VAN ZYL, ANNA MARIA

THE SULPHIDES OF THE UITKOMST COMPLEX, BADPLAAS, SOUTH AFRICA

MSc UP 1996

The sulphides of the Uitkomst Complex, Badplaas, South Africa

by

Anna Maria van Zyl

Submitted in partial fulfilment of the requirements

for the degree of

MAGISTER SCIENTIAE

in the Faculty of Science

University of Pretoria

Pretoria

April 1996

Supervisor: Prof. S.A. de Waal

Co-supervisor: Dr. R.K.W. Merkle

ABSTRACT

The Uitkomst Complex is situated on the farms Uitkomst 541JT and Slaaihoek 540JT, twenty kilometres north of Badplaas, in the Mpumalanga Province, South Africa. It is a mineralized, layered, basic to ultrabasic intrusion of Bushveld age (2,05 - 2,06 Ga). The Complex is intruded into sedimentary rocks of the lower Transvaal Supergroup. It is elongated in a north-westerly direction and is exposed over a total distance of 9km. The intrusion is interpreted by earlier workers to have an anvil-shaped cross section with a true thickness of approximately 800m. It is enveloped by metamorphosed, and in places brecciated, country rocks. Post-Bushveld diabase intrusions caused considerable vertical dilation of the Complex, which consists of six lithological units (from bottom to top): Basal Gabbro (Bgab), Lower Harzburgite (Lhzbg), Chromitiferous Harzburgite (PCR), Main Harzburgite (Mhzbg), Pyroxenite (PXT) and Gabbronorite (GN).

The lower three units carry potentially economic quantities of base metal sulphides with some PGE enrichment. The sulphide minerals occur as disseminated, net-textured, and massive segregations. The primary sulphides are pyrrhotite (po), pentlandite (pn), and chalcopyrite (cp), with cubanite (cb), mackinawite (mc), pyrite (py), millerite (ml), and cobaltite (cob) occurring with these at depth in the Complex. The assemblages are comprised of po + pn + cp; po + pn + cp + cb (Mhzbg); po + pn + cp + mc (Mhzbg and PCR); po + pn + cp + py (Lhzbg, PCR and Bgab); py + cp + ml + po (Lhzbg and PCR) and po + pn + cp + cob (Lhzbg and PCR). Chemical analyses of the sulphide minerals show a definite increase in Ni and decrease in Fe in pentlandite and pyrrhotite towards the base of intrusion. Image analysis indicates that the average grain size of the disseminated sulphide blebs increases towards the base of the intrusion where approximately 80 per cent of the grains are larger than 450 micron. In the Mhzbg, PCR and Lhzbg zones the flame pentlandite forms between 1 and 5 percent of the total pentlandite which is indicative of the lower limit of the nickel losses to be expected in beneficiation. Granular pentlandite has an average grain size of greater than 11 micron and flame pentlandite measures 3 to 10 micron in section.

The Cu/Ni ratio of the sulphide increases towards the base of the Complex.

Serpentinization, saussuritization, uralitization and talc-carbonate alteration are the dominant alteration processes affecting the primary silicate assemblage. Chemical analyses of the primary and secondary silicate minerals associated with the sulphides show Fe-enrichment towards the base of the Complex. This increase in Fe is interpreted as the combined effects of fractionation and the cooling effects of the country rock on the intruding magma. The occurrence of talc and carbonate in the mineralized zone suggest the development of a deuteric CO_2-rich environment in the lower three lithologies. Secondary silicate minerals (serpentine, talc, amphibole and chlorite) are intergrown with the sulphide. These intergrowths will have a bearing on the beneficiation of the sulphide.

UITTREKSEL

Die Uitkomstkompleks is geleë op die plase Uitkomst 541JT en Slaaihoek 540JT, ongeveer 20 km noord van Badplaas, in die Mpumalanga Provinsie, Suid Afrika. Dit is 'n gelaagde, basiese tot ultrabasiese intrusie van Bosveld ouderdom (2.05 - 2.06 Ga) en is gemineraliseerd. Die Kompleks het in die gesteentes van die onderste gedeelte van die Transvaal Supergroep ingedring. Dit is verleng in 'n noordwestelike rigting en dagsoom oor 'n totale afstand van 9 km. Volgens vorige werkers het die Kompleks 'n aambeeldvormige dwarsprofiel met 'n ware dikte van omtrent 800m. Dit word omsluit deur gemetamorfoseerde, en in plekke gebreksieerde, omgewingsgesteentes. Na-Bosveld diabaas indringings het aansienlike vertikale verdikking van die Kompleks veroorsaak. Die Kompleks bestaan uit 6 litologiese eenhede (van onder na bo): Basale Gabbro (Bgab), Laer Hartzburgiet (Lhzbg), Chroomryke Harzburgiet (PCR), Hoof Harzburgiet (Mhzbg), Pirokseniet (PXT) en Gabbronoriet (GN).

Die onderste 3 eenhede dra potensieël ekonomiese hoeveelhede onedel metaalsulfied met ondergeskikte PGM verryking. Die sulfied kom voor in gedissemineerde vorm, met 'n nettekstuur, asook as massiewe liggame. Die primêre sulfiedassosiasie bestaan uit pirrotiet, pentlandiet en chalkopiriet, met ondergeskikte kubaniet, mackinawiet, piriet; milleriet en kobaltiet wat op gegewe dieptes in die Kompleks saam met die primêre mineraalversameling voorkom. Die onderskeie sulfiedassosiasies bestaan uit po + pn + cp + cb (Mhzbg); po + pn + cp + mc (Mhzbg en PCR); po + pn + cp + py (Lhzbg, PCR en Bgab); py + cp + ml + po (Lhzbg en PCR) en po + pn + cp + cob (Lhzbg en PCR). Chemiese ontledings van die sulfied minerale dui op 'n duidelike toename in Ni en afname in Fe in pentlandiet en pirrotiet na die basis van die Kompleks. Beeldanalise dui daarop dat die gemiddelde korrelgroote van die gedissemineerde sulfied toeneem na die Basale Gabbro, waar dit omtrent 80 persent groter as 450 mikron is. In die Mhzbg, PCR en Lhzbg sones beslaan die vlampentlandiet tussen 1 en 5 persent van die totale pentlandiet, wat 'n aanduiding is van die minimum hoeveelheid Ni wat verlore sal gaan tydens veredeling. Granulêre pentlandiet het 'n gemiddelde korrelgroote van groter as 11 mikron en vlampentlandiet wissel tussen 3 en 10 mikron in deursnit, in

poleerde snit. Die Cu/Ni verhouding van die sulfied neem toe na die basis van die Kompleks.

Die primêre silikaatversameling in Uitkomst is meesal geserpentinitiseerd, gesoussuritiseerd, ge-uralitiseerd en toon ook talk-karbonaat verandering. Chemiese ontledings van primêre en sekondêre silikaatminerale geassosieerd met sulfied, toon Fe-verryking nader aan die basis van die Kompleks. Hierdie toename in Fe word geinterpreteer as die gekombineerde uitwerking van fraksionele kristalisasie en die afkoelingseffek van die omgewingsgesteentes op die magma. Die voorkoms van talk en karbonaat in die gemineraliseerde sone getuig van die ontwikkeling van 'n deuteriese, CO_2 -ryke omgewing in die laer drie litologieë. Sekondêre silikaatminerale (serpentyn, talk, amfibool en chloriet) is vergroei met die sulfiede. Hierdie vergroeing sal moontlik 'n invloed hê op die veredeling van die sulfiede.

INDEX

1:INTRODUCTION..... 1

2:PREVIOUS WORK..... 5

2.1 Background..... 5

2.2 Mineralization..... 7

2.2.1 Assay information..... 8

3: EXPERIMENTAL PROCEDURES..... 9

3.1 Sampling..... 9

3.2 Microscopy..... 9

3.3 Electron microprobe..... 9

3.4 X-ray Diffraction..... 11

3.4.1 Quantitative estimation of alteration minerals..... 11

3.4.2 Crystal structure of pyrrhotite..... 12

3.5 Image Analysis..... 12

3.5.1 Background..... 12

3.5.2 Present study..... 15

3.5.3 Problems related to image analysis in the present study..... 18

4: RESULTS..... 21

4.1 Bulk variation of Cu, Co, Ni, Pt, Pd and S in the main lithological units..... 21

4.2 Sulphide minerals..... 27

4.2.1 Systematic description..... 27

4.2.2 Distribution of the sulphide minerals in relation to the lithological units..... 43

4.2.3 Chemical variation of the sulphide minerals in relation to the lithological units..... 44

4.2.4 Crystal structure of pyrrhotite..... 48

4.2.5 Grain size of the disseminated sulphide..... 53

4.2.6 Granular versus flame pentlandite: quantitative results..... 55

4.3 Oxide minerals..... 57

4.4 Silicate minerals..... 61

4.4.1 Primary magmatic minerals..... 61

4.4.2 Secondary minerals..... 77

4.4.3 Quantitative estimation of secondary minerals..... 91

5: DISCUSSION..... 98

5.1 Chemical variation in the sulphide and associated silicate minerals..... 98

5.2 Alteration and sulphide mineralization..... 98

5.3 Beneficiation of the sulphide..... 99

5.3.1 Overview of flotation..... 99

5.3.2 Expected performance of the Uitkomst ore during beneficiation..... 103

6: CONCLUSIONS..... 108

7: ACKNOWLEDGEMENTS..... 111

8: REFERENCES..... 112

9: APPENDICES..... 120

Appendix A: *Microprobe analysis of the sulphide minerals*..... 122

Appendix B: *Microprobe analysis of the silicate minerals*..... 131

Appendix C: *A mineral list compiled from the microscopic investigation on samples from the Uitkomst Complex*..... 154

Appendix D: *Data compiled on the grain size of disseminated and net-textured sulphide in boreholes UD 1, 2, 5, 13, 17, 21, 26, 28, 32, 34, 35, 36, 45, 56, 59, 62, 64, 83, 89, and 93*.. 156

Appendix E: *Assay values for boreholes UD 1, 5, 34, 45, 59 and 64*..... 169

List of Figures

Figure 1.1: Locality map of the Uitkomst Complex (after Gauert et al, 1995)..... 2

Figure 1.2: A geological map of the Uitkomst Complex on the farm Uitkomst 541JT (after Gauert et al, 1995)..... 3

Figure 1.3: A schematic cross section through the Uitkomst Complex (after Gauert et al, 1995)..... 4

Figure 3.1: Sketch map of the approximate positions of the boreholes in the Uitkomst Complex used in this study for image analysis and microscopy (blocked)..... 10

Figure 3.2: (a) Photomicrograph of sulphide minerals. (b) Pentlandite are detected through thresholding. (c) A grey-level/intensity histogram. (d) The binary image of pentlandite. (See text for description)..... 14

Figure 3.3: Bias resulting from measurements that are not made on true section (Holmes effect). (a) Material in relief in polished section in reflected light as a result of differential polishing of the hard and soft components. (b) Thin section in transmitted light. (From Oosthuyzen, 1983)..... 16

Figure 3.4: Minimum projection..... 17

Figure 3.5: Maximum projection..... 18

Figure 3.6: Width..... 18

Figure 4.1a: Essay values from borehole UD 1 for Cu, Ni, Co and S (in wt %) plotted against depth (in m)..... 22

Figure 4.1b: The Ni/S, Cu/Ni and Pt/Pd weight ratio for UD 1..... 22

Figure 4.2a: Essay values from borehole UD 5 for Cu, Ni, Co and S (in wt %) plotted against depth (in m)..... 22

Figure 4.2b: The Ni/S, Cu/Ni and Pt/Pd weight ratio for UD 5 versus depth (in m)..... 23

Figure 4.3a: Essay values from borehole UD 34 for Cu, Ni and S (in wt %) versus depth (in m)..... 23

Figure 4.3b: The Ni/S, Cu/Ni and Pt/Pd weight ratio for UD 34 versus depth (in m)..... 23

Figure 4.4a: Essay values from borehole UD 45 for Cu, Ni, Co and S (in wt %) versus depth (in m)..... 24

Figure 4.4b: The Ni/S, Cu/Ni and Pt/Pd weight ratio for UD 45 versus depth (in m)..... 24

Figure 4.5a: Essay values from borehole UD 59 for Cu, Ni, Co and S (in wt %) versus depth (in m)..... 24

Figure 4.5b: The Ni/S, Cu/Ni and Pt/Pd weight ratio for borehole UD 59 versus depth (in m)..... 25

Figure 4.6a: Essay values from borehole UD 64 for Cu, Ni, Co and S (in wt %) versus depth (in m)..... 25

Figure 4.6b: The Ni/S, Cu/Ni and Pt/Pd weight ratio for UD 64 versus depth (in m)..... 25

Figure 4.7: Compositions of natural pentlandites in nickel sulphide assemblages (Misra and Fleet, 1973)..... 32

Figure 4.8: Fe/S atomic ratio of pyrrhotite versus elevation above base (depth)..... 44

Figure 4.9: Ni-content (atomic %) of pyrrhotite..... 45

Figure 4.10: Fe/Ni atomic ratio in pentlandite versus elevation above base..... 46

Figure 4.11: Ni/Co atomic ratio in pentlandite versus elevation above base..... 46

Figure 4.12: Ni-content in pyrrhotite versus Ni-content in pentlandite (atomic %)..... 47

Figure 4.13: Fe/S atomic ratio of pyrite versus elevation above base..... 47

Figure 4.14: Upper: X-ray chart records of the 11 re-examined pyrrhotite samples. Lower: X-ray chart records and intensity ratios of various weighed mixtures of hexagonal and monoclinic pyrrhotite. I (LHP) and I (RHP) represent the intensity of the left- and right hand peaks, respectively..... 50

Figure 4.15: X-ray chart records for samples UD 2/8 (a), UD 2/12 (b), UD 59/8 (c) and UD 59/9 (d).... 51

Figure 4.16: X-ray chart records for samples UD 45/4 (a), UD 45/6 (b), UD 2/17 (c) and UD 1/9 (d)..... 52

Figure 4.17: Grain size distribution in the Mhzbg..... 54

Figure 4.18: Grain size distribution in the PCR..... 54

Figure 4.19: Grain size distribution in the Lhzbg..... 54

Figure 4.20: Grain size distribution in the Bgab..... 55

Figure 4.21: Olivine compositions in molar percentage plotted against elevation in metre above base of intrusion (from Gauert et al, 1995)..... 63

Figure 4.22: Microprobe analyses of pyroxenes plotted on a Q - J diagram where Q = Ca + Mg + Fe^2 and J = 2Na..... 65

Figure 4.23: Microprobe analyses of pyroxenes plotted on a triangular diagram showing the four component system $CaMgSi_2O_6$-$CaFeSi_2O_6$-$MgSiO_3$-$FeSiO_3$..... 66

Figure 4.24: Variation of Mg (cation percent) against elevation above base (metres) in the Uitkomst Complex. The lowermost Bgab is not marked, but is represented by the first 15 m in the diagram.(from Gauert et al, 1995)..... 67

Figure 4.25: Plagioclase compositions plotted on the triangular diagram $KAlSi_3O_8$-$NaAlSi_3O_8$-$CaAl_2Si_2O_8$..... 69

Figure 4.26: A diagram of the phlogopite - biotite compositional field with Al in the tetrahedral position versus the Fe/(Fe + Mg) ratio. The division between them is arbitrarily chosen to be where Mg:Fe = 2:1..... 76

Figure 4.27: Microprobe analyses of phlogopites plotted according to lithology on a diagram of the phlogopite-biotite compositional field with Al in the tetrahedral position versus the Fe/(Fe + Mg) ratio. The division between them is arbitrarily chosen to be where Mg:Fe = 2:1..... 76

Figure 4.28: Serpentine analyses plotted in terms of Si, Mg and Fe on a ternary diagram (crosses represent analyses where Al_2O_3=0, while the circles represent analyses containing Al_2O_3)..... 79

Figure 4.29: Classification of the Uitkomst chlorite after Hey (1954)..... 80

Figure 4.30: Amphibole analyses plotted on a diagram showing the different amphibole subgroups, with Na in the B position versus Ca+Na in the B position..... 84

Figure 4.31: The series cummingtonite-grunerite with Si versus Mg/Mg+Fe..... 85

Figure 4.32: Calcic amphiboles where (Na + K)A< 0.5 and Ti< 0.5..... 86

Figure 4.33: Calcic amphiboles where (Na + K)A> 0.5; Ti< 0.5 and Fe^3< Al^6..... 86

Figure 4.34: Calcic amphiboles were (Na + K)A> 0.5; Ti< 0.5 and Fe^3> Al^6..... 87

Figure 4.35: The corrected NIR for serpentine-chlorite versus depth (m) in borehole UD 45..... 93

Figure 4.36: The corrected NIR for amphibole versus depth (m) in borehole UD 45..... 93

Figure 4.37: The corrected NIR for calcite versus depth (m) in borehole UD 45..... 94

Figure 4.38: The corrected NIR for talc versus depth (m) in borehole UD 45..... 94

Figure 4.39: The corrected NIR for mica versus depth (m) in borehole UD 45..... 94

Figure 4.40: Mass % sulphide plotted against the corrected NIR for serpentine-chlorite in borehole UD 45..... 95

Figure 4.41: Mass % sulphide plotted against the corrected NIR for amphibole in borehole UD 45..... 95

Figure 4.42: Mass % sulphide plotted against the corrected NIR for calcite in borehole UD 45..... 96

Figure 4.43: Mass % sulphide plotted against the corrected NIR for talc in borehole UD 45.... 96

Figure 4.44: Mass % sulphide plotted against the corrected NIR for mica in borehole UD 45.... 96

Figure 5.1: The effects of product size on the specific energy required for cominution (after Cohen, 1983)..... 100

List of Tables

Table 1:	The reproducability of X-ray diffraction line intensities.....	12
Table 2:	Average Cu/Cu+Ni and Pt/Pt+Pd assay values for the lithologies at Uitkomst.....	26
Table 3:	Cu/(Cu+Ni) and Pt/(Pt+Pd) ratios for various layers and pipes in the Bushveld Complex (Von Gruenewaldt, 1979).....	26
Table 4:	Average composition of pyrrhotite at Uitkomst.....	27
Table 5:	Summary of pentlandite compositions (Duke and Naldrett, 1976).....	33
Table 6:	Average composition of pentlandite at Uitkomst.....	33
Table 7:	Average composition of chalcopyrite at Uitkomst.....	36
Table 8:	Average composition of pyrite at Uitkomst..	38
Table 9:	Platinum-group minerals observed at Uitkomst.....	42
Table 10:	Sulphide assemblages of the Uitkomst Complex.....	43
Table 11:	A summary of the compositions, d-values, and structural types of the 11 re-examined pyrrhotites after Arnold (1966).....	48

Table 12: Quantitative data on flame and granular pentlandite (all measurements in micron).... 56

Table 13: The grain size (micron) for granular and flame pentlandite in borehole UD 45..... 56

Table 14.1: Average composition for brown phlogopite at Uitkomst..... 70

Table 14.2: Average composition for white phlogopite at Uitkomst..... 72

Table 14.3: Average composition for green phlogopite at Uitkomst..... 74

Table 15: Calcic amphibole in metamorphic ultramafic rocks: Relation to metamorphic facies, critical mineral parageneses, aluminium phase, and typical Si-content of calcic amphibole (after Robinson et al, 1982)..... 88

Table 16: The depth (m), normalized intensity ratios (NIR), and volume % sulphide of the samples used for X-ray diffraction..... 92

Table 17: The corrected values for the normalized intensity ratios (NIR) and volume % sulphide of the samples used for X-ray diffraction... 92

Table 18: Classification of sulphide minerals based on the relative abundance of surface sulphide sites (Herrera-Urbina, 1990)..... 101

List of Photographs

Plate 1A: Granular pentlandite with characteristic octahedral cleavage and chalcopyrite with smaller islands of pyrrhotite. Sample 45/4, magnification x20, plane polarized light... 29

Plate 1 B: Flame pentlandite occurring on the grain boundaries, around cracks, around holes and in the lattice of pyrrhotite. Sample 45/4, magnification x20, plane polarized light.... 29

Plate 1 C: Pentlandite islands in violarite with surrounding chalcopyrite. The violarite has almost totally replaced the granular pentlandite. Sample 59/1, magnification x50, plane polarized light..... 30

Plate 1 D: Granular pentlandite occurring with magnetite (left) and pyrrhotite with chalcopyrite (right). Mackinawite flames (yellow- bluish gray anisotropism) occurs in the pentlandite. Sample 5/D, magnification x20, crossed polarizers..... 30

Plate 2 A: Cubanite with chalcopyrite exsolution occurring in pyrrhotite. Flame pentlandite exsolves in the cubanite- chalcopyrite grain. Sample 5/A, magnification x50, crossed polarizers..... 35

Plate 2 B: Islands of pyrrhotite occurring in chalcopyrite. Sample 1/9 a, magnification x20, plane polarized light..... 35

Plate 2 C: Subhedral, spongy pyrite (left) and mottled pentlandite (right) in pyrrhotite. Chalcopyrite occurs in the pyrrhotite next to the pyrite and as discrete grains in the gangue. Sample 59/9, magnification x20, plane polarized light..... 37

Plate 2 D: Pyrite, chalcopyrite, pentlandite, and magnetite occurring in pyrrhotite. The pentlandite has a mottled appearance which is caused by violarite replacing the pentlandite. Sample 59/9, magnification x20, plane polarized light..... 37

Plate 3 A: Cubanite and chalcopyrite exsolution in pyrrhotite. Sample 5/A, magnification x50, plane polarized light..... 39

Plate 3 B: Granular pentlandite and chalcopyrite occurring in pyrrhotite. Euhedral bluish-white cobaltite seems to cut over the existing sulfides, thereby indicating its secondary nature. Sample 1/9 a, magnification x20, plane polarized light.... 39

Plate 3 C: Anhedral aggregates of millerite (blue to yellow anisotropism) occurring in pyrite. Sample 34/A, magnification x20, crossed polarizers..... 41

Plate 3 D: White-pinkish cobaltite occurring in pyrrhotite. Very small yellowish-white grains (*) occur in the cobaltite consisting of Pd, Bi and Te. The cobaltite in bluish in places. Granular pentlandite (above, left) seems more orangy than the usual light yellow. Sample 45/3, magnification x50, plane polarized light..... 41

Plate 4 A: Fine magnetite exsolutions in pyrrhotite, which exsolves parallel to the flame pentlandite. Sample 59/9, magnification x50, plane polarized light..... 59

Plate 4 B: Primary magnetite with exsolutions of ulvöspinel and ilmenite, occuring adjacent to sulphide. Sample 1/6, magnification x20, plane polarized light..... 59

Plate 4 C: Secondary magnetite rimming chromite and sulphide which are surrounded by phlogopite. Lenses of magnetite (below, left) parallel to the cleavage of phlogopite can be seen. Sample 5/A, magnification x20, plane polarized light..... 60

Plate 4 D: A subhedral grain of ilmenite, surrounding pyrrhotite with exsolutions of flame pentlandite, which is in turn surrounded by primary magnetite. Sample 1/8, magnification x20, plane polarized light..... 60

Plate 5 A: Olivine poikilitically enclosed by pyroxene. Sample 45/1, magnification x6.3, crossed polarizers..... 62

Plate 5 B: Clinopyroxene enclosed by plagioclase. Sample 34/9, magnification x3.2, crossed polarizers..... 62

Plate 5 C: Phlogopite - brown on one side (left) and colourless on the other (right). Sample 5/5, magnification x10, plane polarized light.... 71

Plate 5 D: Phlogopite of plate 5 C under crossed polarizers. Note the difference in birefringe between the left (brown) side and the right (colourless) side. Sample 5/5, magnification x10..... 71

Plate 6 A: Brown phlogopite altering to chlorite surrounded by talc and carbonate. The chlorite displays anomalous blue interference colours. Sample 5/1, magnification x10, crossed polarizers..... 73

Plate 6 B: Pyroxene replaced by green phlogopite. Sample 64/6, magnification x5, plane polarized light..... 73

Plate 6 C: Pyroxene replaced by a green amphibole and green phlogopite. The green phlogopite shows a brown colour in the middle of the grain surrounded by green on the side. Sample 64/6, magnification x5, plane polarized light..... 75

Plate 6 D: Green phlogopite enclosing a sulphide grain (just like brown phlogopite usually do). The green phlogopite is platy and coarse-grained directly next to the sulphide, becoming more fine-grained further away, as well as where it is replacing pyroxene. Sample 64/6, magnification x5, plane polarized light.... 75

Plate 7 A: Pyroxene (purple) replaced by amphibole (green) from the grain boundaries inwards. The amphibole forms a rim around the pyroxene. Epidote - zoisite occurs to the right. Sample 59/1, magnification x3.2, crossed polarizers..... 83

Plate 7 B: Grains of carbonate surrounding a sulphide grain. Brown phlogopite with chromite are in association with the carbonate and sulphide. Serpentine occurs in the background. Sample 1/3, magnification x10, plane polarized light..... 83

Plate 7 C: A plagioclase-quartz intergrowth. The section is thicker than usual, hence the orange interference colour of quartz. Sample 34/9, magnification x3.2, crossed polarizers..... 91

Plate 8 A: Pyrrhotite with granular pentlandite surrounded by a rim of magnetite. The magnetite also occurs in the cleavage of the granular pentlandite. Sample 45/1, magnification x20, plane polarized light.... 104

Plate 8 B: Pyrrhotite with granular pentlandite and chalcopyrite occurring on the side of the pyrrhotite grain. Silicate needles are intergrown with the sulphide, resulting in grain size reduction of pentlandite and chalcopyrite. Sample 34/4, magnification x20, plane polarized light..... 104

Plate 8 C: Needles of serpentine growing into sulphide. Carbonate occurs in the sulphide and talc in the serpentine. Sample 34/4, magnification x10, crossed polarizers..... 106

Plate 8 D: Colourless, diamond-shaped shards of amphibole growing into the sulphide. Sample 64/7, magnification x3.2, crossed polarizers..... 106

Plate 9 A: Sulphide surrounded by carbonate with needle-like serpentine growing into the carbonate. The carbonate seems to act as a buffer, thus preventing sulphide-silicate intergrowth. Talc occurs around the serpentine. Sample 1/3, magnification x10, plane polarized light..... 107

Plate 9 B: Sulphide surrounded by carbonate with needle-like serpentine growing into the carbonate. The carbonate seems to act as a buffer, thus preventing sulphide-silicate intergrowth. Talc occurs around the serpentine. Sample 1/3, magnification x10, crossed polarizers..... 107

1. INTRODUCTION

The Uitkomst Complex is situated on the farms Uitkomst 541JT and Slaaihoek 540JT twenty kilometres north of Badplaas in the Mpumalanga Province, South Africa **(Figure 1.1).** It is a mineralized, layered, basic to ultrabasic intrusion of Bushveld age (2,05 - 2,06 Ga) as indicated by a single Rb-Sr determination (Kenyon et al, 1986). The Complex intruded into sedimentary rocks of the lower Transvaal Supergroup (Button, 1973; Clendenin et al, 1991; Schreiber, 1991; Eriksson et al, 1993). It is elongated in a north-westerly direction and is exposed over a total distance of 9km **(Figure 1.2).** The intrusion is interpreted by Gauert et al (1995) to have an anvil-shaped cross section **(Figure 1.3)** with a true thickness of approximately 800m. It is enveloped by metamorphosed, and in places brecciated, country rocks. Post-Bushveld diabase intrusions caused considerable vertical dilation of the Complex, which consists of six lithological units (from bottom to top): Basal Gabbro, Lower Harzburgite, Chromitiferous Harzburgite, Main Harzburgite, Pyroxenite and Gabbronorite (Gauert et al, 1995).

The investigation reported on here is concerned with the lower four lithological units which are present on the farm Uitkomst. The lower three units, collectively referred to in this study as **the mineralized zone**, carry potentially economic quantities of base metal sulphides with some PGE enrichment. The economic potential of the deposit warranted a detailed mineralogical study of the sulphide minerals and their relation to the silicate host rocks. The sulphide minerals occur as disseminated, net-textured, and massive segregations and the report is largely confined to the **disseminated and net-textured sulphides**.

The main purpose of the research was to elucidate the mineralogical aspects pertaining to beneficiation of the sulphide ore. However, the wide range of observations made in this process also has definite significance for petrologists and economic geologists.

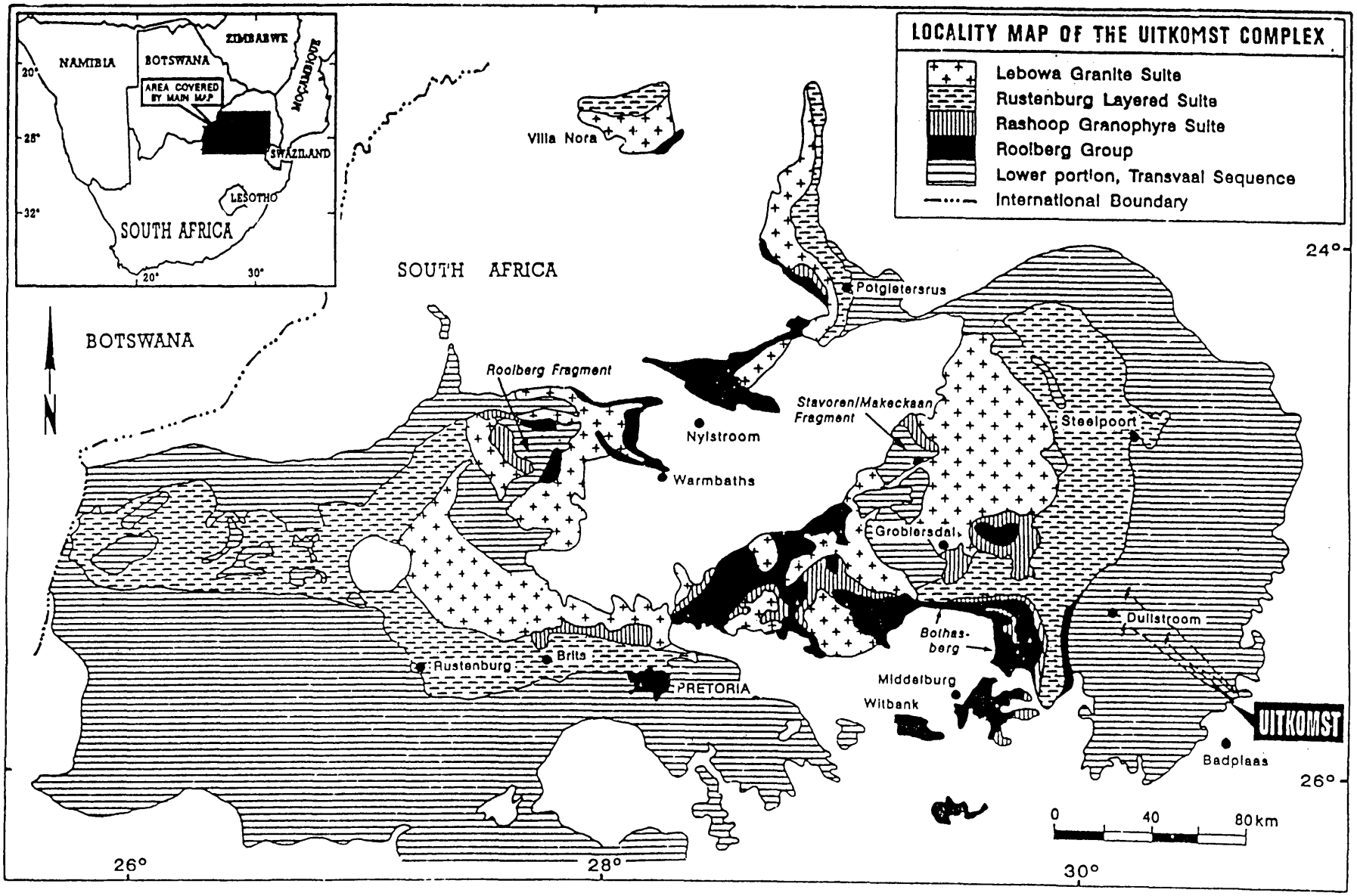

Figure 1.1: Locality map of the Uitkomst Complex (after Gauert et al, 1995).

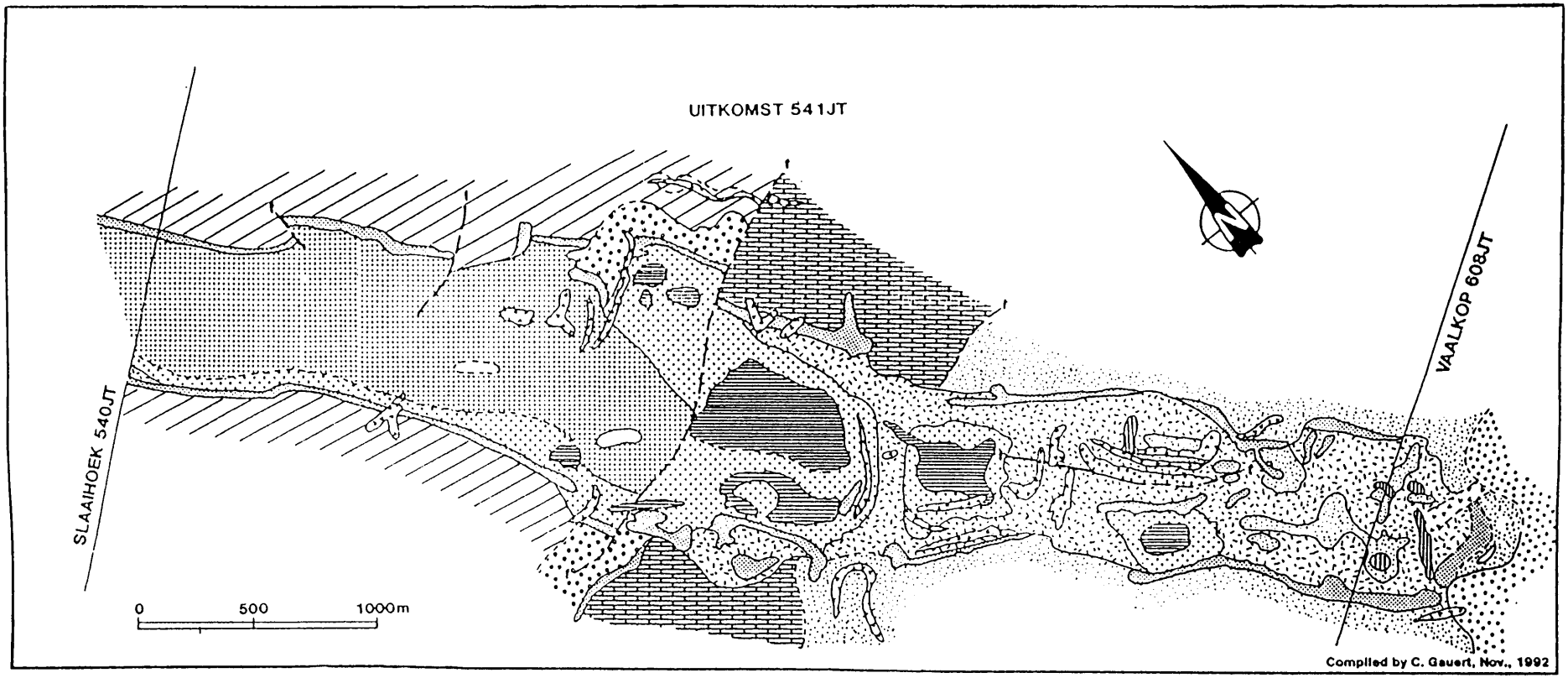

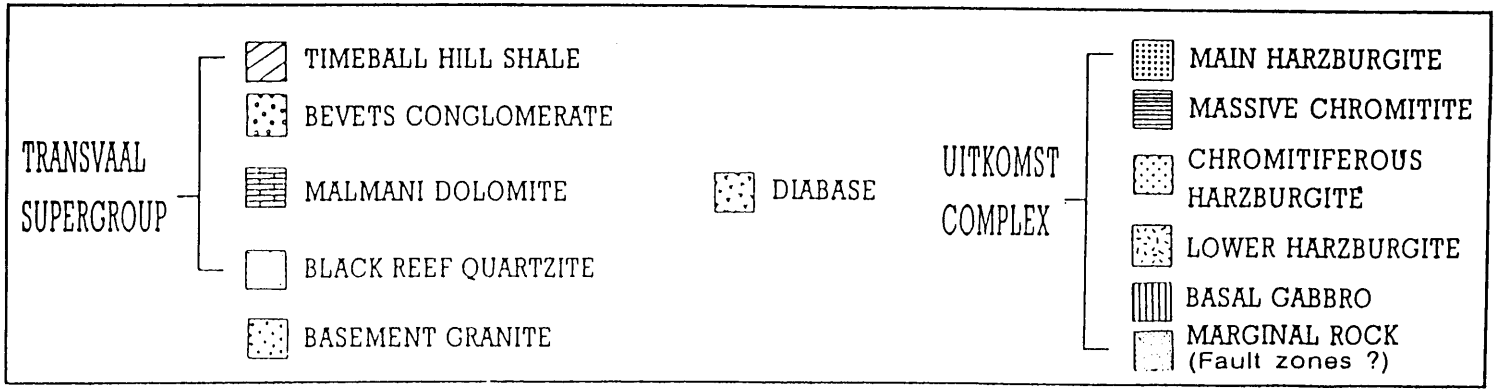

Figure 1.2: A geological map of the Uitkomst Complex on the farm Uitkomst 541JT (after Gauert et al, 1995).

Figure 1.3: A schematic cross section through the Uitkomst Complex (after Gauert et al, 1995).

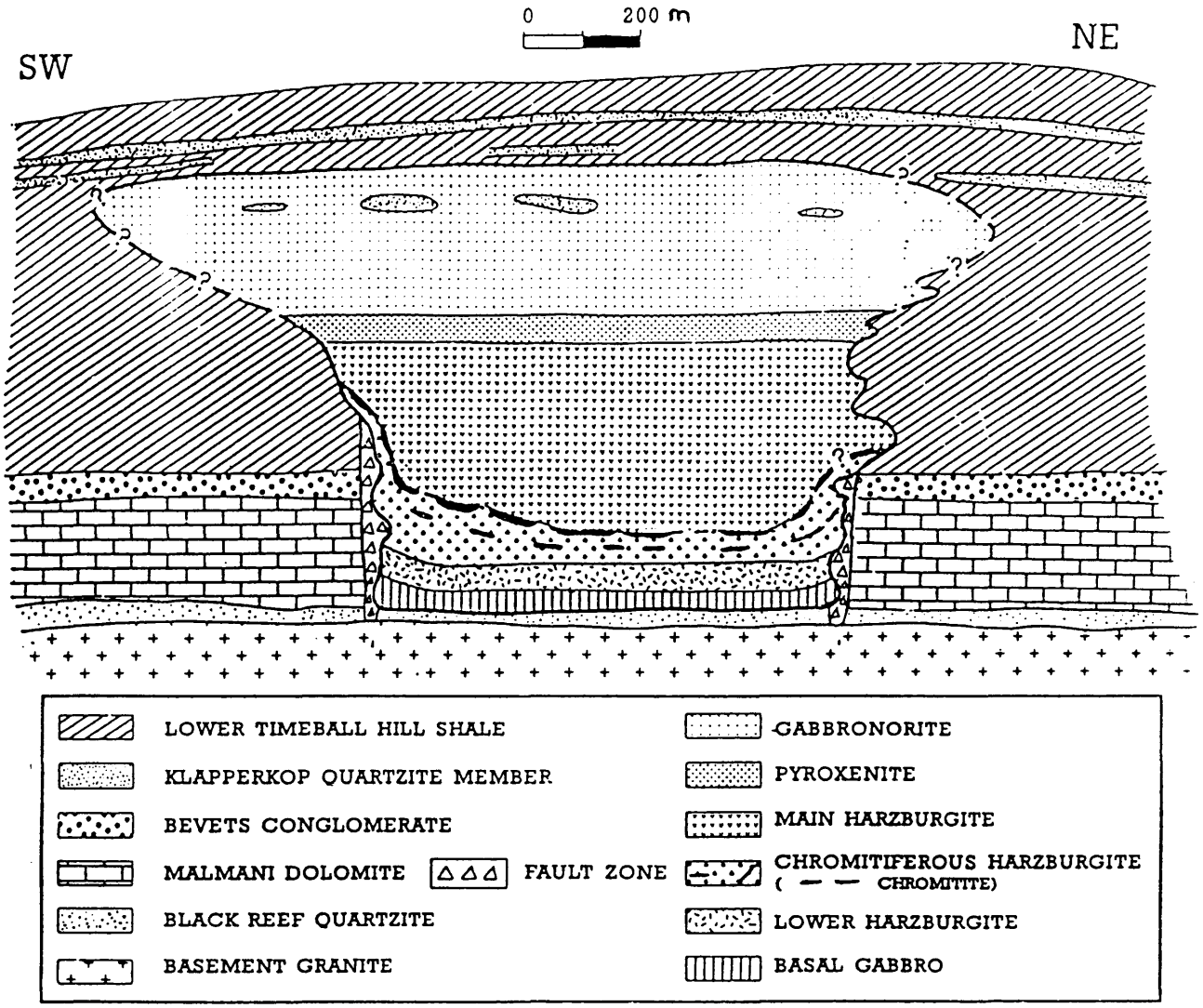

2.PREVIOUS WORK

2.1 Background

The Uitkomst Complex was described by a number of previous workers (Wagner, 1929; Kenyon, 1979 and Kenyon et al, 1986; Von Scheibler, 1990a and 1990b; Allen, 1990; Kiviets, 1991) and more recently by Gauert et al (1995, 1996). The following background on the Complex is a summary compiled from Gauert et al (1995, 1996).

The Complex consists of six lithological units (from bottom to top): Basal Gabbro, Lower Harzburgite, Chromitiferous Harzburgite, Main Harzburgite, Pyroxenite and Gabbronorite.

The Basal Gabbro (Bgab) unit, with an average thickness of 6m, is developed at the base of the intrusion and shows a narrow chilled margin, 0,2 - 1,5m thick, against the floor rocks. The contact of the Basal Gabbro with the Black Reef Quartzite Formation is defined by a strongly sheared talc-chlorite-carbonate rock, varying in thickness from less than one to several metres. The gabbroic rock constituting Basal Gabbro shows intense saussuritization and uralitization. In spite of this degree of alteration, the original sub-ophitic texture is still visible.

The Basal Gabbro grades upwards into the sulphide-rich, pyroxenitic and xenolith-bearing sequence of the Lower Harzburgite (Lhzbg) unit wich has an average thickness of 50m. This unit is highly altered and contains abundant quartzitic and carbonaceous xenoliths, flattened in the direction of the original sedimentary layering, and forming rafts that are orientated parallel to the igneous layering. The dominant poikilitic harzburgite of the Lower Harzburgite includes local variations of feldspar-bearing lherzolite, grading into sulphide-rich feldspatic olivine-wehrlite, and amphibolite. In places, especially in the vicinity of country rock inclusions, a pegmatoidal pyroxenite is developed. Although the primary magmatic minerals are intensely altered through serpentinization, saussuritization and uralitization, the original igneous textures are still well preserved.

The Lower Harzburgite is overlain with a gradational contact by the chromite-rich harzburgite of the Chromitiferous Harzburgite (PCR) unit

(average thickness 60m). The unit consists of sheared chromitite lensoids with a distinct "schlieren"-type structure embedded in highly altered harzburgite. The chromite increases in abundance upwards in the sequence and the top of this unit is a three to four metre thick massive chromitite. The original magmatic minerals of this unit are almost completely replaced by talc, carbonate, mica, chlorite and serpentine.

The Main Harzburgite (Mhzbg) unit with a thickness of 330m follows on the Chromitiferous Harzburgite. It is represented by a rather monotonous sequence of harzburgitic rock, grading locally into dunite, and visibly lacking mineralization except for the lowermost ten metres. Serpentinization is the main alteration type. Talc-carbonate alteration is rare.

The Pyroxenite (PXT) unit follows on the Main Harzburgite with a narrow transitional contact and is approximately 60 m thick. The Pyroxenite can be subdivided into three sub-units i.e. a lower olivine-orthopyroxenite, followed by pure orthopyroxenite, with only minor accessory chromite and sulphide, and an upper norite to gabbronorite showing increasing plagioclase, clinopyroxene and minor quartz towards the top. The pyroxenitic rocks are markedly unaffected by secondary alteration.

The Gabbronorite (GN) unit follows with a gradational contact on the Pyroxenite. It is approximately 250 m thick and forms the uppermost sequence of the intrusion. In boreholes on the farm Little Mamre 538JT the upper contact of the gabbronorite against the lower Timeball Hill Shale has a distinctly chilled character, reaching submicroscopic grain sizes. Xenoliths of quartzitic and argillaceous rocks are found in places.

Field relations, petrography, and mineral and whole rock chemistry suggest the following sequence of events. The original emplacement of magma took place from north-west to south-east. The intrusion was bounded between two major fracture zones that gave rise to an elongated body which acted as a conduit for later magma heaves. The first magma pulses initially intruded along the contact of the Black Reef Quartzite with the overlying Malmani Dolomite of the Transvaal Supergroup and formed the chilled margin of the intrusion. Later pulses stoped upwards to cut across the Malmani Dolomite subgroup, the overlying Bevets Conglomerate Member of the Rooihoogte Formation, and the lower shale member of the Timeball Hill Formation. The

Lower Harzburgite and Chromitiferous Harzburgite units, judged from the abundance of xenoliths, originated by crystal settling from a contaminated basic magma. The Main Harzburgite crystallised from a magma of constant, probably also basic, composition, which flowed through the conduit after formation of the lower three lithological units. At a late stage of emplacement, after replenishment in the conduit came to an end, closed system conditions developed in the upper part of the Complex, resulting in a magma fractionation trend of increasing incompatible element contents towards the top of the intrusion. The oblong shape of the intrusion seems to have been controlled by a major fracture and fault system which strikes in a north-westerly direction.

2.2 Mineralization

According to Gauert et al (1996) the bulk of the sulphide mineralization is confined to the three lowermost lithologies, namely the Chromitiferous Harzburgite, Lower Harzburgite and Basal Gabbro, whereas the upper lithologies (Main Harzburgite, Pyroxenite and Gabbronorite) are virtually barren of sulphide. The sulphide mineralization ranges from disseminated grains, through interstitial net-textured sulphides, to massive lenses and lodes. The net-textured sulphides are common to the Chromitiferous and Lower Harzburgites, whereas the more massive sulphide concentrations tend to be restricted to the Lower Harzburgite and the immediately underlying floor rocks. Allen (1990) described massive and semi-massive sulphides in "assimilated feldspatic zones" as well as above and below xenoliths in the Lower Harzburgite. The Basal Gabbro contains disseminated to semi-massive sulphide mineralization in the form of blebs and interstitial ore, often with Cu-to-Ni ratios exceeding one.

Gauert et al (1996) concluded from sulphur isotope work that magmatic sulphur has been augmented by sedimentary sulphur. Increased oxygen fugacity caused by assimilation of the sediments could have caused sulphur saturation and sulphide liquid segregation to form the mineralization. According to Gauert et al (op. cit.) mass balance calculations indicate that the assimilation of approximately 10 mass percent of sediment by the mafic magma could yield the sulphur isotope ratios observed in the Uitkomst Complex.

Von Scheibler et al (1995) also considers sedimentary rock to be a feasible source for augmenting magmatic sulphur at Uitkomst, but gives preference to the assimilation of Timeball Hill shale in contrast to dolomite as suggested by Gauert et al (1996). The latter authors discussed the effects of both the shale and the dolomite being assimilated, as well as the iron-rich character of the Basal Gabbro. They came to the conclusion that the oxidative influence of the dolomite plus the addition of more sulphur from the sediments caused the limits of sulphur solubility of the magma (already enriched in iron and carrying large amounts of sulphur close to capacity) to be exceeded and precipitation to be triggered.

2.2.1. Assay Information

Anglo American Corporation and the International Nickel Company of Canada (INCO) drilled almost 30 000 m of borehole core during an extensive drilling campaign in the 1970's and 1980's (Gauert, 1995, pers. com.). These boreholes were sampled by the two companies and assayed for Cu, Ni and Co using a total nickel digestion method. The assay values used in this thesis are derived from this source and have been kindly provided by the Anglo American Corporation for the purpose of this study.

3. EXPERIMENTAL PROCEDURES

3.1 Sampling

Representative sections of twenty boreholes **(Figure 3.1)**, each showing the complete section of the mineralized zone, were sampled over five metre intervals. To compare the mineralogy in the unmineralized Main Harzburgite with that in the mineralized zone, the Main Harzburgite was also sampled on a five metre interval in borehole UD 45 (112 m).

From the twenty boreholes six boreholes were selected for detailed microscopic, microprobe and X-ray diffraction work **(Figure 3.1).** UD 1 and 5 falls in the upper north-western (deeper) corner, UD 45 and UD 34 in the middle, while UD 59 and 64 represents the lower south-eastern corner of the Complex on the farm Uitkomst.

Grain size analysis and quantitative image analysis were performed on all the samples from all twenty boreholes sampled.

3.2 Microscopy

Polished thin sections and polished sections were studied by reflected and transmitted light using Leitz and Jenapol petrographic microscopes.

3.3 Electron microprobe analysis

Electron microprobe analyses of sulphide and silicate minerals were carried out on selected samples using a fully automated Jeol 733 Superprobe (University of Pretoria) with four spectrometers. The accelerating potential was 20 kV with a beam current of 20nA. Counting time for each element was 20 seconds and standard data reduction software programmes were used.

Figure 3.1: Sketch map of the approximate positions of the boreholes in the Uitkomst Complex used in this study for image analysis and microscopy (blocked).

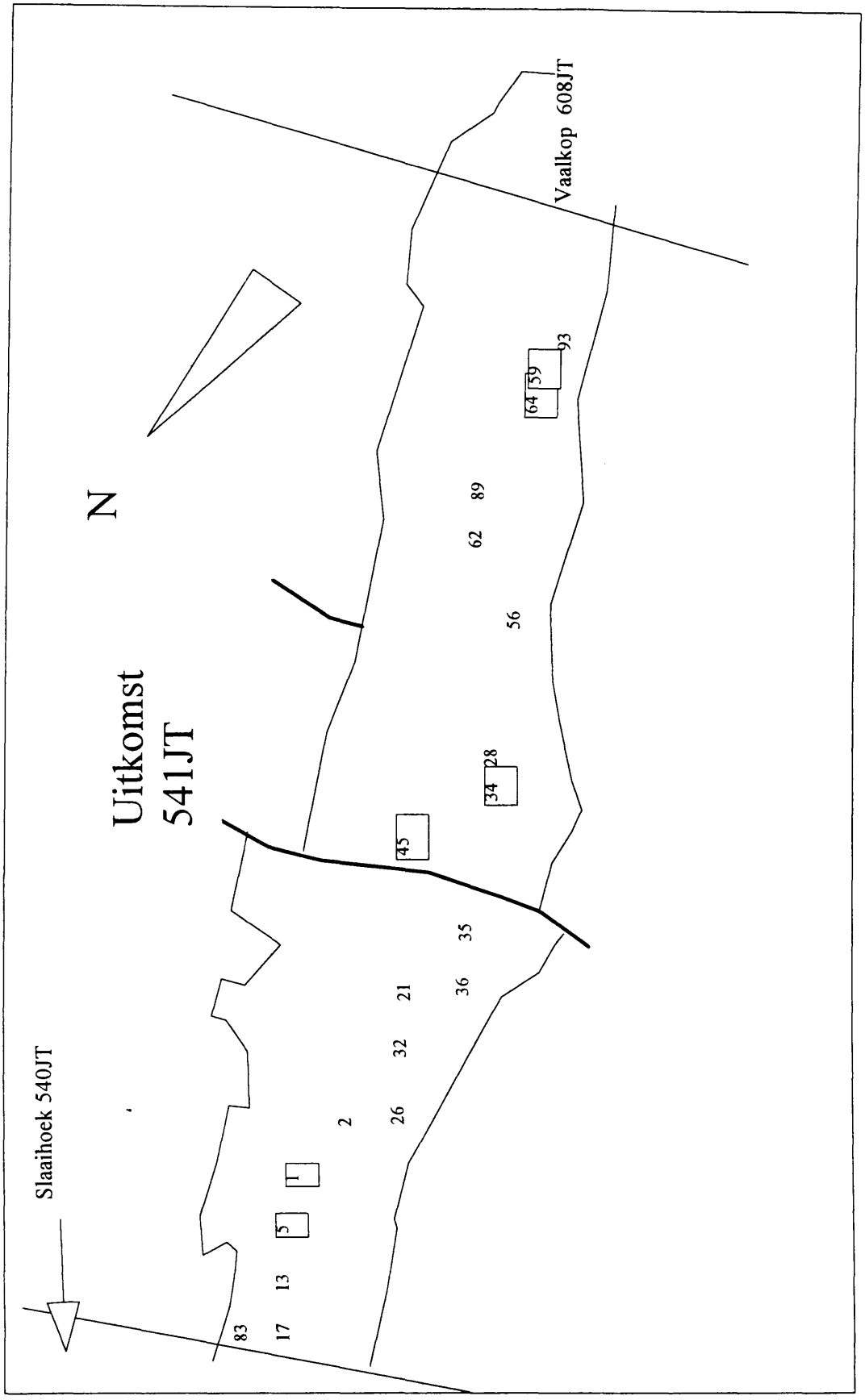

3.4 X-ray Diffraction

3.4.1 Quantitative estimation of the alteration minerals

Following from the observation of Gauert et al (1996) on the association of mineralization and alteration in the mineralized zones, attempts were made to illustrate the possible correlation between the amounts of secondary and sulphide minerals. For this purpose, semi-quantitative X-ray diffraction analyses, with MgO as internal standard, were performed on thirteen samples covering the whole depth of UD 45. The relative proportions of serpentine, chlorite, talc and amphibole were determined. Serpentine and chlorite were grouped as one mineral because of their similar d-values at 7 Ängstrom units. The normalized intensity ratios (NIR), based on peak height of the X-ray diffraction lines of the alteration minerals, were then correlated with the mass percentage of the sulphide minerals present.

The detail of this quantitative X-ray study is as follows. Representative portions of the core samples, powdered to -200 micron and mixed with MgO internal powder standard in a ratio of 4:1, were thorougly homogenized by grinding in an agate mill for five minutes. The mixtures were analyzed at the University of Pretoria on an automated Siemens D501 diffractometer with a forty position sample changer. Monochromated Cu Kα radiation at 25 mA and 30 kV, at a scanning speed of 3° 2θ/min (stepsize = 0,05° 2θ, measuring time = 1 sec.) was used. Patterns were recorded from 5° to 75° 2θ. After background corrections, the peak intensities of selected lines were normalized to the intensity of the MgO *200* diffraction peak. The variance due to sample preparation (five replicate preparations) and instrumental reproducibility (five replicate measurements) was estimated using the formula given by Kaiser and Specker (1956) and listed in **Table 1.**

Table 1: The reproducibility of X-ray diffraction line intensities.

Range of NIR's measured

	Talc:	Amph:	Serp-chl:	Calcite:	Mica:
mean	0.46	0.80	1.09	0.20	0.16
minimum	0	0	0.18	0	0
maximum	2.41	2.32	2.4	0.76	0.85

Reproducibility as determined on replicate samples

	Talc:	Amph:	Serp-chl:	Calcite:	Mica:
1s	0.11	0.15	0.09	0.02	0.09
2s	0.22	0.3	0.18	0.04	0.18
3s	0.33	0.45	0.27	0.06	0.27

(s = sample standard deviation)

3.4.2 Crystal structure of pyrrhotite

X-Ray diffraction was also used to determine the crystal structure of the pyrrhotite in Uitkomst sulphide assemblages. Eight samples were selected from the Chromitiferous Harzburgite, Lower Harzburgite and the Basal Gabbro. The core samples were powdered to -200 micron, mounted and analyzed. Monochromated Cu Kα radiation at 25 mA and 30 kV, at a scanning speed of 3° 2θ/min (stepsize = 0,02° 2θ, measuring time = 1 sec.) was used. Diffraction patterns from 40° to 50° 2θ were recorded.

3.5 Image Analysis

3.5.1 Background

Image analysis is the quantitive measurement of geometrical features, such as area, number, perimeter, projection, form, size and distribution pattern, as observed on a two-dimensional image (Oosthuyzen, 1983). Accordingly, the image can be seen as geometrical information that is:

(a) contained in planar sections of three-dimensional objects (e.g. a polished section of an ore)

(b) contained in projection of a thin film or a thin slice of a three-dimensional object (e.g. a thin section of a rock or mineral) viewed in transmitted light, and

(c) contained in any two-dimensional replica of three-dimensional objects (e.g. microscopic images of unsectioned materials such as unmounted mineral

grains, scanning electron microscope photographs, ordinary photographs, and geological maps)(Oosthuyzen, 1983)

The image is captured by camera or any other suitable device, digitised and displayed on an electronic screen. Such images are made up of pixels, representing the smallest portions of an image that can be addressed. Each pixel contains specific information of the image. The electrical signal from each pixel is fed into a detector which allocates a grey scale value (between 0 and 255), based on the strength of the signal, to each pixel. The detector also allows the classification of pixels according to grey scale which makes it possible to separate different phases in the displayed image on account of their relative "brightness" in the image. By using the principle of thresholding grey level images can be converted into binary images. This means that a specific mineral with its characteristic "brightness" (reflectivity in a polished section) can be extracted from the image if an appropriate threshold and band width of the grey scale are selected (Oosthuyzen, 1983). In the binary image, the selected grey scale interval for a specific mineral or phase is allocated a value of 1 and appears white, whereas the remaining phases receive a value of 0 and forms the background that appears black. Using this binary image, the computer can now generate a variety of morphological parameters including areas, widths, lengths etc.

The procedure to obtain a binary image from an original image can be explained with **Figure 3.2. Figure 3.2a** represents an image acquired from a microscope. The light-coloured grains are pentlandite, the medium grey phase (left) is chalcopyrite and the slightly darker grey phase is pyrrhotite (right). Through tresholding, the pentlandite is detected on basis of grey-level scale **(Figure 3.2b). Figure 3.2c** is called the intensity/gray-level histogram, which plots the 256 possible gray-levels (y-axis) against the number of pixels in an image (x-axis). The white part represents the band width (bin) that contains all the grey-scale levels that correspond to the reflectivity of pentlandite. **Figure 3.2d** presents the binary image of pentlandite. The selected gray-scale interval of pentlandite now has a value = 1, and the background a value = 0.

According to Petruk (1982), the analysis of a sample may be precise, but the results may not be representative of the sample after it has been mounted and prepared as a polished (thin) section. This is because the

Figure 3.2: (a) Photomicrograph of pentlandite (light grey) in chalcopyrite (medium grey), pyrrhotite (dark grey) and silicate (black) (scale: 15 mm =115.5 μm). (b) The pentlandite is detected through thresholding. (c) A grey - level/intensity histogram. (d) The binary image of the pentlandite. (See text for description).

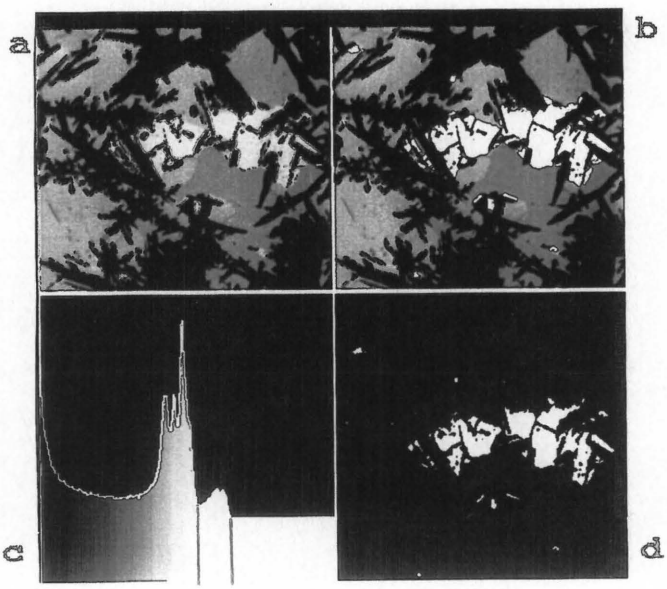

polished section exposes a slice through the middle of some grains and the edges of others **(Figure 3.3).** Grains that are cut through the edges appear smaller than what they actually are.

3.5.2 Present study

Image analysis on Uitkomst samples were done in two phases. In phase one the objective was to determine the grain size of the total sulphide fraction in the selected boreholes. Measurements were made on a binary image created from microphotographs, which were taken from polished sections. The following parameters were measured:

1. **Area:** The number of the pixels in the particle converted to the appropriate units of dimension.

2. **Minimum projection:** The minimum possible particle projection. This value is also determined through the use of the convex vertices. In this case, the shortest altitude of all triangles with a vertex on one side and base on the opposite side of the particle is found **(Figure 3.4).**

3. **Maximum projection:** The maximum possible projection. This value is determined by finding the vertices of the convex perimeter and then searching these vertices for the pair farthest apart **(Figure 3.5).**

4.**Mean projection:** This is the mean of all those distances considered in the determination of the maximum and minimum projections.

5.**Standard deviation projection:** The standard deviation projection considers only those distances used in the determination of the maximum and minimum projections.

6.**Width:** The particle projection perpendicular to the maximum projection. This distance may only vary from the minimum projection **(Figure 3.6).**

7.**Aspect ratio:** $= \frac{\text{Maximum projection}}{\text{Width}}$

Figure 3.3: Bias resulting from measurements that are not made on true section (Holmes effect). (a) Material in relief in polished section in reflected light as a result of differential polishing of the hard and soft components. (b) Thin section in transmitted light. (From Oosthuyzen, 1983).

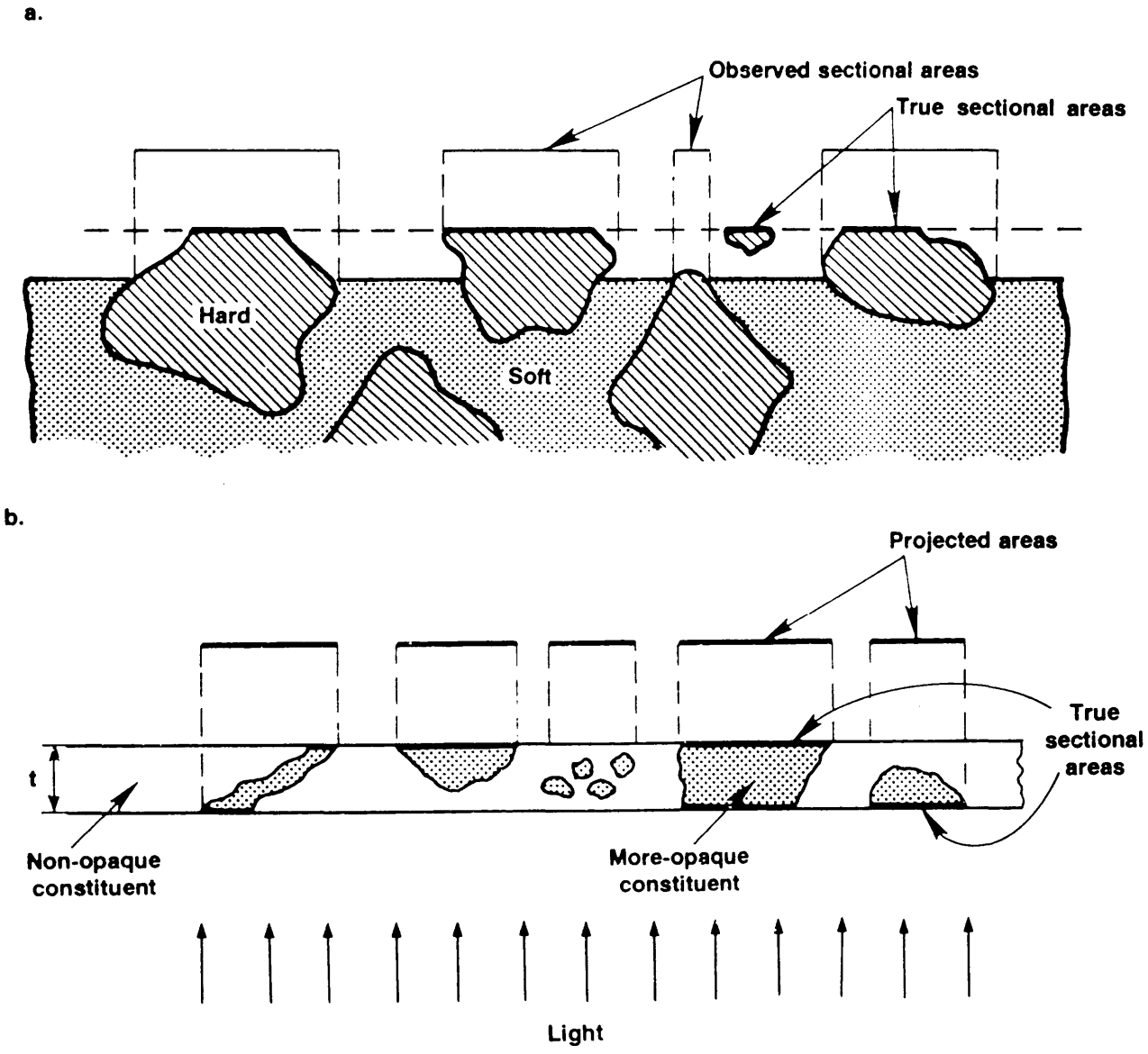

8.**Volume percentage sulphide:** The total area representing sulphide on a polished (thin) section expressed as a percentage of the total area of minerals.

The following boreholes were measured **(Figure 3.1):** UD 1, 2, 5, 13, 17, 21, 26, 26, 28, 32, 34, 35, 36, 45, 56, 59, 64, 83, 89, 93. A table for each borehole with mean values for each parameter measured, as well as a diagram with cumulative volume percentage sulphide plotted against grain size (mean projection) can be seen in Appendix D. The diagrams were plotted on a grain size sorted base.

In phase two of the study microscope images (x20, oil immersion) from polished sections were used directly to measure the ratio of granular:flame pentlandite, as well as the grain size of the flame pentlandite and the minimum grain sizes of the granular pentlandite. Using the total sulphide volume percentage as determined on the photomicrographs of the polished sections, the relative concentration of
flame and granular pentlandite in each polished section could be calculated.

Figure 3.4: Minimum projection.

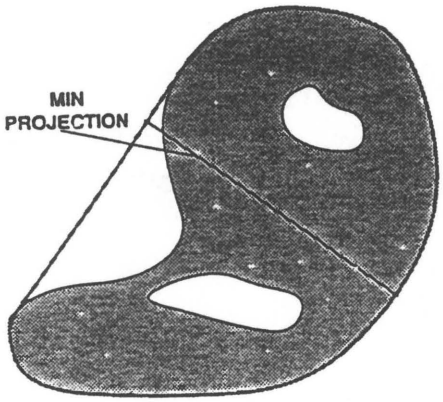

Figure 3.5: Maximum projection:

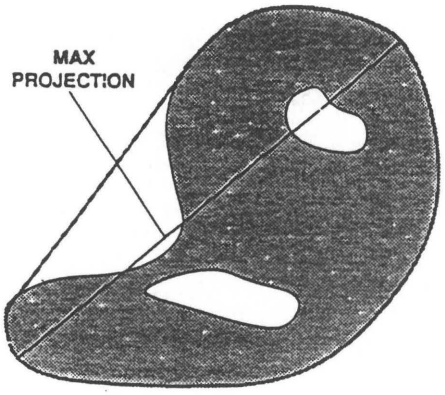

Figure 3.6: Width:

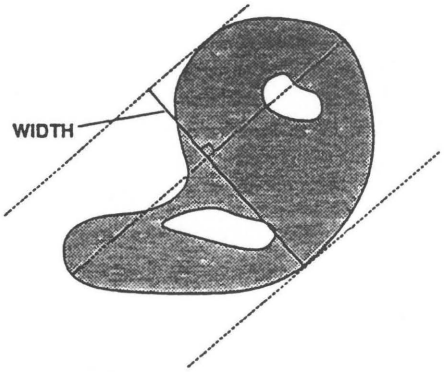

4.5.3 Problems related to image analysis in present study

* The camera field (the field seen on the screen of the image analyzer) with a x20 magnification, oil immersion lense is only 259 mm in width and constitutes about one fifth of the actual microscope field. Most of the chalcopyrite and granular pentlandite grains are bigger than 259 mm. To measure them will take a sequence of camera fields to put together the whole pentlandite or chalcopyrite grain. Because each frame measures its own statistics, these values for area and grain size have to be summed from

field to field. This is acceptable for area, but will result in statistically incorrect data for grain size. As a result it was only possible to determine a minimum grain size for granular pentlandite and chalcopyrite.

* The granular pentlandite occurs as blocky grains which have a rectilinear fracture pattern. The large, blocky pentlandite grains consist of a mosaic of tabular subgrains separated by thin veinlets of silicate material. As a result of this mosaic texture, the actual granular pentlandite grains measured are not those of the larger, composite grains, but the smaller mosaic subgrains (also described in Weiblen and Morey, 1976). According to Weiblen and Morey (1976) these subgrains are two orders of a magnitude smaller than other interstitial sulphides like pyrrhotite and chalcopyrite.

* Chalcopyrite, although easily distinguished from pyrrhotite is difficult for image analysis systems to separate from pyrrhotite because their reflectances, when averaged across the white light spectrum, are similar (Craig et al, 1981). On the x20 magnification lense it is difficult but possible. On the x3.2 magnification lense the system could not distinguish between pyrrhotite and chalcopyrite.

* It would have been advantageous to measure the chalcopyrite and granular pentlandite from the black and white photomicrographs of polished thin sections. However, chalcopyrite was difficult to distinguish from pyrrhotite on the photographs and the small difference in tone that could be noted on the photographs, was inadequate for image analysis. The type of mineralization (disseminated or net-textured) also played a role here. The smaller the grain size of the mineralization, the more difficult it became to distinguish between the different ore minerals.

* Another problem with the black and white photomicrographs was the uneven spread of the light source resulting in the one edge of the photo (furthest from the light source) being darker than the rest. When such an image is converted to a grey-scale image, it is difficult to set a threshold for pentlandite, because it overlaps with grey-scale values for pyrrhotite and chalcopyrite on one edge of the image. The same applies for the other minerals.

* When the data collected through image analysis are processed, each grain smaller than 4 pixels (equal to an area of 6204,4 mm2) are discarded since no other parameter besides area can be measured on it. However, experiments conducted during this study indicate that this procedure is considered not to affect the final results in any significant way (Appendix D, Tables 1, 2, 3).

4. RESULTS

4.1 Bulk rock variation of Cu, Co, Ni, Pd, Pt and S in the main lithological units

Assay values in weight percent for copper, nickel, cobalt, sulphur, platinum and palladium from six boreholes (UD 1, 5, 34, 45, 59 and 64) (Appendix E) were plotted to illustrate the variation of these elements with depth **(Figures 4.1, 4.2, 4.3, 4.4, 4.5 and 4.6).**

From these figures the following observations can be made about the bulk variation of Cu, Ni, Co, Pt, Pd and S in the different lithological units:

* The sulphide is more abundant in the lower lithological units **(Figures 4.1a, 4.2a and 4.4a)**
* A negative relationship exists between the Cu/Ni and Ni/S ratios **(Figures 4.1b, 4.2b).** The Cu/Ni ratio increases **(Figures 4.1b, 4.2b, 4.4b and 4.5b)** and Ni/S ratio decreases **(Figures 4.1b, 4.2b and 4.5b)** towards the base of the Complex
* The Pt/Pd ratio is apparently independent of the Cu/Ni and Ni/S ratios **(Figures 4.1b, 4.2b).**
* The sulphur decreases as the bottom contact is approached **(Figures 4.1a, 4.3a, 4.4a, 4.5a and 4.6a)**
* The occurrence of xenoliths have an influence on the amounts of Cu, Ni, Co and S present. The Cu values and Cu/Ni ratio tend to increase in the vicinity of a xenolith **(Figures 4.3, 4.4a, 4.5).** The Ni/S ratio seems to be low in the vicinity of a xenolith **(Figures 4.3b, 4.5b, 4.6b),** except for UD 45 **(Figure 4.4b)** where it has a high value at 69m were a xenolith is described. This high Ni/S ratio on 69m could be explained by the lower S value **(Figure 4.4a)** that occur at 69m.

The average Cu/(Cu+Ni) ratio **(Table 2)** is low (0.16) in the Main Harzburgite and increases with increasing depth to 0.44 in the Basal Gabbro. The Pt/(Pt+Pd) ratio, at about 0.31, appears to be constant throughout the Complex. When these values are compared with those from various localities in the Bushveld Complex **(Table 3)**(Von Gruenewaldt, 1979), the Pt/(Pt+Pd) values for Uitkomst correspond to that found on the

Figure 4.1a: Essay values from borehole UD 1 for Cu, Ni, Co and S (in wt %) plotted against depth (in m).

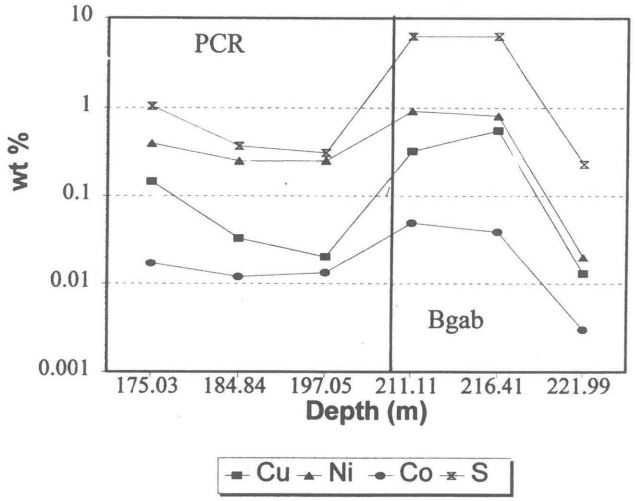

Figure 4.1b: The Ni/S, Cu/Ni and Pt/Pd weight ratio for UD 1.

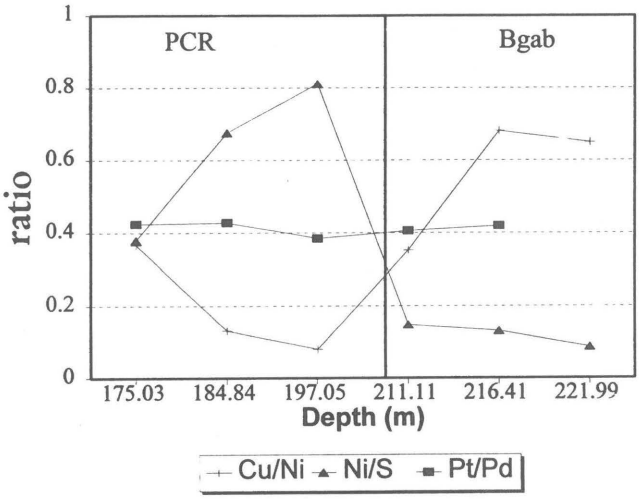

Figure 4.2a: Essay values from borehole UD 5 for Cu, Ni, Co and S (in wt %) plotted against depth (in m).

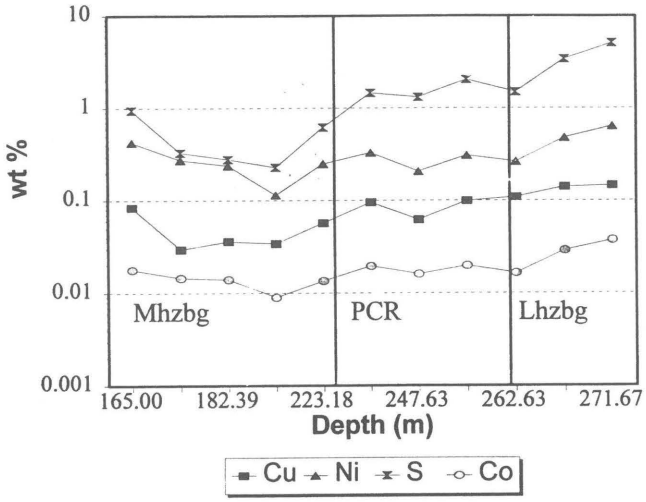

Figure 4.2b: The Ni/S, Cu/Ni and Pt/Pd weight ratio for UD 5 versus depth (in m).

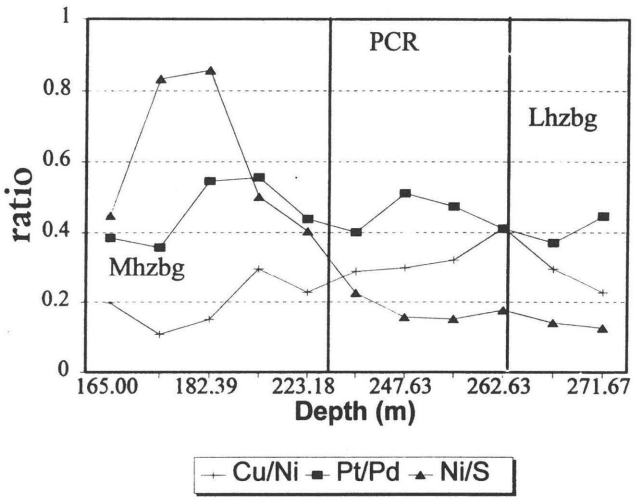

Figure 4.3a: Essay values from borehole UD 34 for Cu, Ni and S (in wt %) versus depth (in m).

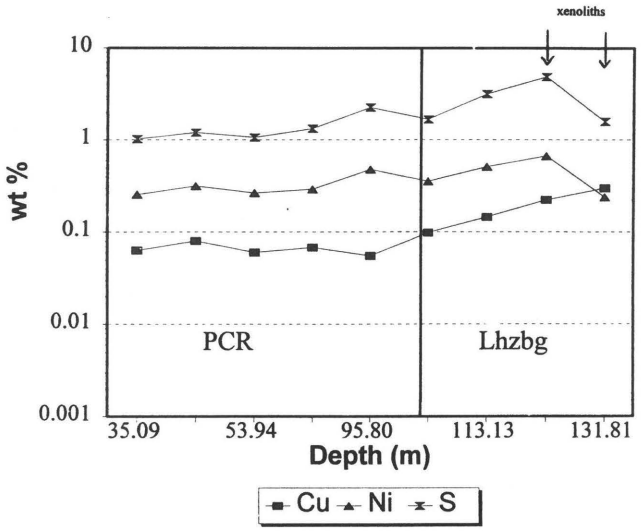

Figure 4.3b: The Ni/S, Cu/Ni and Pt/Pd weight ratio for UD 34 versus depth (in m).

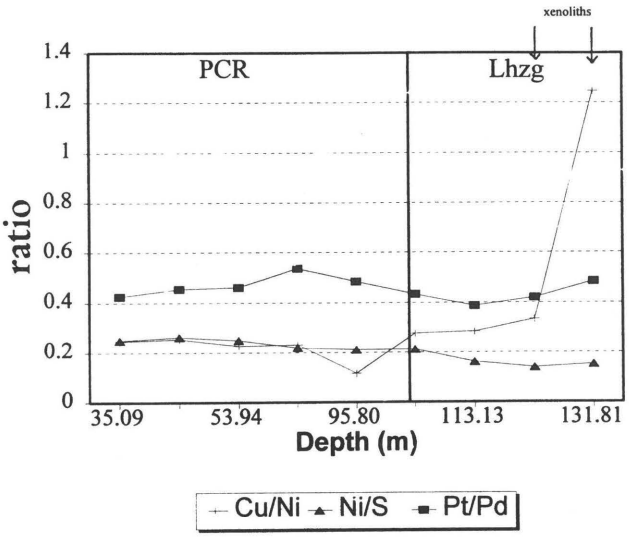

Figure 4.4a: Essay values from borehole UD 45 for Cu, Ni, Co and S (in wt %) versus depth (in m).

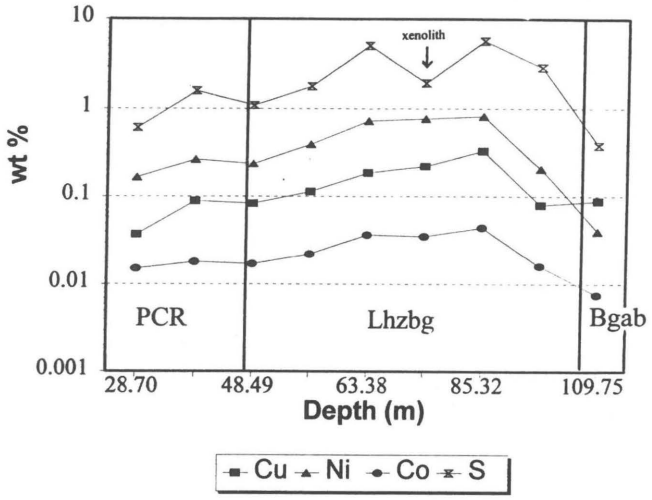

Figure 4.4b: The Ni/S, Cu/Ni and Pt/Pd weight ratio for UD 45 versus depth (in m).

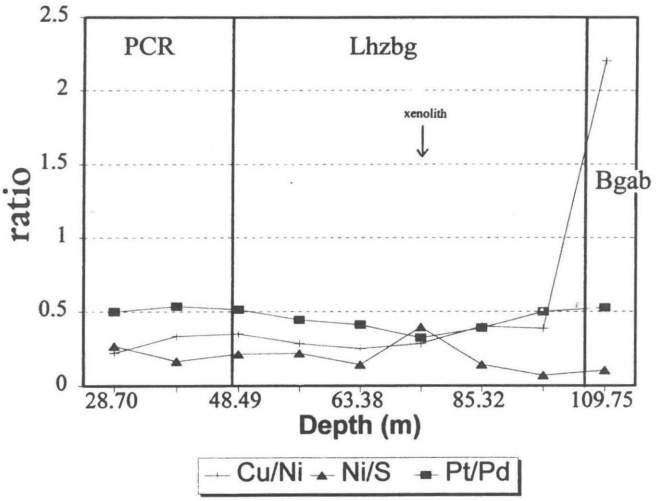

Figure 4.5a: Essay values from borehole UD 59 for Cu, Ni, Co and S (in wt %) versus depth (in m).

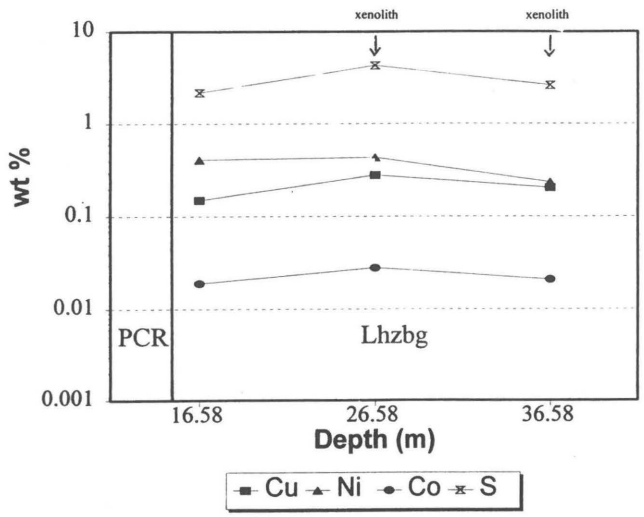

Figure 4.5b: The Ni/S, Cu/Ni and Pt/Pd weight ratio for UD 59 versus depth (in m).

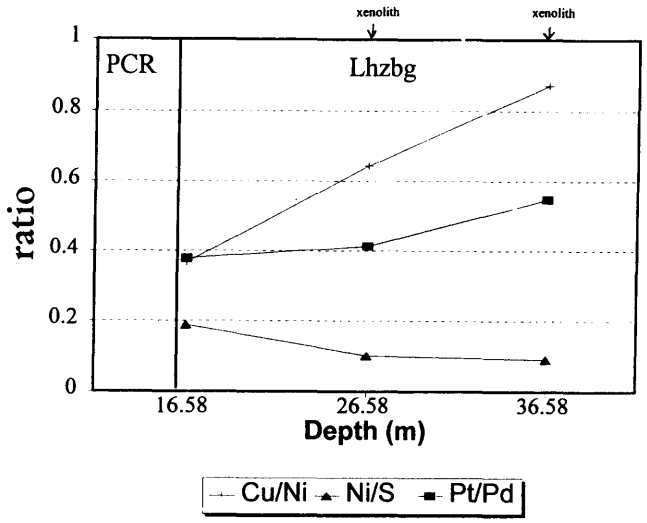

Figure 4.6a: Essay values from borehole UD 64 for Cu, Ni, Co and S (in wt %) versus depth (in m).

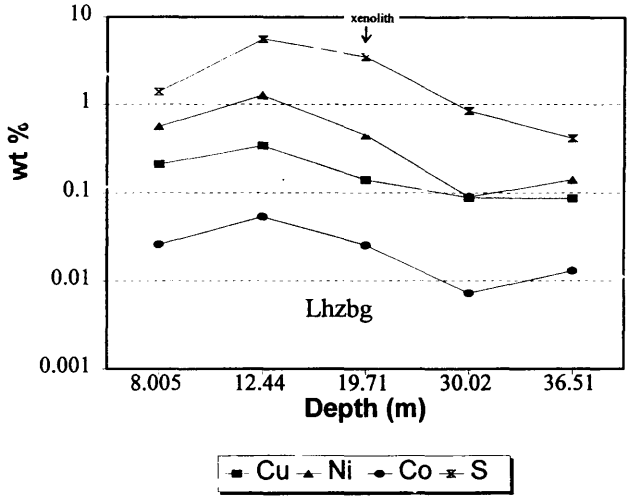

Figure 4.6b: The Ni/S, Cu/Ni and Pt/Pd weight ratio for UD 64 versus depth (in m).

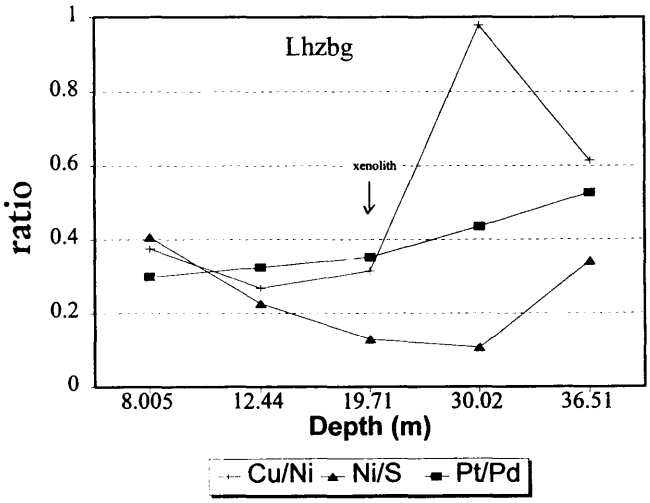

outer edges of the Vlakfontein nickel pipes. The Cu/(Cu+Ni) values for the Chromitiferous Harzburgite and Lower Harzburgite are roughly similar to those given for the UG2 chromitite layer, while values for the Basal Gabbro correspond to those for the Platreef.

Table 2: Average Cu/Cu+Ni and Pt/Pt+Pd assay values for the lithologies at Uitkomst.

		Cu/Cu+Ni		Pt/Pt+Pd	
	n	mean	s	mean	s
Mhzbg	5	0.16	0.05	0.31	0.04
PCR	13	0.19	0.06	0.32	0.02
Lhzbg	20	0.29	0.10	0.29	0.03
Bgab	4	0.44	0.18	0.31	0.03

s=sample standard deviation

Table 3: Cu/(Cu+Ni) and Pt/(Pt+Pd) ratios for various layers and pipes in the Bushveld Complex (after Von Gruenewaldt, 1979).

	Cu/(Cu+Ni)	Pt/(Pt+Pd)
upper zone, below main magnetite layer	0.82	
upper zone, below lower magnetite layer 2	0.86	0.45
Bethal area, top of mineralized zone	0.60	
Bethal area, bottom of mineralized zone	0.40	
Merensky reef, average	0.38	0.70
Pseudoreef		0.64
Platreef, average	0.44	0.48
UG 2 chromitite layer	(0.22)*	0.55
Vlakfontein nickel pipes, centre	0.07	0.50
Vlakfontein nickel pipes, edge	0.59	0.29
Onverwacht dunite pipe		0.99
Tweefontein (in floor-rocks)	0.65	

*includes Ni in chromite

4.2 Sulphide minerals

4.2.1 Systematic description

4.2.1.1 Pyrrhotite

Pyrrhotite is the principal sulphide mineral. It occurs interstitially to the primary silicate minerals as disseminated grains and coarser blebs and as net-textured segregations. Pyrrhotite forms a host to other sulfide minerals such as pentlandite, chalcopyrite, pyrite, cobaltite and platinum-group minerals.

Two varieties of pyrrhotite, bluish and pinkish in reflected light, were noted. The bluish phase tends to surround the pinkish phase or forms irregular tongues in the pinkish phase. Following Kelly and Vaughan (1983) the darker phase could consist of monoclinic pyrrhotite and the lighter phase of hexagonal pyrrhotite. Fine, roundish grains of pyrrhotite were noted in pyrite and anhedral grains in magnetite stringers. When secondary magnetite occurs, magnetite is usually intimately intergrown with the pyrrhotite as irregular rims on the edges of the pyrrhotite grains, or as anhedral, irregular grains enclosed in the pyrrhotite. In some sections serpentine, amphibole and talc are also very finely intergrown with the pyrrhotite, resulting in a pronounced reduction of the pyrrhotite grain size.

Microprobe analyses of pyrrhotite are listed in Appendix A. The bulk average composition of the pyrrhotite analyzed is given in **Table 4**. The iron content varies between 45.61 and 49.42 with an average of 46.85 atomic per cent. A maximum of 0.75 atomic per cent nickel is recorded.

Table 4: Average atomic percentage composition of the pyrrhotite at Uitkomst (n=90, s= standard deviation).

	Fe	Ni	Cu	Co	S
mean	46.85	0.29	0.04	0.04	52.78
s	1.11	0.19	0.08	0.03	0.99
min	45.61	0	0	0	50.58
max	49.42	0.75	0.33	0.08	53.70

4.2.1.2. Pentlandite

Pentlandite occurs throughout the Complex and is observed as two distinct textural varieties:

* as granular, polycrystalline aggregates associated with the pyrrhotite **(Plate 1 A)** or,
* as flame-like exsolutions in the pyrrhotite.

The granular pentlandite occurs on the grain boundaries of the pyrrhotite, along cracks or as worms or veinlets in the pyrrhotite. In places the granular pentlandite is so coarse-grained that the pyrrhotite forms islands in the pentlandite. Granular pentlandite is also present as discrete grains in the gangue.

The flame pentlandite is found along pyrrhotite grain boundaries, along and orientated perpendicular to cracks in the pyrrhotite, along crystal boundaries **(Plate 1 B),** on the boundaries between granular pentlandite and pyrrhotite, on the contact between pyrrhotite and chromite where the pyrrhotite is interstitial to the chromite, as well as on the contacts between pyrrhotite and secondary magnetite, or chalcopyrite. Pentlandite flames were also noted where chalcopyrite-cubanite intergrowth exists in the pyrrhotite.

Where the pentlandite is situated on the margins of the pyrrhotite, it is also affected by the needle-like intergrowth of the silicates. Here, the secondary magnetite forms irregular rims around the pentlandite and/or occurs as veins in the cracks existing in the granular pentlandite.

The pentlandite alters to violarite along cracks which gives the former a mottled appearance. In places the violarite has almost completely replaced the pentlandite so that only tiny islands of pentlandite can be distinguished in the violarite **(Plate 1 C).** Mackinawite seems to exsolve from the pentlandite along crystallographic planes **(Plate 1 D).**

The formation of granular and flame pentlandite was discussed by a number of authors e.g. Kelly and Vaughan (1983), Durazzo and Taylor (1982), Francis et al (1976), Misra and Fleet (1973), and Hawley and Haw

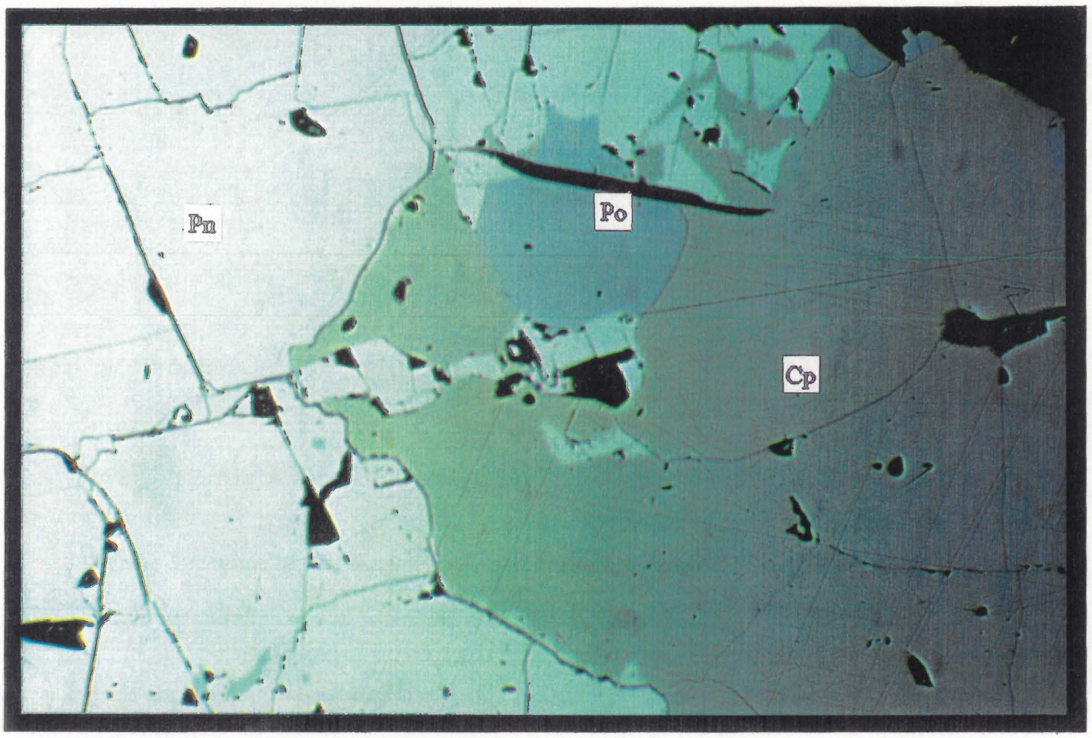

Plate 1 A : Granular pentlandite (pn) with characteristic octahedral cleavage and chalcopyrite (cp) with smaller islands of pyrrhotite (po). Sample 45/4, magnification x20, plane polarized light.

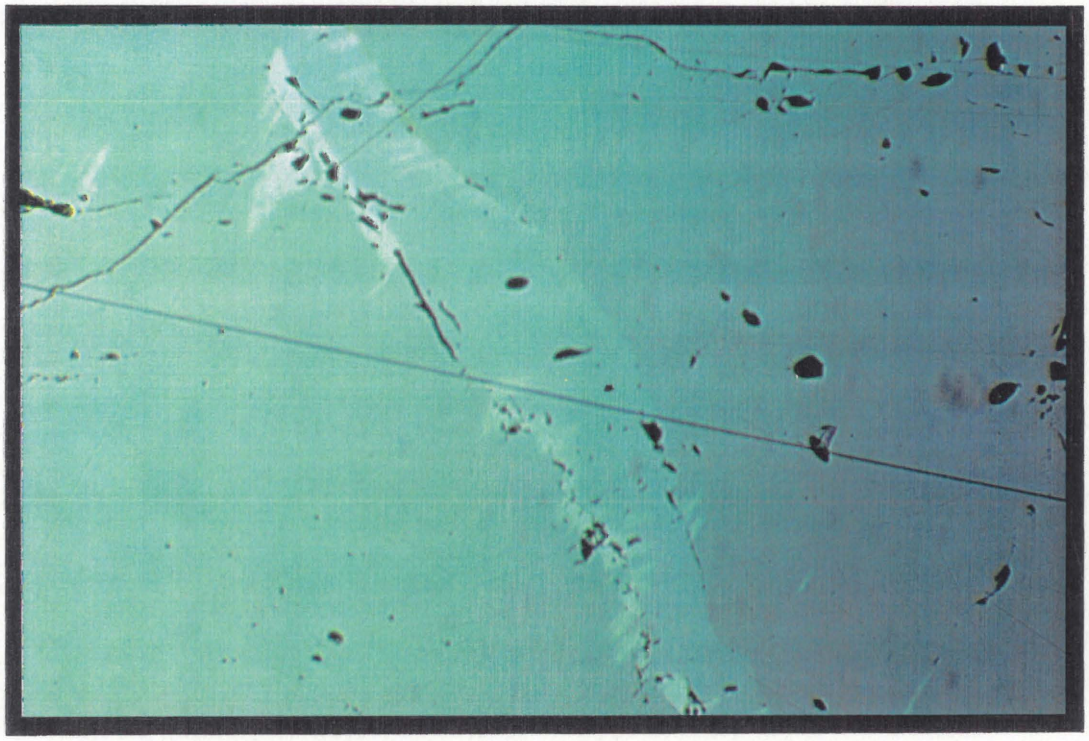

Plate 1 B : Flame pentlandite occurring on the grain boundaries, around cracks, around holes and in the lattice of pyrrhotite. Sample 45/4, magnification x20, plane polarized light.

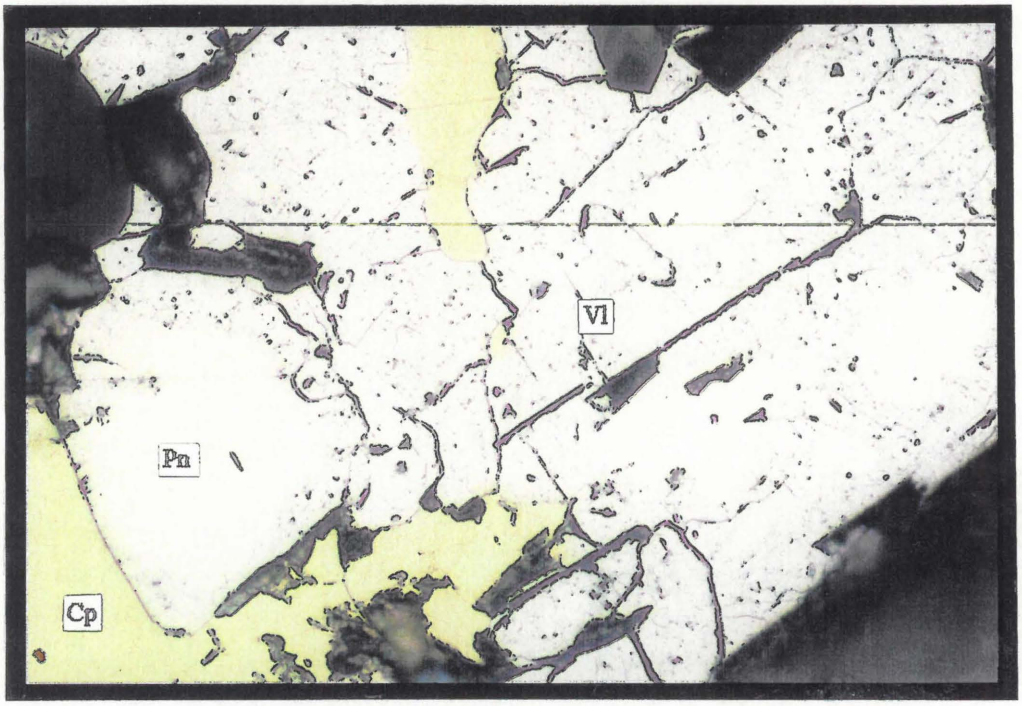

Plate 1 C : Pentlandite (pn) islands in violarite (vl) with surrounding chalcopyrite (cp). The violarite has almost totally replaced the granular pentlandite. Sample 59/1, magnification x50, plane polarized light.

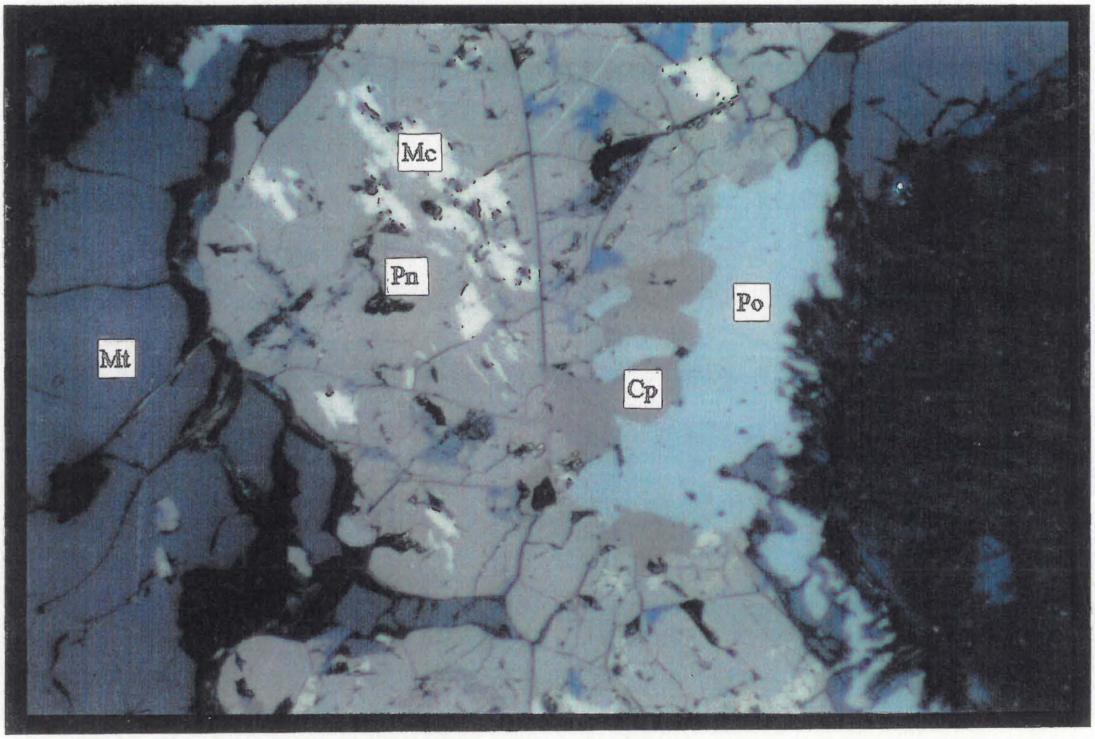

Plate 1 D : Granular pentlandite (pn) occurring with magnetite (mt) (left) and pyrrhotite (po) with chalcopyrite (cp) (right). Mackinawite (mc) flames (yellow-bluish gray anisotropism) occurs in the pentlandite. Sample 5/D, magnification x20, crossed polarizers.

(1957). Kelly and Vaughan (1983) describe the formation of granular and flame pentlandite as follows:

From 900 °C down to 270 °C the Fe-Ni-S system is dominated by a complete solid solution between $Fe_{1-x}S$ and $Ni_{1-x}S$ termed the monosulphide solid solution (Mss). Pentlandite becomes stable at approximately 610 °C. Kullerud (1963) gives a temperature of 613 °C. On cooling of the sulphide nickel ores below 600 °C, the originally homogeneous Mss will exsolve a more Ni-rich pentlandite, thus leaving the residual Mss matrix progressively more Fe- and S-rich until, eventually, it stabilizes as pyrrhotite. The composition of the Mss phase is very different from that of pentlandite, the former having the NiAs-type structure (Francis, 1974; Misra and Fleet, 1973) and the latter an unusual cubic structure with most of the metals in tetrahedral coordination (Rajamani and Prewitt, 1973; Vaughan
and Craig, 1978). Because of this, exsolution involves a nucleation event with the agglomeration and stabilization of small clusters of atoms with pentlandite structure occurring within the Mss matrix. Heterogeneous nucleation initially occurs at the grain boundaries leading to the development of rim pentlandite. With slow cooling these may develop into more granular pentlandite at triple junctions. In finer grained mosaics of Mss, smaller distances are involved so that complete segregation of interstitial pentlandite grains may occur. As cooling continues, volume diffusion of Fe, Ni, and S within Mss grains decreases exponentially (Condit et al, 1974; Klotsman et al, 1963). Therefore compositional changes required within the Mss matrix will become increasingly difficult, leading to further undercooling and departure from equilibrium. Heterogeneous nucleation of orientated pentlandite particles becomes possible leading to flame-like bladed particles at grain boundaries or as extensions to previously formed pentlandite rims. These will be orientated along planes of least mismatch, thereby reducing the strain energy involved in growth. The increased driving force for nucleation allows flames to form at less potent defects such as fractures. Further cooling will reduce the distances over which diffusion is effective. Ni left within the Mss, particularly within larger grains, may be removed by homogeneous nucleation of oriented lamellae which coarsen into flames. The greatest degree of lattice match occurs for the orientation (*111*) pentlandite to (*001*) Mss (Francis et al, 1976). The proportion of flame pentlandite found within pyrrhotite

grains markedly increases in grains equal to and bigger than 2000 mm in diameter.

From this explanation by Kelly and Vaughan (1983), it seems that at Uitkomst the granular pentlandite formed at the highest temperatures, followed by flame pentlandite situated at cracks, grain boundaries and extensions of granular pentlandite. Flames situated within the pyrrhotite crystal units resemble the lowest temperatures of formation.

Microprobe analyses (Appendix A) indicate that the iron, nickel, and cobalt content of the pentlandite vary throughout the Complex. Iron ranges from 23.40 to 28.85 with an average of 25.80 atomic per cent. Nickel varies from 23.08 to 27.43 with an average of 25.67 atomic per cent, while the cobalt shows a minimum of 0.30 and a maximum of 1.75 with an average of 0.97 atomic per cent. When the Ni-content of pentlandite from Uitkomst is compared with that of other occurrences **(Figure 4.7)** compiled by Misra and Fleet (1973), it is seen to overlap with the following assemblages: troilite + hexagonal pyrrhotite + pentlandite, hexagonal pyrrhotite + monoclinic pyrrhotite + pentlandite, and monoclinic pyrrhotite + pentlandite.

Figure 4.7: Compositions of natural pentlandites in nickel sulphide assemblages (after Misra and Fleet, 1973).
(tr=troilite, aw=awaruite, pn=pentlandite, hpo=hexagonal pyrrhotite, mpo=monoclinic pyrrhotite, py=pyrite, ml=millerite, vl=violarite, hz=haezelwoodite, gs=gersdorffite)

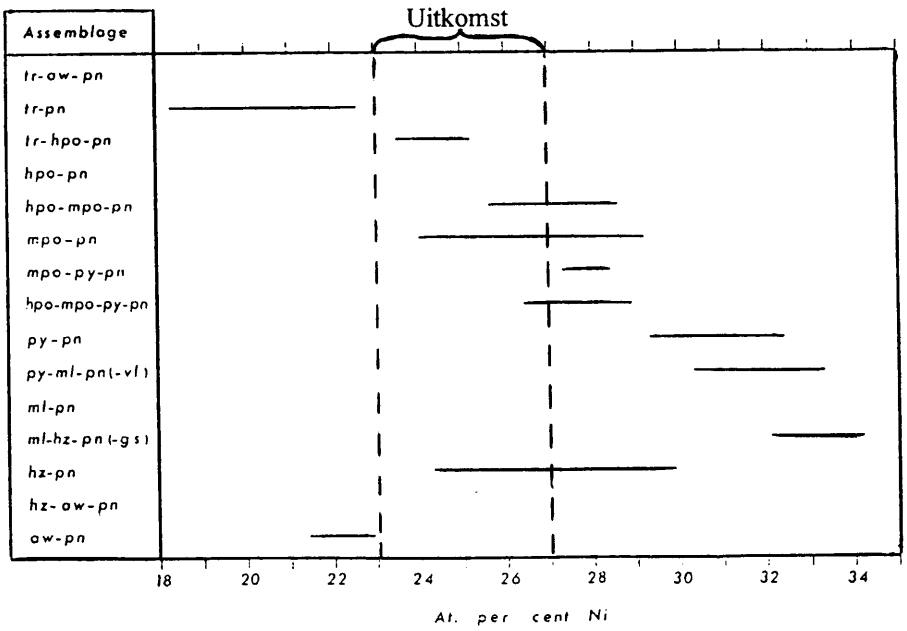

In **Table 5** the Uitkomst pentlandite, co-existing with pyrrhotite and pyrite (Appendix A), is compared with pentlandite in similar associations from different localities as compiled by Duke and Naldrett (1976). It seems that Uitkomst pentlandite shows a higher Fe-contents (~25 atomic per cent) and lower Ni-contents (~26.65 atomic per cent) relative to the other localities. The Co-contents are about the same. The bulk average composition of the pentlandite analyzed is given in **Table 6.**

Table 5: Summary of pentlandite compositions (after Duke and Naldrett, 1976).

Atomic percent	Fe	Ni	Co	S
Pentlandite co-existing with pyrite and pyrrhotite				
Harris & Nickel (1972)	**24.2**	**27.7**	**0.90**	**47.2**
6 samples	(0.9)	(0.7)	(0.83)	(0.6)
Misra & Fleet (1973)	**24.6**	**27.9**	**0.82**	**46.7**
15 samples	(0.50)	(0.8)	(0.62)	(0.4)
Ramsden (1975)	**24.2**	**28.1**	**0.50**	**47.2**
37 samples	(0.8)	(1.0)	(0.14)	(0.6)
Duke & Naldrett (1976)	**23.9**	**27.3**	**1.70**	**47.1**
3 samples	(0.4)	(0.5)	(0.40)	(0.2)
Pentlandite from Sudbury ores				
Hawley (1962)	**24.9**	**27.0**	**0.64**	**47.5**
12 samples	(0.8)	(0.5)	(0.03)	(1.3)

Numbers in parantheses are standard deviations

Table 6: Average atomic percentage composition of pentlandite at Uitkomst (n=132).

	Fe	Ni	Cu	Co	S
mean	25.80	25.67	0.02	0.97	47.54
s	1.53	1.36	0.02	0.31	0.70
min	23.40	23.08	0	0.30	46.74
max	28.85	27.43	0.09	1.75	49.97

s=sample standard deviation

According to Harris and Nickel (1972) a distinction can be made between pentlandite compositions in assemblages containing both hexagonal pyrrhotite and monoclinic pyrrhotite and those containing only

monoclinic pyrrhotite. The pentlandite in assemblages containing both hexagonal and monoclinic pyrrhotite shows atomic per cent Ni = 27.7. From this it could possibly be concluded that both hexagonal and monoclinic pyrrhotite occur with the pentlandite from Uitkomst.

From X-ray diffraction work done on the crystal structure of pyrrhotite (see section 4.5) it is evident that both monoclinic and hexagonal pyrrhotite exist at Uitkomst, with monoclinic pyrrhotite dominating over hexgonal pyrrhotite in these two-phase mixtures.

4.2.1.3. Chalcopyrite

Chalcopyrite is almost obiquitously present in the sulphide assemblages and occurs as anhedral aggregates or grains in pyrrhotite and granular pentlandite, as discrete grains in the silicate gangue, in pyrite usually accompanied by millerite, in places interstitial to chromite and in grains and stringers of magnetite. It is intergrown with cubanite in places and these intergrowths occur in pyrrhotite **(Plate 2 A).** Where the chalcopyrite was noted in pyrrhotite, it usually occurs along the pyrrhotite grain boundaries as if replacing the pyrrhotite from its margins inwards. In places islands of pyrrhotite occur in the chalcopyrite **(Plate 2 B).** Similar irregular islands of pyrrhotite in chalcopyrite were also described by Boucher (1975) and Bonnichsen (1972) who suggested that the chalcopyrite replaces the earlier pyrrhotite. The discrete chalcopyrite grains occurring in the silicate gangue varies extensively in grain size from very fine (< 10 micron) to blebs (> 100 micron). In places secondary magnetite rims the chalcopyrite. Pyrite, cobaltite, pentlandite, and worms of mackinawite were noted in chalcopyrite.

Microprobe analyses (Appendix A) shows that the chemistry of chalcopyrite is very consistent throughout the Complex with an average Fe, Cu, and S of respectively 25.24, 24.92, and 49.81 atomic per cent. The bulk average composition of the chalcopyrite analyzed is given in **Table 7.**

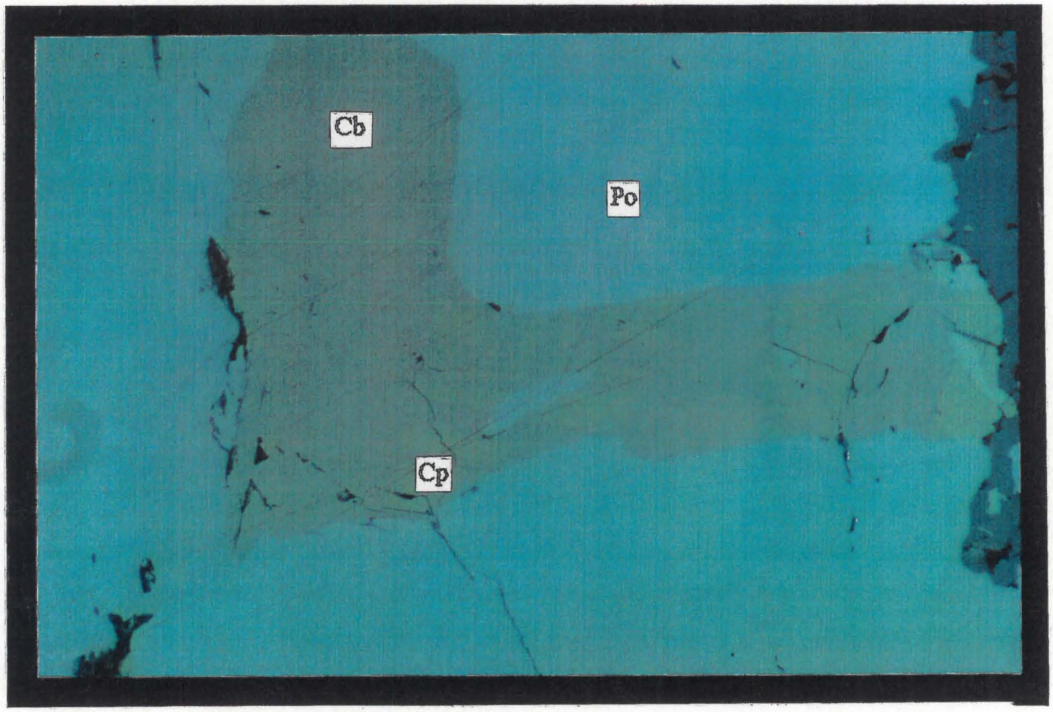

Plate 2 A : Cubanite (cb(with chalcopyrite (cp) exsolution occurring in pyrrhotite (po). Flame pentlandite exsolves in the cubanite- chalcopyrite grain. Sample 5/A, magnification x50, crossed polarizers.

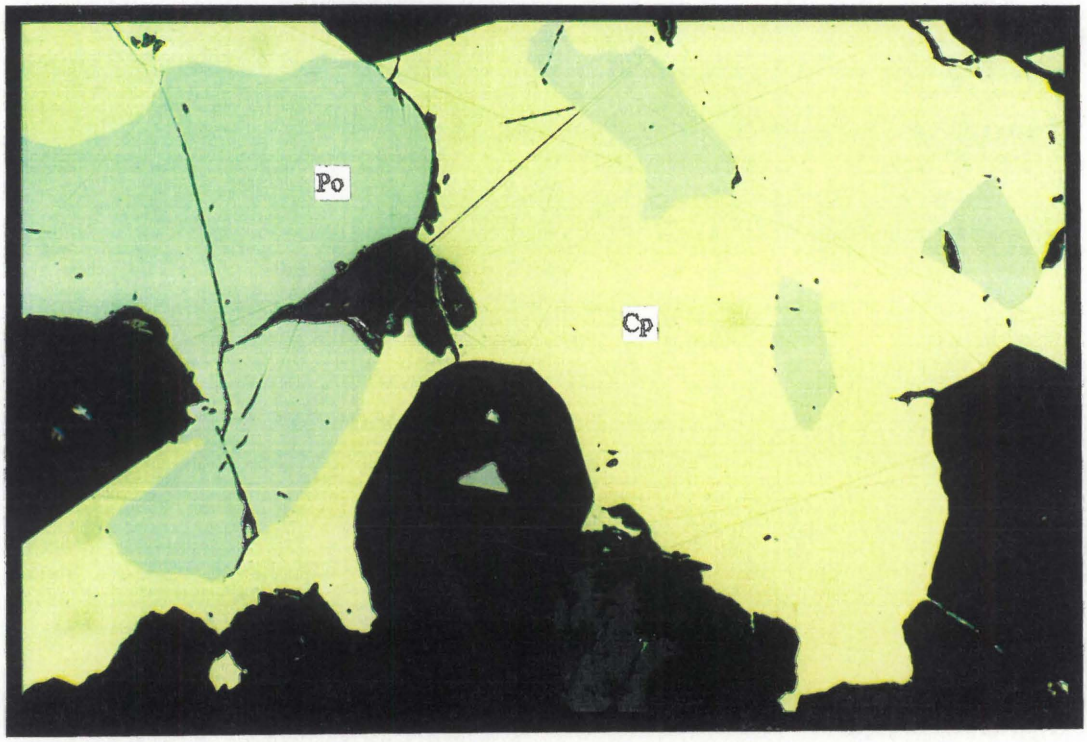

Plate 2 B : Islands of pyrrhotite (po) occurring in chalcopyrite (cp). Sample 1/9 a, magnification x20, plane polarized light.

Table 7: Average atomic percentage composition of the chalcopyrite at Uitkomst (n=94).

	Fe	Ni	Cu	Co	S
mean	25.24	0.01	24.92	0.02	49.81
s	0.14	0.01	0.35	0.01	0.35
min	24.95	0	24.08	0	49.33
max	25.53	0.04	25.35	0.03	50.57

(s= standard deviation)

4.2.1.4. Pyrite

Subhedral to anhedral, spongy-looking pyrite occurs in pyrrhotite **(Plates 2C and D)** and chalcopyrite, as dicrete grains disseminated in the silicate gangue, as well as interstitial to chromite and then associated with millerite and chalcopyrite. Pyrite encloses pyrrhotite with pentlandite exsolutions, chalcopyrite, magnetite, millerite, and one occurrence of galena.

Based on 34 microprobe analyses (Appendix A) average pyrite shows Fe = 32.8 and S = 66.62 atomic per cent. The nickel and copper contents show maxima of 0.70 and 0.43 atomic per cent, respectively. The cobalt content of the pyrite ranges between 0.15 and 1.08 atomic per cent. According to Cambel and Jarkovsky (1968) when pyrite and pyrrhotite from the same sample are considered, due to metamorphic recrystallization, Ni is concentrated in the pyrrhotite and Co in the pyrite. Thus, highly metamorphic pyrite shows increased Co-contents in comparison with that in pyrrhotite and pyrrhotite shows increased Ni-contents compared to that in pyrite. Microprobe analyses of three samples (UD 1/3, 59/4, and 1/9 in Appendix B) with co-existing pyrite and pyrrhotite support this notion except that the Ni-content in the pyrite from UD 1/3 is higher than that in the pyrrhotite. The bulk average composition of the pyrite analyzed is given in **Table 8.**

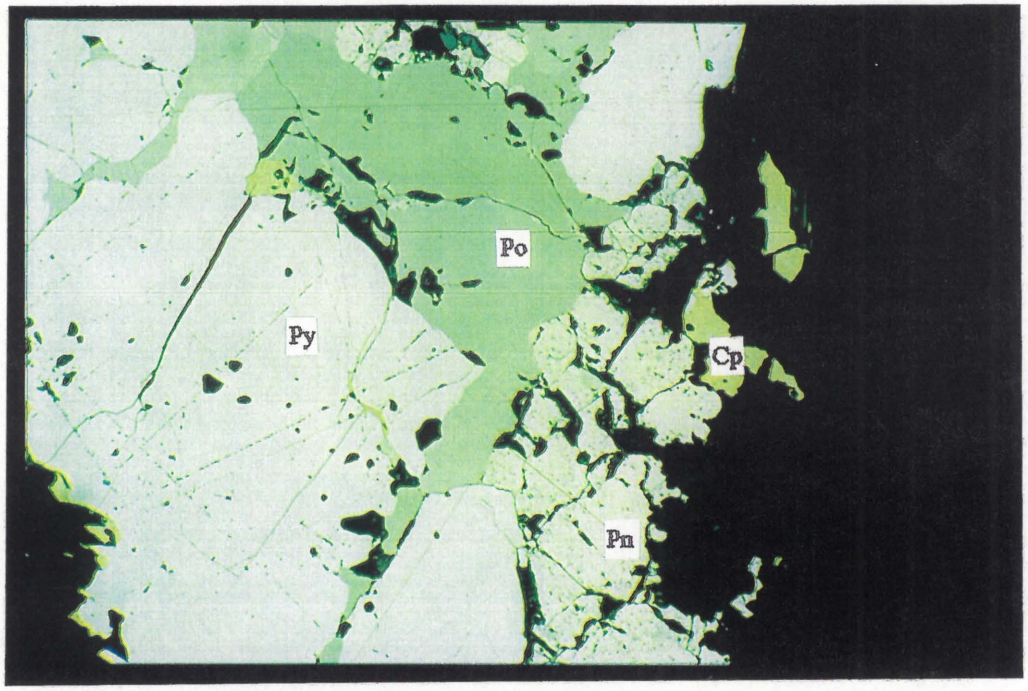

Plate 2 C : Subhedral, spongy pyrite (py) (left) and mottled pentlandite (pn) (right) in pyrrhotite (po). Chalcopyrite (cp) occurs in the pyrrhotite next to the pyrite and as discrete grains in the gangue. Sample 59/9, magnification x20, plane polarized light.

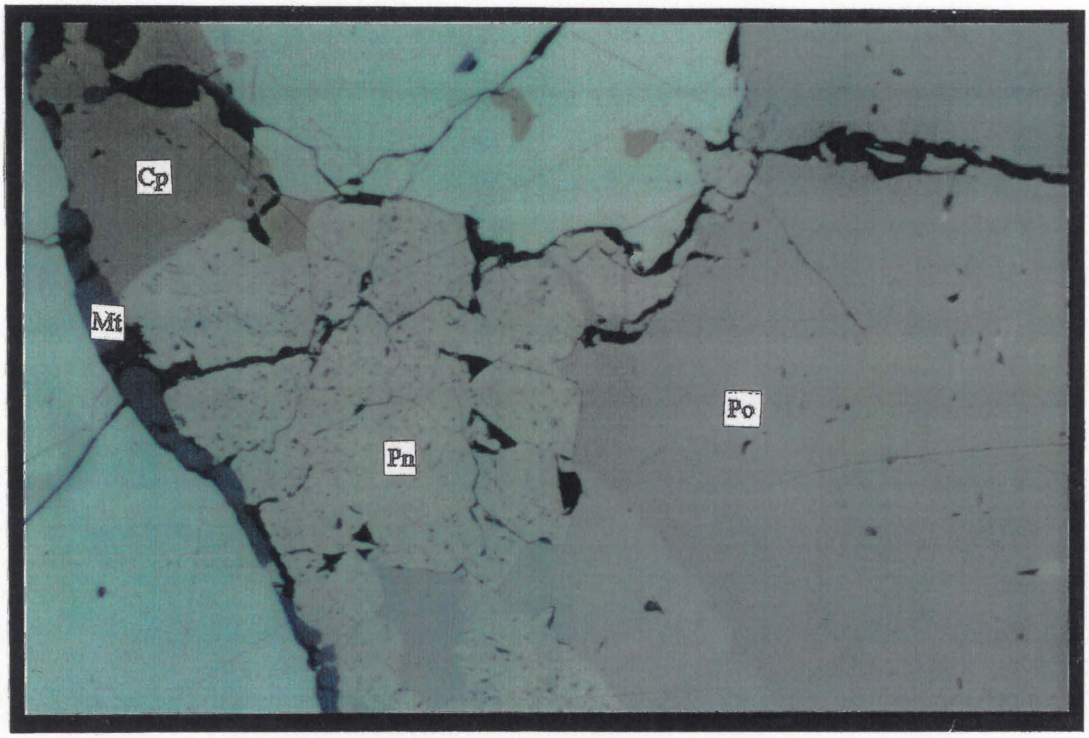

Plate 2 D : Pyrite (py), chalcopyrite (cp), pentlandite (pn) and magnetite (mt) occurring in pyrrhotite (po). The pentlandite has a mottled appearance which is caused by violarite replacing the pentlandite. Sample 59/9, magnification x20, plane polarized light.

Table 8: Average atomic percentage composition of pyrite at Uitkomst (n=34).

	Fe	Ni	Cu	Co	S
mean	32.58	0.18	0.12	0.48	66.62
s	0.30	0.34	0.21	0.41	0.38
min	32.29	0	0	0.15	66.10
max	32.99	0.70	0.43	1.08	66.96

(s= standard deviation)

4.2.1.5. Cubanite

Cubanite was only noted in three samples, all of which come from the Main Harzburgite zone. It is difficult to distinguish optically from pyrrhotite. In polished sections it appears to have a greenish tint relative to pyrrhotite **(Plate 3 A)**. It usually occurs as chalcopyrite-cubanite exsolutions in pyrrhotite. According to Ramdohr (1981) cubanite exsolutions in chalcopyrite indicate a minimum temperature of formation at approximately 250 °C. A few microprobe analyses are listed in Appendix A.

4.2.1.6. Cobaltite

Euhedral, bluish-white grains of cobaltite occur as discrete grains in the gangue but also in pyrrhotite, where it cuts across the grain boundaries of pyrrhotite and pentlandite **(Plate 3 B)**. This indicates that the cobaltite formed later than the pyrrhotite and pentlandite. Pyrrhotite, pentlandite, and chalcopyrite inclusions were noted in the cobaltite. In one sample (UD 45/3, located in the Lower Harzburgite) anhedral bluish-white to pinkish grains of cobaltite occur within the pyrrhotite. This cobaltite hosts an unidentified whitish-yellow mineral which, by qualitative microprobe analyses, proves to consist of Pd, Te, and Bi.

Microprobe analyses of the euhedral cobaltite are listed in Appendix A.

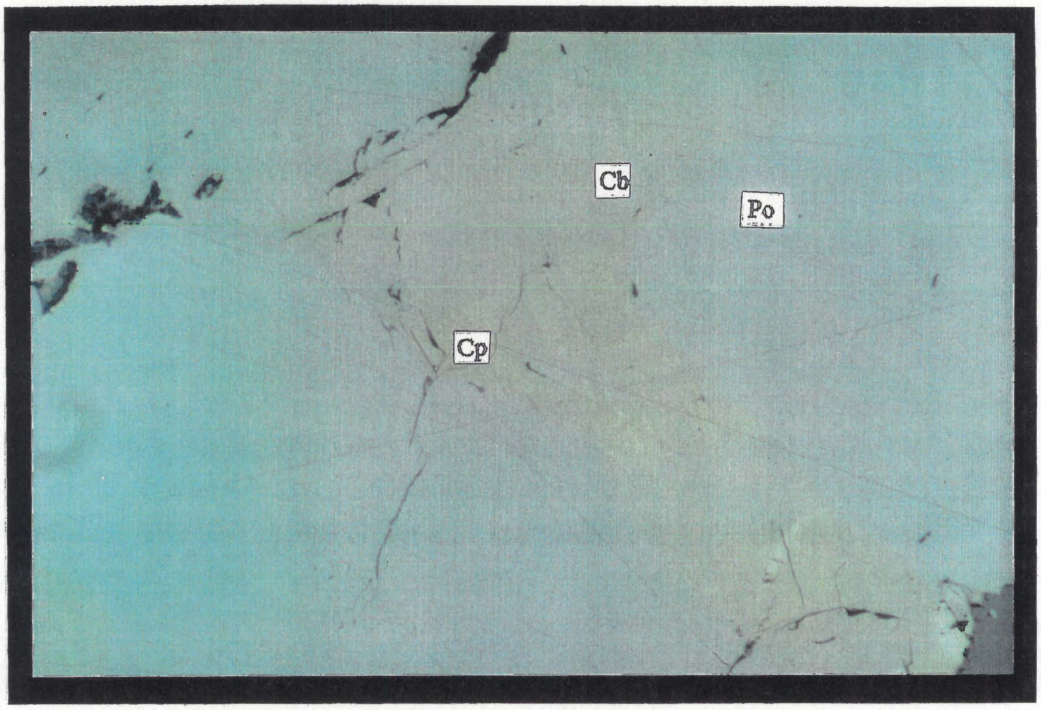

Plate 3 A : Cubanite (cb) and chalcopyrite (cp) exsolution in pyrrhotite (po). Sample 5/A, magnification x50, plane polarized light.

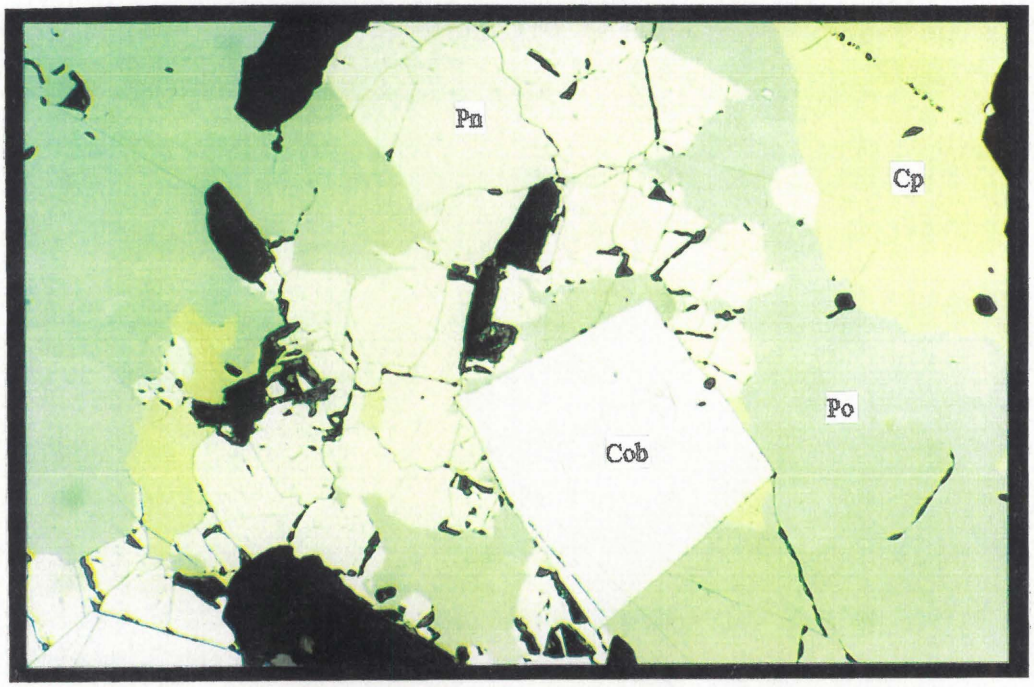

Plate 3 B : Granular pentlandite (pn) and chalcopyrite (cp) occurring in pyrrhotite (po). Euhedral bluish- white cobaltite (cob) seems to cut over the existing sulfides, thereby indicating its secondary nature. Sample 1/9 a, magnification x20, plane polarized light.

4.2.1.7. Mackinawite

Mackinawite forms exsolutions in granular pentlandite and shows characteristic strong pleochroism of light yellow to brownish pink and anisotropism from blue-grey to yellow **(Plate 1 D).** It was also noted as inclusions in pyrrhotite and chalcopyrite. In one sample (UD 5/5), located in the Chromitiferous Harzburgite, worm-like mackinawite was observed in chalcopyrite. Mackinawite was found in the Main Harzburgite, Chromitiferous Harzburgite, and Lower Harzburgite.

4.2.1.8. Millerite

Bright yellow millerite, with strong anisotropism from yellow to light blue **(Plate 3 C),** was only observed in assemblages consisting of chromite, pyrite, chalcopyrite, pyrrhotite, and millerite. In such samples the primary silicates are completely replaced by secondary amphibole, serpentine, phlogopite, talc, chlorite, and carbonate. The millerite forms anhedral, worm-like aggregates in the pyrite and exhibits uneven extinction. Small grains of chalcopyrite occur in the millerite. Temperatures below 200 °C are suggested by the presence of pyrite and millerite (Craig, 1973). Groves et al (1974) described a pyrite + millerite + chalcopyrite assemblage in talc-carbonate rocks.

Microprobe analyses of millerite are listed in Appendix A.

4.2.1.9. Violarite

Violarite, creamy bluish in colour, occurs along cracks in the granular pentlandite. In places entire pentlandite grains have been replaced by violarite. Flame pentlandite, especially that occurring on grain boundaries or along cracks in the pyrrhotite, was also noted to be replaced by violarite. Flame pentlandite situated along crystallographic planes in the pyrrhotite seems to be unaffected. This, and the fact that the violarite occurs along cracks in the granular pentlandite, seem to emphasize accessibility by the circulating fluids. Unaffected flames were not accessable to fluids. Where the pentlandite is replaced by violarite, it commonly has a mottled appearance **(Plate 2 D).** According to Harris and Nickel (1972), violarite appears to be almost always

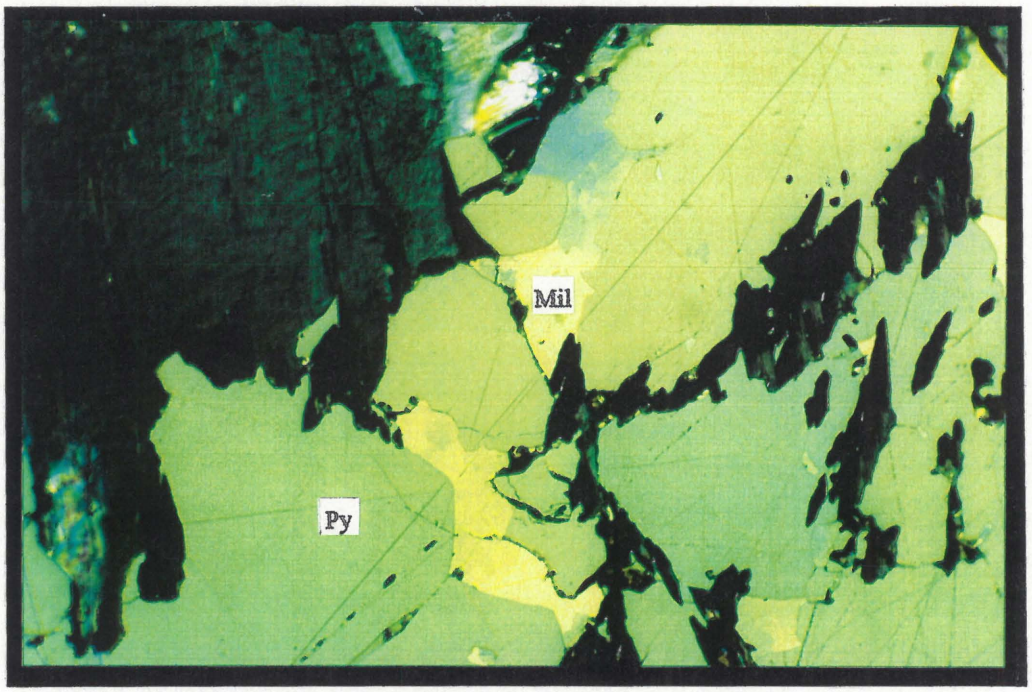

Plate 3 C : Anhedral aggregates of millerite (mil) (blue- yellow anisotropism) occurring in pyrite (py). Sample 34/A, magnification x20, crossed polarizers.

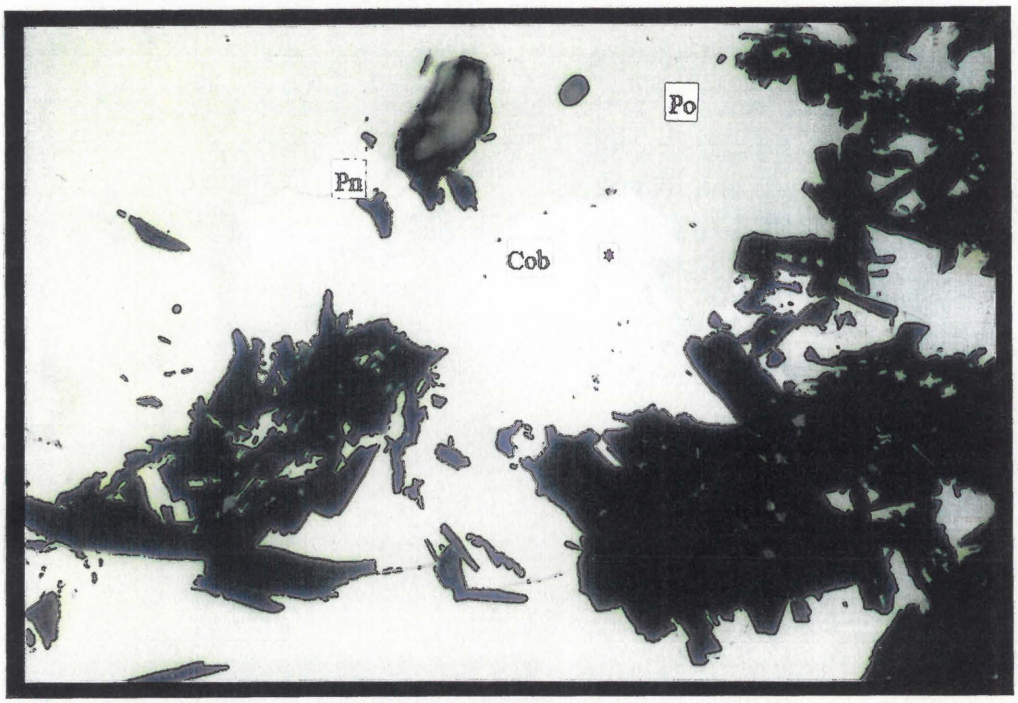

Plate 3 D : White- pinkish cobaltite (cob) occurring in pyrrhotite (po). Very small yellowish- white grains (*) in the cobaltite consisting of Pd, Bi and Te. The cobaltite is bluish in places. Granular pentlandite (pn) (above, left) appears more orangy than the usual light yellow. Sample 45/3, magnification x50, plane polarized light.

secondary and the texture seen at Uitkomst of violarite after pentlandite supports this notion.

4.2.1.10. Galena, sphalerite, and graphite

One small grain of bluish galena was observed in pyrite in a chromite-pyrite-chalcopyrite-pyrrhotite-millerite assemblage located in the Chromitiferous Harzburgite.

Two occurrences of small grains of sphalerite in pyrrhotite from the Lower Harzburgite were noted.

One occurrence of brown-grey graphite with a strong yellow to charcoal anisotropism was noted occuring in pyrrhotite next to magnetite, as well as along cracks in the pyrrhotite.

4.2.1.11 Platinum - group minerals

Although the detection and descripion of the platinum-group minerals fell outside the scope of this study, a limited number of these minerals **(Table 9)** have been observed and qualitatively analyzed.

Table 9: Platinum-group minerals observed at Uitkomst.

Mineral:	Colour:	Composition:	Association:
1.	yellow-white **(Plate 3D)**	Pd, Bi, Te	cobaltite and pyrrhotite
2.	light blue	Pb, Te, Fe	pyrrhotite
3.	two-phase grain (creamy brown and yellow)		pyrrhotite

According to Swash et al, 1991, the main platinum-group minerals found at Uitkomst are kotulskite [Pd(Te,Bi)], merenskyite [(Pt,Pd)$(Te,Bi)_2$], stibiopalladinite [$(Pd,Cu)_5Sb_2$] and sperrylite ($PtAs_2$).

Te and Bi concentrations in base metal sulfides play an important roll in controlling the extent of the exsolution process and, therefore, the amount of Platinum Group Elements remaining in solid solution (Pactunc et al, 1990). Vermaak and Hendriks (1976) and Genkin and Evstigneeva (1986) proposed that PGE tellurides, bismutho-tellurides and arsenides are later than PGE sulfides and alloys in the sequence of crystallization.

4.2.2 Distribution of the sulphide minerals in relation to the lithological units

From the microscopic investigation it is evident that six sulphide assemblages exist at Uitkomst. The primary assemblage consists of pyrrhotite, pentlandite and chalcopyrite. Cubanite, mackinawite, pyrite, millerite, violarite and cobaltite occur with the primary assemblage at certain depths in the Complex **(Table 10).** The assemblages are:

1) po + pn + cp
2) po + pn + cp + cb (Mhzbg)
3) po + pn + cp + mc (Mhzbg and PCR)
4) po + pn + cp + py (Lhzbg, PCR and Bgab)
5) py + cp + ml + po (Lhzbg and PCR)
6) po + pn + cp + cob + vl (Lhzbg and PCR)

The ocurrence of these assemblages are listed in **Table 10.**

Table 10: Sulphide assemblages of the Uitkomst Complex.

	Po	Pn	Cp	Py	Ml	Cob	Vl	Mc	Cb
Mhzbg	*	*	*					*	*
PCR	*	*	*	*	*	*	*	*	
Lhzbg	*	*	*	*	*	*	*		
Bgab	*	*	*	*	*	*			

According to Craig and Kullerud (1969) the following three assemblages are the result of low temperature reactions within most massive Ni-Cu ores:

* Chalcopyrite + pyrite + monoclinic pyrrhotite + pentlandite
* Chalcopyrite + monoclinic pyrrhotite + hexagonal pyrrhotite + pentlandite
* Chalcopyrite + cubanite + hexagonal pyrrhotite + pentlandite

4.2.3 Chemical variation of the sulphide minerals in relation to the lithological units

With one exception (UD 5/7, Chromitiferous Harzburgite) the Fe/S ratio of the pyrrhotite **(Figure 4.8)** shows a variation from 0.85 to 0.90 in the mineralized zone. The mineral assemblage of the anomalous sample consists of pyrrhotite + pentlandite + chalcopyrite + mackinawite + PbTe. In the Main Harzburgite, however, the Fe/S is higher and varies from 0.91 to 0.975. These samples have mineral assemblages consisting of pyrrhotite + pentlandite + chalcopyrite + mackinawite + cubanite.

Figure 4.8: Fe/S atomic ratio of pyrrhotite versus elevation above base (depth). The crosses represent all the points analyzed in a section, while the triangles represent the average values for each section.

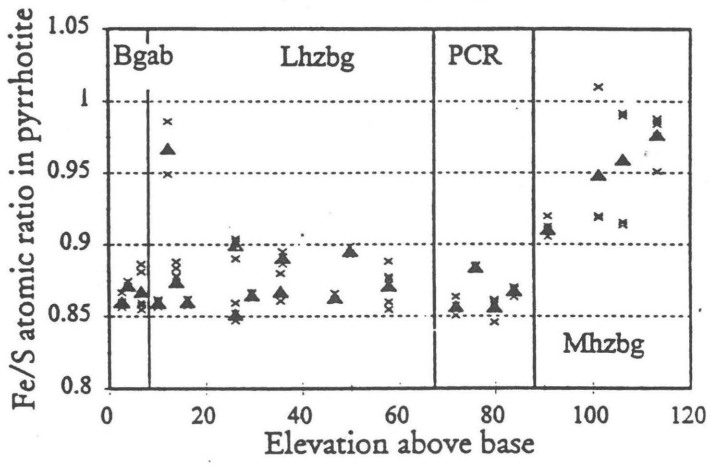

The Ni in pyrrhotite **(Figure 4.9)** varies between 0 to 0.85 atomic per cent, but is generally lower in the Main Harzburgite than in the mineralized zone.

Figure 4.9: Ni-content (atomic per cent) of pyrrhotite (symbols as for Figure 4.8).

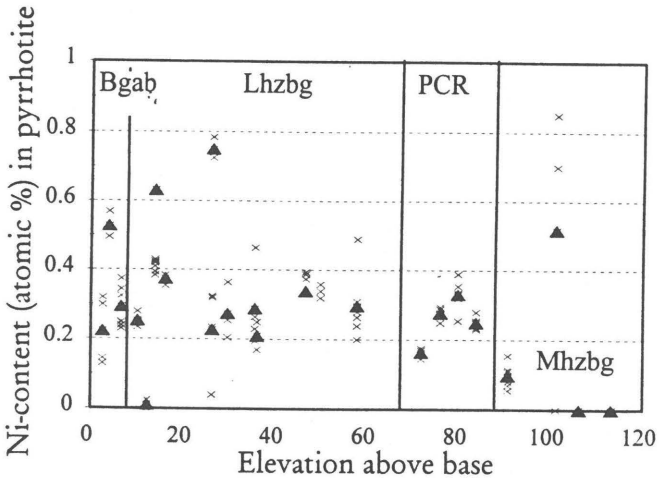

The Fe/Ni ratio of the pentlandite **(Figure 4.10)** scatters between 0.85 and 1.1 , and roughly follows the Fe/S ratio for pyrrhotite **(Figure 4.8)**. The Main Harzburgite exhibits an overall higher ratio of 1.1 to 1.24. These higher ratios of Fe/Ni in the Main Harzburgite as well as for the one sample (UD 5/7) could be attributed to the existence of mackinawite in the mineral assemblage. The Ni-content of the pentlandite, which have a direct influence on the Ni/Fe ratio, seems to be lower where mackinawite exists in the assemblage. Mackinawite was noted in the Main Harzburgite as well as in the one sample from the Chromitiferous Harzburgite (mineral map in Appendix C). This corresponds with what has been said by Graterol and Naldrett (1971), Harris and Nickel (1972), Misra and Fleet (1973b), and Craig (1973) about the composition of natural pentlandite being intimately related to the sulphide assemblage in which it occurs.

Figure 4.10: Fe/Ni atomic ratio in pentlandite versus elevation above base (symbols as for Figure 4.8).

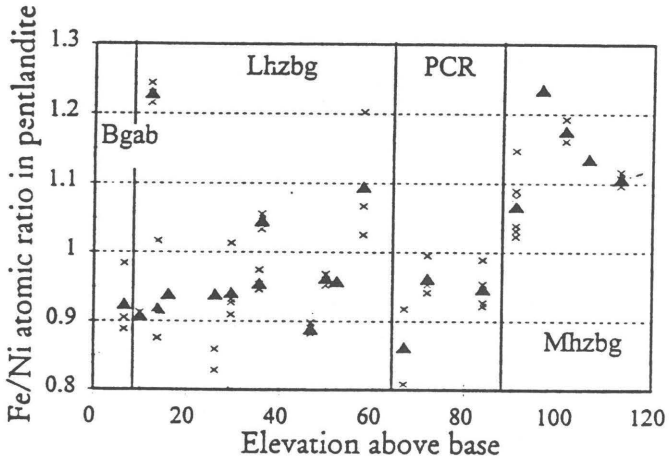

The Ni/Co atomic ratio of pentlandite **(Figure 4.11)** ranges between 15 and 45 throughout the Complex, except for one outlier (UD 5/1, Chromitiferous Harzburgite) with a Ni/Co ratio of 90 and a mineral assemblage consisting of pyrrhotite + pentlandite + chalcopyrite + cobaltite. This sample shows a low 0.30 atomic per cent Co for pentlandite which could perhaps be ascribed to the presence of cobaltite in the assemblage.

Figure 4.11: Ni/Co atomic ratio in pentlandite versus elevation above base (symbols as for Figure 4.8).

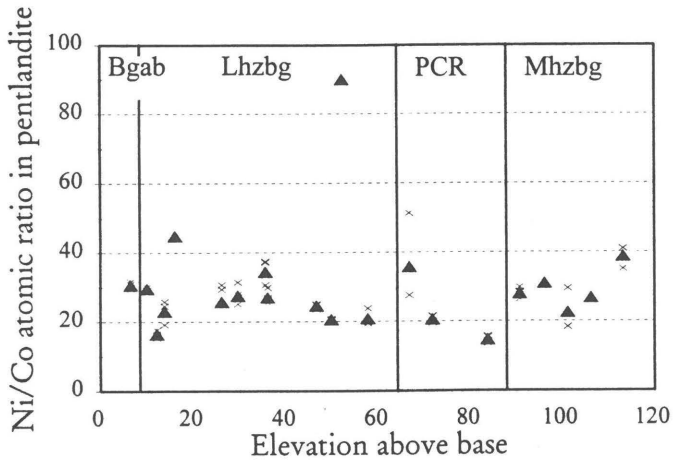

Plotting the Ni-contents of pyrrhotite and pentlandite against each other **(Figure 4.12)**, shows an approximate positive linear relationship.

Figure 4.12: Ni-content in pyrrhotite versus Ni-content in pentlandite (atomic per cent) (symbols as for Figure 4.8).

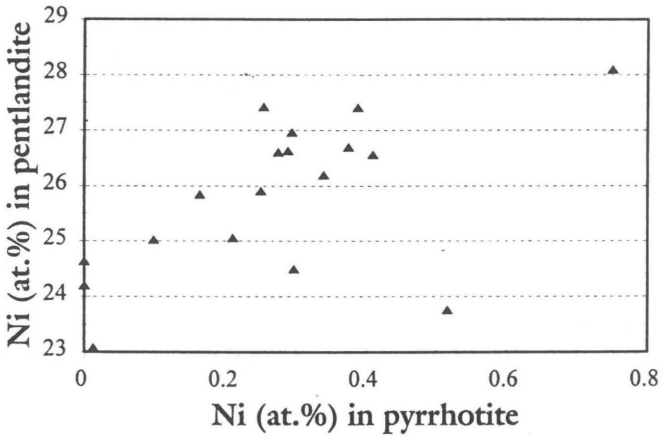

Based on the few analyses of pyrite (Appendix A), the Fe/S ratio **(Figure 4.13)** of the pyrite seems to decrease towards the base of the Complex.

Figure 4.13: Fe/S atomic ratio of pyrite versus elevation above base (symbols as for Figure 4.8).

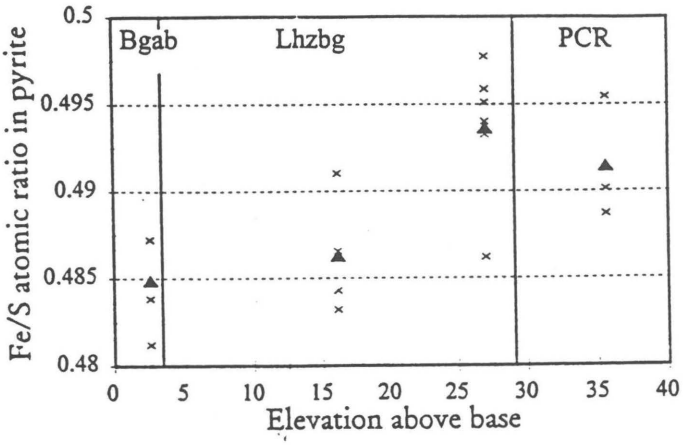

4.2.4 Crystal structure of pyrrhotite

Arnold and Reichen (1962) proposed that the relationship between composition and the d-spacing of the (*1012*) reflection (d_{102}) of pyrrhotite can be used to estimate the metal content of natural, hexagonal pyrrhotite provided that the concentrations of impurities in solid solution are low. This they demonstrated by the good correlation between d_{102} and the metal content of synthetic, hexagonal pyrrhotite as well as for 14 chemically analyzed natural pyrrhotites.

Arnold (1966) re-examined 11 of these same natural pyrrhotites that were previously thought to be hexagonal pyrrhotite, and revealed that 2 are hexagonal, 8 are mixtures of hexagonal and monoclinic types and 1 is monoclinic. **Table 11** summarizes the compositions, d-values and structural types of the 11 re-examined pyrrhotites.

Table 11: A summary of the compositions, d-values, and structural types of the 11 re-examined pyrrhotites after Arnold (1966).

Samples	**Arnold and Reichen (1962)**		**New data**	
	Atomic % metals	**d_{102} (Ä)**	**d_{102} (Ä)**	**Structural types ‡**
McAfee, N.J.	47.80	2.0711	2.0698	H
Bergbau, Austria	47.67	2.0677	2.0666	H
Moise River, Quebec	47.63	2.0701	†	H>>M
Toncray, Virginia	47.53	2.0687	2.0664*	H>>M
Hybla, Ontario	47.50	2.0682	2.0673	H>M
Bluebell, B.C.	47.28	2.0668	2.0663	H>M
Highland Surprise, Idaho	47.26	2.0645	†	H~M
Funter Bay, Alaska	47.19	2.0659	2.0643	H<M
Riondell, B.C.	46.90	2.0588	2.0575	H<<M
Clearwater Brook, N.B.	46.90	2.0592	†	H<<M
Kisbanya, Romania	46.70	2.0587	2.0574	M

* Heated at 350°C for 30 minutes before measuring
† No fresh lumps available for heating and re-measuring
‡ Determined from x-ray charts and optical examination of etched polished surfaces
H and M represent hexagonal and monoclinic pyrrhotite, respectively

A single, sharp, symmetrical 102 X-ray reflection is indicative of hexagonal pyrrhotite. A split reflection consisting of two peaks (202 $-20\bar{2}$) of about equal intensity is indicative of monoclinic pyrrhotite (Bÿstrom, 1945), and a split reflection, with the high angle reflection ($20\bar{2}$) being significantly lower in intensity than the other (102, 202 superimposed) is indicative of a mixture of hexagonal and monoclinic pyrrhotite (Bÿstrom, 1945). This interpretation of a split reflection is valid only for pyrrhotites with less than about 47.5 atomic per cent metal.

The split reflection for various weighed mixtures of hexagonal and monoclinic pyrrhotite is illustrated in **Figure 4.32 (lower)** (Arnold, 1966). There is a good correlation between structural type and composition. The two most metal-rich pyrrhotites are wholly hexagonal, the most metal-deficient pyrrhotite is wholly monoclinic and pyrrhotites with intermediate compositions are mixtures of the hexagonal and monoclinic types. A correlation also exists between the bulk composition of two-phase mixtures and the ratio of hexagonal to monoclinic pyrrhotite. Two-phase mixtures high in metals have a high ratio of hexagonal to monoclinic pyrrhotite and two-phase mixtures low in metals have a low ratio of hexagonal to monoclinic pyrrhotite. Arnold (1966) explains this relationship by a two-phase field with approximate boundaries at 47.6 and 46.7 atomic per cent metals. This is roughly in agreement with a low temperature two-phase field of hexagonal and monoclinic pyrrhotite with field boundaries at 47.4 and 46.73 atomic per cent Fe, postulated by Grønvold and Haraldsen (1952) on the basis of synthetic pyrrhotites.

Figure 4.14: Upper: X-ray chart records of the 11 re-examined pyrrhotite samples. Lower: X-ray chart records and intensity ratios of various weighed mixtures of hexagonal and monoclinic pyrrhotite. I (LHP) and I (RHP) represent the intensity of the left- and right hand peaks, respectively.

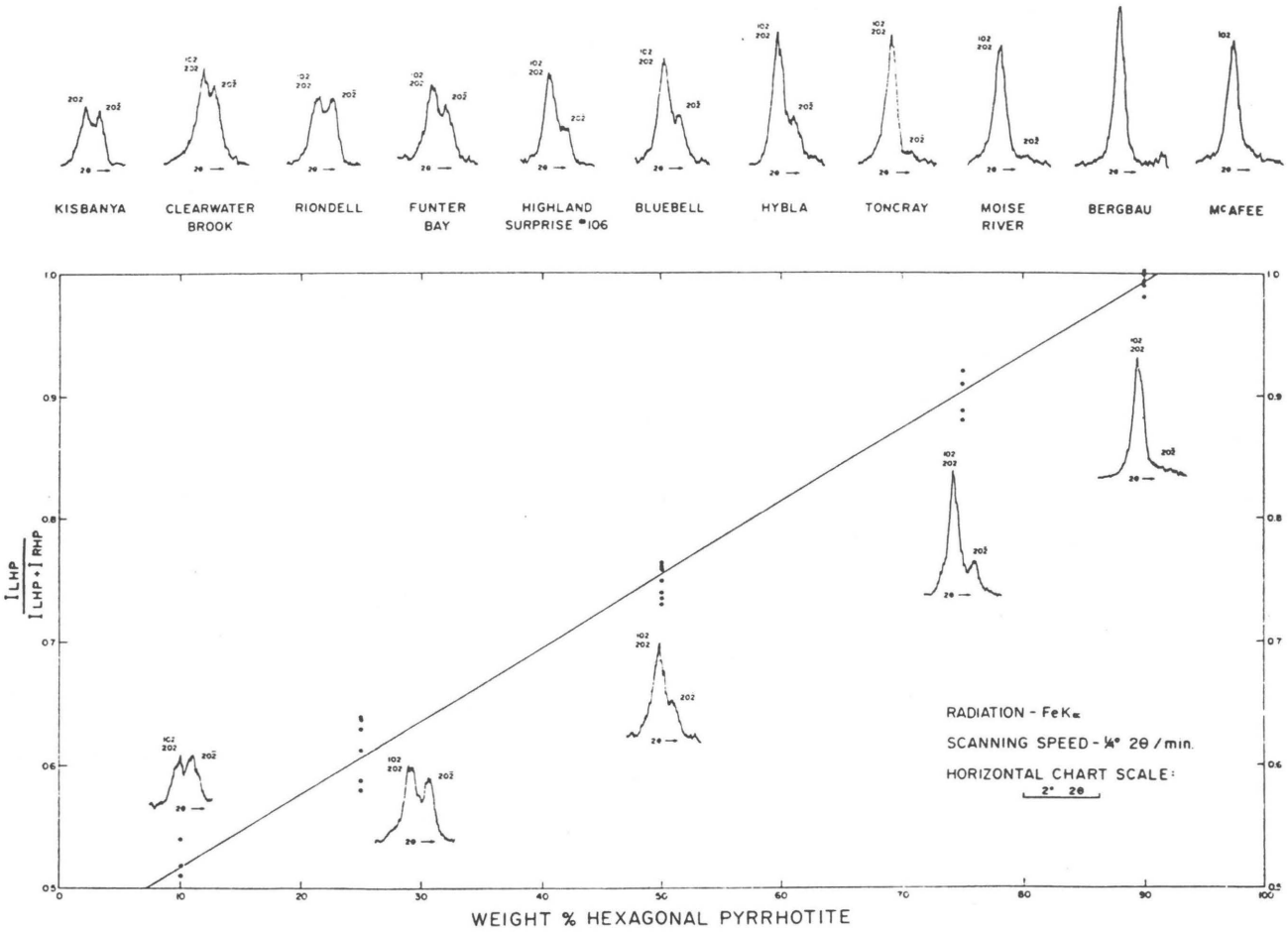

In an attempt to determine the phases of pyrrhotite present in the Uitkomst ore, X-ray traces of Uitkomst samples were compared with **Figure 4.14** from Arnold (1966). From this comparison, one sample (**Figure 4.15c,** UD 59/8, Lower Harzburgite) and possibly another (**Figure 4.15a,** UD 2/8, Chromitiferous Harzburgite) could be classified as monoclinic pyrrhotite, while the other six samples **(Figures 4.15b, d; 4.16a, b, c, d)** consist of a mixture of hexagonal and monoclinic pyrrhotite. These mixtures could further be classified from **Figure 4.14** as having a low ratio (about 20 per cent hexagonal pyrrhotite) of hexagonal to monoclinic pyrrhotite. Thus, monoclinic pyrrhotite seems to dominate over hexagonal pyrrhotite in these two-phase mixtures.

Figure 4.15: X-ray chart records for samples UD 2/8 (a), UD 2/12 (b), UD 59/8 (c) and UD 59/9 (d).

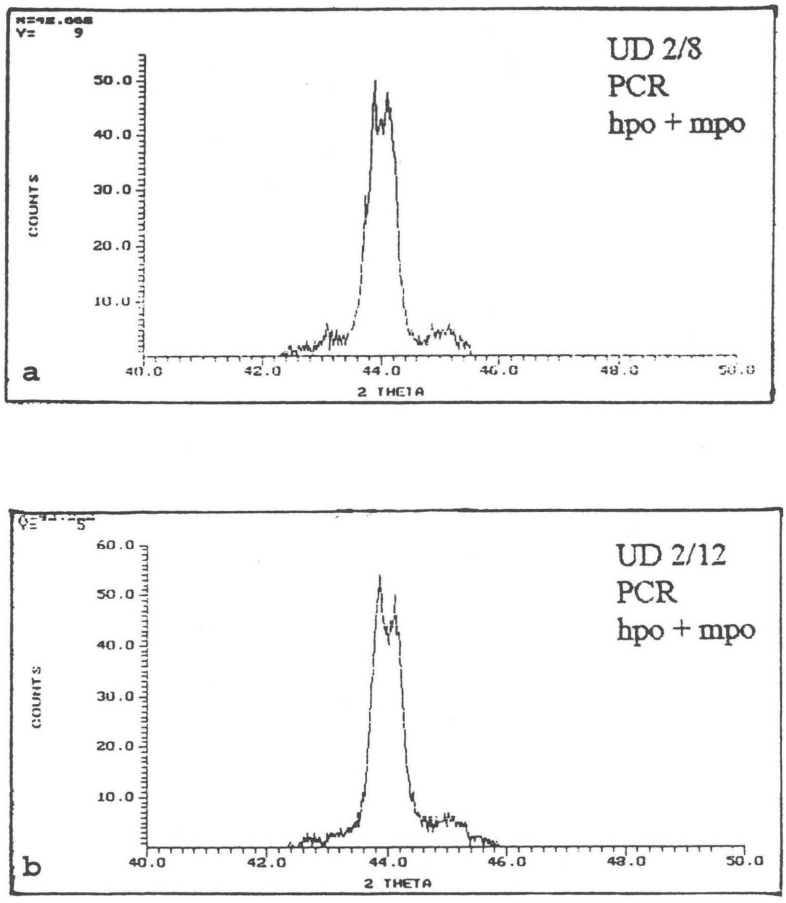

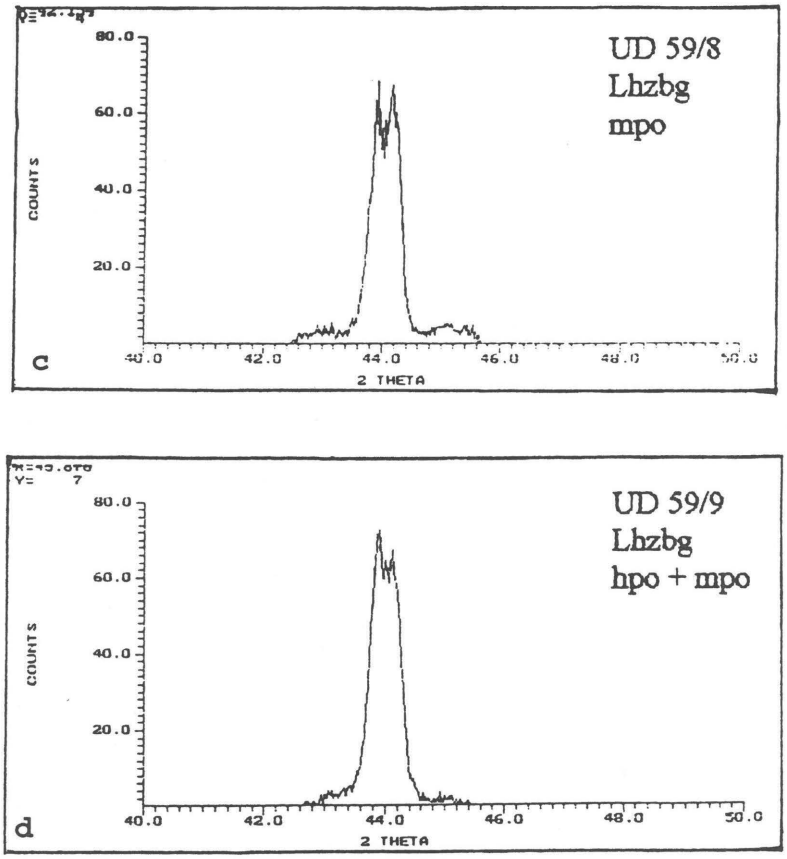

Figure 4.16: X-ray chart records for samples UD 45/4 (a), UD 45/6 (b), UD 2/17 (c) and UD 1/9 (d).

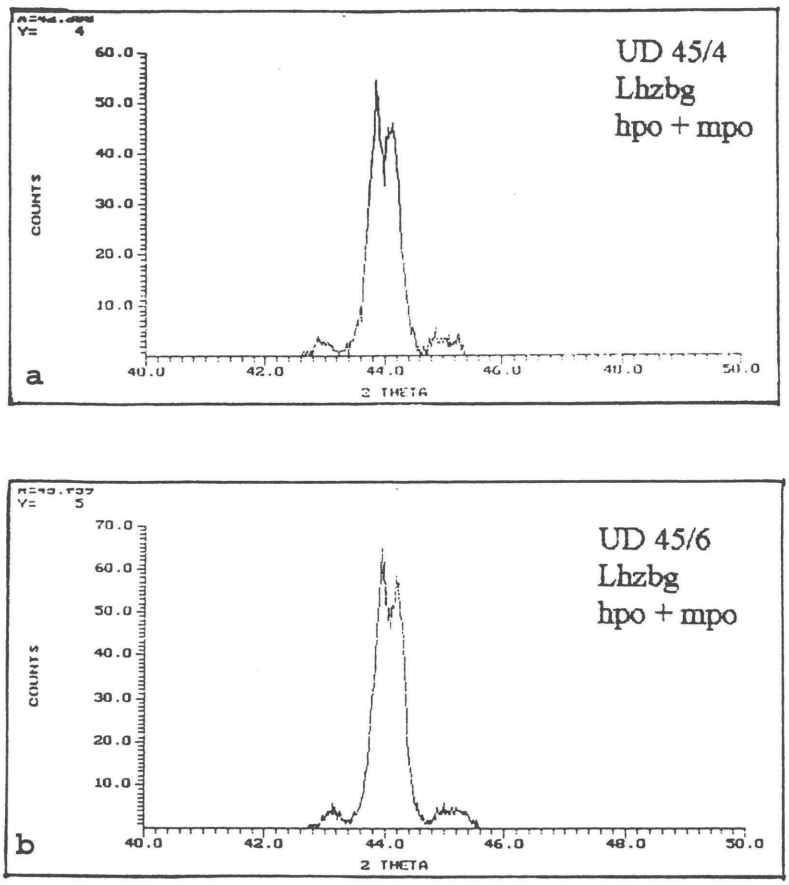

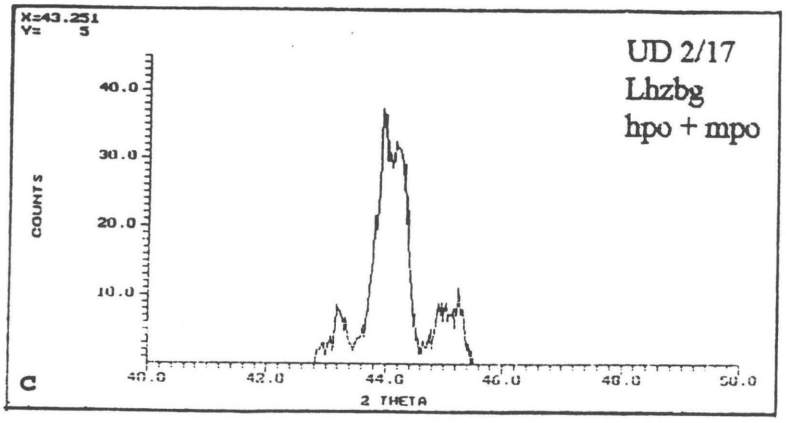

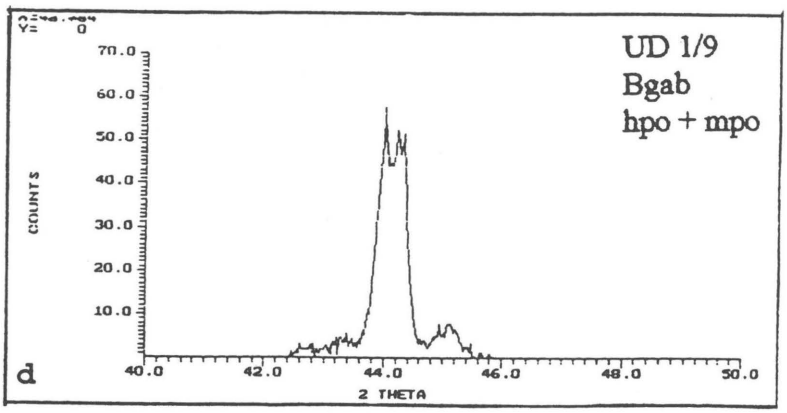

4.2.5 Grain size of the disseminated sulphide

From **Figures 4.17, 4.18, 4.19, and 4.20** the following can be said about the grain size distribution in each lithology at Uitkomst:

The sulphide grain size increases from the Main Harzburgite (80 per cent larger than 275 micron) downwards through the Chromitiferous Harzburgite (80 per cent larger than 347 micron) and the Lower Harzburgite (80 per cent larger than 325 micron) to the Basal Gabbro (80 per cent larger than 473 micron).

As shown earlier (chapter 3), sulphide mineralization in the Main Harzburgite is scarce and usually disseminated. This is probably the reason for the smallest sulphide grain size occurring in the Main Harzburgite. Most of the sulphide mineralization occurs in the Chromitiferous Harzburgite, Lower Harzburgite and Basal Gabbro as blebs, pods and net-textured ore. Massive ore was described in the Basal Gabbro. This is in line with the larger sulphide grains towards the bottom of the Complex.

Figure 4.17: Grain size distribution in the Main Harzburgite.

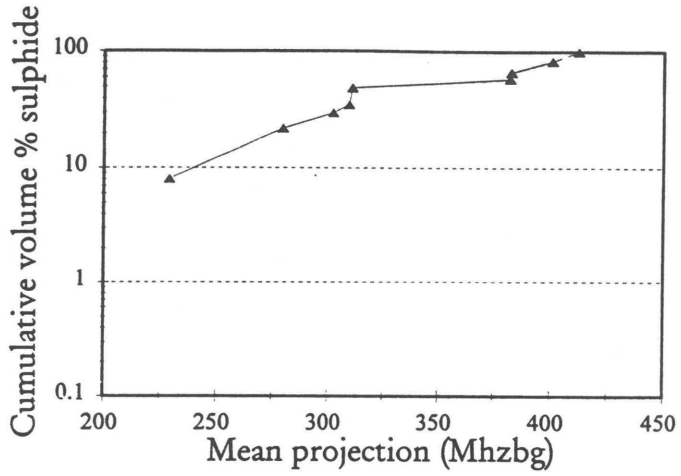

Figure 4.18: Grain size distribution in the Chromitiferous Harzburgite.

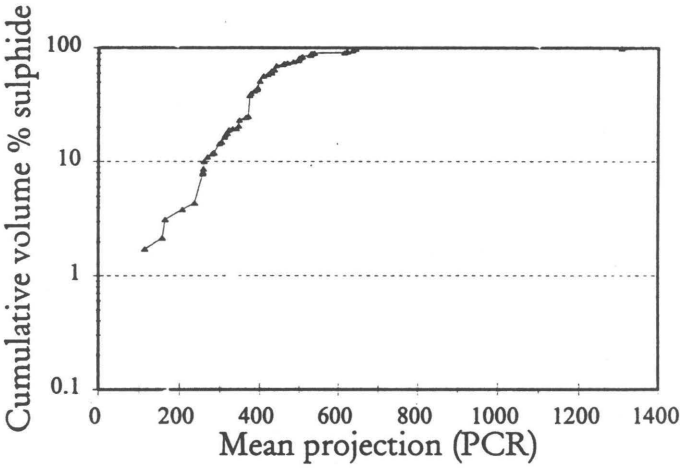

Figure 4.19: Grain size distribution in the Lower Harzburgite.

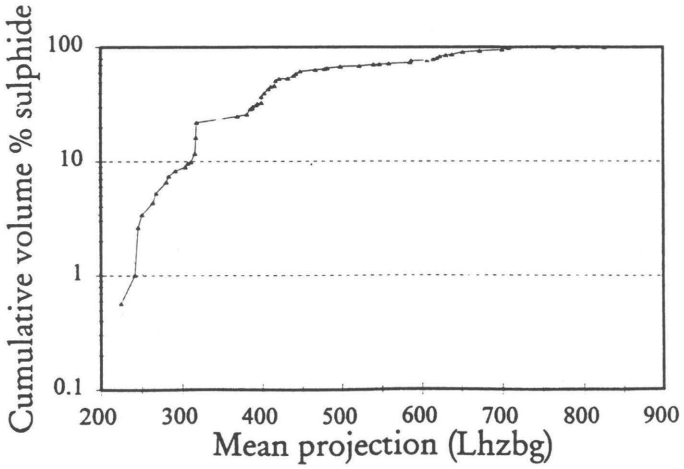

Figure 4.20: Grain size distribution in the Basal Gabbro.

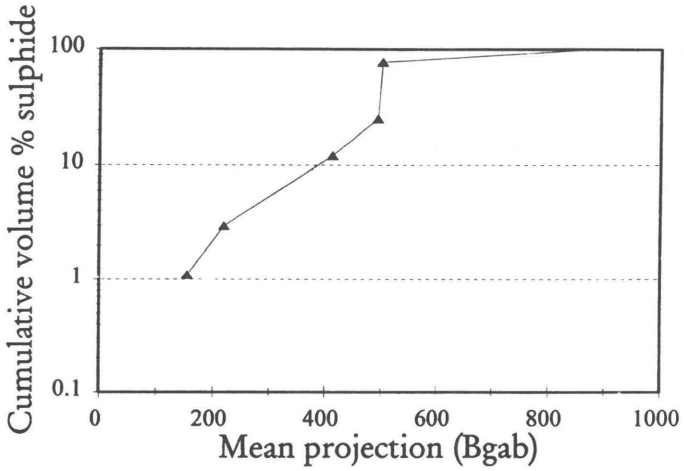

However, because only a few samples were measured from the Basal Gabbro, in comparison to the other lithologies, the results for the Basal Gabbro should be used with caution.

4.2.6 Granular versus flame pentlandite: quantitative results

The results of the quantitative measurements on granular and flame pentlandite are listed in **Table 12**. It is evident that approximately 1-5 per cent of the total nickel is confined in flame pentlandite. In the Basal Gabbro it is 35.78 per cent, but this figure is questionable. The granular pentlandite as a percentage of the sulphide fraction is higher in the upper part of the mineralized zone than towards the bottom of the Complex, whereas the reverse is true for the flame pentlandite.

The grain sizes for granular and flame pentlandite are listed in **Table 13.**

Table 12: Quantitative data on flame and granular pentlandite (all measurements in micron):

Sample.no:	Lithology	Total sulfide area % (*1)	N (granular)	%Granular pentlandite (*2)	N (flame)	%Flame pentlandite (*2)	100*Flame/(Flame +Granular)
UD 5/C	Mhzbg	0.8335	11988	25.018	22	0.003	0.01
UD 45/A	Mhzbg	0.9247	4786	20.821	110	0.053	0.25
UD 45/C	PCR	1.3412	7507	11.819	1764	0.528	4.28
UD 45/1	PCR	1.263	3390	12.177	509	0.082	0.67
UD 45/3	Lhzbg	6.6032	4561	4.581	1875	0.169	3.56
UD 45/F	Lhzbg	1.0998	145	0.479	15	0.008	1.64
UD 45/G	Bgab	0.3189	339	0.725	278	0.404	35.78
			32716		**4573**		

*1= as % of sample surface
*2= as % of total sulphide

Table 13: The grain sizes (in micron) for granular and flame pentlandite in borehole UD 45.

Sample no:	Flame: mean projection	Granular: mean* projection
	µm	µm
UD 5/C	3.95	8.80
UD 45/A	8.24	11.24
UD 45/C	8.25	9.11
UD 45/1	5.59	13.01
UD 45/3	9.12	14.04
UD 45/F	9.77	13.29
UD 45/G	8.12	6.53
mean	7.58	10.86
s	2.06	2.79
minimum	3.95	6.53
maximum	9.77	14.04

* the particle size of the granular pentlandite excludes the larger grains which could not be accommodated in the microscope field (see section on experimental methods)

The grain size for flame pentlandite varies between 3.95 and 9.77 micron. The minimum grain size for granular pentlandite ranges between 6.53 and 14.04 micron. There appears to be an overlap in the minimum grain sizes

for granular pentlandite and the mean grain size for flame pentlandite but this may be an artifact due to the measuring procedure.

4.3. Oxide Minerals

4.3.1 Chromite

Subhedral chromite grains with planar faces and rounded edges occur interstitially to olivine, as well as enclosed by pyrrhotite, chalcopyrite, and pyrite. In places secondary magnetite rims the chromite grains. Cracks in the chromite are also filled with magnetite. Rounded chromite grains were also noted in secondary magnetite rims of sulphide grains. In one sample olivine enclosed by chromite was noted. Numerous descriptions of silicates included by chromite appear in the literature (Kruparz and van Rensburg, 1965; McDonald, 1965; Jackson, 1966; and Hulbert and Von Gruenewaldt, 1985). According to Hulbert and Von Gruenewaldt (1985) chromite grains that mantle olivine are considered to be postcumulus textures related to sintering. The sintering process is described in detail in their paper. Chromite shows a strong association with brown phlogopite, occurring in and around the latter.

4.3.2. Magnetite

Three types of magnetite can be distinguished at Uitkomst:

* fine exsolution lamellae in the pyrrhotite
* primary magnetite with exsolution lamellae of ilmenite and ulvöspinel
* secondary magnetite associated with the sulphide and chromite and as disseminated grains and stringers in the gangue

The fine exsolution lamellae in the pyrrhotite are less than a micron in width and exsolved along the same crystallographic planes (*001*) in the pyrrhotite as the pentlandite flames **(Plate 4 A).** It is very easy to mistake these magnetite rods for polishing scratches on the surface of the pyrrhotite. Flames were noted parallel to the magnetite, as well as at one or both ends of these magnetite rods. It was only observed in the Lower Harzburgite. From Graham et al (1987) it is clear that oxygen is soluble in pyrrhotite to the extent of at least 0.37 per cent at 700 °C

(1.35 per cent magnetite) and that magnetite exsolves at lower temperatures.

Primary magnetite occurs as discrete sub- to anhedral grains in the gangue or associated with sulphide and is usually more than 20mm in diameter **(Plate 4 B).** It displays more or less straight contacts with the sulphides. In places it encloses pyrrhotite (with or without pentlandite) and chalcopyrite. The exsolution lamellae of ilmenite and needle-like ulvöspinel are characteristic of primary magnetite. The ilmenite and ulvöspinel exsolve parallel to (*111*) and (*100*) of the magnetite respectively. The presence of these exsolution phases in magnetite has been taken as evidence that the magnetite and the rock containing these intergrowths have been formed within a temperature range of about 700-1000 °C (Augustithis, 1979). This magnetite shows a strong association with brown mica and was only found in the lower Lower Harzburgite and in the Basal Gabbro. According to Skinner and Peck (1969) the existence of primary magnetite can suggest an immiscible sulphide melt with a high oxygen content. Alternatively, the high Ti-content is indicative of rapid in situ crystallization where relatively large quantities of unfractionated liquid is caught between the first-formed crystals. This process differs from that higher up in the sequence where fractional separation of the intercumulus melt was more efficient.

The secondary magnetite coats sulphide grains consisting of pyrrhotite, pentlandite, and chalcopyrite by forming a rim around the grains **(Plate 4 C).** These rims differ in thickness from 1-2 micron to larger than 10 micron and are anhedral, irregular, and lobate. It also occurs in the respective sulphides as irregular grains and in the cracks of granular pentlandite. The disseminated grains in the sulphide ranges in size from 10 mm to 45 mm and is usually anhedral. More blocky, subhedral, fine disseminated grains occur in and around serpentinized olivine and seem to form a rim of beads around the serpentinized olivine. According to Augustithis (1979) serpentinization is accompanied by topo-metasomatic iron oxide mobilization in that the iron from olivine which is not accomodated in the lattice of the serpentine is topo-metasomatically mobilized and forms iron oxide granules which are often following the initial olivine grain boundary. In places the magnetite stringers carry grains of pyrrhotite with or without pentlandite and chalcopyrite as

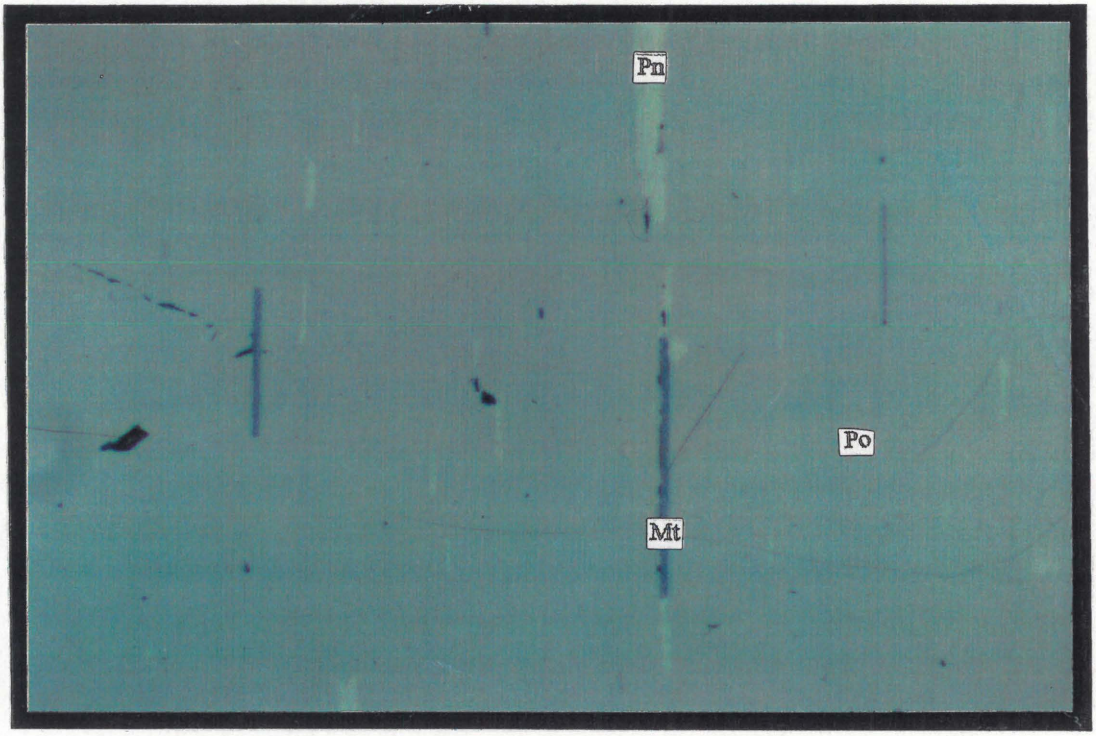

Plate 4 A : Fine magnetite (mt) exsolutions in pyrrhotite (po), which exsolve parallel to the flame pentlandite (pn). Sample 59/9, magnification x50, plane polarized light.

Plate 4 B : Primary magnetite (mt) with exsolutions of ulvöspinel and ilmenite, occuring adjacent to sulphide. Sample 1/6, magnification x20, plane polarized light.

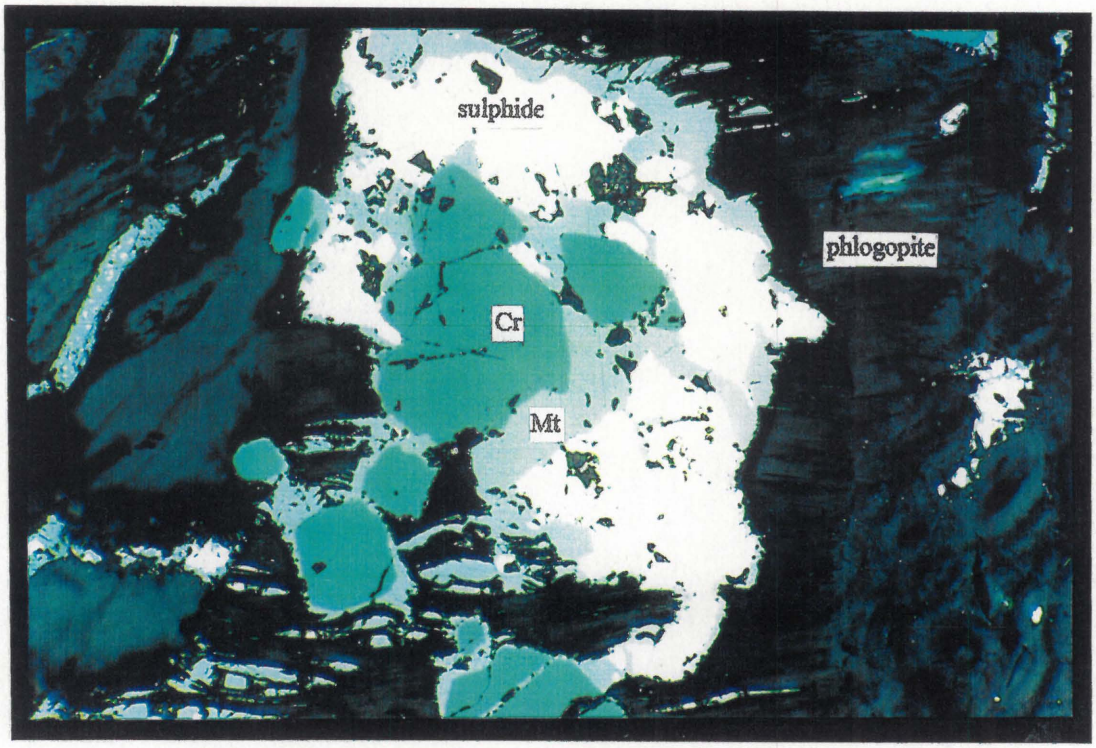

Plate 4 C : Secondary magnetite (mt) rimming chromite (chr) and sulphide which are surrounded by phlogopite. Lenses of magnetite (below, left) parallel to the cleavage of phlogopite can be seen. Sample 5/A, magnification x20, plane polarized light.

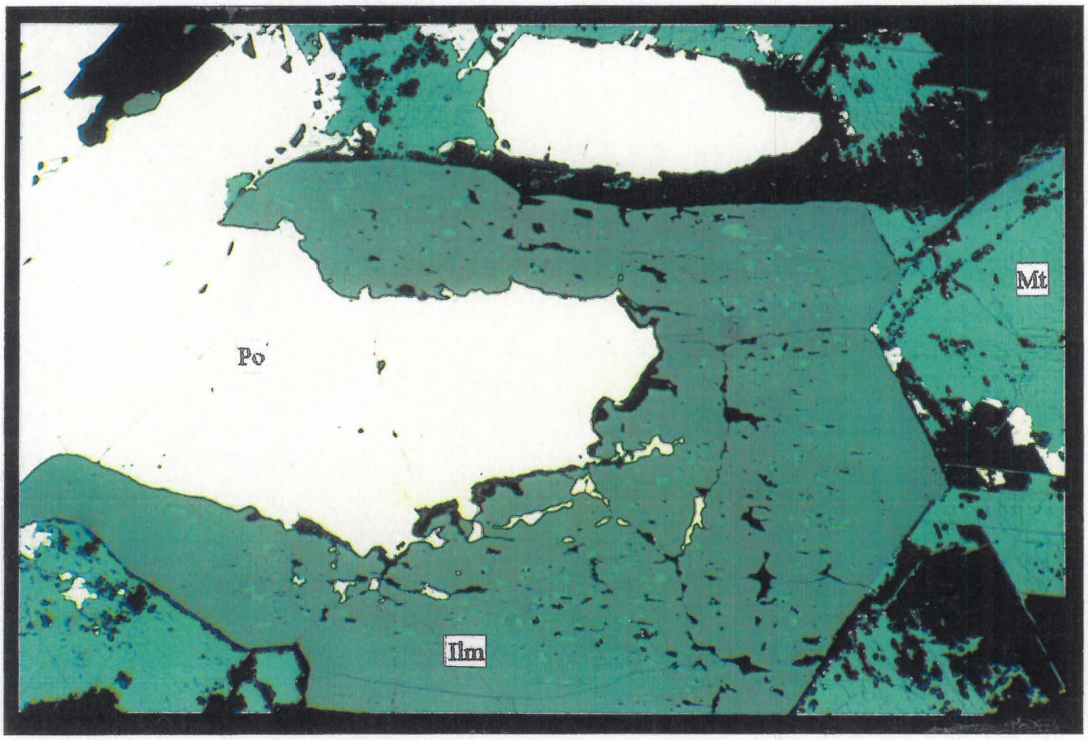

Plate 4 D : A subhedral grain of ilmenite (ilm), surrounding pyrrhotite (po) with exsolutions of flame pentlandite, which is in turn surrounded by primary magnetite (mt). Sample 1/8, magnification x20, plane polarized light.

well as chromite. Lenses of magnetite, parallel to the cleavage, were noted in the brown mica. The stringers occur in the gangue, especially in the cleavages and cracks of gangue minerals. The disseminated grains and stringers of magnetite often exhibit a spongy texture.

4.3.3. Ilmenite

Ilmenite has a strong pinkish-brown to light grey pleochroism that makes it easy to distinguish it from magnetite. It occurs as fine to broad lamellae in magnetite and also as discrete grains of various sizes in the gangue **(Plate 4 D)**. In places the surrounding magnetite is removed completely, leaving behind a skeleton consisting only of ilmenite. The ilmenite usually alters around its grain boundaries to a dark grey anisotropic mineral, possibly pseudobrookite or anatase. It exhibits an association with brown mica by occuring in or enclosing brown mica.

4.4. SILICATE MINERALS

4.4.1 Primary magmatic minerals

4.4.1.1 Olivine

The olivine occurs as anhedral or rounded, equigranular grains poikilitically enclosed by pyroxene **(Plate 5A)** and plagioclase. It is colourless to light brown and in most cases show second order interference colours, which is typical of Mg-rich olivine. Olivine shows a high relief with irregular cracks and very poor cleavage.

According to Deer et al (1985) olivine is very susceptible to hydrothermal alteration, low grade metamorphism and effects of weathering. The most common products are serpentine, chlorite, talc, carbonates and various iron oxides. At Uitkomst, the olivine alters to serpentine. This alteration is present along the irregular fractures of the olivine grains and where pervasive serpentinization was noted, the olivine crystal is totally replaced by serpentine, accompanied by a release of iron which forms fine magnetite stringers as well as disseminated magnetite grains in the serpentine. In one section a carbonate replacing the olivine was noted.

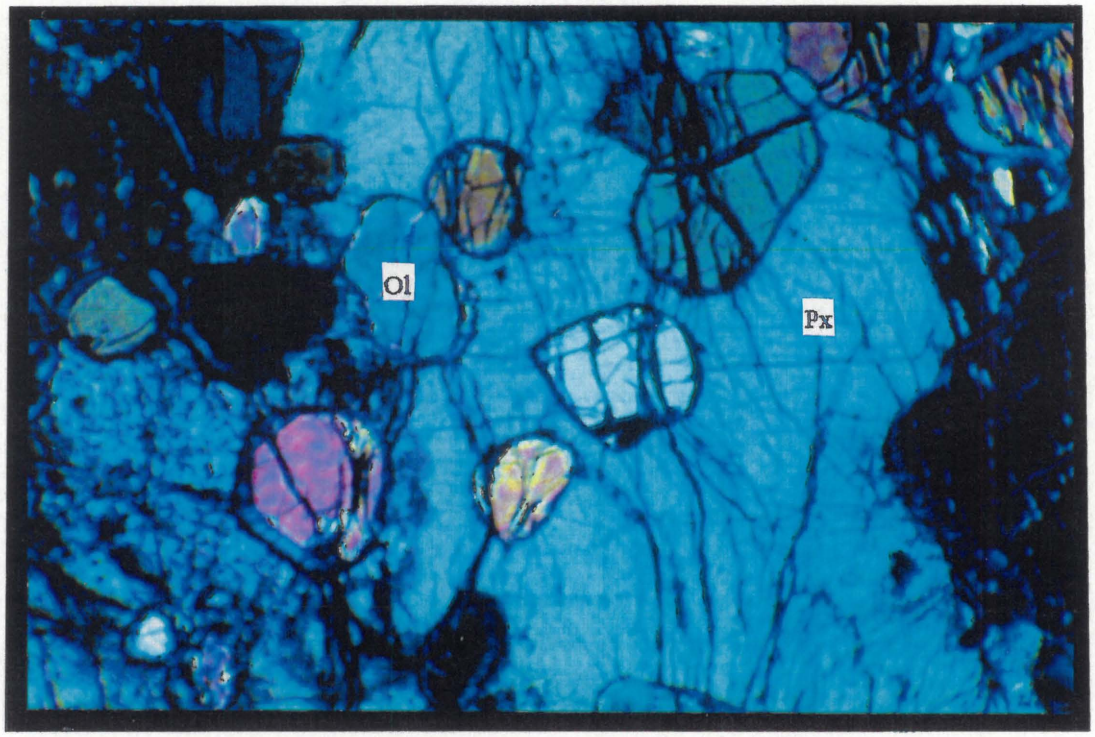

Plate 5 A: Olivine (ol) poikilitically enclosed by pyroxene (px). Sample 45/1, magnification x6.3, crossed polarizers.

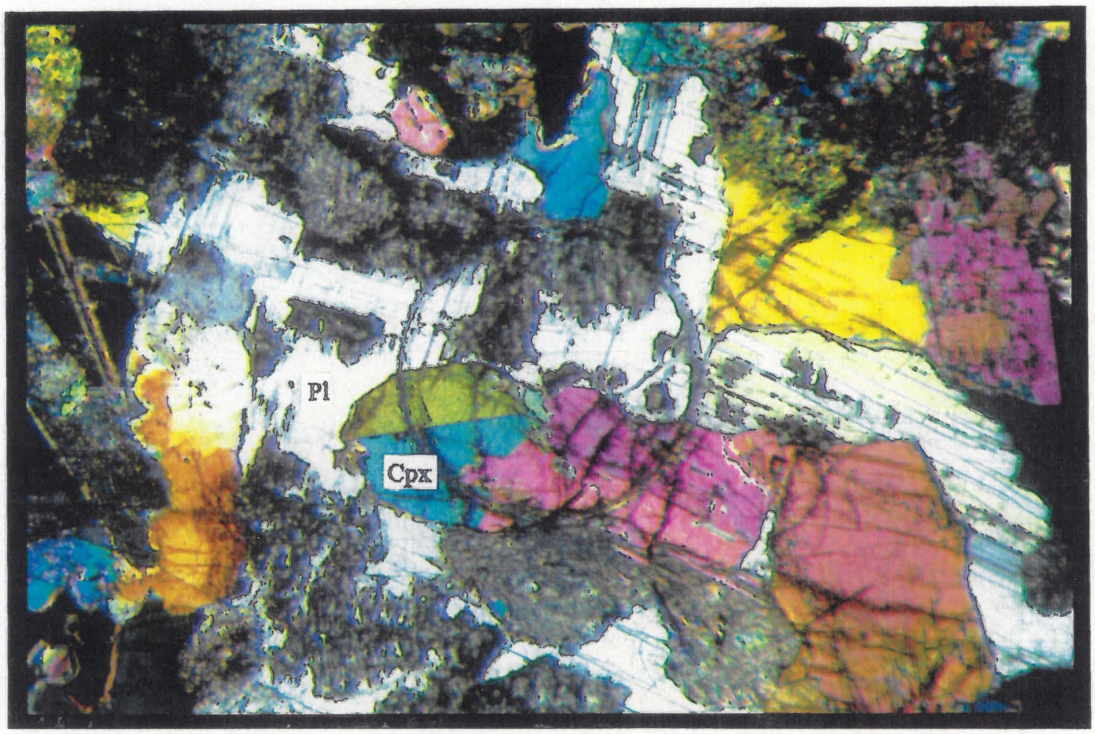

Plate 5 B: Clinopyroxene (cpx) enclosed by plagioclase (pl). Sample 34/9, magnification x3.2, crossed polarizers.

Microprobe analyses on the primary silicate minerals of Uitkomst by Gauert (1995, pers. comm.) where combined with those made in this study (**Figure 4.21**, Appendix B). These analyses show that the olivine varies from Fo88 in the Main Harzburgite to Fo79 in the Lower Harzburgite. Thus, samples from the Main Harzburgite (upper part of the Complex) are relatively more Mg-rich than samples from the Lower Harzburgite (lower part of the Complex). This is consistent with Gauert et al (1995).

Figure 4.21: Olivine compositions in molar percentage plotted against elevation in metre above base of intrusion (from Gauert et al, 1995).

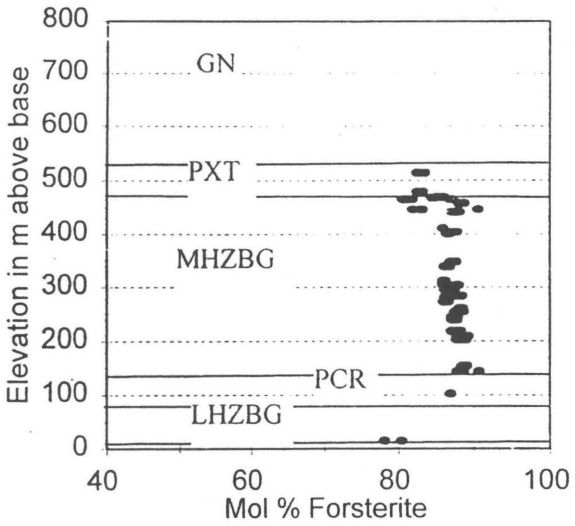

From the microprobe analyses it is evident that the manganese content of the olivine also increases towards the base of the Complex. This could be because of the diadochy that exists between iron and manganese. Small amounts of calcium are also present in the olivine. Deer et al (1985) describe diadochy between Mg and Fe^2, and Fe^2 and Mn in the fosterite-fayalite series and mention small amounts of Ca present in olivine.

4.4.1.2 Pyroxene

The pyroxene, together with plagioclase, encloses olivine and chromite grains poikilitically **(Plate 5B).**The orthopyroxene show a high relief and a

characteristic light pinkish to greenish pleochroism. Under crossed nicols, it shows parallel extinction and the interference colours are first order yellow to orange-red. Talc and amphibole were noted replacing the orthopyroxene along fractures and grain boundaries.

The process of converting orthopyroxene to talc is called talcification and is a common alteration process in ultramafic and mafic rocks. It usually occurs according to the following reaction :

$$3(MgO.SiO_2) + H_2O + SiO_2 = 3(MgO.4SiO_2\ H_2O)$$

enstatite → talc

(Bonnichsen, 1984)

The clinopyroxene is colourless to light brown and have a lower relief than orthopyroxene. The interference colours are middle second order green and blue. Cleavage in one direction as well as typical pyroxene cleavage (two sets forming almost 90° angles) are characteristic. Simple twinning was observed in some sections. Amphibole tend to replace the clinopyroxene from the grain boundaries inwards, thereby forming a rim around the pyroxene. When this occurs, the pyroxene grain is littered by fine, disseminated opaques.

This process of formation of amphibole from pre-existing ferromagnesian minerals like pyroxene is called uralitization. A typical reaction illustrating the effect is:

$$5(CaO.MgO.2SiO_2) + H_2O$$

diopside

$$= 2(2CaO.5MgO.8SiO_2.H_2O) + SiO_2 + 3CaO$$

tremolite

(Bonnichsen, 1984)

The pyroxene analyses (Appendix B) were plotted on a Q-J diagram where Q = $Ca+Mg+Fe^2$ and J = 2Na. It shows that all the Uitkomst samples fall into the quadrilateral (Ca-Mg-Fe) field **(Figure 4.22).**

Figure 4.22: Microprobe analyses of pyroxene plotted on a Q-J diagram where Q = Ca+Mg+Fe^2 and J = 2Na.

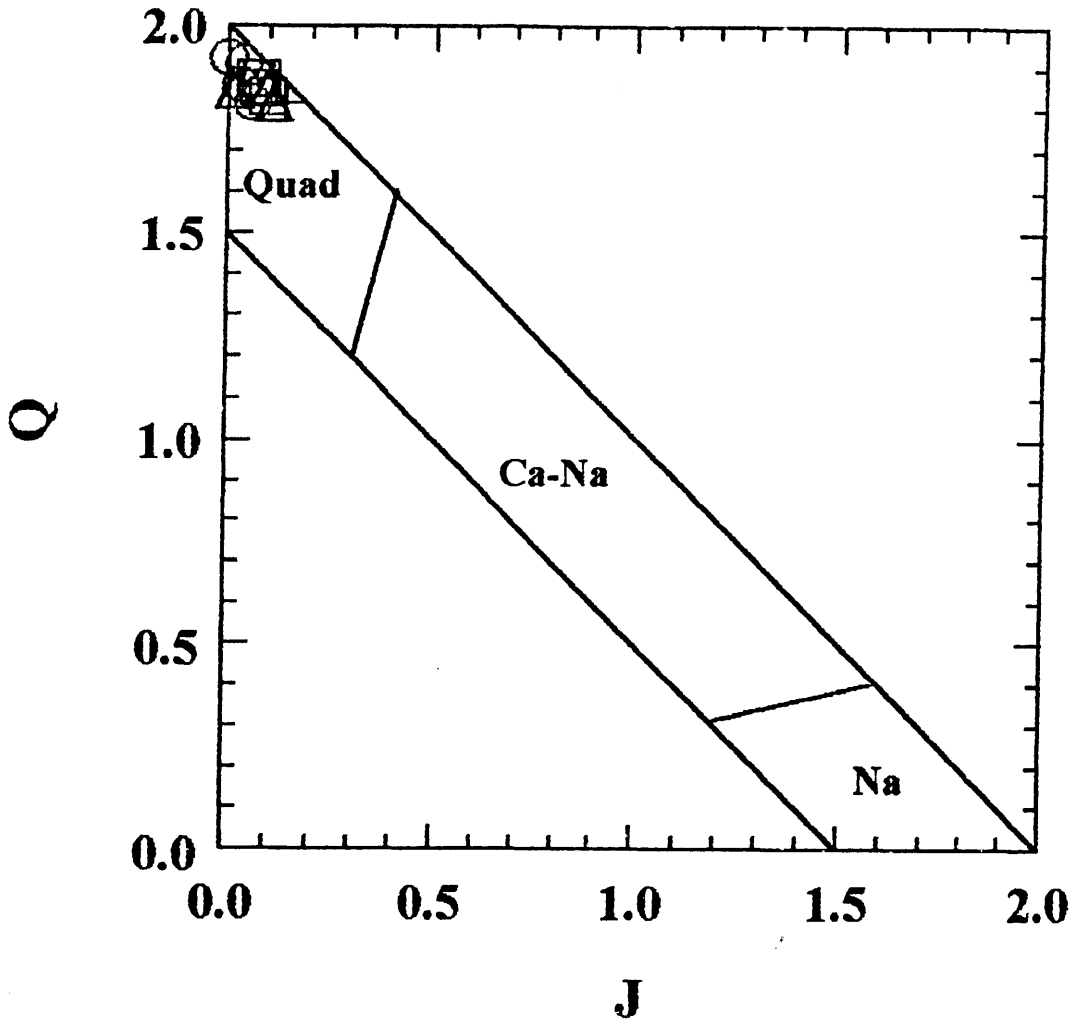

The same analyses, plotted on a triangular diagram (following Morimoto, 1989) showing the four component system $CaMgSi_2O_6$-$CaFeSi_2O_6$-$MgSiO_3$-$FeSiO_3$. **(Figure 4.23),** fall largely in the augite field. The samples plotting in the augite field represent al four the lithologies (Main Harzburgite, Chromitiferous Harzburgite, Lower Harzburgite and the Basal Gabbro). However, two groupings were noted. The Main Harzburgite and Chromitiferous Harzburgite analyses are less Fe-rich than the Lower Harzburgite and Basal Gabbro samples. This indicates an increase in Fe from the upper part to the lower part of the Complex over the interval investigated.

Figure 4.23: Microprobe analyses of pyroxene plotted on a triangular diagram showing the four component system $CaMgSi_2O_6$ - $CaFeSi_2O_6$ - $MgSiO_3$ - $FeSiO_3$.

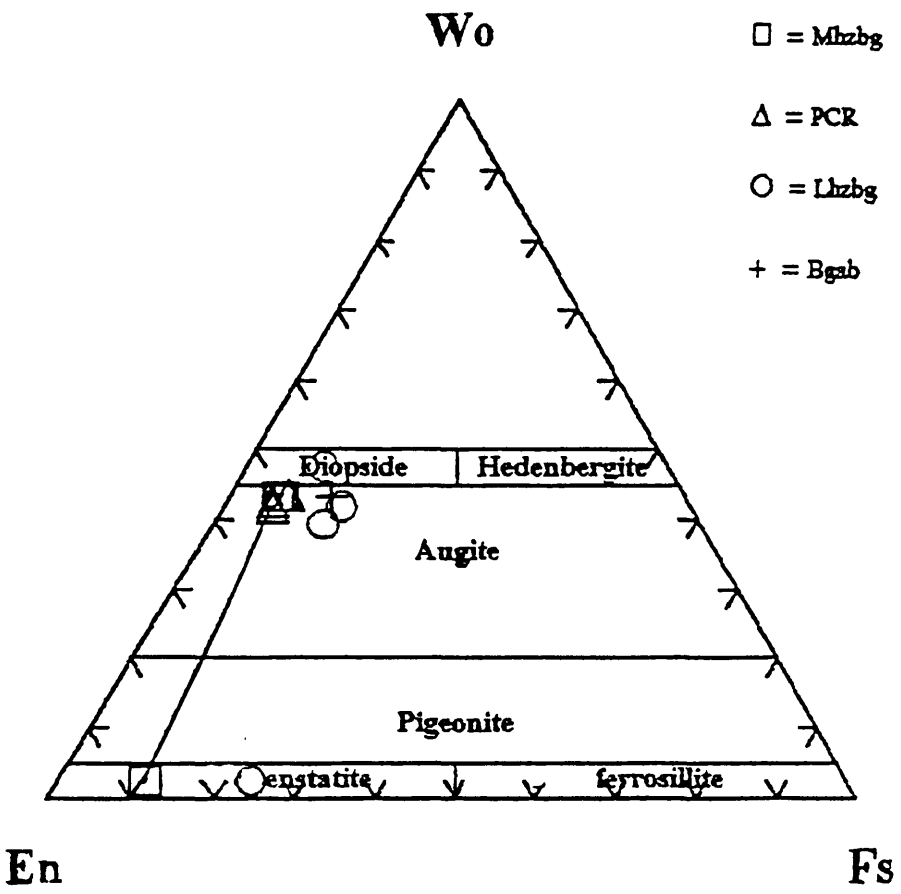

The sample in **Figure 4.23** that plots in the diopside field is from the Lower Harzburgite. The samples in the enstatite field are from the Main Harzburgite and Lower Harzburgite respectively. Here, the increase in Fe can once again be seen in the two groupings. A tieline linking the Fe-poor grouping in the augite field with the same grouping in the enstatite field is indicated. Hess (1941) first described tielines joining the compositions of many co-existing ortho- and clinopyroxene pairs for igneous pyroxenes, expressed in terms of their Wo (wollastonite), En (enstatite) and Fe (ferrosilite) contents. The increase in Fe from the Main Harzburgite to the

Basal Gabbro, observed for the pyroxene, is consistent with the whole rock geochemical data for Mg **(Figure 4.11)** described by Gauert et al (1995).

Figure 4.24: Variation of whole rock Mg (cation percent) against elevation above base (metre) in the Uitkomst Complex. The lowermost Bgab is not marked, but is represented by the first 15 m in the diagram (from Gauert et al, 1995).

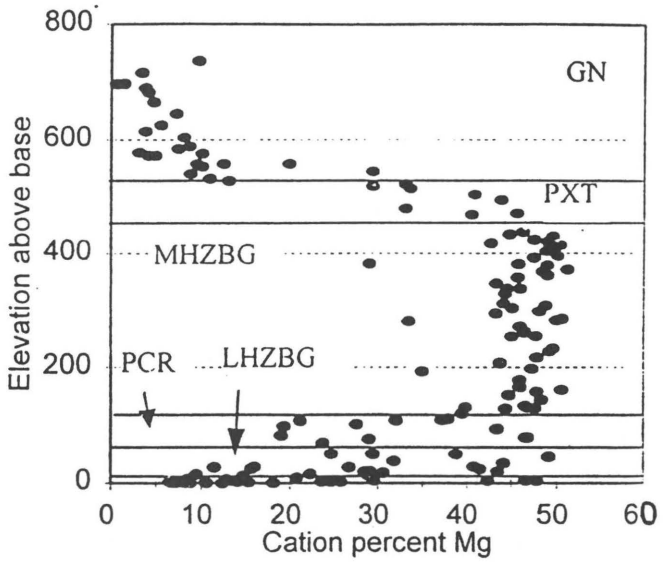

4.4.1.3 Plagioclase

The plagioclase is colourless with pale brown to brown patches where alteration has occurred. It shows low first order grey interference colours with characteristic polysynthetic twinning. Two cleavages {*001*} and {*010*}, intersecting at nearly right angles on a (*100*) section, were noted. The plagioclase occurs interstitially to pyroxene and in places encloses olivine poikilitically. Fresh plagioclase was seldomly found because it is mostly seritisized or saussuritisized, the latter more frequently. Saussuritization is the process of replacing plagioclase by zoisite, epidote, albite and sometimes calcite, sericite and zeolites. It is commonly accompanied by the chloritization of the ferromagnesian minerals (Bonnichsen, 1984). At Uitkomst the saussuritization of plagioclase is usually accompanied by the formation of a green phlogopite.

This process can be illustrated using the following reactions :

$$4(CaO.Al_2O_3.2SiO_2) + 4H_2O$$
anorthite
$$= 4CaO.3Al_2O_3.6SiO_2.H_2O + Al_2O_3 + 2SiO_2$$
zoisite

$$2[2(CaO.Al_2O_3.2SiO_2).(Na_2O.Al_2O_3.6SiO_2)] + H_2O + Fe_2O_3$$
epidote
$$= 4CaO.2Al_2O_3.Fe_2O_3.6SiO_2.H_2O + 2(Na_2O.Al_2O_3.6SiO_2)$$
albite
$$+ 2Al_2O_3 + 2SiO_2$$

If CO_2 is available, calcite can be formed.

$$CaO.Al_2O_3.2SiO_2 + CO_2 = CaO.CO_2 + Al_2O_3 + 2SiO_2$$
anorthite calcite

In these reactions, the Al_2O_3 released by the breakdown of calcium plagioclase would be available to combine with ferromagnesian minerals to form chlorite (Bonnichsen, 1984).

Microprobe analyses of plagioclase (Appendix B) are plotted on the triangular diagram $KAlSi_3O_8$ - $NaAlSi_3O_8$ - $CaAl_2Si_3O_8$ **(Figure 4.25)**. Most samples plot in the labradorite (An 50-70) field while one sample falls in the andesine (An 30-50) field. The samples plotted as labradorite is located in the Lower Harzburgite, and the andesine sample in the Basal Gabbro.

Figure 4.25: Plagioclase compositions plotted on the triangular diagram $KAlSi_3O_8$ - $NaAlSi_3O_8$ - $CaAl_2Si_2O_8$.

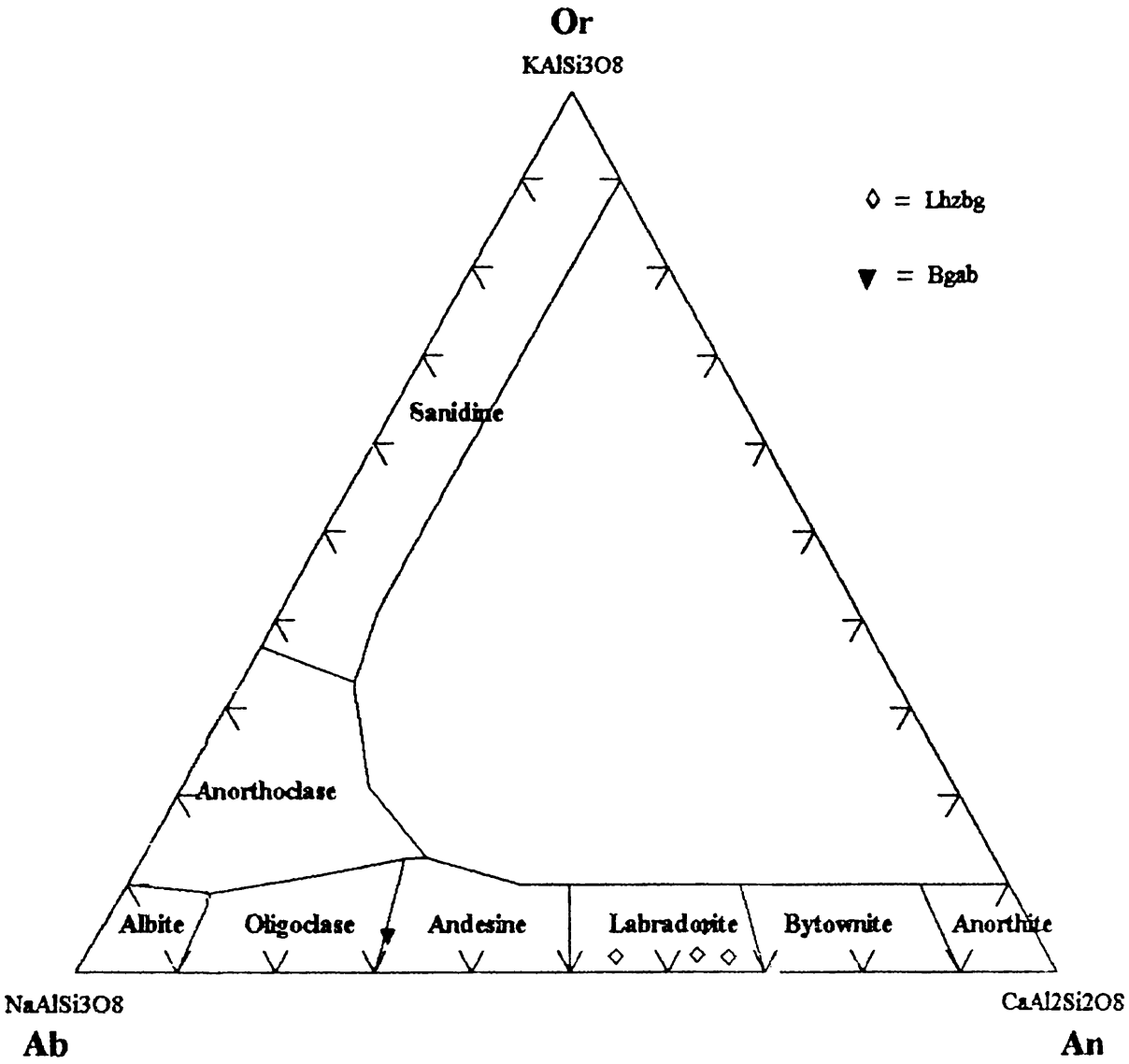

4.4.1.4 Phlogopite

On the basis of colour, three types of phlogopites can be distinguished at Uitkomst, i.e. brown, colourless, and green phlogopite. The colourless and green phlogopites are strictly secondary in nature, but will nevertheless be described here.

The brown phlogopite is pleochroic from colourless to pale brown in some sections to strong orange-brown to redbrown and black in others. It occurs throughout the Complex. Birds eye texture (a mottled appearance best seen under crossed polars when close to extinction) is typical with a high third order green to pink interference colours. Where the phlogopites are intensely coloured, the strong colour masks the interference colours. In places needles of rutile occur in the brown phlogopites. Microprobe analyses (see Appendix B) of sections where rutile occurs as acicular inclusions in brown phlogopite (perpendicular to {*010*} and at 60° intervals) has the highest titanium contents of all the phlogopites. An average composition for brown phlogopite from Uitkomst is given in **Table 14.1.**

Table 14.1: Average composition of brown phlogopite at Uitkomst.

n=34	SiO_2	TiO_2	Al_2O_3	Cr_2O_3	FeO	MnO	MgO	CaO	Na_2O	K_2O
mean	38.22	3.34	13.45	0.72	9.14	0.03	19.83	0.04	0.52	8.08
s	1.29	1.71	0.96	0.75	5.43	0.07	3.54	0.22	0.49	0.65
minimum	34.66	0.23	10.96	0	4.76	0	9.62	0	0	6.63
maximum	40.86	8.01	15.68	2.05	24.70	0.26	23.55	1.26	1.35	9.04

s = standard deviation

The colourless phlogopite occurs as discrete grains but also as an intergrowth in the brown phlogopite. In the latter case the brown phlogopite grades into the colourless variety towards the grain boundaries, or one part of a grain is brown while the other part is colourless **(Plate 5C, D).** Microprobe analyses of these sections show that the main chemical difference between the colourless and brownish phlogopite lies in the titanium content. The brown mineral has a higher titanium content than the

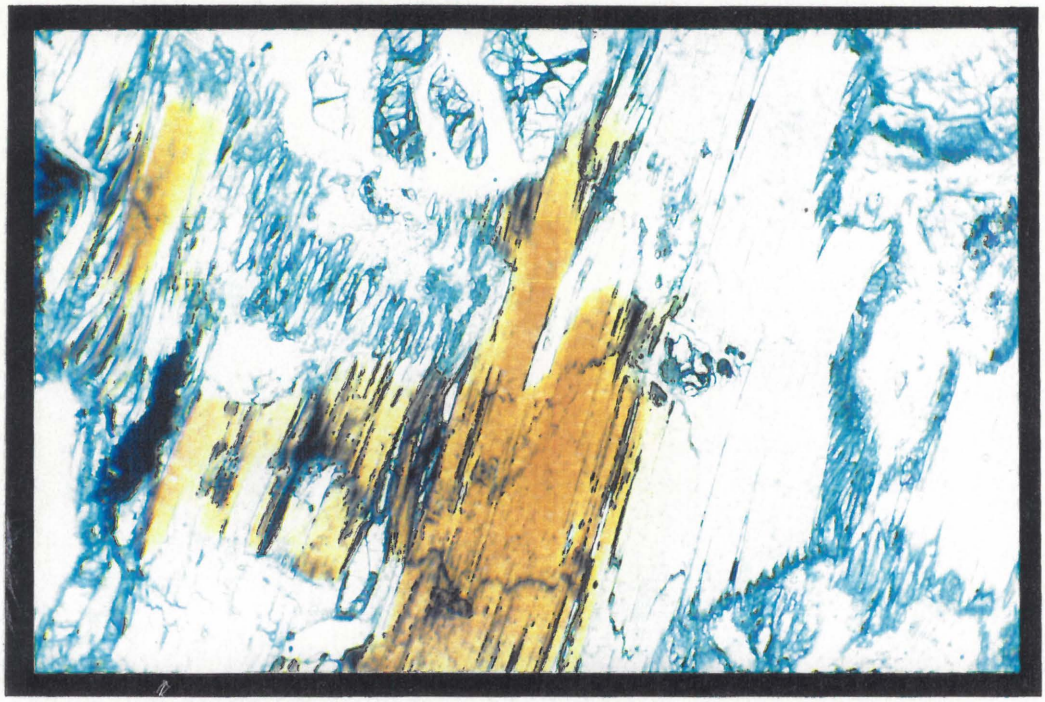

Plate 5 C: Phlogopite- brown on one side (left) and colourless on the other (right). Sample 5/5, magnification x10, plane polarized light.

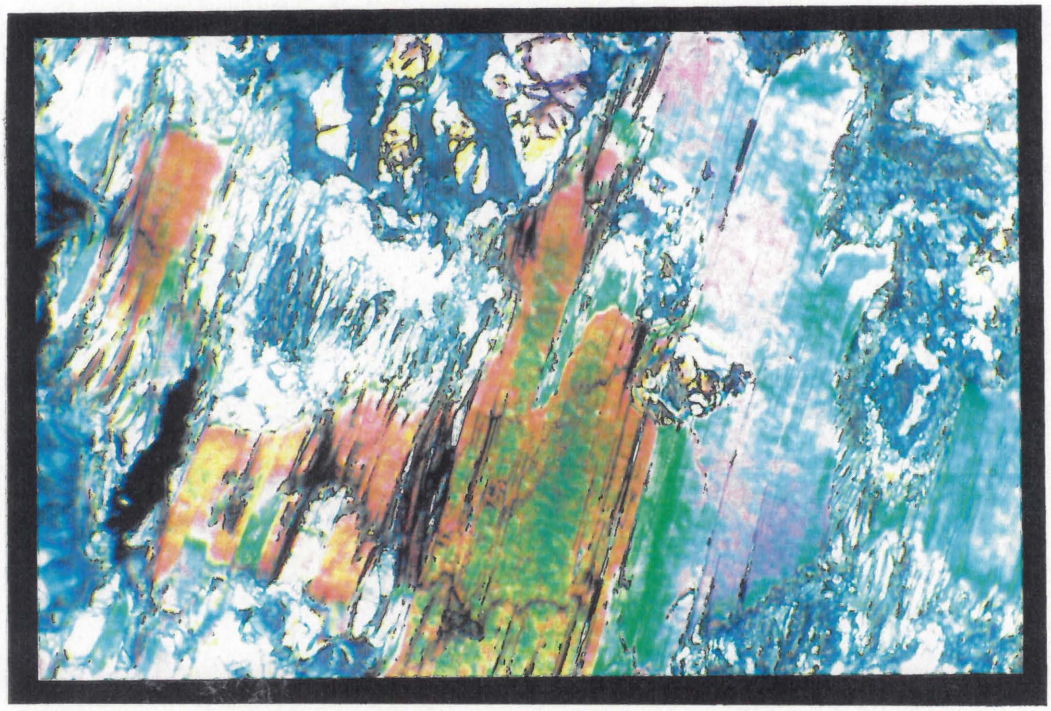

Plate 5 D: Phlogopite of plate 5 C under crossed polarizers. Note the difference in birefringe between the left (brown) side and the right (colourless) side. Sample 5/5, magnification x10.

colourless variety. An average composition for white phlogopite can be seen in **Table 14.2.**

Table 14.2: An average composition for white phlogopite from Uitkomst.

n=3	SiO_2	TiO_2	Al_2O_3	FeO	MgO	Na_2O	K_2O
mean	38.94	0.05	13.48	7.38	25.37	0.40	5.82
s	3.36	0.09	1.42	4.41	4.02	0.36	3.53
minimum	35.30	0	12.09	3.35	21.72	0	2.05
maximum	41.93	0.15	14.93	12.09	29.68	0.67	9.04

(s= standard deviation)

The brown and colourless phlogopite occur as anhedral grains interstitial to the primary silicates. This texture is magmatic, the phlogopite being late magmatic occurring as an interstitial phase between the cumulus olivine, plagioclase and pyroxene. Opaque minerals (chromite, ilmenite, magnetite, sulphide) are associated with the phlogopite, in which they are often enclosed. Carbonates, sulphides and magnetite form lenses in and parallel to the cleavage of the phlogopite.

The phlogopite alters to chlorite along cleavage and grain boundaries **(Plate 6A).** This chloritization can be illustrated by the following reaction:

$$5(K_2O.6MgO.6SiO_2.Al_2O_3.2H_2O)+Al_2O_3+14H_2O$$
phlogopite
$$=6(5MgO.Al_2O_3.3SiO_2.4H_2O)+K_2O+12SiO_2$$
clinochlore

According to Deer et al (1985) the colour of phlogopite is influenced mainly by iron and titanium content. Those rich in titanium are usually reddish brown regardless of their Mg:Fe ratio. Those poor in titanium and rich in ferrous iron tend to be bluegreen or shades of brown according to the ferric iron content.

The green phlogopite occurs only in the Chromitiferous Harzburgite and the Lower Harzburgite and is usually associated with the products of the

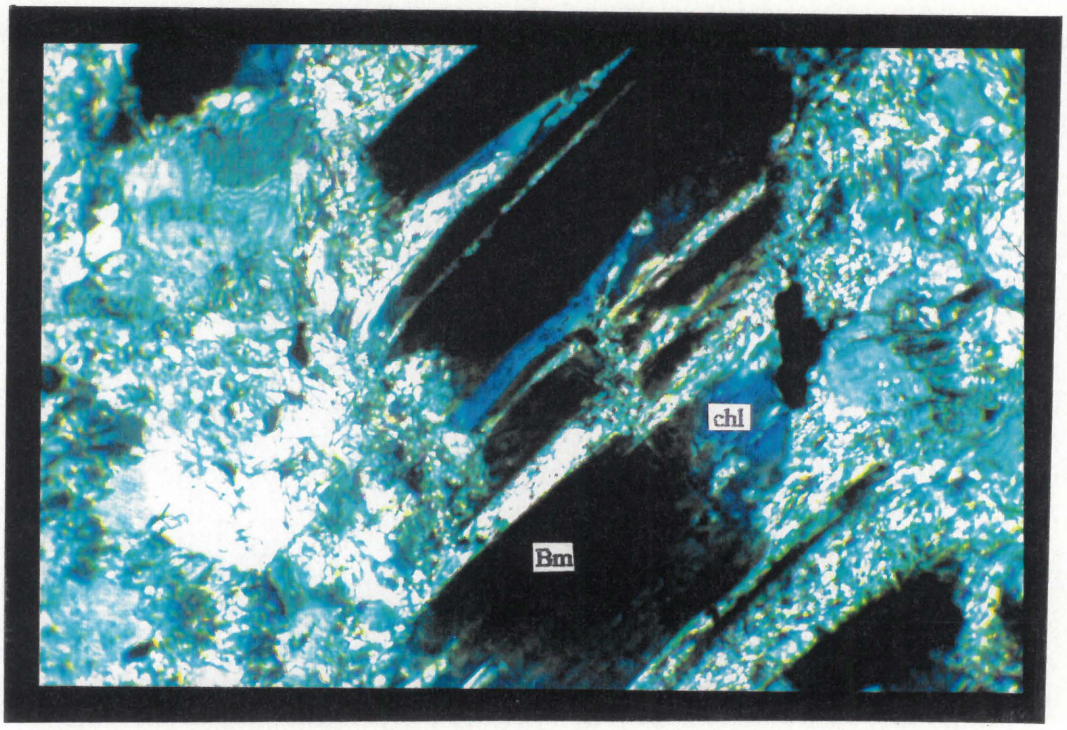

Plate 6 A: Brown phlogopite (bm) altering to chlorite (chl) surrounded by talc and carbonate. The chlorite displays anomalous blue interference colours. Sample 5/1, magnification x10, crossed polarizers.

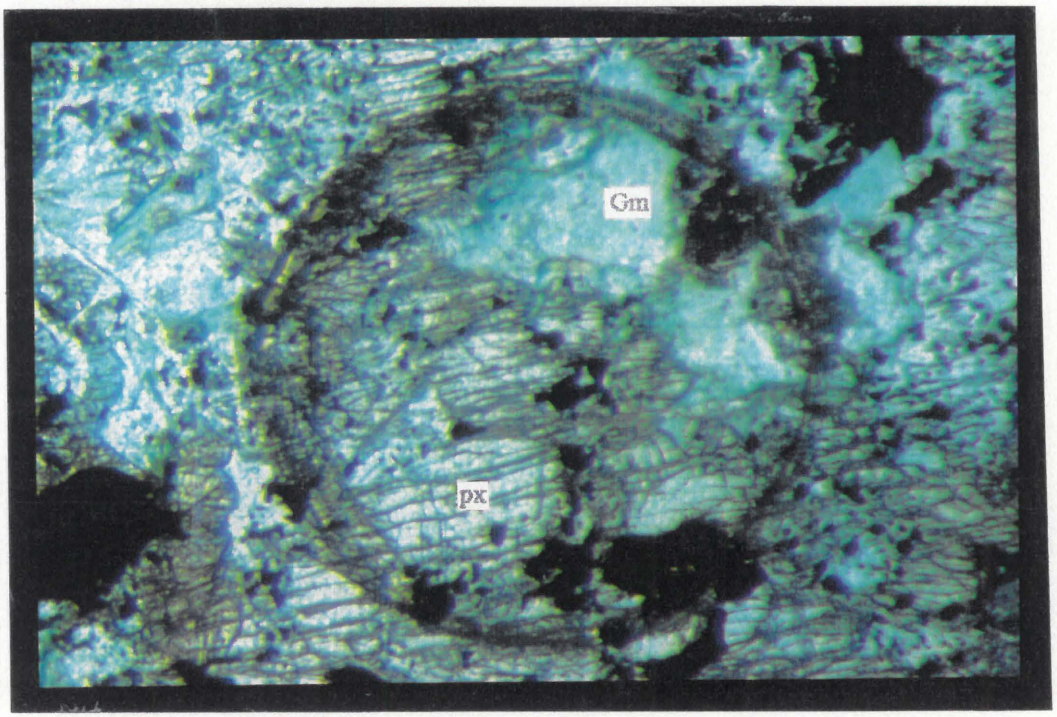

Plate 6 B: Pyroxene (px) replaced by green phlogopite (gm). Sample 64/6, magnification x5, plane polarized light.

saussuritization of plagioclase, i.e. epidote and zoisite. It has a light green to dark green pleochroism. Unlike the late-magmatic brown and white phlogopite, the green phlogopite seems to be secondary in nature as it forms anhedral masses that replace the earlier minerals **(Plate 6B).** It is usually dark green on the edges of the grains, with a more uniform light green in the central parts of the grains. The dark green parts tend to show high third order interference colours with birds-eye texture and is coarser-grained, while the light green part is fine-grained and shows low greenish gray interference colours. The green phlogopite also occurs as veins in the surrounding minerals. Some grains, located in the Lower Harzburgite, show remnants of brown phlogopite surrounded by green phlogopite **(Plate 6C).** These grains are usually coarse-grained and the mode of occurrence is very similar to that of brown phlogopite **(Plate 6D).** Microprobe analyses (Appendix B) of these sections indicate that the green part (64/6-14C, analysis 48) is higher in titanium than the brown part (64/6-15C, analysis 49). An average composition for the green phlogopite at Uitkomst can be seen in **Table 14.3.**

Table 14.3: An average composition for the green phlogopite at Uitkomst.

n=11	SiO_2	TiO_2	Al_2O_3	Cr_2O_3	FeO	MnO	MgO	CaO	Na_2O	K_2O
mean	39.19	0.58	14.02	0.01	8.90	0.04	21.34	0.55	0.39	8.16
s	2.43	1.37	2.74	0.04	4.02	0.12	3.32	1.24	0.33	1.20
minimum	34.90	0	9.82	0	4.50	0	13.76	0	0	5.30
maximum	44.28	4.67	20.41	0.15	15.57	0.39	24.37	3.78	0.81	9.76

(s= standard deviation)

In **Figure 4.26** microprobe analyses (see Appendix C) are plotted on a diagram depicting phlogopite-biotite compositional fields. It is clear that all the white and green varieties can be classified as phlogopite, whereas some of the brown varieties fall in the biotite field.

When the phlogopite is plotted according to lithology **(Figure 4.27),** samples located in the Main Harzburgite, Chromitiferous Harzburgite and Lower Harzburgite can be classified as phlogopites, whereas the samples from the Basal Gabbro (these are all brown micas) fall into the biotite

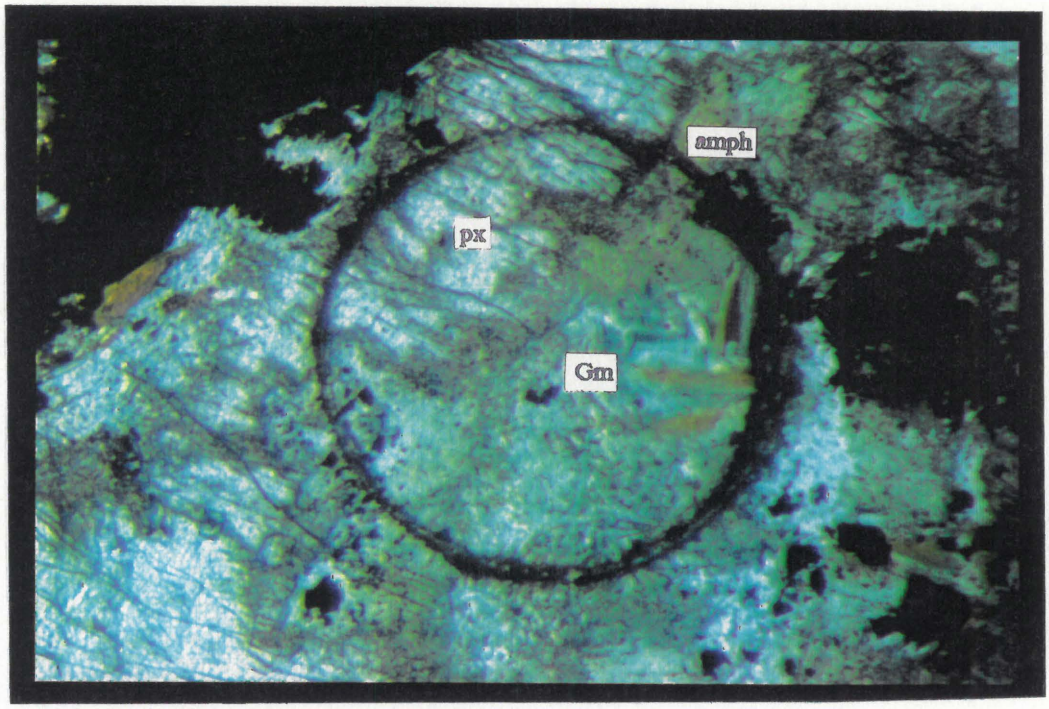

Plate 6 C: Pyroxene (px) replaced by a green amphibole (amph) and green phlogopite (gm). The green phlogopite shows a brown colour in the middle of the grain surrounded by green on the edge. Sample 64/6, magnification x5, plane polarized light.

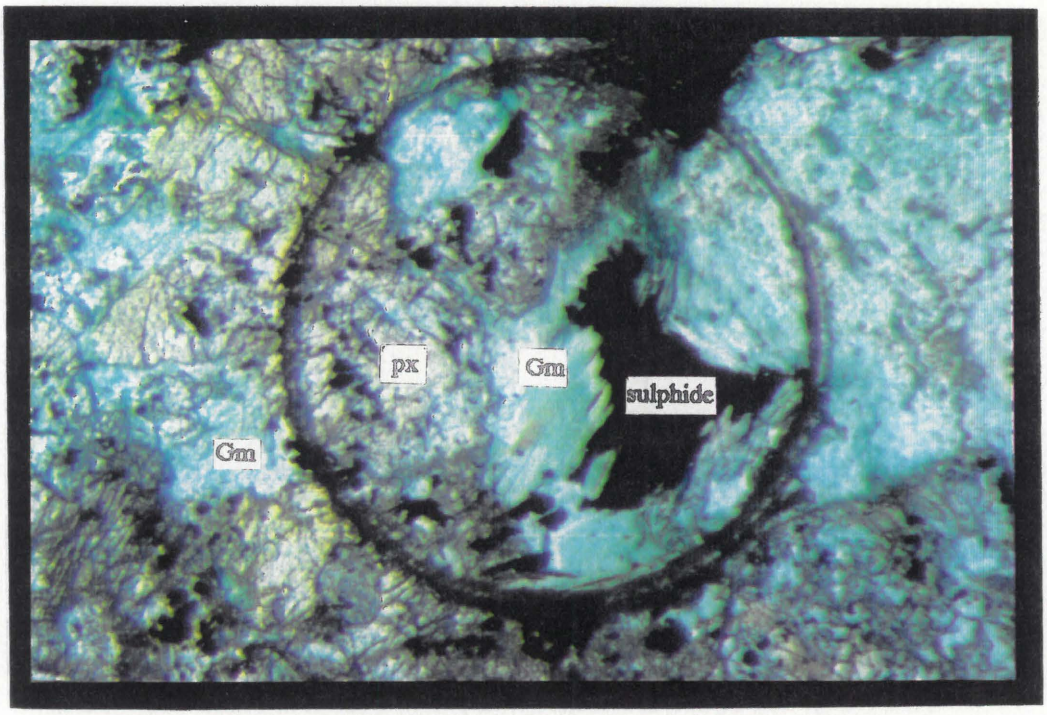

Plate 6 D: Green phlogopite (gm) enclosing a sulphide grain (just like brown phlogopite usually do). The green phlogopite is platy and coarse-grained directly next to the sulphide, becoming more fine-grained further away, as well as where it is replacing pyroxene (px). Sample 64/6, magnification x5, plane polarized light.

Figure 4.26: A diagram of the phlogopite - biotite compositional field with Al in the tetrahedral position versus the Fe/(Fe + Mg) ratio. The division between phlogopite and biotite is arbitrarily chosen to be where Mg:Fe = 2:1.

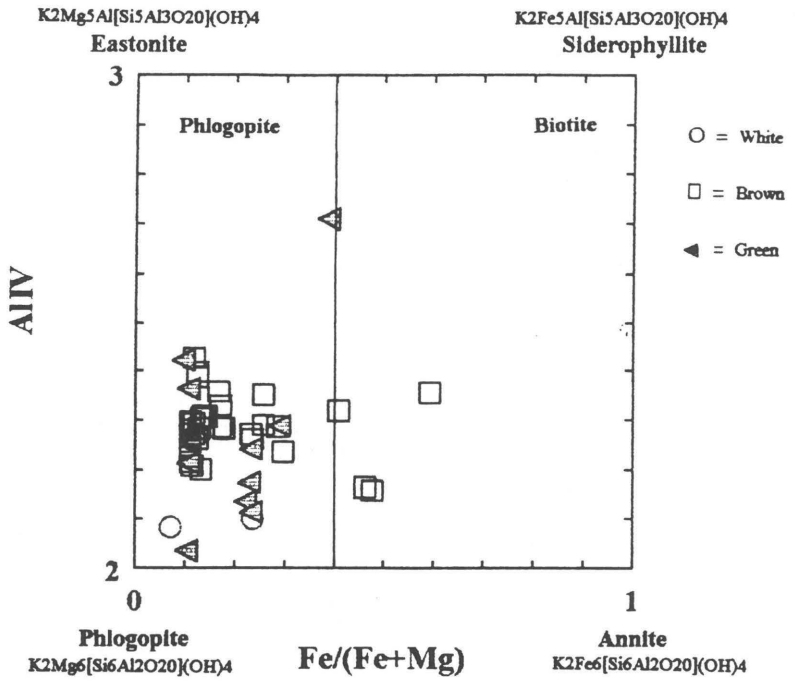

Figure 4.27: Microprobe analyses of phlogopite plotted according to lithology on a diagram of the phlogopite - biotite compositional field with Al in the tetrahedral position versus the Fe/(Fe + Mg) ratio. The division between phlogopite and biotite is arbitrarily chosen to be where Mg:Fe = 2:1.

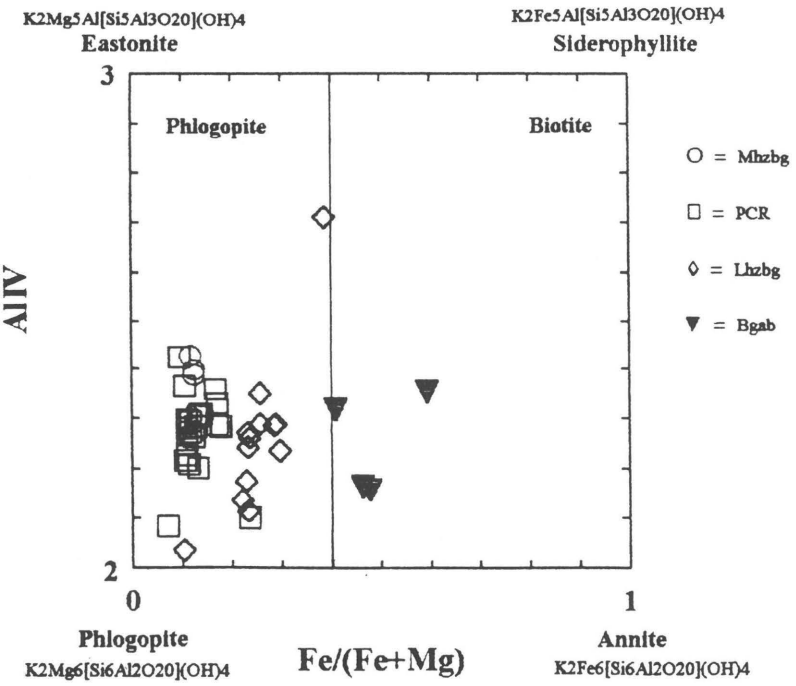

field. According to Deer et al (1985) the following changes in chemistry can be noted between phlogopite and biotite. The Mg is replaced by ferrous iron and also by trivalent ions (Fe^3, Al), and Al replaces Si in the tetrahedral sites usually beyond the ratio of Al:Si = 2:6.

In terms of Fe-content, samples located in the Main Harzburgite and Chromitiferous Harzburgite show Fe/(Fe+Mg) ratios between 0 and 0,2. Samples from the Lower Harzburgite show ratios between 0,2 and 0,3, whereas samples from the Basal Gabbro varies from 0,4 to 0,6. Thus, there seems to be an increase of Fe/(Fe+Mg) from the Main Harzburgite downwards to the Basal Gabbro. This local trend of Fe-enrichment towards the base of the Complex was also evident from olivine and pyroxene and is consistent with the mineral chemistry and whole-rock geochemical data of the Complex as described by Gauert et al (1995).

4.4.2 Secondary minerals

4.4.2.1 Serpentine

The serpentine minerals lizardite, chrysotile and antigorite are tri-octahedral hydrous phyllosilicates based on 1:1 layer structures. The principal minerals of the serpentine group all have the approximate composition $Mg_3[Si_2O_5](OH)_4$ and comparatively little substitution of Mg by other cations is found to occur in natural specimens. Chrisotile has a fibrous nature, while lizardite and antigorite are tabular (Deer et al, 1985). Lizardite is formed during the alteration of ultrabasic igneous rocks at temperatures below 400°C. Serpentine is an alteration product of olivine in H_2O-rich environments.

At Uitkomst, serpentine is most prevalent in the Main Harzburgite where serpentinization is common (section 4.5), but lesser amounts of serpentine occur in all the other lithologies. As described under olivine, the serpentine is present in the fractures of the olivine or has completely replaced the olivine, forming a typical mesh structure (irregular, platy serpentine combined with areas of cross- and slip-fibre serpentine) (Nockolds et al, 1978). Fine magnetite and lesser pyrrhotite veinlets occur in the serpentine. Around the mesh structure, fine needle-like and sometimes spherulitic serpentine grows into the sulphide. Serpentine also forms veins in pyroxene. According to Augustithis (1979) the

serpentinization of olivine is a process which involves expansion of volume, consequently when olivine is enclosed by pyroxene and alteration of the olivine takes place, cracks may develope transversing both the olivine and surrounding pyroxene. These cracks are then occupied by serpentine. In places fine, colourless tremolite needles occur in the mesh centres of the serpentine. Talc, carbonate and mica were noted in association with serpentine. At Uitkomst, the textures are mostly pseudomorphic, with the outlines of the original olivine grains as well as its fracture patterns well preserved. Some sections show non-pseudomorphic textures, with the original ultramafic textures more or less destroyed.

Serpentine is only stable at very small values of XCO_2. The presence of serpentine in a rock is a very good indicator that the fluid phase present during rock alteration contained very little CO_2. The XCO_2 must have been less than 10 mole per cent, otherwise serpentine would have been converted to magnesite + quartz or talc (Winkler, 1979).

Microprobe analyses (Appendix B) were compared with those given for serpentine in Deer et al (1985). The Uitkomst samples all show much higher FeO and in places higher Al_2O_3 contents. In **Figure 4.28** the serpentine analyses were plotted in terms of Si, Mg and Fe (atomic percentage) on a ternary diagram. It is evident that the Uitkomst serpentine are Fe-rich. The analyses with Al_2O_3 are generally more Fe-rich and extend towards an average Uitkomst chlorite analysis plotted on the diagram. This could be an indication that small amounts of chlorite are sub-microscopically intermixed with the serpentine. This idea is supported by the fact that, in places, the serpentine showed slightly bluish birefringence.

From Deer et al (1985) we know that Si can be replaced by Al, and Mg by Al, Fe^2 and Fe^3 in the serpentine structure. The Uitkomst samples showing high Al_2O_3, also show lower SiO_2, so it is possible that Al is here substituting for Si. Furthermore, the high degree of substitution of Mg by Fe is notable. Serpentine generally does not accommodate significant amounts of Fe in the structure (Deer et al, 1985; Whittaker and Wicks, 1970). Wicks and Plant (1979) report maximum FeO values of 12 per cent for antigorite, 9 per cent for chrysotile and 16 per cent for lizardite. The FeO content of the Uitkomst serpentines ranges from 1.4 to 9.8 percent, which is high but within the range of values quoted by Wicks and Plant (op cit). The high FeO

content of the serpentine could be ascribed to relatively low oxygen fugacities or high SiO_2 activities during serpentinization.

Figure 4.28: Serpentine analyses plotted in terms of SiO_2, MgO and FeO on a ternary diagram (crosses represent analyses where Al_2O_3=0, while the circles represent analyses containing Al_2O_3).

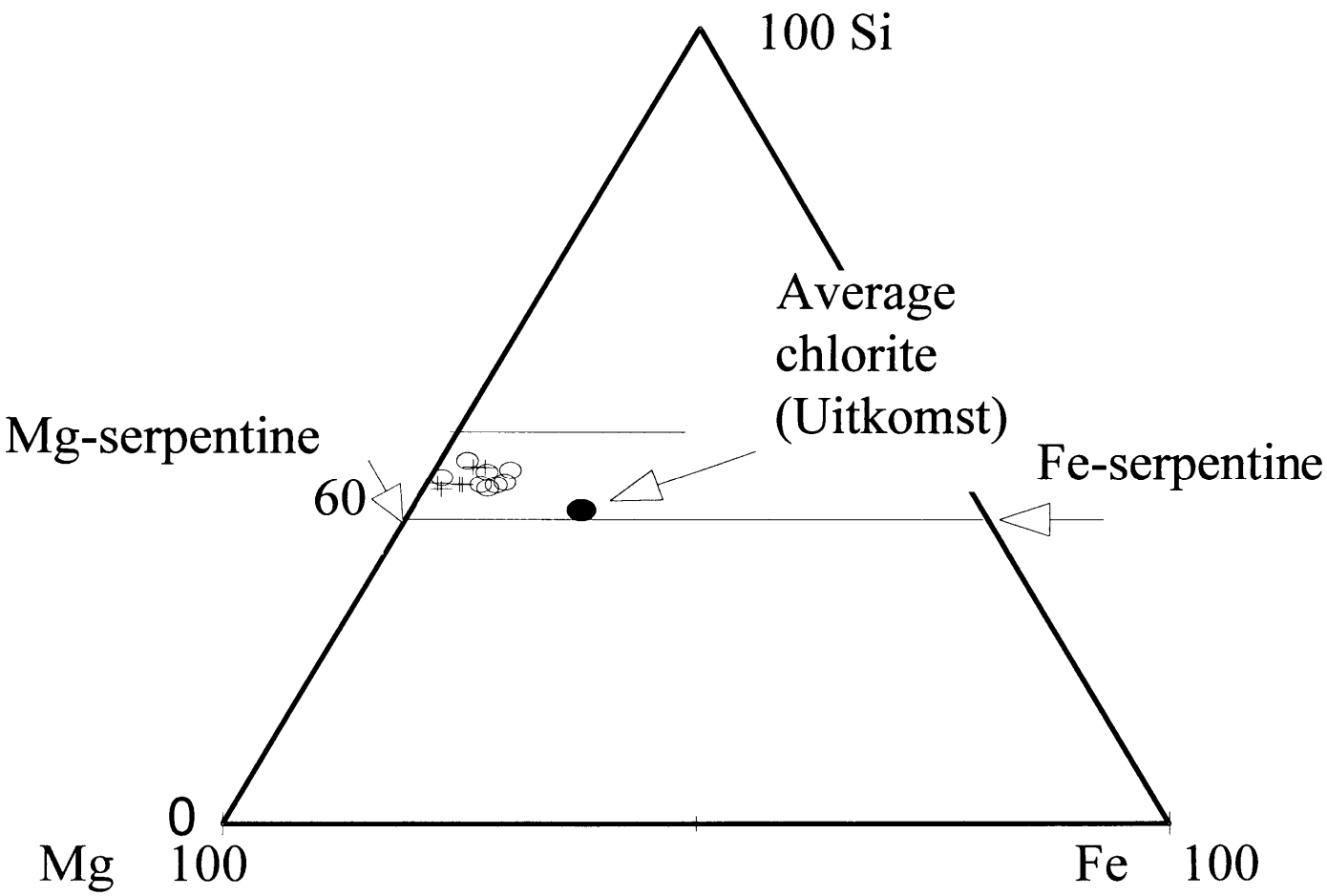

4.4.2.2 Chlorite

Chlorite in ultramafic rocks occurs usually as secondary minerals formed by deuteric or hydrothermal alteration of primary ferromagnesian minerals, such as mica, pyroxene, amphibole, garnet and olivine (Bailey, 1988). The structure of chlorite consists of alternating talc-like $Y_6Z_8O_{20}(OH)_4$ and brucite-like $Y_6(OH)_{12}$ sheets. It has a general formula of $(Mg,Al,Fe)_{12}[(Si,Al)_8O_{20}](OH)_{16}$ (Deer et al, 1985).

The chlorite at Uitkomst is colourless to pale green. It has a low birefringence and does not always display the characteristic anomalous blue and brown interference colours. The pale green chlorite is more fine-grained than the colourless variety and usually occurs in association with green phlogopite. In this association it is difficult to distinguish between the chlorite and the green phlogopite, because both have a light green colour and the birefringence of the green phlogopite is generally low. Phlogopite (brown) alters to chlorite along cleavage planes and grain boundaries. Chlorite veins occur in plagioclase and amphibole. Fan-like or spherulitic grains of chlorite are embedded in carbonate grains. Chlorite occurs throughout the Complex, but is especially abundant in the Lower Harzburgite, where it is associated with the saussuritization products of plagioclase (epidote-zoisite, green phlogopite).

Microprobe analyses (Appendix B) of chlorite compares well with the analyses of a pycnochlorite in Deer et al (1985). These chlorite analyses were plotted on a diagram **(Figure 4.29)** after Hey (1954). All the analyses plot in the pycnochlorite-diabantite field.

Figure 4.29: Classification of the Uitkomst chlorite after Hey (1954).

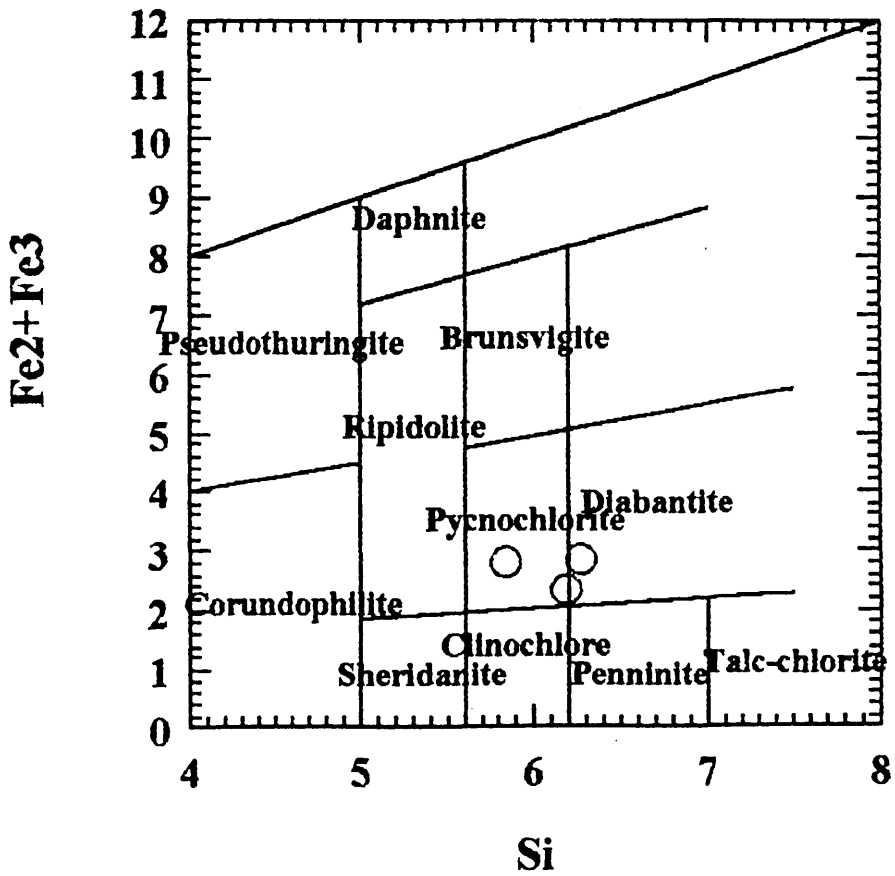

4.4.2.3 Talc

Talc is the tri-octahedral phyllosilicate consisting of simple 2:1 layers. The structure resembles that of pyrophyllite except that octahedral sites in the composite layers are occupied by magnesium instead of aluminium. It has a chemical formula of $Mg_6[Si_8O_{20}](OH)_4$ (Deer et al, 1985).

In the rocks of the mineralized zone at Uitkomst, the talc is usually colourless to light brown and occurs as fine grained needles in random orientation. It has a high birefringence with third order interference colours. In places, two generations of talc are found in one section, i.e. fine grained needles or blades, and coarser, fan-like grains.

The talc tends to be intergrown with the sulphide grains, and is usually associated with tremolite and carbonate with lesser serpentine and chlorite. Talc was also noted as an alteration product of pyroxenes and in places olivines. Where talc has replaced pyroxene, a pseudomorphic texture of the original igneous texture exists, with talc (previously pyroxene) now poikilitically enclosing serpentine (previously olivine). Talc is a dominant mineral in the Chromitiferous Harzburgite, occurring with chromite, tremolite, chlorite and carbonate.

McKie (1959) reported a talc sample with 3.95 weight per cent Al_2O_3. Based on experimental work, others (Yoder, 1952; Stemple and Brindley, 1960; Fawcett, 1962; Fawcett and Yoder, 1966) established that about 4.0 weight per cent is the apparent maximum Al substitution possible. For samples with silicon deficiency, Al (up to about 0.1 atoms per 4 tetrahedral sites) may occupy the tetrahedral sites (Evans and Guggenheim, 1988).

Microprobe analyses of talc (Appendix B) correspond well with those of talc in altered peridotite published in Deer et al, 1985, except for Na_2O and Al_2O_3. Analyses from Uitkomst show Na_2O contents to be generally higher than 0.5 weight per cent and one sample (UD 5/1) contains a high Al_2O_3 content of 2.83 weight per cent.

Steatization, the process of converting serpentine to talc, is commonly associated with serpentinization. It may occur through the addition of silica and removal of magnesia, or by the addition of CO_2 :

$$2Mg_3Si_2(OH)_4 + 3CO_2 = Mg_3Si_4O_{10}(OH)_2 + 3MgCO_3 + 3H_2O$$
serpentine — talc — magnesite

At low temperatures in the greenschist facies, both tremolite and chlorite may be converted to talc by CO_2 metasomatism (Deer et al, 1985). Talc is stable in a binary H_2O-CO_2 fluid up to an $X(CO_2)$ of about 0,95. In the presence of magnesite, dolomite and calcite, respectively, the stability of talc is progressively reduced to more restricted portions of the T-$X(CO_2)$ diagram. Access of H_2O and CO_2 to ultramafic rocks is shown by the conversion of serpentinites to rocks consisting of talc + magnesite ± dolomite (Winkler, 1979).

According to Naldrett (1966), talc-carbonate alteration of ultramafic rocks is not to be confused with steatization. Both talc and carbonate are essential products of talc-carbonate alteration, whereas for steatization, talc is the main product and minerals such as chlorite, serpentine and carbonate are accessories.

Although steatitization may have played a role in the formation of talc at Uitkomst, the balance of evidence, especially the strong association of carbonate and talc, suggests that talc-carbonate alteration was the more probable alteration process. This is especially true for the mineralized zone, where talc and carbonate are well developed. The Main Harzburgite is dominated by serpentine as the secondary mineral after the primary magmatic silicate minerals.

4.4.2.4 Amphibole

The amphibole at Uitkomst is secondary in nature and occurs as rims around pyroxene **(Plate 7A)**, as anhedral grains, as elongated prismatic grains or as fibrous, spherulitic masses. Diamond shaped cross sections are common. Depending on the type of amphibole, the colour and pleochroism varies from colourless, colourless to lightgreen, green pleochroic and brown to green pleochroic. It has a lower relief than pyroxene with interference colours ranging from low first order (for tremolitic amphibole) to upper second order for hornblendes. Polysynthetic as well as simple twinning are common. The fibrous amphibole tends to grow into the sulphide grains. Amphibole

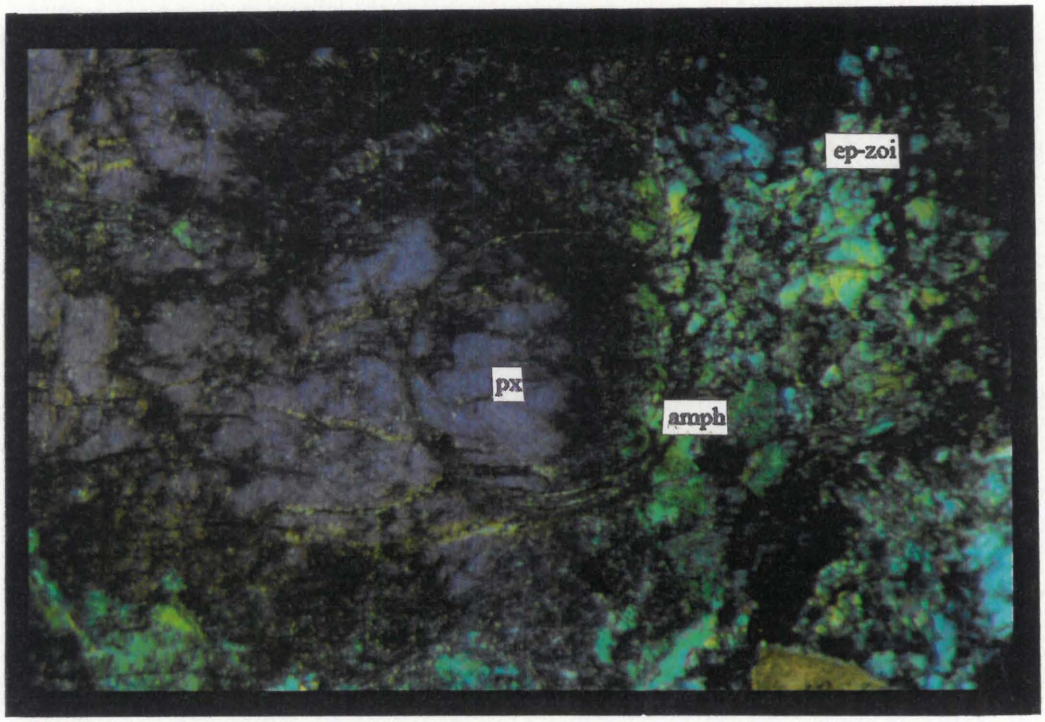

Plate 7 A: Pyroxene (px) (purple) replaced by amphibole (amph) (green) from the grain boundaries inwards. The amphibole forms a rim around the pyroxene. Epidote - zoisite (ep-zoi) occurs to the right. Sample 59/1, magnification x3.2, crossed polarizers.

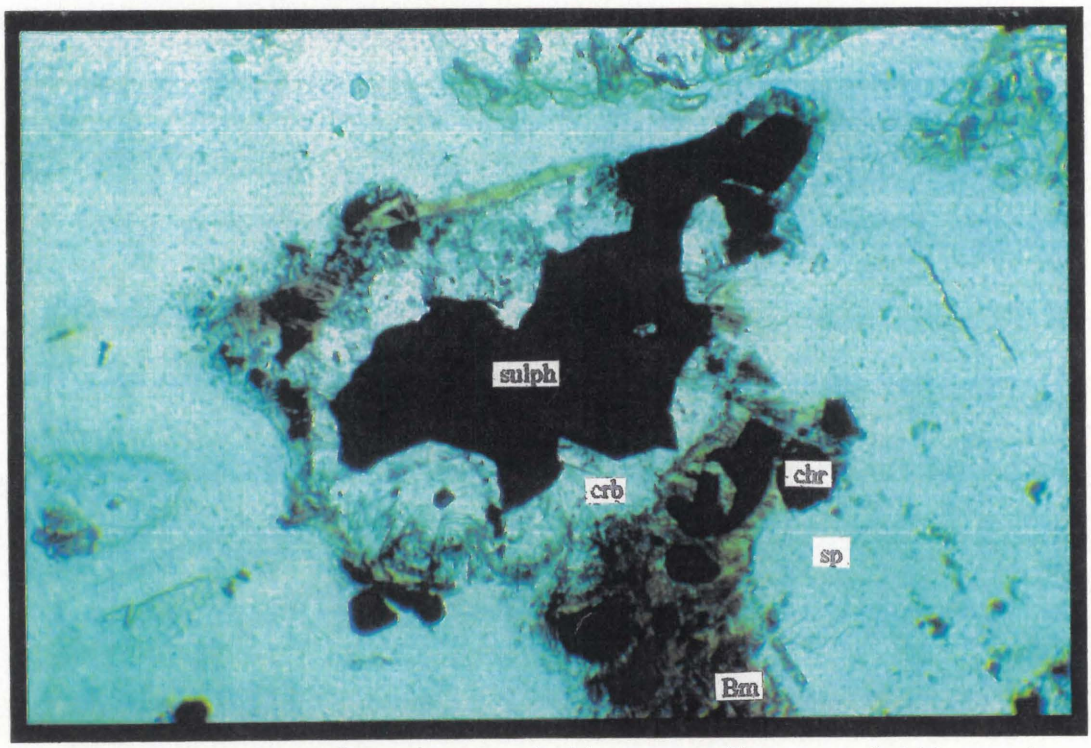

Plate 7 B: Grains of carbonate (crb) surrounding a sulphide grain. Brown phlogopite (bm) with chromite (chr) are in association with the carbonate and sulphide. Serpentine (sp) occurs in the background. Sample 1/3, magnification x10, plane polarized light.

usually alters to talc and chlorite and is commonly intergrown with carbonate and talc. Long, thin colourless needles of tremolite are also found in serpentine mesh centres.

Actinolite rimming pyroxene was also described by Deer et al (1985) and they conclude that the pyroxene is being marginally altered to amphibole by the pneumatolitic action of the residual H_2O-enriched magmatic fluids. This process is referred to as amphibolitization.

Microprobe analyses (Appendix B) were plotted on a diagram showing the amphibole subgroups with Na in the B-position versus Ca+Na in the B-position **(Figure 4.30).** This diagram indicates that most of the amphiboles are calcic with a few Fe-Mg-Mn amphiboles. These Fe-Mg-Mn analyses were classified as magnesio-cummingtonites **(Figure 4.31).**

Figure 4.30: Amphibole analyses plotted on a diagram showing the different amphibole subgroups, with Na in the B position versus Ca+Na in the B position.

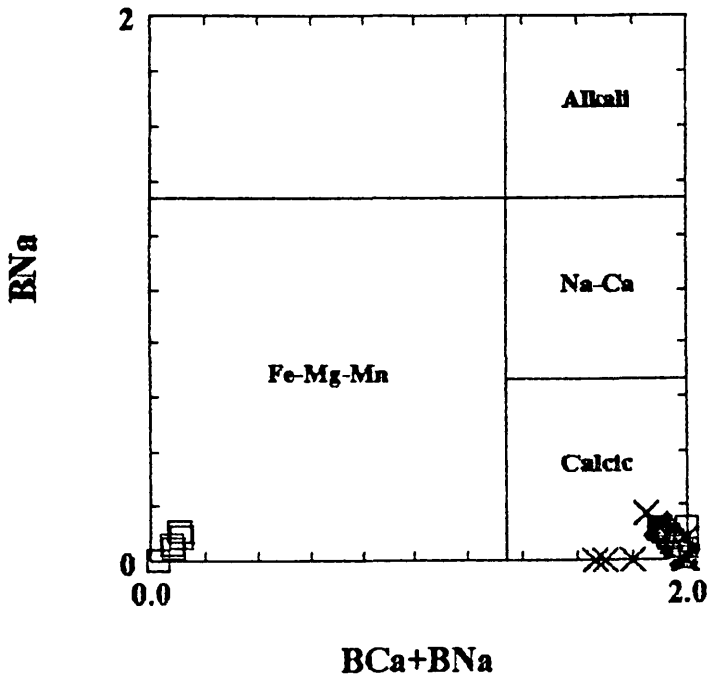

Figure 4.31: The series cummingtonite-grunerite with Si versus Mg/Mg+Fe.

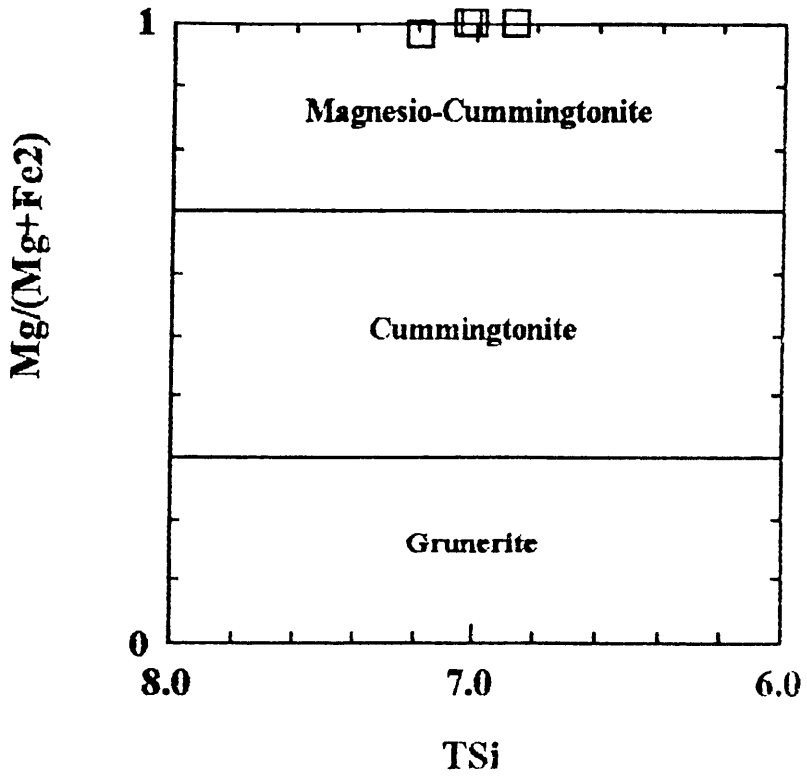

From **Figures 4.32, 4.33 and 4.34** it is clear that a wide range of calcic amphiboles occurs, namely, tremolite-ferroactinolite, tremolitic hornblende, actinolitic hornblende, magnesio-hornblende, edenite, edenitic hornblende, magnesian hastingsitic hornblende and hastingsite.

The tremolite-ferroactinolite occurs throughout the Chromitiferous Harzburgite, Lower Harzburgite and Basal Gabbro. Tremolitic varieties are usually colourless to light green whereas the ferroactinolite is pleochroic in shades of green. The tremolite occurs mostly in the Chromitiferous Harzburgite and Lower Harzburgite and becomes more actinolitic in the lower lithologies, where ferroactinolite occurs in the Basal Gabbro.

The tremolitic-, actinolitic- and magnesio-hornblende are found in the Chromitiferous Harzburgite and Lower Harzburgite, while the edenite and edenitic hornblende occur in the Lower Harzburgite, and the hastingsitic hornblende and hastingsite are prevalent in the Basal Gabbro. According to Robinson et al (1982) the progressive metamorphism of ultramafic rocks

Figure 4.32: Calcic amphiboles where (Na + K)A< 0.5 and Ti< 0.5.

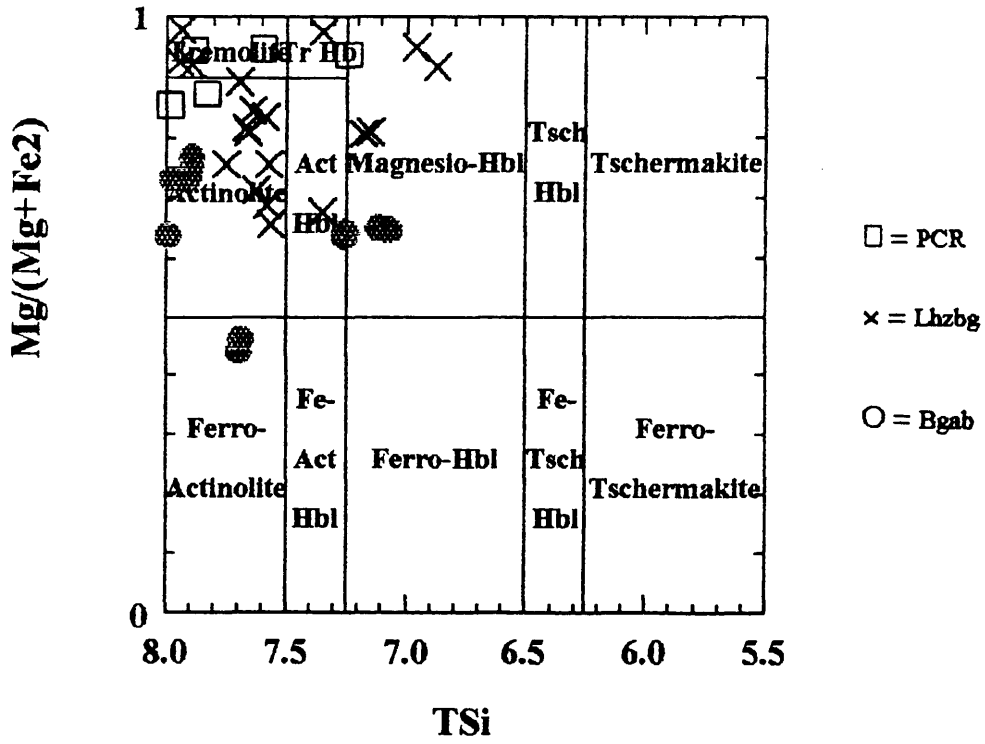

Figure 4.33: Calcic amphiboles where (Na + K)A> 0.5; Ti< 0.5 and Fe^3< Al^6.

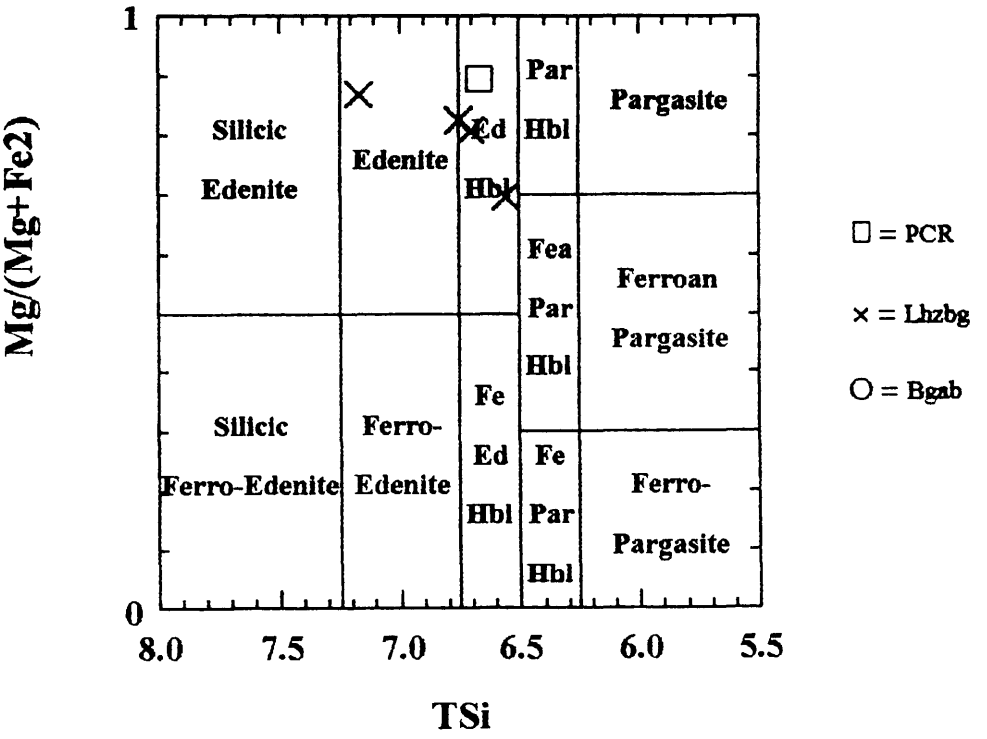

Figure 4.34: Calcic amphiboles were (Na + K)A> 0.5; Ti< 0.5 and Fe^3> Al^6.

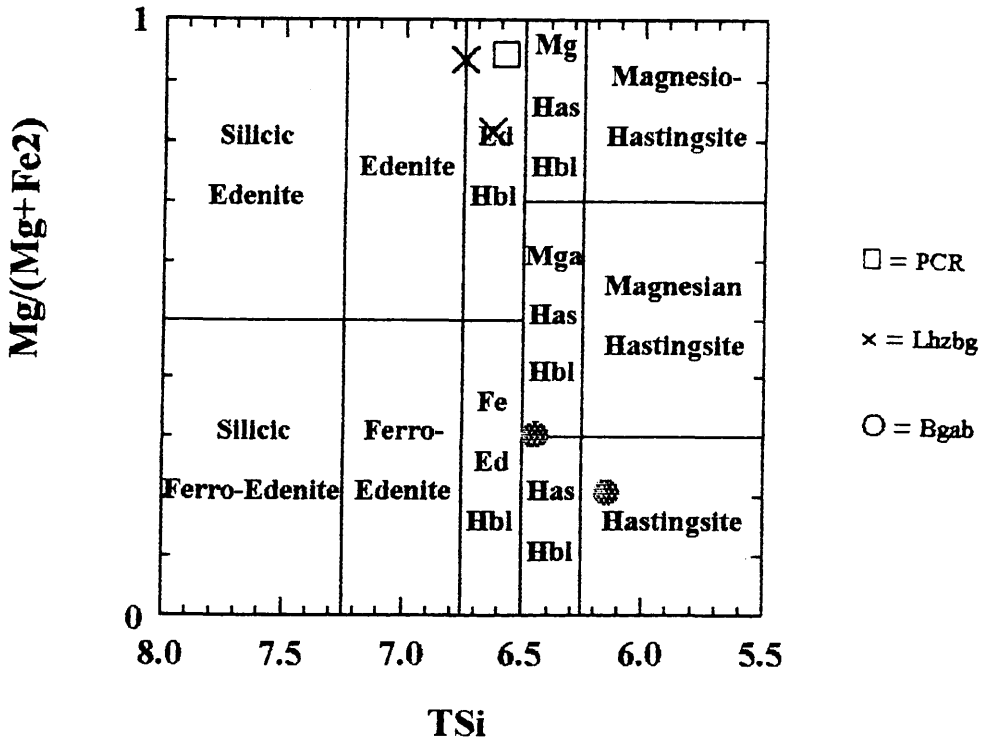

produces a continuous trend from tremolite, through tremolitic hornblende, magnesio hornblende and pargasitic hornblende to pargasite. For Uitkomst the more acceptable alternative is that the amphibole in the Basal Gabbro reflects the gabbroic nature of the latter unit relative to the more harzburgitic units higher up in the sequence. The range in amphibole described reflects therefore rock composition rather than P-T conditions of formation.

The magnesio-cummingtonite is found in the Chromitiferous Harzburgite together with tremolite-actinolite. Robinson et al, 1982 (op cit) also describes magnesio-cummingtonite in association with tremolite-bearing rocks where saturation in the tremolite component provides a chemical environment favourable for magnesio-cummingtonite.

It has already been mentioned that the amphibole tends to grow into the sulphide grains resulting in severe reduction of the effective grain size of the sulphide. The amphibole present in these intergrowths is Mg-rich, mostly tremolite-actinolite, tremolitic and magnesio-hornblende which occur as spherulitic aggregates or elongated blades. The more Fe-rich

hornblenditic amphibole is more prismatic and tends to have more regular contacts with the sulphide.

According to Bailey the Si-value of the amphibole formula is the compositional parameter most sensitive to metamorphic grade **(Table 15)**. The gradual change in Si-content from 8,0 (tremolite) to 6,0 (pargasite) is accompanied by a change in habit from slender prisms with excellent development of {*110*} prism faces, to stout prisms or equidimensional grains with poor development of prism faces. At the same time, colour in thin section changes from colourless to pale green or brown, and there is an increase in refractive indices.

Calcic and magnesian amphiboles have been shown to be stable over a range of P-T conditions in model ultramafic rock compositions. Tremolite, magnesio-hornblende and pargasite can be regarded as substituting for the clinopyroxene, whereas anthophyllite and magnesio-cummingtonite may be regarded as presenting the orthopyroxene. Replacement of pyroxene by amphibole indicates retrograde metamorphism of ultramafic rocks (Robinson et al, 1982).

Table 15: Calcic amphibole in metamorphic ultramafic rocks: Relation to metamorphic facies, critical mineral parageneses, aluminium phase, and typical Si-content of calcic amphibole (after Robinson et al, 1982).

Facies	Critical Paragenesis	Al-phase	Si Content
prehnite-pumpellyite	chrys + talc + tremolite	chlorite	
pumpellyite-actinolite	chrys + antig + tremolite	chlorite	
	chrys + antig + diopside	chlorite	8.0 to 7.9
greenschist and blueschist	brucite + antig + diopside	chlorite	
	olivine + antig + diopside	chlorite	
amphibolite and hornblende hornfels	olivine + antig + tremolite	chlorite	
	olivine + talc + tremolite	chlorite	
	olivine + Mg-amph + tremolite	chlorite/chromite	8.0 to 7.8
	olivine + opx* + tremolite	chlorite/chromite	7.9 to 7.5
	olivine + opx* + {tremolitic hornblende / Mg-hornblende}	spinel	7.6 to 6.5
granulite pyroxene hornfels eclogite (garnet lherzolite)	olivine + opx** + cpx {edenitic hornblende,	spinel	6.6 to 5.9
	olivine + opx** + cpx + {pargasitic hornblende,	plagioclase	
	olivine + opx** + cpx {or pargasite	garnet	

*CaO in opx: <0.20 wt.%; ** CaO in opx: 0.1 to 0.7 wt.%

4.4.2.5 Carbonate

The carbonates form a group of minerals in which the essential structural unit is the $(CO_3)^{-2}$ ion (Deer et al, 1985). This discrete $(CO_3)^{-2}$ ion may be considered as a single anion in structure, but it is in fact a trigonal planar complex with carbon in the centre of an equilateral triangle formed by three oxygens (Gribble and Hall, 1992).

The carbonate minerals at Uitkomst are colourless to brownish and show a high third order birefringe. Rhombohedric cleavage and twinning are observed. The carbonate forms aggregates and occurs usually in association with serpentine and talc as well as with amphibole. It is also interstitial to chromite. In some sections the carbonate replaces the olivine, or is intergrown with colourless phlogopite. Carbonate, in various amounts, is well distributed throughout all the lithologies, but in the Chromitiferous Harzburgite it forms a common assemblage with talc, chlorite and tremolite.

The carbonate shows a strong association with sulphide blebs or grains, enclosing them or being enclosed in the sulphide **(Plate 7B).** Where it encloses sulphide, it usually forms a buffer protecting the sulphide from intergrowth with the fine serpentine crystals.

Qualitative microprobe analyses (n = 20) of the carbonate show that it is mostly dolomitic (Ca and Mg with lesser Fe), with minor calcite (Ca) and magnesite (Mg with lesser Ca and Fe).

4.4.2.6 The Epidote Group

Members of the epidote group crystallize in both the orthorombic and monoclinic systems. Their structure consists of chains of AlO_6 and $AlO_4(OH_2)$ octahedra linked by independent SiO_4 and Si_2O_7 groups. Zoisite is the orthorombic member, while clinozoisite and epidote are monoclinic. The group formula is : $X_2Y_3Z_3\ (O,OH,F)_{13}$

Epidote shows a colourless to yellowgreen pleochroism with bright third order interference colours. Zoisite-clinozoisite are colourless with anomalous blue and yellow interference colours.

At Uitkomst the epidote group minerals are largely confined to the Lower Harzburgite, but were also noted in the Main Harzburgite and Chromitiferous Harzburgite. Their occurrence is usually associated with the saussuritization of plagioclase due to late stage hydrothermal action. Clusters of epidote were also seen associated with amphiboles. Epidote may form from the breakdown of amphiboles in basic igneous rocks.

Microprobe analyses of the epidote-group minerals (Appendix B) show the presence of both epidote and clinozoisite-zoisite and compare well with those presented in Deer et al, 1985.

4.4.2.7 Quartz

Quartz is a minor constituent of the Uitkomst rocks and was only noted in four sections in the Chromitiferous Harzburgite, Lower Harzburgite and Basal Gabbro. In one section (UD 34/9), the quartz is intergrown with plagioclase **(Plate 7C).** Micropegmatite typically is the product of eutectic crystallization and such intergrowths have been considered to result from the simultaneous crystallization of alkali feldspar and quartz (Deer et al, 1985).

4.4.2.8 Chrome-bearing mica

In one section appreciable amounts of chromium were found in what seems as fuchsitic micas (analyses 37 and 50; Appendix B). The one mica is colourless and occurs as relatively coarse-grained spherulites in carbonate grains (34/1). The second mica is light peppermint green in colour and forms a mass of very fine grained needles around chromite schlieren (34/1-11D). This section consists mostly of chromite, carbonate, amphibole and these chrome-rich micas.

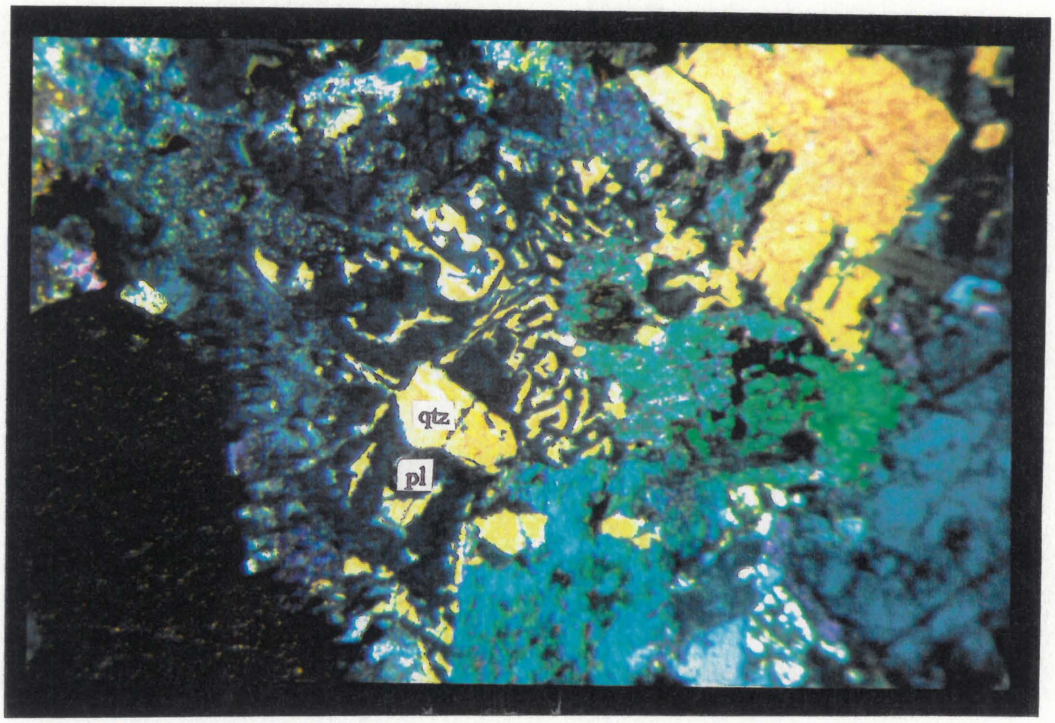

Plate 7 C: A plagioclase-quartz intergrowth. The section is thicker than usual, hence the orange interference colour of quartz. Sample 34/9, magnification x3.2, crossed polarizers.

4.4.3 Quantitative estimation of secondary minerals

In **Table 16** the normalized intensity ratios (NIR) and volume percentage sulphide for the secondary minerals in borehole 45 are listed.

To be able to do quantitative comparisons between the secondary minerals and the sulphide it was necessary to convert the sulphide volume percent to sulphide mass percent and to express the NIR's in terms of the non-sulphide fraction in each sample. For these calculcalculations the average densities of the sulphide and silicate fractions were taken as 4.6 and 2.9, respectively. The corrected values are listed in **Table 17** and have been used in the graphical presentations.

Table 16: The depth (m), normalized intensity ratio (NIR), and volume percentage sulphide of the samples used for X-ray diffraction.

Sample no:	Depth:	Volume % sulphide:	Talc:	Amphibole:	Serpentine -chlorite:	Calcite:	Mica:
	(m)		(NIR)	(NIR)	(NIR)	(NIR)	(NIR)
45/A	18	1.48	0.73	0	1.59	0.11	0
45/B	24	0	0.82	0	1.08	0	0
45/C	29	1	0.47	0.2	1.66	0.38	0
45/D	33	3.2	0	0.24	1.29	0.19	0
45/1	41	5.38	0	0.36	1.56	0	0.14
45/2	46	2.2	2.41	0.6	1.21	0	0
45/3	55	8.36	0.29	1.05	2.4	0.2	0.13
45/4	63	8.92	0.3	0.69	0.7	0.76	0
45/5	68	24.09	0	0.9	0.29	0.54	0.14
45/E	99	6.26	0.507	1.41	1.35	0.29	0
45/F	105	0.72	0.45	2.32	0.34	0.17	0.85
45/G	109	0.25	0	0.72	0.18	0	0.65
45/H	111	0.15	0	1.95	0.46	0	0.16
		mean	0.46	0.80	1.09	0.20	0.16
		minimum	0	0	0.18	0	0
		maximum	2.41	2.32	2.4	0.76	0.85

Table 17: The corrected values for normalized intensity ratio (NIR), and mass percentage sulphide of the samples used for X-ray diffraction.

Sample no:	Depth:	Mass % sulphide:	Talc:	Amphibole:	Serpentine-chlorite:	Calcite:	Mica:
			(NIR)	(NIR)	(NIR)	(NIR)	(NIR)
45/A	18	2.33	0.75	0.00	1.63	0.11	0.00
45/B	24	0.00	0.82	0.00	1.08	0.00	0.00
45/C	29	1.58	0.48	0.20	1.69	0.39	0.00
45/D	33	4.90	0.00	0.25	1.36	0.20	0.00
45/1	41	7.97	0.00	0.39	1.70	0.00	0.15
45/2	46	3.42	2.50	0.62	1.25	0.00	0.00
45/3	55	11.86	0.33	1.19	2.72	0.23	0.15
45/4	63	12.56	0.34	0.79	0.80	0.87	0.00
45/5	68	27.95	0.00	1.25	0.40	0.75	0.19
45/E	99	9.16	0.56	1.55	1.49	0.32	0.00
45/F	105	1.15	0.46	2.35	0.34	0.17	0.86
45/G	109	0.40	0.00	0.72	0.18	0.00	0.65
45/H	111	0.24	0.00	1.95	0.46	0.00	0.16

To see the variation of the proportion of each mineral, the corrected NIR values were plotted against depth. From these graphs **(Figures 4.35, 4.36, 4.37, 4.38, 4.39)** it is evident that serpentine-chlorite **(Figure 4.35)** shows a decreasing trend from the Mhzbg towards the Bgab whereas amphibole **(Figure 4.36)** exhibits an increasing trend from the Mhzbg to the Bgab reaching a maximum in the Lhzbg. Maximum values for calcite **(Figure 4.37)** occur in the Lhzbg. Talc **(Figure 4.38)** occurs throughout the Complex with a maximum value in the PCR. Mica **(Figure 4.39)** increases towards the Bgab with a maximum in the Lhzbg.

Figure 4.35: The corrected NIR for serpentine-chlorite versus depth (m) in borehole UD 45.

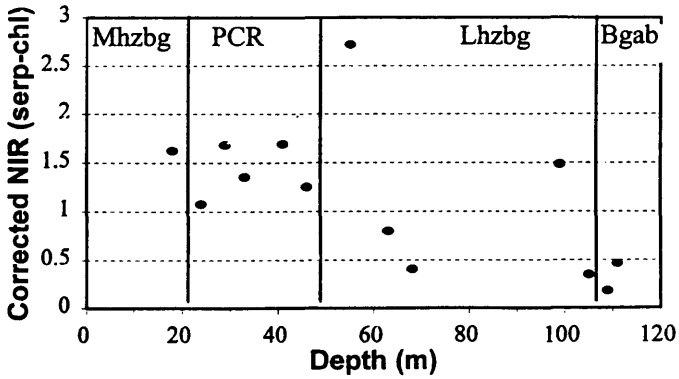

Figure 4.36: The corrected NIR for amphibole versus depth (m) in borehole UD 45.

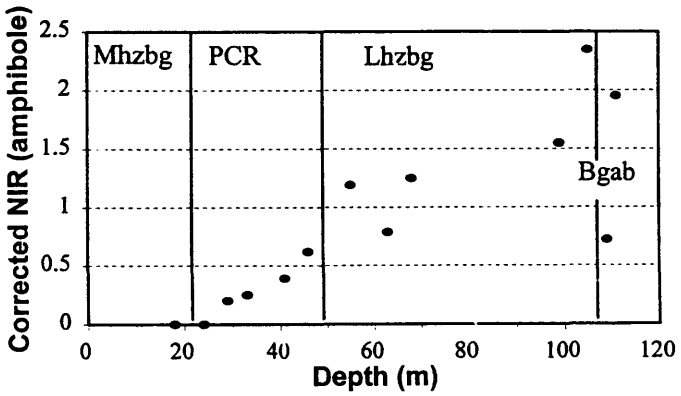

Figure 4.37: The corrected NIR for calcite versus depth (m) in borehole UD 45.

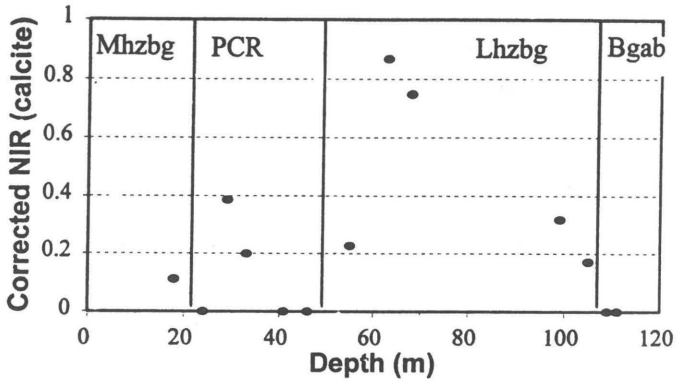

Figure 4.38: The corrected NIR for talc versus depth (m) in borehole UD 45.

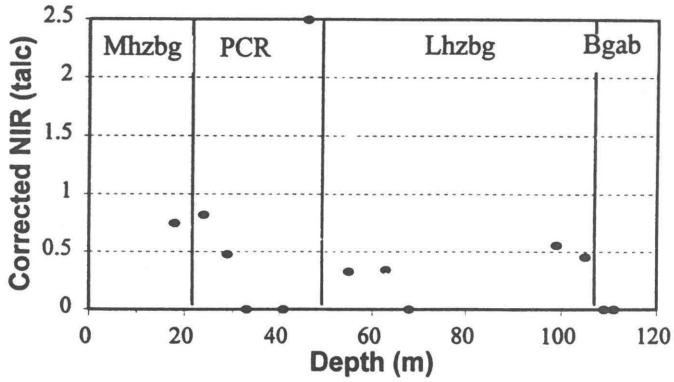

Figure 4.39: The corrected NIR for mica versus depth (m) in borehole UD 45.

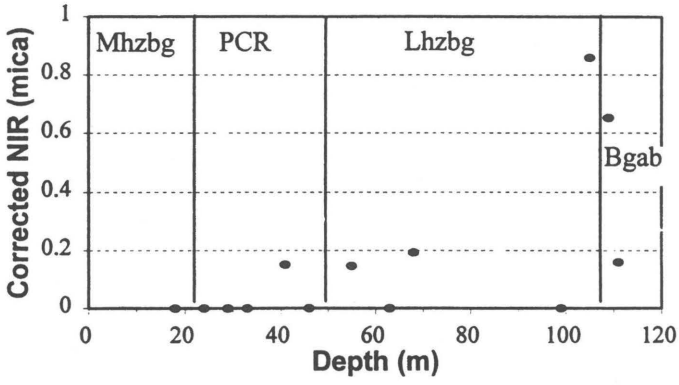

In **Figures 4.40, 4.41, 4.42, 4.43, and 4.44** the mass percentage sulphide is plotted against the corrected NIR's of each mineral. Serpentine-chlorite **(Figure 4.40)** and talc **(Figure 4.43)** do not show a discernible trend with mineralization, whereas amphibole **(Figure 4.41)** and calcite **(Figure 4.42)** exhibit a crude correlation with mineralization. Mica **(Figure 4.44)** exhibits maximum values at low mass percentages of sulphide.

Figure 4.40: Mass per cent sulphide plotted against the corrected NIR for serpentine-chlorite in borehole UD 45.

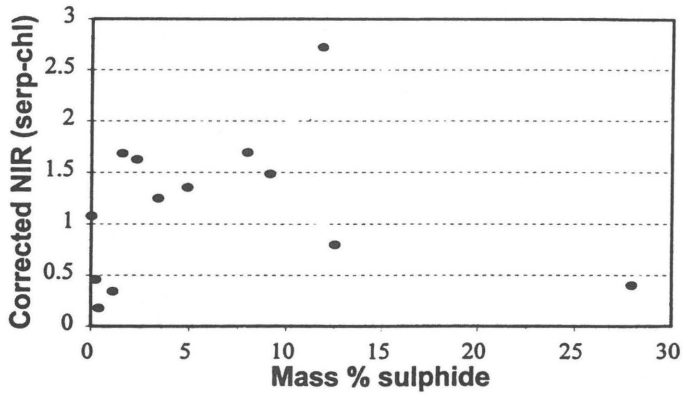

Figure 4.41: Mass per cent sulphide plotted against the corrected NIR for amphibole in borehole UD 45.

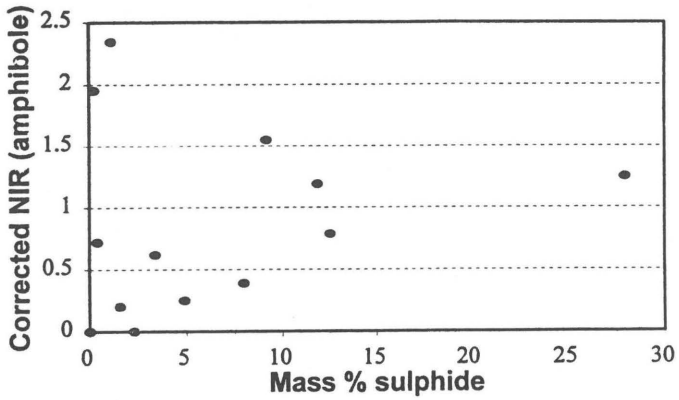

Figure 4.42: Mass per cent sulphide plotted against the corrected NIR for calcite in borehole UD 45.

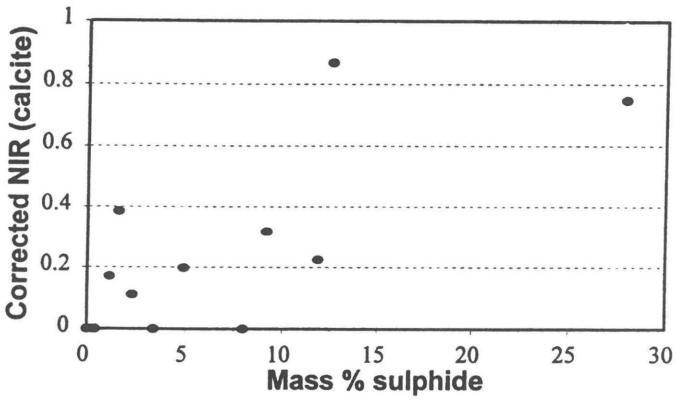

Figure 4.43: Mass per cent sulphide plotted against the corrected NIR for talc in borehole UD 45.

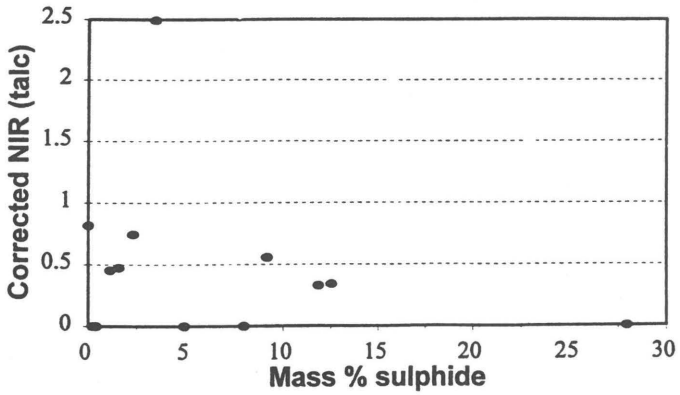

Figure 4.44: Mass per cent sulphide plotted against the corrected NIR for mica in borehole UD 45.

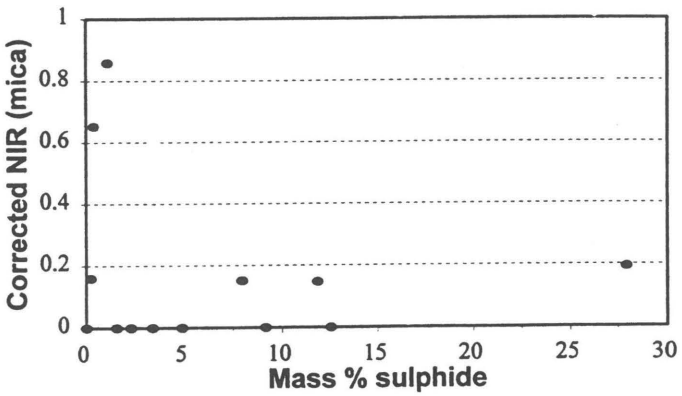

From this exercise it is possible to conclude that serpentine-chlorite dominates the upper part of the mineralized zone and decreases towards the base. Amphibole dominates the lower part of the mineralized zone and decreases towards the top. Calcite is more prominent in the Lower Harzburgite and Chromitiferous Harzburgite and mica increases towards the base of the Complex. Talc occurs throughout the mineralized zone. A crude correlation exist between mineralization and the occurrence of calcite and amphibole.

5: Discussion

5.1 Chemical variation in the sulphide and associated silicate minerals

The data presented in the previous sections show that the primary and secondary silicate minerals are enriched in Fe towards the base of the Complex (Basal Gabbro). The amphibole has a more complex chemistry in the Basal Gabbro than higher up in the sequence and the Cu/Ni ratios of the sulphides increase towards the Basal Gabbro. These features suggest that the early injections of magma cooled rapidly against the country rocks, thus giving rise to more gabbroic rock towards the basal contact of the intrusion. Higher up in the sequence the cooling rate was much lower which allowed more complete fractional crystallization. Accordingly, the bulk chemistry of the rocks changed from gabbroic (Basal Gabbro) to harzburgitic/dunitic (Lower Harzburgite, Chromitiferous Harzburgite, and Main Harzburgite) higher up in the sequence. The observed mineralogy and geochemistry in the primary and secondary minerals, as well as the Cu/Ni ratio reflect the change in chemistry of the bulk rocks.

5.2 Alteration and sulphide mineralization

From the mineral descriptions reported here, it is evident that the Main Harzburgite and mineralized zone of the Uitkomst Complex has been subjected to secondary alteration. Microscopic investigations and X-ray diffraction work confirm that:

* serpentinization was the dominant alteration process in the Main Harzburgite
* the Chromitiferous Harzburgite is characterized by tremolite-talc-carbonate and talc-chlorite-carbonate alteration.
* the Lower Harzburgite is altered by saussuritization, amphibolitization and lesser serpentinization.
* intense amphibolitization and saussuritization took place in the Basal Gabbro.

These alteration processes were also mentioned by Gauert et al (1995).

The introduction of H_2O under metamorphic conditions converts ultramafic rocks into serpentinites, consisting mainly of serpentine with minor amounts of talc, quartz, brucite and magnetite, while an admixture of CO_2

in the fluid results in the formation of talc and carbonate (Winkler, 1979). In the Main Harzburgite the alteration minerals consist mainly of serpentine, while in the Chromitiferous Harzburgite and lower down carbonate, talc, chlorite, amphibole and lesser serpentine form the dominant alteration minerals. The occurrence of abundant talc and carbonate in the mineralized zone, but not in the Main Harzburgite, suggests the development of a distinctly different late stage alteration environment for the mineralized zone. A deuteric, CO_2-rich fluid is postulated for the lower three lithologies, whereas a H_2O-rich deuteric fluid was probably responsible for the serpentinization of the Main Harzburgite. The crude correlation that exists between the quantity of carbonate and the sulphide mineralization **(Figure 4.42)** in the mineralized zone supports this hypothesis and is also in agreement with the postulation of Gauert et al, 1996, that dolomite was assimilated by the intruding magma.

It should be emphasized, however, that it is not implied that the spatial relation of the sulphide minerals and the secondary silicates and carbonate is an indication that the mineralization is a result of alteration. The sulphide, as suggested by Gauert et al, 1996, was precipitated under high CO_2 partial pressures and the latter also finally, in the deuteric stage, caused the secondary alteration of the primary minerals.

5.3 Beneficiation of the sulphide

5.3.1 Overview of flotation as beneficiation process

According to Tomanec and Milovanovic (1994) most of the industrial plants for mineral processing use mainly electric power. The most important concentration operations are virtually all physical in nature and involve crushing and grinding, surface conditioning, physical separation (concentration) of the minerals, and de-watering processes such as thickening, filtering and drying. Cohen (1983) concludes that crushing and grinding account for more than 30- 50 per cent of the total power used in the concentration process, but this can rise as high as 70 per cent for hard and/or finely dispersed and intergrown ores. Crushing is relatively cheap in energy terms, but grinding is the most energy-intensive step in mineral processing, and the least efficient. Liberation of economic minerals from a low grade and texturally complex ore necessitates very fine grinding and very high energy consumption.

Figure 5.1 shows the dramatic increase of grinding energy as the product size required for liberation decreases below about 100 mm (Cohen, 1983). The main purpose of grinding is mineral liberation from complex ores at the coarsest possible grind. The product size directly depends on the grain size of the ground ore (Tomanec and Milovanovic, 1994). Mineral liberation is accomplished by grain size reduction until the grain (crystal aggregates) of the desired mineral have become separated and free from accessory minerals to the degree to be efficiently concentrated into a product of specific qualities. A significant liberation will only begin when the mean size of the particles reaches the same or lower magnitudes than the mean size of the grains in the ore (Tomanec and Milovanovic, 1994).

Figure 5.1: The effects of product size on the specific energy required for cominution (after Cohen, 1983).

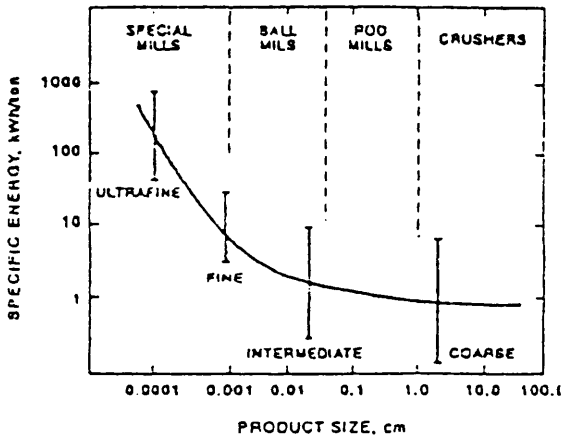

According to Herrera-Urbina et al (1990) flotation involves the interaction of a mineral with amphipathic surfactants, which are called collectors in flotation terminology, that adsorb at the solid/solution interface and make the attachment of an air bubble to the mineral surface thermodynamically favourable. When an air bubble is attached to a particle, the particle floats. The surfaces of the particles can be chemically classified as sulphur-deficient and sulphur-rich depending on the relative abundance of sulphur atoms **(Table 18).** The sulphur-rich surfaces (class A, **Table 18**) have been found to respond well to flotation with thiol collectors. The sulphur-deficient group (class B, **Table 18**) responds poorly to thiol flotation or does not float at all.

Table 18: Classification of sulphide minerals based on the relative abundance of surface sulphide sites (Herrera-Urbina, 1990).

Sulphur-rich surfaces class A	Sulphur-deficient surfaces class B
Pyrrhotite	Wurtzite
Marcasite	Sphalerite (Blende)
Arsenopyrite	Niccolite
Pyrite	Bismuthinite
Cinnabar	Stibnite
Molybdenite	Tetrahedrite
Covellite	
Chalcocite	
Bornite	
Galena	
Chalcopyrite	
Realgar	

From Wellham et al (1992), fast and slow floating minerals can be separated by the staged addition of a collector. The fast floating minerals, for which no collector is needed, are first floated off. Then, starting with low concentrations, the collector is increased in stages until the maximum amount of collector is needed for the slowest floating mineral. Thus, at low collector dosages the fast floating minerals are recovered, whereas at high collector dosages the slows are recovered.

According to Agar (1991) the mineralogical composition of individual ores, and in particular the gangue minerals, have an important impact on the method of treatment required to maximize the recovery of valuable constituents while rejecting the optimum amount of gangue.

According to Edwards et al (1980) serpentine forms slime coatings on the sulphide surface. These positively charged slimes such as chrysotile and lizardite were found to severely reduce the flotation of negatively charged pentlandite. Changing the polarity of the slimes surface charge reduces or eliminates the depression effect by preventing slime coating. Edwards et al (1980) found that the addition of a small amount of chrysotile to the flotation pulp (0.05 g/l) dramatically decreased the pentlandite flotation recovery from 90 per cent to 5 per cent, whereas the effect of lizardite was much less. According to Wellham et al (1992) nickel sulphide flotation is depressed by slime coating of magnesia-bearing

gangue minerals (serpentine, talc, tremolite), and carboxy methyl cellulose (CMC) does not disperse these slimes sufficiently at an economically viable dosage. The CMC acts as a slime dispersant by activating the Ni (Edwards et al, 1980; Pugh, 1989) but the dosage required to achieve satisfactory nickel recovery is uneconomically high. Ten percent sodium chloride, compared to CMC, give superior results particularly in the flotation of fine material.

Iwasaki (1988) describes pyrrhotite as an iron deficient iron sulphide ($Fe_{1-x}S$) which occurs either in monoclinic or hexagonal forms. According to him, monoclinic pyrrhotite is richer in sulphur and ferromagnetic, whereas hexagonal pyrrhotite is non- or weakly magnetic and poorer in sulphur. The ferromagnetic properties of natural pyrrhotites increase with increasing sulphur content (Grønvold and Haraldson, 1952). Agar (1991) concludes that the rejection of pyrrhotite is important to the control of sulphur emissions, because virtually all of the sulphur that is contained in the flotation concentrate is emitted from the smelter as sulphur dioxide. Cost studies (Bruce and Orr, 1986) have revealed that the rejection of pyrrhotite is the most cost-effective method of reducing SO_2 emissions. Pyrrhotite is also notoriously reactive and generates acidic tailing water which must be treated with lime to neutralize the water for recycling and to control dissolved metal ion concentrations (Agar, 1991). Non-magnetic pyrrhotite is known to be more floatable than magnetic pyrrhotite and hence the combination of flotation and magnetic separation may be utilized to maximize the recovery or the rejection of this mineral (Boldt and Queneau, 1967; Kubo, 1957).

The very fine-grained nature of flame pentlandite makes liberation from pyrrhotite difficult. Reducing the Ni-losses in the tailings can only be obtained by increasing the liberation of pentlandite from pyrrhotite by additional grinding, and improving the recovery of the pentlandite fines (the poor Ni-recoveries in the very fine particles [<10 micron] is due to the poor recovery of fine free pentlandite) (Sizgoric and Alcock, 1981). Additional grinding is very expensive, so it is very important to know how much Ni is lost to the tailings. If it is a very small percentage (e.g. between 1-5 per cent in the Main Harzburgite, Chromitiferous Harzburgite and Lower Harzburgite from work done in this

thesis), additional grinding to liberate these small particles would not be economically viable.

5.3.2 Expected performance of the Uitkomst ore during beneficiation

As previously mentioned, the sulphide mineralization at Uitkomst varies from net-textured ore as well as blebs, stringers, and irregular aggregates in a silicate matrix to massive ore. The massive sulphide ore is not discussed in this study. Several mineral intergrowths, which will have a bearing on the beneficiation of the ore are present in the Uitkomst ore. The intergrowths are:

* magnetite rims on pyrrhotite, pentlandite and chalcopyrite
* mackinawite with granular pentlandite
* violarite with granular and flame pentlandite
* flame pentlandite with pyrrhotite
* serpentine, tremolite, talc and chlorite with sulphide

From previous experience it is believed that the occurrence of platy and fibrous alteration minerals like serpentine, amphibole and talc in a rock usually causes the rock to be tough and more resistant to grinding. This could result in higher energy consumption during comminution.

The magnetite which is intergrown with pentlandite and chalcopyrite could interfere with flotation of the economic sulphide **(Plate 8A).** On grinding, the grains could retain magnetite as a shield that interferes with their floatability. The extent to which this may be a problem depends on the specific flotation strategies followed, and on the level of the alteration in the mineralized zone. Secondary magnetite is more prevalent where the secondary alteration of the silicate minerals is most intense.

The mackinawite at Uitkomst is extremely fine and in complex intergrowth with pentlandite, and would, for the most part, not be liberated from pentlandite during grinding. Since the pentlandite can contain up to 30 per cent mackinawite, the Ni-content of the composite pentlandite-mackinawite grains could be as low as 25 per cent. The net effect of this dilution of the pentlandite would be to reduce the nickel grade of the concentrate (Sizgoric and Alcock, 1981). This is also true for violarite replacing pentlandite.

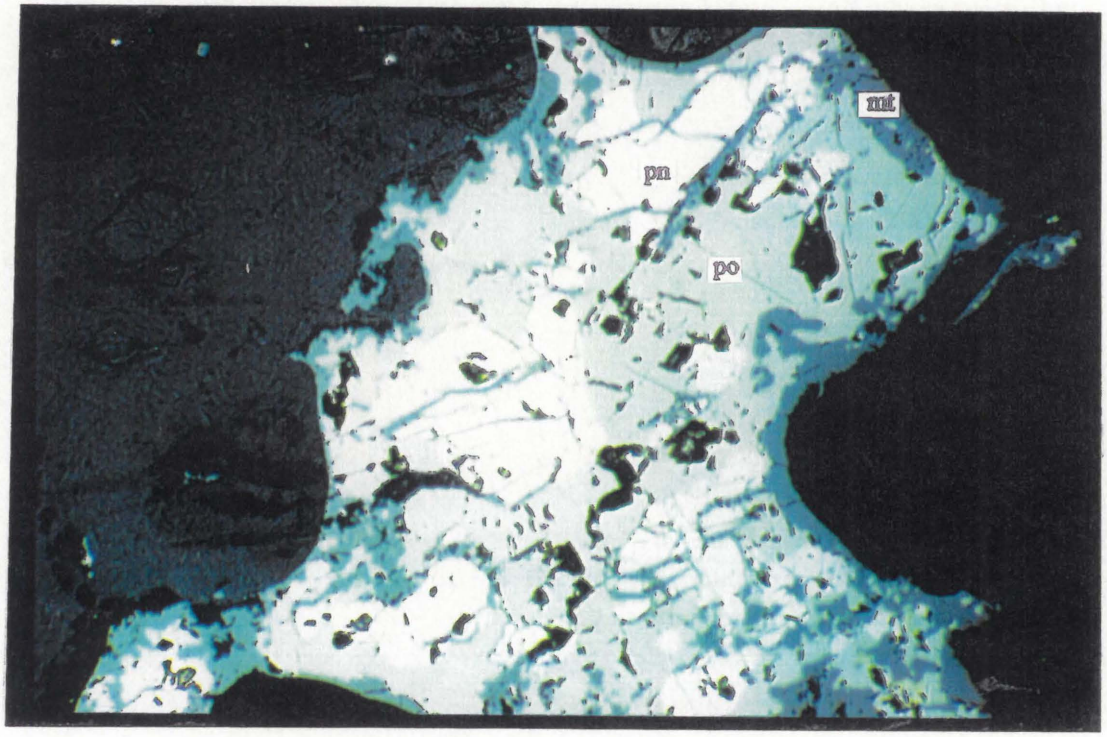

Plate 8 A: Pyrrhotite (po) with granular pentlandite (pn) surrounded by a rim of magnetite (mt). The magnetite also occurs in the cleavage of the granular pentlandite. Sample 45/1, magnification x20, plane polarized light.

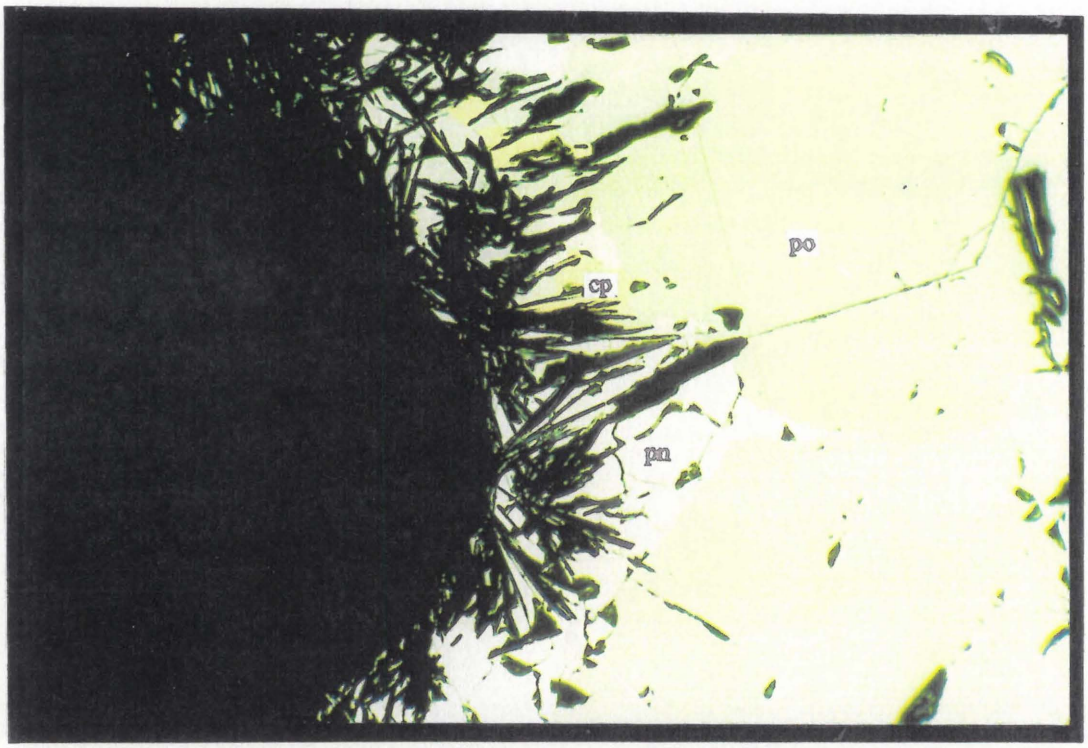

Plate 8 B: Pyrrhotite (po) with granular pentlandite (pn) and chalcopyrite (cp) occurring on the side of the pyrrhotite grain. Silicate needles are intergrown with the sulphide, resulting in grain size reduction of pentlandite and chalcopyrite. Sample 34/4, magnification x20, plane polarized light.

Serpentine, talc, chlorite and amphibole are finely intergrown with the sulphide grains in the Uitkomst ore. This has an implication for the beneficiation of the sulphide. Firstly, these intergrowths tend to increase sliming of the sulphide, thus reducing sulphide recovery. Secondly, because of this fine intergrowth between sulphide and silicate, the silicate tends to coat the sulphide and thereby reduces its floatibility **(Plate 8B).**

Microscopic investigation of the silicate-sulphide intergrowth reveals that fine serpentine needles are most commonly intergrown with the sulphide grains, with lesser talc, amphibole, and chlorite **(Plate 8C, 8D).** The serpentine is mostly found in the Main Harzburgite, but also occurs as a subordinate constituent in the other lithologies. Where carbonate occurs in association with the sulphide, it forms a rim around the sulphide which acts as a barrier against the intergrowing serpentine needles **(Plate 9A, 9B).** The fibrous varieties of amphibole like tremolite-actinolite, tremolitic-, and magnesio-hornblendes concentrated in the Chromitiferous Harzburgite and Lower Harzburgite cause more severe reduction of the sulphide grain sizes than the more prismatic hornblendes located towards the base of the Complex.

Talc is known to be naturally hydrophobic and it is readily floated with only a frother. The talc content has a much greater influence on the flotation results than would be expected from its content in the ore. When nothing is done to suppress the flotation of talc the rougher flotation froth is extremely voluminous and there does not appear to be any sulphides present (Agar, 1991). Where talc is intergrown with sulphide, it adheres itself to the sulphide surface because of its platy nature, thereby reducing the floatibility of the sulphide.

The fact that pyrrhotite is highly reactive and generates acidic water (Agar, 1991) has definite implications for the environment. De Waal (1984) describes the transformation of pyrrhotite to marcasite as a very rapid reaction that can be simulated in the laboratory within days. This will have to be kept in mind in the placement of the flotation tailings dumps.

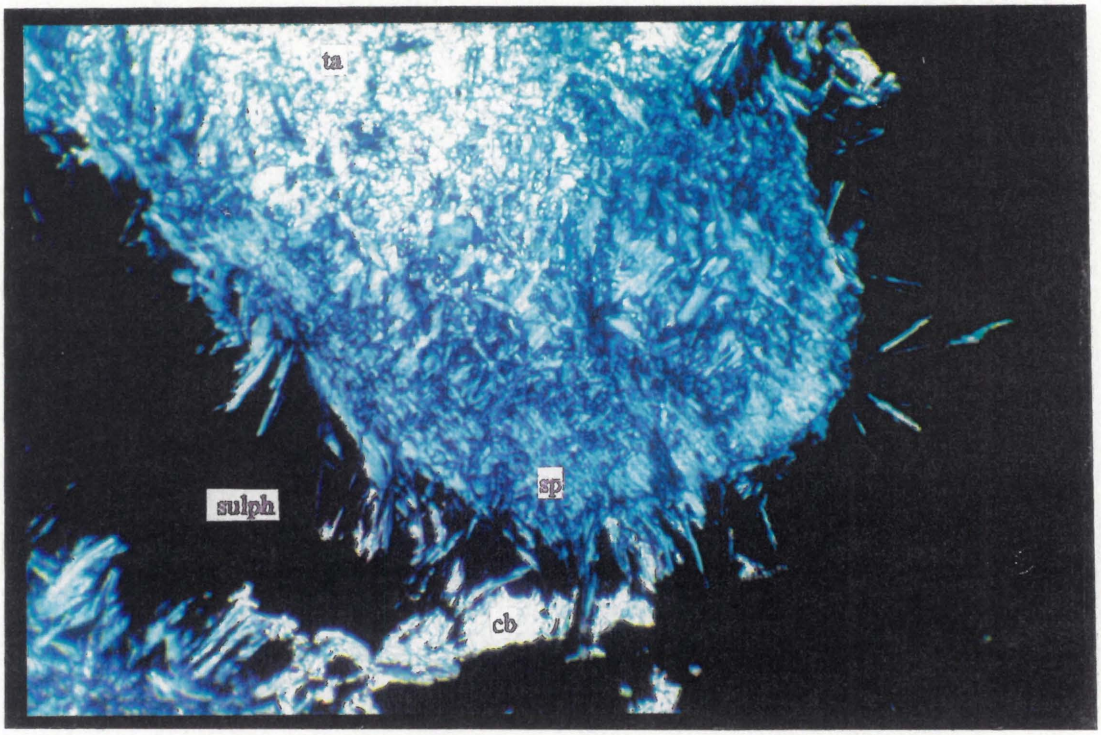

Plate 8 C: Needles of serpentine (sp) growing into sulphide (sulph). Carbonate (crb) occurs in the sulphide and talc (ta) in the serpentine. Sample 34/4, magnification x10, crossed polarizers.

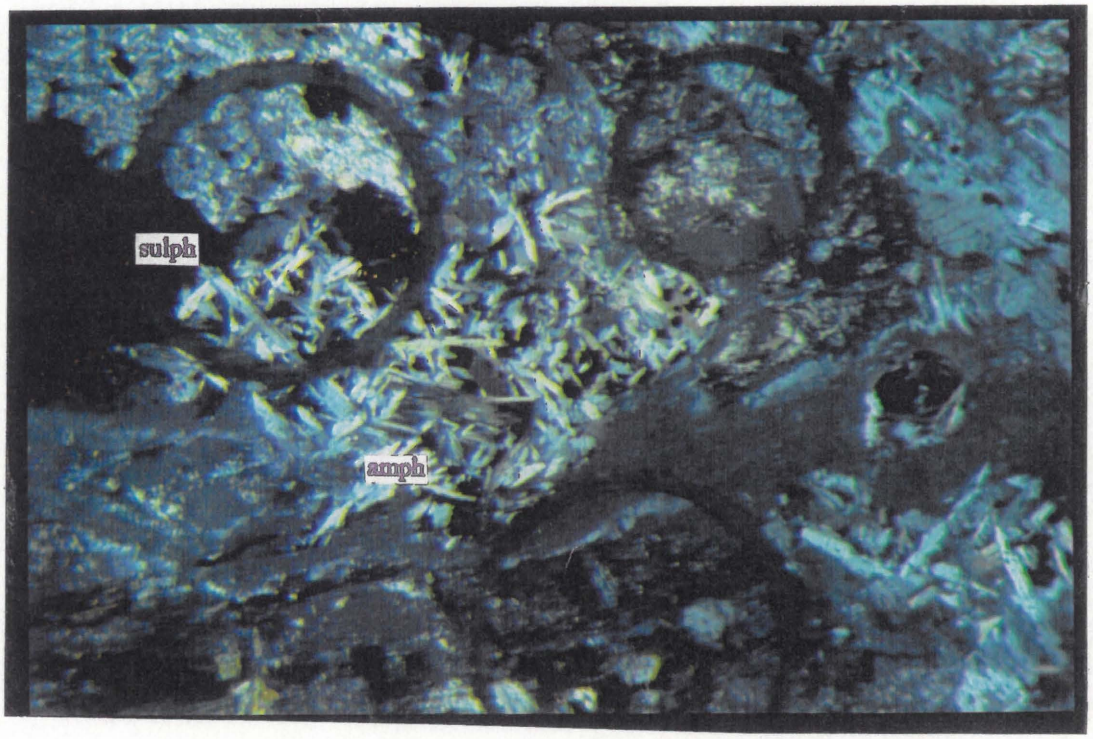

Plate 8 D: Colourless, diamond-shaped shards of amphibole (amph) growing into the sulphide (sulph). Sample 64/7, magnification x3.2, crossed polarizers.

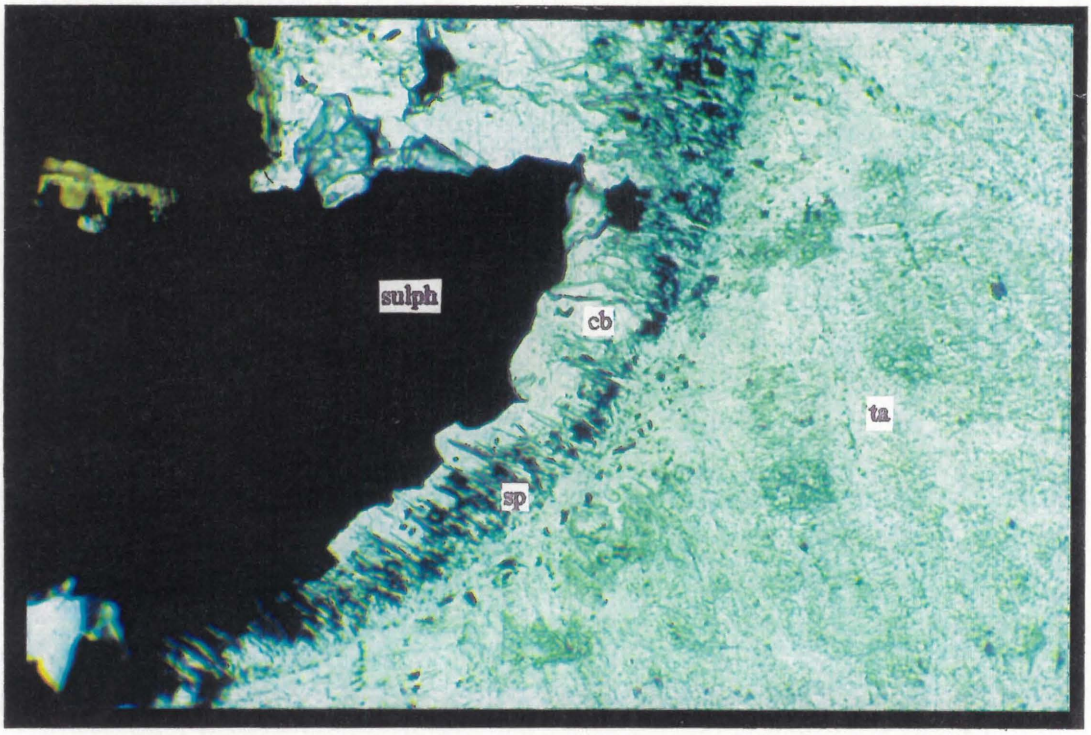

Plate 9 A: Sulphide (sulph) surrounded by carbonate (cb) with needle-like serpentine (sp) growing into the carbonate. The carbonate seems to act as a buffer, thus preventing sulphide-silicate intergrowth. Talc (ta) occurs around the serpentine. Sample 1/3, magnification x10, plane polarized light.

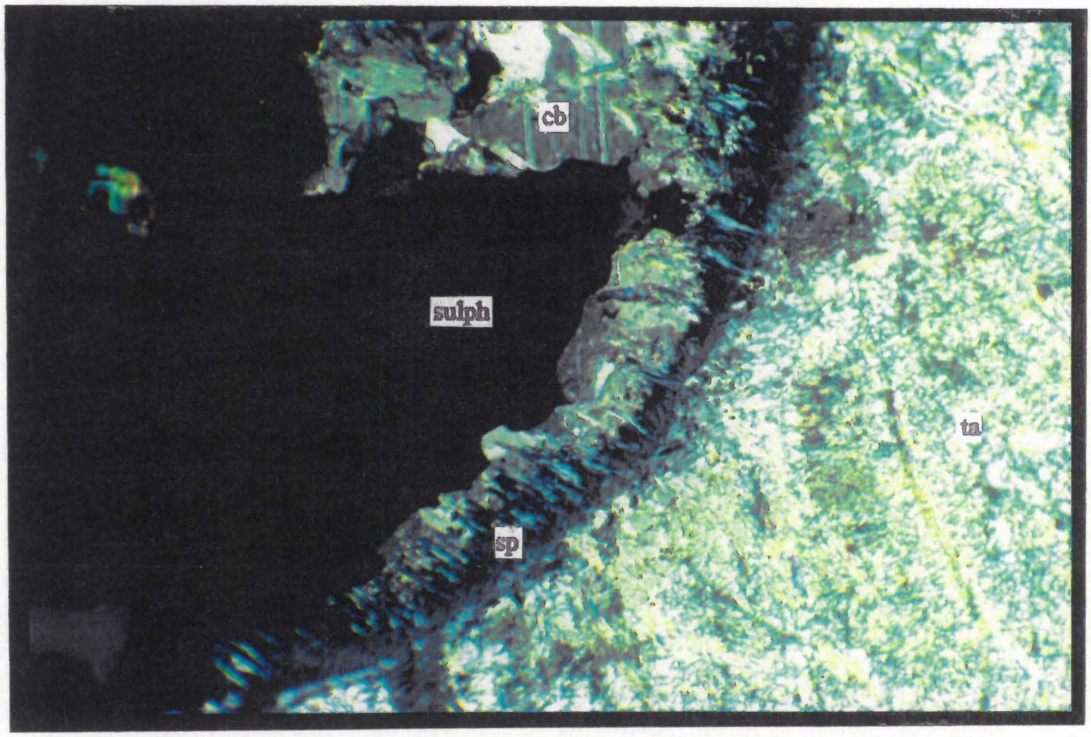

Plate 9 B: Sulphide (sulph) surrounded by carbonate (cb) with needle-like serpentine (sp) growing into the carbonate. The carbonate seems to act as a buffer, thus preventing sulphide-silicate intergrowth. Talc occurs around the serpentine. Sample 1/3, magnification x10, crossed polarizers.

6. Conclusions

* The sulphide mineralization at Uitkomst occurs as massive and net-textured ore as well as blebs, stringers, and irregular aggregates in a silicate matrix.

* The primary sulphide assemblage consists of pyrrhotite, pentlandite and chalcopyrite with cubanite, mackinawite, pyrite, millerite, violarite and cobaltite occurring with the primary assemblage at given depths in the Complex. The assemblages comprise of po + pn + cp; po + pn + cp + cb (Main Harzburgite); po + pn + cp + mc (Main Harzburgite and Chromitiferous Harzburgite); po + pn + cp + py (Lower Harzburgite, Chromitiferous Harzburgite and Basal Gabbro); py + cp + ml + po (Lower Harzburgite and Chromitiferous Harzburgite) and po + pn + cp + vl + cob (Lower Harzburgite and Chromitiferous Harzburgite).

* Serpentinization was the dominant alteration process in the Main Harzburgite.

* The Chromitiferous Harzburgite is characterized by tremolite-talc-carbonate and talc-chlorite-carbonate alteration.

* The Lower Harzburgite is altered by saussuritization, uralitization and lesser serpentinization.

* Intense amphibolitization and saussuritization took place in the Basal Gabbro.

* From the assay values it is concluded that the Cu/Ni ratio of the sulphide increases towards the base of the Complex.

* Chemical analyses of the sulphide minerals show a definite increase in Ni and decrease in Fe in pentlandite and pyrrhotite with decreasing elevation above the base of intrusion.

* Chemical analyses of the primary and secondary silicate minerals associated with the sulphides show Fe-enrichment towards the base of the Complex. This increase in Fe is interpreted as the combined effects of

fractionation and the cooling effects of the country rock on the intruding magma.

* From the X-ray diffraction work on the secondary silicate minerals, a crude correlation is shown to exist between calcite abundance and mineralization.

* The abundance of talc and carbonate in the mineralized zone, but not in the Main Harzburgite, suggests the development of a deuteric CO_2-rich environment in the lower three lithologies. The role of CO_2 in the lower parts of the Complex is in accord with the postulation by Gauert et al, 1995, that dolomite was assimilated by the intruding magma. This does not exclude the assimilation of Timeball Hill shale as suggested by Von Scheibler et al, 1995.

* Image analysis indicates that the average grain size of the disseminated sulphide blebs increases towards the base of the intrusion where it measures about 80 per cent larger than 450 micron.

* The granular pentlandite in the Uitkomst ore has an average grain size of ±11 micron and flame pentlandite measures 3 to 10 micron in section.

* In the Main Harzburgite, Chromitiferous Harzburgite and Lower Harzburgite the flame pentlandite forms between 1 and 5 percent of the total pentlandite which is indicative of the lower limit of the nickel losses to be expected in beneficiation.

* Where the secondary alteration of the silicate minerals is most intense, pyrrhotite shows a marginal replacement by magnetite as well as intergrowths with secondary silicate minerals. These intergrowths also affect pentlandite, and to a lesser extent chalcopyrite, and will have a bearing on the beneficiation of the sulphide.

* Pentlandite is in places extensively altered to violarite and mackinawite, which results in the reduction of the effective grain size of pentlandite. Sliming during comminution is likely to be a problem in beneficiation of these altered ores.

* The presence of talc in the mineralized zone may interfere with the flotation behaviour of the sulphide minerals.

7: ACKNOWLEDGEMENTS

The writer wishes to thank the following persons and institutions:
Anglo American Prospecting Services, Roy Corrans and Steve Marsh in person, respectively, for financial support and interest in the project.
André Botha, Sabine Verryn and Nasco Atanasov for their analytical and technical assistance.
Prof. C.P. Snyman, Drs. G. Grantham, T. Wallmach and J. Harmer of the Department of Geology, University of Pretoria, for useful insets at times in the duration of the project.
A special note of thanks is extended to Prof. S.A. de Waal and Dr. R.K.W. Merkle for their continued interest and guidance through this thesis.
I thank my husband, Etienne and the rest of our friends and family for their love and support during this study.
Last, but not least, I praise our Creator for giving me the strength and the courage to finish this thesis, when at times I thought I had none left.

9: References

Agar, G.E. (1991) Flotation of chalcopyrite, pentlandite and pyrrhotite ores. International Journal of Mineral Processing **33,** 1-19.

Allen, I.V.L. (1990) The geology and geochemistry of the Uitkomst Layered Complex, Eastern Transvaal. BSc. Hons.Thesis, University of the Witwatersrand; 49 p.

Arnold, R.G. (1966) Mixtures of hexagonal and monoclinic pyrrhotite and the measurement of the metal content of pyrrhotite by X-ray diffraction. American Mineralogist **51,** 1221-1227.

Arnold, R.G. and Reichen, L.E. (1962) Measurement of the metal content of naturally occurring metal-deficient, hexagonal pyrrhotite by an X-ray spacing method. American Mineralogist **47,** 105-111.

Augustithis, S.S. (1979) Atlas of the textural patterns of basic and ultrabasic rocks and their genetic significance. Walter de Gruyter, Berlin & New York, 393 p.

Bailey, S.W. (1988) Chlorites: Structures and crystal chemistry. In: Bailey, S.W. (editor) Hydrous Phyllosilicates (Exclusive of Micas). Mineralogical Society of America, Reviews in Mineralogy, **19,** 347-403.

Boldt, J.R.j. and Queneau, P. (1967) The Winning of Nickel. Van Nostrand, New York, 487 p.

Bonnichsen, B. (1972) Sulfide minerals in the Duluth Complex. In: Sims, P.K. and Morey, G.B. (editors) Geology of Minnesota: a Centennial Volume. Geological Survey of Minnesota, 388-393.

Bonnichsen, B. (1984) Alteration of mafic minerals and rocks. In: Siems, P.L. (editor) Hydrothermal Alteration for Mineral Exploration Workshop. Department of Geology, University of the Witwatersrand, Johannesburg, 33-41.

Boucher, M.L. (1975) Cu-Ni mineralization in a drill core from the Duluth Complex of Northern Minnesota. U. S. Bur. Mines Rep. Invest. **8084**.

Bruce, T.J. and Orr, R.G. (1986) Pyrrhotite rejection at INCO Ltd. Manitoba Division. In: Ozberk, E. and Marcuson, S.W. (editors) Nickel Metallurgy, Proceedings of the 25th Annual Conference of Metallurgy. The Canadian Institute of Mining and Metallurgy, Montreal, Quebec, 57-94.

Button, A. (1973) A regional study of the stratigraphy and the development of the Transvaal basin in the eastern and north-eastern Transvaal. PhDThesis, University of the Witwatersrand; 358 p.

Cambel, B. and Jarkovsky, J. (1968) Geochemistry of nickel and cobalt in pyrrhotites of different genetic types. 23rd Int. Geol. Congress (Prague) **6,** 169-183.

Clendenin, C.W., Henry, G., and Charlesworth, E.G. (1991) Characteristics of and influences on the Black Reef depositional sequence in the Eastern Transvaal. South African Journal of Geology **94,** 321-327.

Cohen, H.E. (1983) Energy usage in mineral processing. Transactions of the Institution of Mining and Metallurgy, Section C: Mineral Processing and Extractive Metallurgy **92,** 160-164.

Condit, R.H., Hobbins, R.R., and Birchenall, C.E. (1974) Self-diffusion of iron and sulfur in ferrous sulfide. Oxidation of Metals **8(6),** 409-455.

Craig, J.R. (1973) Pyrite-pentlandite assemblages and other low-temperature relations in the Fe-Ni-S system. American Journal of Science **273-A,** 496-510.

Craig, J.R. and Kullerud, G. (1969) Phase relations in the Cu-Fe-Ni-S system and their application to magmatic ore deposits. In: Wilson, H.D.B. (editor) Magmatic Ore Deposits. Economic Geology Monograph, **4,** 344-358.

Craig, J.R., Yoon, R.H., Haralick, R.M., Pong, T.C., and Choi, W. (1981) The application of General Image Processing System (GIPSY) to mineral beneficiation studies. In: Hausen, D.M. and Park, W.C. (editors) Process Mineralogy 2: applications in metallurgy, ceramics and geology. Metallurgical Society of AIME, Warrendale, 55-67.

Deer, W.A., Howie, R.A., and Zussman, J. (1985) An Introduction to the Rock Forming Minerals. Longman Group Limited, Harlow, Essex, England, 528 p.

De Waal, S.A. (1984) Experimental simulation of the supergene reaction: pyrrhotite → marcasite + Fe^{2} + electrons. Transactions of the Geological Society of South Africa **87**, 273-279.

Duke, J.M. and Naldrett, A.J. (1976) Sulfide Mineralogy of the Main Irruptive, Sudbury, Ontario. Canadian Mineralogist **14,** 450-461.

Durazzo, A. and Taylor, L.A. (1982) Exsolution in the Mss - pentlandite system: textural and genetic implications for Ni-sulfide ores. Mineralium Deposita **17,** 313-332.

Edwards, C.R., Kipkie, W.B., and Agar, G.E. (1980) The effect of slime coatings of the serpentine minerals, chrysotile and lizardite, on pentlandite flotation. International Journal of Mineral Processing **7,** 33-42.

Eriksson, P.G., Schweitzer, J.K., Bosch, P.J.A., Schreiber, U.M., Van Deventer, J.L., and Hatton, C.J. (1993) The Transvaal Sequence: An overview. Journal of African Earth Sciences **16.**

Evans, B.W. and Guggenheim, S. (1988) Talc, pyrophyllite, and related minerals. In: Bailey, S.W. (editor) Hydrous Phyllosilicates (Exclusive of Micas). Mineralogical Society of America, Reviews in Mineralogy, **19,** 225-294.

Fawcett, J.J. (1962) The alumina content of talc. Carnegie Inst. Wash. Yearb. **62,** 139-140.

Fawcett, J.J. and Yoder, H.S. (1966) Phase relationships of chlorites in the system MgO-Al2O3-SiO2-H2O. American Mineralogist **51,** 353-380.

Francis, C.A. (1974) A crystallographic study of the $Fe_{1-x}S$-$Ni_{1-x}S$ monosulfide solid solution. MSc.Thesis, Virginia Polytechnic Institution and State University.

Francis, C.A., Fleet, M.E., Misra, K., and Craig, J.R. (1976) Orientation of exsolved pentlandite in natural and synthetic nickeliferous pyrrhotite. American Mineralogist **61,** 913-920.

Gauert, C.D.K., De Waal, S.A., and Wallmach, T. (1995) Geology of the ultrabasic to basic Uitkomst Complex, Eastern Transvaal, South Africa: an overview. Journal of African Earth Sciences **21,** 553-570.

Gauert, C.D.K., Jordaan, L., De Waal, S.A., and Wallmach, T. (1996) Isotopic constraints on the source of sulphur for the base-metal sulphides of the Uitkomst Complex, Badplaas, South Africa. South African Journal of Geology (in press).

Genkin, A.D. and Evstigneeva, T.L. (1986) Associations of platinum-group minerals of the Noril'sk copper-nickel sulfide ores. Economic Geology **81,** 1203-1212.

Graham, J., Bennett, C.E.G., and van Riessen, A. (1987) Oxygen in pyrrhotite: 1. Thermomagnetic behavior and annealing of pyrrhotites containing small quantities of oxygen. American Mineralogist **72,** 599-604.

Graterol, M. and Naldrett, A.J. (1971) Mineralogy of the Marbridge no. 3 and no. 4 nickel-iron sulfide deposits, with some comments on low temperature equilibration in the Fe-Ni-S system. Economic Geology **66,** 886-900.

Gribble, C.D. and Hall, A.J. (1992) A Practical Introduction to Optical Mineralogy. Chapman & Hall, London, 249 p.

Gronvold, F. and Haraldson, H. (1952) On the phase relations of synthetic and natural pyrrhotites ($Fe_{1-x}S$). Acta Chemica Scandinavica **6,** 1452-1469.

Groves, D.I., Hudson, D.R., and Hack, T.B.C. (1974) Modification of iron-nickel sulfides during serpentinization and talc-carbonate alteration at Black Swan, Western Australia. Economic Geology **69,** 1265-1281.

Harris, D.C. and Nickel, E.H. (1972) Pentlandite compositions and associations in some mineral deposits. Canadian Mineralogist **11,** 861-878.

Hawley, J.E. and Haw, V.A. (1957) Intergrowths of pentlandite and pyrrhotite. Economic Geology **52,** 132-139.

Herrera-Urbina, R., Hanson, J.S., Harris, G.H., and Fuerstenau, D.W. (1990) Principles and practice of sulphide mineral flotation. In: Gray, P.M.J., Bowyer, G.J., Castle, J.F., Vaughan, D.J. and Warner, N.A. (editors) Sulphide Deposits - their Origin and Processing. The Insitution of Mining and Metallurgy, London, 87-101.

Hess, H.H. (1941) Pyroxenes of common mafic magmas, part 2. Amer. Min. **26,** 573-594.

Hey, M.H. (1954) A review of the chlorites. Mineralogical Magazine **30,** 277-292.

Hulbert, L.J. and Von Gruenewaldt, G. (1985) Textural and compositional features of chromite in the lower and critical zones of the Bushveld Complex south of Potgietersrus. Economic Geology **80,** 872-895.

Iwasaki, I. (1988) Flotation behaviour of pyrrhotite in the processing of copper-nickel ores. In: Tyroler, G.P. and Landolt, C.A. (editors) Extractive Metallurgy of Nickel and Cobalt. The Metallurgical Society, Inc. Warrendale, Pennsylvania, 271-292.

Jackson, E.D. (1966) Liquid immiscibility in chromite seam formation- a discussion. Economic Geology **61,** 777-780.

Kaiser, H. and Specker, H (1956) Bewertung und Vergleich von Analysenfahren. Z.anal.Chem **149**, 46-66.

Kelly, D.P. and Vaughan, D.J. (1983) Pyrrhotite - pentlandite ore textures: a mechanistic approach. Mineralogical Magazine **47,** 453-463.

Kenyon, A.K. (1979) A general mineralogical and pertrological investigation of mafic and ultramafic satellite bodies of the Bushveld Igneous Complex. Anglo American Research Laboratories. Johannesburg. R/48. 125 p.

Kenyon, A.K., Attridge, R.L., and Coetzee, G.L. (1986) The Uitkomst nickel-copper deposit, Eastern Transvaal. In: Anhaeusser, C.R. and Maske, S. (editors) Mineral Deposits of Southern Africa. Geological Society of South Africa, Johannesburg, **1,** 1009-1017.

Kiviets, G.B. (1991) The petrography and geochemistry of chromite seams from the Uitkomst Layered Ultramafic Complex, Eastern Transvaal. BSc. Hons.Thesis, University of Cape Town; 55 p.

Klotsman, S.M., Timofeyev, A.N., and Trakhtenberg, I.S. (1963) Investigation of the diffusion properties of the chalcogenides of transition metals. IV. Temperature dependence of the anisotropy of nickel and sulphur self-diffusion in nickel monosulphide. Physics of Metals and Metallography **16,** 92-98.

Kruparz, H. and Van Rensburg, W.L. (1965) The chromite deposits at Nietverdientd, Marico District, Transvaal. S. Afr. Geol. Surv. Annals **4,** 137-150.

Kubo, H. (1957) Improvements to the methods of treatment of pyrrhotite. Nippon Kogyo Kaishi **73,** 801-809.

Kullerud, G. (1963) Thermal stability of pentlandite. Canadian Mineralogist **7,** 353-366.

McDonald, J.A. (1965) Liquid immiscibility as one factor in chromite seam formation in the Bushveld Igneous Complex. Economic Geology **60,** 1674-1685.

McKie, D. (1959) Yoderite, a new hydrous magnesium iron aluminosilicate from Mautia Hill, Tanganyika. Mineralogical Magazine **32,** 282-307.

Misra, K.C. and Fleet, M.E. (1973) The chemical compositions of synthetic and natural pentlandite assemblages. Economic Geology **68,** 518-539.

Morimoto, N. (1989) Nomenclature of pyroxenes. Canadian Mineralogist **27,** 143-156.

Muir, I.D. and Tilley, C.E. (1958) The compositions of co-existing pyroxenes in metamorphic assemblages. Geological Magazine **95,** 403-408.

Naldrett, A.J. (1966) Talc-carbonate alteration of some serpentinized ultramafic rocks south of Timmins, Ontario. Journal of Petrology **7,** 489-499.

Nockolds, S.R., Knox, R.W.O.B., and Chinner, G.A. (1978) Petrology for Students. University Press, Cambridge, 435p.

Oosthuyzen, E.J. (1983) The application of automatic image analysis to mineralogy and extractive metallurgy. In: De Villiers, J.P.R. and Cawthorn, P.A. (editors) ICAM '81, Proceedings of the 1st International Congress on Applied Mineralogy. Geological Society of South Africa, Johannesburg, Special Publication, **7,** 449-464.

Paktunc, A.D., Hulbert, L.J., and Harris, D.C. (1990) Partitioning of the platinum-group and other trace elements in sulfides from the Bushveld Complex and Canadian occurrences of Nickel-Copper sulfides. Canadian Mineralogist **28,** 475-488.

Petruk, W. (1982) Image analysis in process mineralogy. In: Hagni, R.D. (editor) Process Mineralogy 2: Applications in Metallurgy, Ceramics, and Geology. Metallurgical Society of AIME, Warrendale, Pennsylvania, 39-53.

Pugh, R.J. (1989) Macromolecular organic depressants in sulphide flotation - a review. 1. Principles, types, and application. International Journal of Mineral Processing **25,** 101.

Rajamani, V. and Prewitt, C.T. (1973) Crystal chemistry of natural pentlandites. Canadian Mineralogist **12,** 178-187.

Ramdohr, P. (1981) The ore minerals and their intergrowths.

Robinson, P., Spear, F.S., Schumacher, J.C., Laird, J., Klein, C., Evans, B.W., and Doolan, B.L. (1982) Phase relations of metamorphic amphiboles: Natural occurrence and theory. In: Veblen, D.R. and Ribbe, P.H. (editors) Amphiboles. Mineralogical Society of America, Reviews in Mineralogy, **9B,** 1-390.

Schreiber, U. (1991) A paleoenvironmental study of the Pretoria Group in the Eastern Transvaal. PhD Thesis, University of Pretoria.

Sizgoric, M.B. and Alcock, R.A. (1981) Quantitative mineralogy as an aid to beneficiation of nickel sulfide ores. In: Hausen, D.M. and Park, W.C. (editors) Process Mineralogy: Extractive Metallurgy, Mineral Exploration, Energy Resources. Metallurgical Society of AIME, Warrendale, 419-428.

Skinner, B.J. and Peck, D.L. (1969) An immiscible sulphide melt from Hawaii. In: Wilson, H.D.B. (editor) Magmatic Ore Deposits. Economic Geology Monograph, **4,** 310-322.

Stemple, I.S. and Brindley, G.W. (1960) A structural study of talc and talc-tremolite relations. Journal of the American Ceramic Society **43,** 34-42.

Swash, P.M., Horsch, H.E., and Glatthaar, C.W. (1991) The contribution of applied mineralogy to the development of the Uitkomst Ni-Cu deposit, South Africa. ICAM '91, International Congress on Applied Mineralogy, Papers. Mineralogical Association of South Africa, Pretoria, **2,** Chapter 55, 1-12.

Tomanec, R. and Milovanovic, J. (1994) Mineral liberation prediction based on texture characterization. In: Demirel, H. and Ersayin, S. (editors) Progress in Mineral Processing Technology. Balkema, Rotterdam, 3-9.

Vaughan, D.J. and Craig, J.R. (1978) Mineral Chemistry of Metal Sulfides. Cambridge University Press, 493 p.

Vermaak, C.F. and Hendriks, L.P. (1976) A review of the mineralogy of the Merensky Reef, with specific reference to new data on precious metal mineralogy. Economic Geology **71,** 1244-1269.

Von Gruenewaldt, G. (1979) A review of some recent concepts of the Bushveld Complex, with particular reference to sulfide mineralization. Canadian Mineralogist **17,** 233-256.

Von Scheibler, W. (1990a) The genesis of the Uitkomst Igneous Complex. Anglo American Prospecting Services. Verwoerdburg. June. 12 p.

Von Scheibler, W. (1990b) Report on petrographic examination of Uitkomst 541JT thin sections. Anglo American Prospecting Services. Verwoerdburg. October. 15 p.

Von Scheibler, W.H.T.M., Cawthorn, R.G., Kenyon, A.K., and Allen, I.V.L. (1995) Ni-Cu sulphide mineralization in the Uitkomst Intrusion. Geocongress, Ext. Abstr. 133-136.

Wagner, P.A. (1929) The Platinum Deposits and Mines of South Africa. Oliver & Boyd, London.

Weiblen, P.W. and Morey, G.B. (1976) Textural and compositional characteristics of sulfide ores from the basal contact zone of the South Kawishiwi Intrusion, Duluth Complex, Northeastern Minnesota. Minnesota Geological Survey Reprint **32,** 22-1 to 22-23.

Wellham, E.J., Elber, L., and Yan, D.S. (1992) The role of carboxy methyl cellulose in the flotation of a nickel sulphide transititon ore. Minerals Engineering **5,** 381-395.

Whittaker, E.J.W. and Wicks, F.J. (1970) Chemical differences among serpentine polymorphs: a discussion. American Mineralogist **55,** 1025-1047.

Wicks, F.J. and Plant, A.G. (1979) Electron microprobe and X-ray microbeam studies of serpentine textures. Canadian Mineralogist **17,** 785-830.

Winkler, H.G.F. (1979) Petrogenesis of Metamorphic Rocks. 5th ed. Springer-Verlag, Berlin, Heidelberg, New York, 348 p.

Yoder, H.S. (1952) The MgO - Al_2O_3 - SiO_2 - H_2O system and the related metamorphic facies. American Journal of Science 569-627.

APPENDIX A

Microprobe analyses of the sulphide minerals

Microprobe analyses of pyrrhotite (weight %):
s= standard deviation; ()=number of analyses

Label:	#:	Eab:	Lith:	Mineral assoc:	Fe	Ni	Cu	Co	S	Total:
5/A	5	113.21	Mhzbg	po+pn+cp+mc+	63.61	*	*	*	37.38	100.99
s (5)				cub	0.73	*	*	*	0.16	0.59
5/B	5	106.21	Mhzbg	po+pn+cp+cub	63.35	*	*	*	37.86	101.23
s (5)					1.04	*	*	*	1.04	0.12
5/C	3	101.21	Mhzbg	po+pn+mc	62	0.72	0.4	*	37.52	100.61
s (3)					1.43	0.63	0.69	0.00	1.18	0.85
45/A	6	90.82	Mhzbg	po+pn+cp+mc	60.91	0.13	0.05	0.07	38.40	99.55
s (6)					0.18	0.05	0.03	0.01	0.27	0.34
45/C	4	83.82	PCR	po+pn+vl+cp	60.06	0.34	0.13	0.08	39.68	100.30
s (4)					0.11	0.03	0.04	0.01	0.25	0.35
45/D	5	79.82	PCR	po+pn+vl+cp	59.34	0.45	0.05	0.08	39.76	99.67
s (5)					0.54	0.06	0.05	0.01	0.15	0.62
34/4	4	76	PCR	po+pn+cp	60.99	0.38	0.01	0.08	39.59	101.02
s (4)					0.13	0.03	0.01	0.01	0.11	0.23
45/1	5	71.82	PCR	po+pn+vl+cp	59.42	0.22	0.05	0.07	39.80	99.55
s (5)					0.39	0.02	0.02	0.01	0.56	0.95
45/3	6	57.82	Lhzbg	po+pn+vl+cp	59.93	0.40	0.01	0.07	39.48	99.86
s (6)				+cob	0.31	0.14	0.02	0.01	0.41	0.36
45/4	2	49.82	Lhzbg	po+pn+cp	60.68	0.46	0.01	0.07	38.88	100.16
s (3)					0.23	0.11	0.01	0.00	0.10	0.22
UD 1/1	3	46.58	PCR	po+pn+cp	59.38	0.53	0.02	*	39.48	99.41
s (3)					0.21	0.02	0.02	*	0.10	0.27
34/7	3	36	Lhzbg	po+pn+cp	61.36	0.28	0.04	0.05	39.53	101.31
s (3)					0.21	0.06	0.05	0.04	0.16	0.34
UD1/3	4	35.58	PCR	po+pn+cp+py	60.48	0.40	0.04	0.07	40.04	101.00
s(2)					0.11	0.05	0.01	0.00	0.11	0.10
UD1/4	3	29.58	PCR	po+pn+cp+py	60.3	0.38	0.01	0.07	40.03	100.79
s (4)					0.25	0.17	0.04	0.01	0.23	0.20
UD 5/5	5	26.21	PCR	po+pn+cp+mc	60.12	0.30	0.03	*	38.33	98.79
s (5)					0.08	0.15	0.04	*	0.22	0.13
59/1	4	26.11	Lhzbg	po+pn+cp+vl+py	59.6	1.03	0.03	0.09	40.16	100.89
s (4)				+sf	0.23	0.04	0.02	0.01	0.13	0.18
59/4	3	16.11	Lhzbg	po+pn+cp+py	60.07	0.51	0.00	0.07	40.10	100.71
s (3)					0.08	0.03	0.01	0.00	0.09	0.13
45/E	7	13.82	Lhzbg	po+pn+cp	59.17	0.83	0.01	0.11	38.85	98.98
s (7)					0.88	0.80	0.01	0.10	0.16	0.16
UD 5/7	2	12.21	PCR	po+pn+cp+mc+	61.93	0.02	*	*	36.73	98.66
s (2)				PbTe	0.60	0.02	*	*	0.67	0.11
59/9	4	10.11	Lhzbg	po+pn+cp+py	59.96	0.35	0.05	0.07	40.03	100.46
s (4)					0.12	0.02	0.01	0.01	0.10	0.13
UD1/8	6	6.58	Bgab	po+pn+cp	60.38	0.38	0.05	0.08	39.94	100.84
s (6)					0.41	0.09	0.07	0.00	0.61	0.79
45/G	3	3.82	Bgab	po+pn+cp+py	59.83	0.72	0.04	0.08	39.40	100.07
s (3)					0.13	0.05	0.01	0.02	0.09	0.13
UD 1/9	4	2.58	Bgab	po+pn+cp+py	59.09	0.30	0.49	*	39.45	94.27
s (4)					0.27	0.13	0.27	0	0.19	10.23

Microprobe analyses of pyrrhotite (atomic %):

Label:	#:	Eab:	Lith:	Mineral assoc:	Fe	Ni	Cu	Co	S
5/A	5	113.2	Mhzbg	po+pn+cp+mc+	**49.42**	*	*	*	**50.58**
s (5)				cub	0.39	*	*	*	0.39
5/B	5	106.2	Mhzbg	po+pn+cp+cub	**48.97**	*	*	*	**51.03**
s (5)					1.09	*	*	*	1.09
5/C	3	101.2	Mhzbg	po+pn+mc	**48.32**	**0.52**	**0.27**	*	**50.92**
s (3)					1.68	0.45	0.46	*	1.03
45/A	6	90.82	Mhzbg	po+pn+cp+mc	**47.58**	**0.10**	**0.04**	**0.05**	**52.24**
s (6)					0.13	0.04	0.02	0.01	0.17
45/C	4	83.82	PCR	po+pn+vl+cp	**46.29**	**0.25**	**0.09**	**0.06**	**53.31**
s (4)					0.09	0.02	0.03	0.01	0.09
45/D	5	79.82	PCR	po+pn+vl+cp	**45.95**	**0.33**	**0.04**	**0.06**	**53.63**
s (5)					0.2	0.05	0.03	0.01	0.16
34/4	4	76	PCR	po+pn+cp	**46.75**	**0.28**	**0.00**	**0.06**	**52.88**
s (4)					0.04	0.02	0.01	0.01	0.05
45/1	5	71.82	PCR	po+pn+cp+vl	**46.03**	**0.16**	**0.04**	**0.05**	**53.7**
s (5)					0.18	0.02	0.01	0.01	0.20
45/3	6	57.82	Lhzbg	po+pn+vl+cp	**46.40**	**0.30**	**0.00**	**0.05**	**53.24**
s (6)				+cob	0.36	0.10	0.01	0.01	0.35
45/4	2	49.82	Lhzbg	po+pn+cp	**47.08**	**0.34**	**0.01**	**0.05**	**52.55**
s (3)					0.12	0.08	0.01	*	0.03
UD 1/1	3	46.58	PCR	po+pn+cp	**46.15**	**0.39**	**0.01**	*	**53.47**
s (3)					0.09	0.01	0.01	*	0.06
34/7	3	36	Lhzbg	po+pn+cp	**47.01**	**0.21**	**0.03**	**0.04**	**52.74**
s (3)					0.10	0.04	0.04	0.03	0.15
UD1/3	4	35.58	PCR	po+pn+cp+py	**46.28**	**0.29**	**0.03**	**0.05**	**53.34**
s(2)					0.11	0.03	0.01		
UD1/4	3	29.58	PCR	po+pn+cp+py	**46.23**	**0.28**	**0.01**	**0.05**	**53.43**
s (4)					0.19	0.12	0.03	0.00	0.30
UD 5/5	5	26.21	PCR	po+pn+cp+mc	**47.25**	**0.228**	**0.017**	*	**52.49**
s (5)					0.12	0.12	0.03	*	0.22
59/1	4	26.11	Lhzbg	po+pn+cp+vl+py	**45.61**	**0.75**	**0.02**	**0.06**	**53.56**
s (4)				+sf	0.18	0.03	0.01	0.00	0.15
59/4	3	16.11	Lhzbg	po+pn+cp+py	**46.05**	**0.38**	**0.00**	**0.05**	**53.52**
s (3)					0.09	0.02	0.00	0.00	0.08
45/E	7	13.82	Lhzbg	po+pn+cp	**46.31**	**0.63**	**0.01**	**0.08**	**52.96**
s (7)					0.72	0.59	0.01	0.07	0.14
UD 5/7	2	12.21	PCR	po+pn+cp+mc+	**49.18**	**0.01**	*	*	**50.83**
s (2)				PbTe	0.67	0.02	*	*	0.67
59/9	4	10.11	Lhzbg	po+pn+cp+py	**46.08**	**0.25**	**0.04**	**0.05**	**53.58**
s (4)					0.06	0.02	0.01	0.01	0.08
UD1/8	6	6.58	Bgab	po+pn+cp	**46.28**	**0.29**	**0.03**	**0.06**	**53.35**
s (6)					0.38	0.06	0.05	0.00	0.36
45/G	3	3.82	Bgab	po+pn+cp+py	**46.30**	**0.53**	**0.03**	**0.06**	**53.1**
s (3)					0.05	0.04	0.01	0.01	0.10
UD 1/9	4	2.58	Bgab	po+pn+cp+py	**46**	**0.22**	**0.33**	*	**53.46**
s (4)					0.14	0.10	0.19	*	0.14

Microprobe analyses of pyrite (weight %):

Label:	n	Eab:	Lith:	Assemblage	Fe	Ni	Cu	Co	S	Total
UD1/3	3	35.58	PCR	po+pn+cp+py	45.78	1.03	0.70	0.40	53.47	101.4
s (3)					0.63	0.18	0.70	0.06	0.49	0.304
34/8	6	27	Lhzbg	po+cp+py+ml	46.26	0.05	*	0.24	53.79	100.35
s (6)					0.35	0.08	*	0.30	0.06	0.26
59/4	4	16.11	Lhzbg	po+pn+cp+py	46.11	*	0.03	0.65	54.43	101.2
s (4)					0.20	*	0.00	0.23	0.15	0.21
UD 1/9	4	2.58	Bgab	po+pn+cp+py	45.4	*	0.06	1.59	53.76	100.81
s (4)					0.13	*	0.08	0.36	0.20	0.50

Microprobe analyses of pyrite (atomic %):

Label:	n	Eab:	Lith:	Assemblage:	Fe	Ni	Cu	Co	S
UD1/3	3	35.58	PCR	po+pn+cp+py	32.48	0.70	0.43	0.27	66.10
s (3)					0.28	0.13	0.45	0.03	0.26
34/8	6	27	Lhzbg	po+cp+py+ml	32.99	0.03	*	0.15	66.83
s (6)					0.23	0.05	*	0.21	0.09
59/4	4	16.11	Lhzbg	po+pn+cp+py	32.56	*	0.02	0.44	66.96
s (4)					0.21	*	*	0.15	0.07
UD 1/9	4	2.58	Bgab	po+pn+cp+py	32.29	*	0.04	1.08	66.59
s (4)					0.20	*	0.05	0.24	0.09

Microprobe analyses of pentlandite (weight %):

Label:	n	Eab:	Lith:	Assemblage:	Fe	Ni	Cu	Co	S	Total
5/A	3	113.21	Mhzbg	po+pn+cp+mc+	**33.93**	**32.22**	*	**0.83**	**33.9**	**100.88**
s (3)				cub	0.45	0.19	*	0.10	0.2	0.69
5/B	1	106.21	Mhzbg	po+pn+cp+cub	**34.40**	**31.80**	*	**1.20**	**34.00**	**101.4**
UD 5/C	2	101.21	Mhzbg	po+pn+mc	**34.18**	**30.50**	**0.04**	**1.38**	**33.08**	**99.14**
s (2)					0.46	0.14	0.03	0.39	0.32	0.25
5/D	2	96.21	Mhzbg	po+pn+cp+mc	**35.65**	**30.35**	*	**1.00**	**33.35**	**100.3**
s (2)				+cb	0.21	0.21	*	0.14	0.07	0.08
45/A	6	90.82	Mhzbg	po+pn+cp+mc	**32.68**	**32.18**	**0.13**	**1.15**	**33.18**	**99.28**
s (6)					0.83	0.58	0.18	0.05	0.38	0.56
45/C	4	83.82	PCR	po+pn+vl+cp	**30.03**	**33.26**	**0.07**	**2.26**	**33.44**	**99.05**
s (4)					0.32	0.74	0.02	0.10	0.31	0.17
45/1	4	71.82	PCR	po+pn+cp+vl	**30.54**	**33.36**	**0.07**	**1.62**	**33.74**	**99.30**
s (4)					0.23	0.59	0.05	0.06	0.03	0.38
45/3	3	57.82	Lhzbg	po+pn+vl+cp	**32.80**	**31.48**	*	**1.51**	**33.32**	**99.11**
s (3)				+cob	1.18	1.47	*	0.15	0.32	0.14
UD5/1	1	52.21	PCR	po+pn+cp+cob	**31.40**	**34.40**	*	**0.40**	**32.90**	**99.04**
45/4	3	49.82	Lhzbg	po+pn+cp	**31.08**	**33.92**	**0.052**	**1.65**	**33.35**	**99.99**
s (3)					0.28	0.36	0.03	0.03	0.09	0.67
UD 1/1	4	46.58	PCR	po+pn+cp	**30.26**	**35.79**	**0.04**	**1.49**	**33.54**	**101.08**
s (4)					0.03	0.22	0.08	0.05	0.05	0.24
34/7	5	36	Lhzbg	po+pn+cp	**32.40**	**32.56**	**0.04**	**1.21**	**33.88**	**100.08**
s (5)					0.09	0.29	0.01	0.06	0.08	0.31
UD1/3	4	35.58	PCR	po+pn+cp+py	**31.19**	**34.31**	*	**1.00**	**33.16**	**99.66**
s (4)					0.05	0.47	*	0.09	0.06	0.42
UD1/4	5	29.58	PCR	po+pn+cp+py	**30.63**	**34.20**	*	**1.25**	**33.25**	**99.31**
s (5)					0.68	0.79	*	0.11	0.19	0.44
59/1	3	26.11	Lhzbg	po+pn+cp+vl+py	**29.52**	**32.95**	*	**1.29**	**35.70**	**99.49**
s (3)				+sf	0.68	5.87	*	0.12	4.16	1.06
59/4	2	16.11	Lhzbg	po+pn+cp+py	**30.85**	**34.50**	*	**0.78**	**33.55**	**99.70**
s (2)					0.35	0.14	*	0.06	0.07	0.57
45/E	3	13.82	Lhzbg	po+pn+cp	**29.83**	**34.13**	**0.05**	**1.48**	**33.62**	**99.11**
s (3)					0.33	2.54	0.04	0.12	1.63	0.51
UD 5/7	3	12.21	PCR	po+pn+cp+mc+	**34.63**	**29.62**	**0.04**	**1.80**	**33.00**	**99.14**
s (3)				PbTe	0.31	0.14	0.01	0.10	0.10	0.17
59/9	2	10.11	Lhzbg	po+pn+cp+py	**30.92**	**35.78**	*	**1.21**	**33.30**	**101.21**
s (2)					0.09	0.18	*	0.04	0.09	0.02
UD1/8	3	6.58	Bgab	po+pn+cp	**30.77**	**35.00**	*	**1.15**	**33.45**	**100.39**
s (3)					0.50	1.39	*	0.07	0.38	1.03

Microprobe analyses of pentlandite (atomic %):

Label:	n	Eab:	Lith:	Assemblage:	Fe	Ni	Cu	Co	S
5/A	3	113.2	Mhzbg	po+pn+cp+mc+	**27.28**	**24.63**	*	**0.63**	**47.48**
s (3)				cub	0.25	0.03	*	0.06	0.16
5/B	1	106.2	Mhzbg	po+pn+cp+cub	**27.50**	**24.20**	*	**0.90**	**47.40**
UD 5/C	2	101.2	Mhzbg	po+pn+mc	**27.95**	**23.75**	**0.0225**	**1.05**	**47.175**
s (2)					0.28	0.21	0.02	0.35	0.25
5/D	2	96.21	Mhzbg	po+pn+cp+mc+cb	**28.85**	**23.35**	*	**0.75**	**47.05**
s (2)					0.21	0.07	*	0.07	0.07
45/A	6	90.82	Mhzbg	po+pn+cp+mc	**26.73**	**25.03**	**0.09**	**0.89**	**47.28**
s (6)					0.72	0.46	0.13	0.03	0.32
45/C	4	83.82	PCR	po+pn+vl+cp	**24.58**	**25.91**	**0.05**	**1.75**	**47.69**
s (4)					0.25	0.61	0.02	0.07	0.40
45/1	4	71.82	PCR	po+pn+cp+vl	**24.89**	**25.85**	**0.05**	**1.25**	**47.94**
s (4)					0.24	0.38	0.04	0.05	0.11
45/2	2	66.82	PCR	po+pn+cp+cob	**23.40**	**27.10**	**0.03**	**0.76**	**48.73**
s (2)					1.98	0.14	0.01	0.33	1.52
45/3	3	57.82	Lhzbg	po+pn+vl+cp	**26.85**	**24.50**	*	**1.17**	**47.47**
s (3)				+cob	0.98	1.17	*	0.11	0.33
UD5/1	1	52.21	PCR	po+pn+cp+cob	**25.80**	**26.90**	*	**0.30**	**47.10**
45/4	3	49.82	Lhzbg	po+pn+cp	**25.25**	**26.20**	**0.04**	**1.27**	**47.22**
s (3)					0.15	0.15	0.02	0.02	0.20
UD 1/1	4	46.58	PCR	po+pn+cp	**24.38**	**27.41**	**0.03**	**1.11**	**47.05**
s (4)					0.10	0.13	0.06	0.02	0.04
34/7	5	36	Lhzbg	po+pn+cp	**26.23**	**25.06**	**0.03**	**0.93**	**47.77**
s (5)					0.08	0.17	0.01	0.05	0.09
UD1/3	4	35.58	PCR	po+pn+cp+py	**25.46**	**26.64**	*	**0.77**	**47.15**
s (4)					0.09	0.28	*	0.07	0.16
UD1/4	5	29.58	PCR	po+pn+cp+py	**25.08**	**26.61**	*	**0.96**	**47.38**
s (5)					0.53	0.60	*	0.09	0.33
59/1	3	26.11	Lhzbg	po+pn+cp+vl+py	**23.75**	**25.27**	*	**0.98**	**49.97**
s (3)				+sf	0.18	4.92	*	0.07	4.79
59/4	2	16.11	Lhzbg	po+pn+cp+py	**25.10**	**26.70**	*	**0.60**	**47.60**
s (2)					0.14	*	*	0.05	0.28
45/E	3	13.82	Lhzbg	po+pn+cp	**24.40**	**26.57**	**0.03**	**1.15**	**47.88**
s (3)					0.10	2.14	0.03	0.09	2.01
UD 5/7	3	12.21	PCR	po+pn+cp+mc+	**28.38**	**23.08**	**0.03**	**1.40**	**47.10**
s (3)				PbTe	0.18	0.13	0.01	0.10	0.10
59/9	2	10.11	Lhzbg	po+pn+cp+py	**24.91**	**27.43**	*	**0.93**	**46.74**
s (2)					0.06	0.14	*	0.03	0.11
UD1/8	3	6.58	Bgab	po+pn+cp	**24.95**	**26.97**	*	**0.88**	**47.20**
s (3)					0.63	0.84	*	0.05	0.53

Microprobe analyses of chalcopyrite (weight %):

Label:	n	Eab:	Lith:	Assemblage:	Fe	Ni	Cu	Co	S	Total
UD 5/B	2	106.21	Mhzbg	po+pn+cp+cub	**31.00**	*	**34.15**	*	**35.20**	**100.4**
s (2)					0.14	*	0.07	*	0.14	*
45/A	3	90.82	Mhzbg	po+pn+cp+mc	**30.37**	*	**34.13**	**0.02**	**34.65**	**99.15**
s (3)					0.13	*	0.28	0.01	0.13	0.19
45/C	4	83.82	PCR	po+pn+vl+cp	**31.05**	*	**34.30**	**0.02**	**34.69**	**100.06**
s (4)					0.07	*	0.36	0.01	0.09	0.44
45/D	3	79.82	PCR	po+pn+vl+cp	**30.57**	**0.04**	**34.12**	**0.03**	**33.37**	**99.77**
s (3)					0.08	0.05	0.10	0.01	2.96	0.20
45/1	3	71.82	PCR	po+pn+cp+vl	**30.72**	*	**33.23**	**0.03**	**35.15**	**99.16**
s (3)					0.15	*	0.44	0.00	0.09	0.47
UD 5/1	2	52.21	PCR	po+pn+cp+cob	**30.25**	*	**34.60**	*	**34.00**	**98.90**
s (2)					0.35	*	0.14	*	0.14	0.36
45/4	3	49.82	Lhzbg	po+pn+cp	**30.68**	**0.05**	**34.20**	**0.04**	**34.93**	**99.93**
s (3)					0.10	0.06	0.15	0.00	0.03	0.07
UD 1/1	2	46.58	PCR	po+pn+cp	**30.75**	*	**34.75**	*	**35.1**	**100.6**
s (2)					0.07	*	0.21	*	0.14	0.13
UD1/3	3	35.58	PCR	po+pn+cp+py	**30.77**	*	**35.20**	**0.03**	**34.77**	**100.79**
s (3)					0.20	*	0.43	0.01	0.03	0.41
UD 5/5	4	26.21	PCR	po+pn+cp+mc	**30.75**	*	**34.21**	*	**34.78**	**99.77**
s (4)					0.33	*	0.10	*	0.17	0.46
59/1	3	26.11	Lhzbg	po+pn+cp+vl+py	**31.08**	*	**35.13**	**0.03**	**34.70**	**101.00**
s (3)				+sf	0.16	*	0.21	0.01	0.17	0.24
59/4	4	16.11	Lhzbg	po+pn+cp+py	**30.88**	*	**35.14**	**0.03**	**34.64**	**100.7**
s (4)					0.16	*	0.22	0.01	0.11	0.38
45/E	1	13.82	Lhzbg	po+pn+cp	**30.40**	*	**33.80**	**0.02**	**34.50**	**98.59**
59/9	3	10.11	Lhzbg	po+pn+cp+py	**30.85**	**0.01**	**34.86**	**0.03**	**34.71**	**100.30**
s (3)					0.03	0.02	0.23	0.00	0.04	0.19
UD1/8	2	6.58	Bgab	po+pn+cp	**31.00**	*	**35.28**	**0.03**	**34.90**	**101.19**
s (2)					0.28	*	0.25	0.01	0.14	0.18
45/G	2	3.82	Bgab	po+pn+cp+py	**30.45**	**0.01**	**35.10**	**0.04**	**34.75**	**100.28**
s (2)					0.21	0.01	*	0.01	0.21	0.43
UD 1/9	3	2.58	Bgab	po+pn+cp+py	**30.78**	*	**34.60**	*	**35.23**	**100.64**
s (3)					0.06	*	0.10	*	0.06	0.15

Microprobe analyses of chalcopyrite (atomic %):

Label:	n	Eab:	Lith:	Assemblage:	Fe	Ni	Cu	Co	S
UD 5/B	2	106.2	Mhzbg	po+pn+cp+cub	25.35	*	24.55	*	50.10
s (2)					0.07	*	0.07	*	0.14
45/A	3	90.82	Mhzbg	po+pn+cp+mc	25.15	*	24.83	0.02	50.00
s (3)					0.09	*	0.23	0.01	0.13
45/C	4	83.82	PCR	po+pn+vl+cp	25.53	*	24.75	0.02	49.68
s (4)					0.13	*	0.15	0.00	0.12
45/D	3	79.82	PCR	po+pn+vl+cp	25.12	0.03	24.65	0.03	50.17
s (3)					0.08	0.04	0.05	0.01	0.13
45/1	3	71.82	PCR	po+pn+cp+vl	25.35	*	24.08	0.02	50.57
s (3)					0.05	*	0.25	0.00	0.21
UD 5/1	2	52.21	PCR	po+pn+cp+cob	25.25	*	25.35	*	49.35
s (2)					0.21	*	0.21	*	0.07
45/4	3	49.82	Lhzbg	po+pn+cp	25.22	0.04	24.7	0.03	50.02
s (3)					0.08	0.05	0.13	0.00	0.08
UD 1/1	2	46.58	PCR	po+pn+cp	25.1	*	24.9	*	49.95
s (2)					*	*	0.14	*	0.21
UD1/3	3	35.58	PCR	po+pn+cp+py	25.15	*	25.27	0.03	49.53
s (3)					0.17	*	0.23	0.01	0.10
59/1	3	26.11	Lhzbg	po+pn+cp+vl+py	25.38	*	25.22	0.02	49.33
s (3)				+sf	0.08	*	0.18	0.00	0.15
59/4	4	16.11	Lhzbg	po+pn+cp+py	25.29	*	25.26	0.02	49.40
s (4)					0.06	*	0.11	0.01	0.09
45/E	1	13.82	Lhzbg	po+pn+cp	25.30	*	24.7	0.02	50.00
59/9	3	10.11	Lhzbg	po+pn+cp+py	25.32	0.01	25.04	0.02	49.62
s (3)					0.04	0.02	0.07	0.01	0.03
UD1/8	2	6.58	Bgab	po+pn+cp	25.23	*	25.25	0.03	49.48
s (2)					0.18	*	0.21	0.01	0.04
45/G	2	3.82	Bgab	po+pn+cp+py	24.95	0.01	25.3	0.03	49.65
s (2)					0.07	0.01	0.14	0.01	0.07
UD 1/9	3	2.58	Bgab	po+pn+cp+py	25.1	*	24.83	*	50.05
s (3)					0.05	*	0.10	*	0.05

Microprobe analyses of millerite (atomic %):

Label:	n	Eab:	Lith:	Assemblage:	Ni	Co	S
UD 34/A	6	103	PCR	po+cp+py+ml	**49.67**	*	**50.33**
s (6)					0.12	*	0.12
34/8	2	27	Lhzbg	po+cp+py+ml	49.80	*	50.20
s (2)					**0.14**	*	**0.14**

Microprobe analyses of millerite (weight %):

Label:	n	Eab:	Lith:	Assemblage:	Ni	Co	S	Total
UD 34/A	6	103	PCR	po+cp+py+ml	**64.43**	*	**35.67**	**100.1**
s (6)					0.19	*	0.22	0.34
34/8	2	27	Lhzbg	po+cp+py+ml	**64.30**	*	**35.40**	**99.67**
s (2)					*	*	0.28	0.30

Microprobe analyses of cubanite (atomic %):

Label:	n	Eab:	Lith:	Assemblage:	Cu	Fe	S
UD 5/A	2	113.21	Mhzbg	po+pn+cp+mc+	**16.20**	**33.30**	**50.50**
s (2)				cub	*	0.14	0.14
UD 5/B	5	106.21	Mhzbg	po+pn+cp+cub	**16.50**	**33.27**	**50.24**
s (5)					0.09	0.08	0.07

Microprobe analyses of cubanite (weight %):

Label:	n	Eab:	Lith:	Assemblage:	Cu	Fe	S	Total
UD 5/A	2	113.21	Mhzbg	po+pn+cp+mc+	**22.75**	**41.05**	**35.75**	**99.57**
s (2)				cub	0.07	0.21	0.07	0.06
UD 5/B	5	106.21	Mhzbg	po+pn+cp+cub	**23.27**	**41.23**	**35.77**	**100.3**
s (5)					0.18	0.09	0.07	0.27

Microprobe analyses of cobaltite (weight %):

Label:	n	Eab:	Lith:	Assemblage:	Co	Fe	Ni	As	S	Total
UD 5/1	4	52.21	PCR	po+pn+cp+cob	**20.21**	**3.93**	**13.09**	**45.11**	**16.69**	**99.01**
s (4)					1.04	1.05	0.65	0.58	0.09	0.34

Microprobe analyses of cobaltite (atomic %):

Label:	n	Eab:	Lith:	Assemblage:	Co	Fe	Ni	As	S
UD 5/1	4	52.21	PCR	po+pn+cp+cob	**19.53**	**3.96**	**12.70**	**34.24**	**29.60**
s (4)					0.97	1.10	0.62	0.41	0.16

APPENDIX B

Microprobe analyses of the silicate minerals

Microprobe analyses of olivine (n=10)
s=standard deviation; ( )=number of analyses

Label:	UD 5/A		UD 34/5		UD 59/4	
Lithology:	Mhzbg		PCR		Lhzbg	
		s(6)		s(2)		s(2)
SiO_2	40.18	0.31	39.9	0.15	38.83	0.15
FeO	11.9	0.27	12.99	0.18	19.3	1.27
MnO	0.05	0.09	0.24	0.03	0.39	0
MgO	47.4	0.41	46.02	0.59	41.71	1.29
CaO	0.03	0.06	0.12	0.01	0.21	0.02
NiO	0.36	0.05	0.19	0.27	0.13	0.18
Si	0.996		0.999		0.992	
Fe	0.247		0.272		0.412	
Mn	0.001		0.005		0.008	
Mg	1.752		1.718		1.588	
Ca	0.001		0.003		0.006	
Ni	0.007		0.004		0.003	
Fe/FeMg	0.12		0.14		0.21	
Mg/FeMg	0.88		0.86		0.79	

Microprobe analyses of pyroxene (n=27):
s=standard deviation; ( )=number of analyses

No:	1		2		3	4	5		6	
Sample:	UD 5/A		UD 5/A		UD 5/C	UD 5/D	UD 5/7		UD 1/1	
Lith:	Mhzbg		Mhzbg		Mhzbg	Mhzbg	PCR		PCR	
		s(2)		s(3)	1	1		s(3)		s(4)
SiO2	56.59	0.15	52.84	0.37	52.41	52.84	53.2	0.12	52.41	0.55
TiO2	0	0	0.39	0.1	0.17	0.33	0.06	0.1	0.54	0.08
Al2O3	0.76	0	2.39	0.22	1.51	2.08	1.57	0.11	2.17	0.24
Cr2O3	0.44	0	1.17	0.15	1.02	1.17	1.27	0.08	0.99	0.07
FeO	7.4	0.09	3.99	0.22	3.86	4.37	3.73	0.22	4.44	0.22
MnO	0.06	0.09	0	0	0	0	0	0	0.13	0
MgO	33.17	0.23	17.41	0.99	17.91	17.58	18.13	0.35	17.16	0.29
CaO	1.2	0.08	20.99	0.84	21.41	21.27	20.75	0.53	21.16	0.53
Na2O	0.61	0.1	0.49	0.43	0.67	0.54	0.67	0.13	0.78	0.17
K2O	0	0	0	0	0	0	0	0	0	0
[Total]	100.12	0.45	99.59	0.23	99.15	100.24	99.41	0.48	100.05	1.08
T Si	1.95		1.93		1.92	1.92	1.94		1.91	
T Al	0.03		0.07		0.07	0.08	0.06		0.09	
M1 Al	0		0.03		0	0.01	0.01		0	
M1 Ti	0		0.01		0.01	0.01	0		0.02	
M1Fe	0.08		0.02		0.09	0.06	0.06		0.08	
M1 Cr	0.01		0.03		0.03	0.03	0.04		0.03	
M1 Mg	0.91		0.91		0.88	0.89	0.89		0.87	
M2 Mg	0.79		0.04		0.1	0.06	0.09		0.06	
M2 Fe	0.12		0.1		0.01	0.07	0.05		0.05	
M2 Mn	0.002		0		0	0	0		0	
M2 Ca	0.04		0.82		0.84	0.83	0.81		0.83	
M2 Na	0.04		0.04		0.05	0.04	0.05		0.06	

Microprobe analyses of pyroxene (cont.):

No:	7		8	9		10		11		12
Sample:	UD 45/1 PCR		UD 59/4 Lhzbg	UD 59/9 Lhzbg		UD 64/6 Lhzbg		UD 64/7 Lhzbg		UD 1/8 Lhzbg
		s(4)	1		s(2)		s(3)		s(2)	1
	54.93	0.93	50.06	50.81	0.15	53.13	0.25	52.31	0.15	52.84
	0.29	0.04	1.17	0.75	0.05	0.37	0.12	1	0.24	0.5
Al2O3	2.65	0.56	4.35	2.83	0	2.08	0.19	2.83	0	1.13
Cr2O3	1.06	0.22	0	0.19	0.06	0	0	0	0	0
FeO	3.7	0.06	6.05	9.13	0.36	15.09	0.63	8.56	1	7.72
MnO	0.23	0.06	0	0.32	0.09	0.34	0.07	0.13	0.18	0.26
MgO	17.66	0.52	14.92	15.5	0.12	27.31	0.35	16.25	0.47	15.42
CaO	19.83	0.21	23.23	20.71	0	1.25	0.24	19.17	0.2	21.27
Na2O	0.13	0.27	0.4	0.2	0.29	0	0	0.27	0.38	0.94
K2O	0	0	0	0	0	0	0	0	0	0
[Total]	100.51	0.5	100.14	100.6	0.26	99.73	0.29	100.57	0.69	100.11
T Si	1.99		1.84	1.87		1.92		1.92		1.94
T Al	0.01		0.16	0.12		0.08		0.08		0.05
M1 Al	0.11		0.03	0		0.01		0.04		0
M1 Ti	0.01		0.03	0.02		0.01		0.03		0.01
M1Fe	0		0.13	0.12		0.06		0.04		0.14
M1 Cr	0.03		0	0.01		0		0		0
M1 Mg	0.86		0.82	0.85		0.93		0.89		0.85
M2 Mg	0.1		0	0		0.54		0		0
M2 Fe	0.11		0.06	0.16		0.4		0.22		0.09
M2 Mn	0.01		0	0.01		0.01		0		0.01
M2 Ca	0.77		0.91	0.82		0.05		0.75		0.84
M2 Na	0.01		0.03	0.02		0		0.02		0.07

Microprobe analyses for plagioclase:

Sample	1	2	3	4	5
Analysis	64/7-14A	64/7-21E	64/7-22H	64/7-23H	1/8-15C
Location	Lhzbg	Lhzbg	Lhzbg	Lhzbg	Bgab
SiO2	55.2	52.63	52.84	52.2	59.9
TiO2	*	*	0.17	*	*
Al2O3	27.78	29.29	29.29	29.67	22.86
FeO	0.77	0.77	0.64	0.77	0.52
MgO	*	*	*	*	0.5
CaO	10.35	12.45	12.17	12.59	5.6
Na2O	4.72	3.77	3.91	3.51	7.01
K2O	0.88	0.88	0.34	0.28	0.66
Total	99.1	99.79	99.36	99.01	97.05
Si	10.04	9.61	9.65	9.57	10.98
Al	5.95	6.3	6.3	6.4	4.93
Ti	*	*	0.02	*	*
Fe2	0.12	0.12	0.1	0.12	0.08
Mg	*	*	*	*	0.14
Ca	2.02	2.44	2.38	2.47	1.1
Na	1.66	1.34	1.38	1.25	2.49
K	0.07	0.21	0.08	0.07	0.16
Ab	44.4	33.6	36	32.9	66.5
An	53.8	61.3	62	65.4	29.3
Or	1.8	5.2	2	1.7	4.1

Microprobe analyses of brown (BRW), colourless (WHT) and green (GRN) phlogopite (n=50):

Sample	1	2	3	4	5
Analysis	5A-16G	5A-19G	5C-1A	5C-2A	54-11F
Location	M HZBG	M HZBG	M HZBG	M HZBG	PCR
Mineral	BRW	BRW	BRW	BRW	BRW
SiO2	38.294	38.722	38.080	36.583	39.364
TiO2	2.836	3.002	3.169	3.336	4.003
Al2O3	14.171	14.171	14.171	13.037	13.415
Cr2O3	1.608	1.754	0.877	0.877	2.046
FeO	5.275	5.403	5.532	6.690	4.760
MnO	0	0	0	0	0
MgO	21.723	21.226	21.226	22.553	20.894
CaO	0	0	0	0	0
Na2O	1.078	0.809	0.674	0	1.078
K2O	8.914	8.914	8.794	7.589	8.312
Total	93.90	94.00	92.52	90.66	93.87
Si	5.567	5.614	5.602	5.500	5.683
AlIV	2.426	2.386	2.398	2.308	2.281
AlVI	0.000	0.034	0.057	0.000	0.000
Ti	0.310	0.327	0.351	0.377	0.435
Fe3	-	-	-	-	-
Fe2	0.641	0.655	0.681	0.841	0.575
Cr	0.185	0.201	0.102	0.104	0.233
Mn	0.000	0.000	0.000	0.000	0.000
Mg	4.707	4.588	4.655	5.055	4.497
Ca	0.000	0.000	0.000	0.000	0.000
Na	0.304	0.227	0.192	0.000	0.302
K	1.653	1.649	1.650	1.456	1.531

Sample	6	7	8	9	10
Analysis	54-14F	55-7C	55-8C	55-9C	55-10C
Location	PCR	PCR	PCR	PCR	PCR
Mineral	BRW	BRW	BRW	BRW	BRW
SiO2	38.294	38.936	39.364	39.150	39.578
TiO2	4.170	5.338	0.234	0.500	5.505
Al2O3	13.415	13.415	15.116	14.549	13.415
Cr2O3	1.900	0.585	0	0	0.438
FeO	4.889	5.532	5.661	5.146	4.889
MnO	0	0	0	0	0
MgO	21.558	20.894	23.548	22.884	21.723
CaO	0	0	0	0	0
Na2O	0.944	1.078	0.674	0.944	1.348
K2O	8.191	7.830	7.709	7.950	7.950
Total	93.36	93.61	92.31	91.12	94.85
Si	5.572	5.631	5.727	5.773	5.635
AlIV	2.299	2.285	2.273	2.227	2.249
AlVI	0.000	0.000	0.317	0.300	0.000
Ti	0.456	0.581	0.026	0.055	0.590
Fe3	-	-	-	-	-
Fe2	0.595	0.669	0.689	0.635	0.582
Cr	0.218	0.067	0.000	0.000	0.049
Mn	0.000	0.000	0.000	0.000	0.000
Mg	4.676	4.504	5.107	5.031	4.610
Ca	0.000	0.000	0.000	0.000	0.000
Na	0.266	0.302	0.190	0.270	0.372
K	1.520	1.445	1.431	1.496	1.444

Microprobe analyses of brown (BRW), colourless (WHT) and green (GRN) phlogopite (n=50):

Sample	11	12	13	14	15
Analysis	14-14H	14-15H	11-15H	11-16H	11-17I
Location	PCR	PCR	PCR	PCR	PCR
Mineral	BRW	BRW	BRW	BRW	BRW
SiO2	37.866	38.080	38.294	38.508	39.150
TiO2	2.335	2.502	5.004	4.837	2.502
Al2O3	13.226	13.037	13.415	13.415	13.793
Cr2O3	1.900	1.754	0.585	0.585	0.585
FeO	6.304	5.789	5.789	5.918	6.304
MnO	0	0	0	0	0
MgO	22.055	22.553	20.894	20.563	22.553
CaO	0	0	0	0	0
Na2O	0.539	0.539	1.348	1.348	0.539
K2O	7.830	8.191	7.830	7.830	7.469
Total	92.06	92.45	93.16	93.00	92.90
Si	5.608	5.613	5.586	5.625	5.692
AlIV	2.307	2.263	2.304	2.308	2.308
AlVI	0.000	0.000	0.000	0.000	0.053
Ti	0.260	0.277	0.549	0.531	0.274
Fe3	-	-	-	-	-
Fe2	0.781	0.714	0.706	0.723	0.766
Cr	0.222	0.204	0.067	0.067	0.067
Mn	0.000	0.000	0.000	0.000	0.000
Mg	4.869	4.955	4.544	4.478	4.888
Ca	0.000	0.000	0.000	0.000	0.000
Na	0.155	0.154	0.381	0.382	0.152
K	1.479	1.540	1.457	1.459	1.385

Sample	16	17	18	19	20
Analysis	11-18I	12-11F	12-12F	13-10G	13-11G
Location	PCR	PCR	PCR	PCR	PCR
Mineral	BRW	BRW	BRW	BRW	BRW
SiO2	39.364	36.797	36.155	37.652	37.866
TiO2	2.502	1.668	4.003	2.002	2.168
Al2O3	13.604	13.037	12.848	13.415	13.037
Cr2O3	0.292	1.754	1.315	1.754	1.900
FeO	6.046	8.234	8.362	7.719	8.105
MnO	0.155	0	0	0.129	0
MgO	21.889	21.889	21.392	21.558	21.558
CaO	0	0	0	0	0
Na2O	0	0	0	0	0
K2O	7.348	6.625	6.866	7.228	6.987
Total	91.20	90.00	90.94	91.46	91.62
Si	5.797	5.584	5.453	5.619	5.641
AlIV	2.203	2.330	2.282	2.357	2.287
AlVI	0.156	0.000	0.000	0.000	0.000
Ti	0.277	0.190	0.454	0.225	0.243
Fe3	-	-	-	-	-
Fe2	0.745	1.045	1.055	0.963	1.010
Cr	0.034	0.210	0.157	0.207	0.224
Mn	0.019	0.000	0.000	0.016	0.000
Mg	4.805	4.952	4.810	4.796	4.788
Ca	0.000	0.000	0.000	0.000	0.000
Na	0.000	0.000	0.000	0.000	0.000
K	1.380	1.283	1.321	1.376	1.328

Microprobe analyses of brown (BRW), colourless (WHT) and green (GRN) phlogopite (n=50):

Sample	21	22	23	25	26
Analysis	451-6B	451-8C	451-9C	599-1A	599-2A
Location	PCR	PCR	PCR	L HZBG	L HZBG
Mineral	BRW	BRW	BRW	BRW	BRW
SiO2	39.150	40.647	40.861	38.508	38.722
TiO2	8.007	0.400	1.835	0.617	2.502
Al2O3	13.793	15.683	15.683	14.360	13.793
Cr2O3	1.023	0	0.614	0	0
FeO	4.760	5.403	4.889	12.350	12.093
MnO	0.258	0.258	0	0	0
MgO	19.733	23.382	21.723	19.733	19.402
CaO	0	0.126	0.140	0	0
Na2O	0.539	0	1.213	0	0.944
K2O	8.914	7.950	7.348	8.314	8.191
Total	96.18	93.85	94.31	93.88	95.65
Si	5.529	5.791	5.784	5.709	5.650
AlIV	2.294	2.209	2.216	2.291	2.350
AlVI	0.000	0.422	0.398	0.216	0.020
Ti	0.851	0.043	0.195	0.069	0.275
Fe3	-	-	-	-	-
Fe2	0.562	0.644	0.579	1.531	1.476
Cr	0.114	0.000	0.069	0.000	0.000
Mn	0.031	0.031	0.000	0.000	0.000
Mg	4.155	4.966	4.584	4.361	4.220
Ca	0.000	0.019	0.021	0.000	0.000
Na	0.148	0.000	0.333	0.000	0.267
K	1.606	1.445	1.327	1.573	1.525

Sample	27	28	29	30	31
Analysis	599-3A	599-11E	599-12E	646-18D	18-22F
Location	L HZBG	L HZBG	L HZBG	L HZBG	B GAB
Mineral	BRW	BRW	BRW	BRW	BRW
SiO2	38.936	37.438	37.652	38.080	34.657
TiO2	3.169	5.171	5.004	3.836	4.504
Al2O3	13.226	12.659	13.037	13.037	12.659
Cr2O3	0	0.161	0	0	0
FeO	10.806	12.608	12.350	10.935	24.701
MnO	0	0	0	0	0
MgO	19.899	16.583	17.246	19.899	9.618
CaO	0	0	0	0	0
Na2O	0.809	0.539	0.539	0	0
K2O	8.314	8.794	8.314	8.673	9.035
Total	95.16	93.95	94.14	94.46	95.17
Si	5.680	5.617	5.606	5.610	5.476
AlIV	2.272	2.237	2.286	2.262	2.356
AlVI	0.000	0.000	0.000	0.000	0.000
Ti	0.348	0.584	0.560	0.425	0.535
Fe3	-	-	-	-	-
Fe2	1.318	1.582	1.538	1.347	3.264
Cr	0.000	0.019	0.000	0.000	0.000
Mn	0.000	0.000	0.000	0.000	0.000
Mg	4.327	3.709	3.828	4.370	2.266
Ca	0.000	0.000	0.000	0.000	0.000
Na	0.229	0.157	0.156	0.000	0.000
K	1.547	1.683	1.579	1.630	1.821

Microprobe analyses of brown (BRW), colourless (WHT) and green (GRN) phlogopite (n=50):

Sample	32	33	34	35
Analysis	18-24G	45G-9C	45G-10C	45G-13D
Location	B GAB	B GAB	B GAB	B GAB
Mineral	BRW	BRW	BRW	BRW
SiO2	35.513	38.508	37.011	37.866
TiO2	5.338	4.003	4.003	3.670
Al2O3	12.659	10.959	11.904	12.093
Cr2O3	0	0	0.132	0
FeO	16.853	20.069	20.455	20.069
MnO	0	0	0	0.129
MgO	13.764	12.271	12.603	13.100
CaO	0	1.259	0	0
Na2O	0	0	0	0
K2O	8.553	8.071	9.035	8.914
Total	92.68	95.14	95.14	95.84
Si	5.521	5.884	5.698	5.755
AlIV	2.318	1.972	2.158	2.165
AlVI	0.000	0.000	0.000	0.000
Ti	0.624	0.460	0.464	0.420
Fe3	-	-	-	-
Fe2	2.191	2.564	2.633	2.551
Cr	0.000	0.000	0.016	0.000
Mn	0.000	0.000	0.000	0.017
Mg	3.190	2.795	2.892	2.968
Ca	0.000	0.206	0.000	0.000
Na	0.000	0.000	0.000	0.000
K	1.696	1.573	1.774	1.728

Sample	36	37	38	39	40
Analysis	54-9E	341-11D	451-11D	57-5D	57-6D
Location	PCR	PCR	PCR	PCR	PCR
Mineral	WHT	WHT	WHT	GRN	GRN
SiO2	39.578	32.946	41.931	44.284	38.51
TiO2	0	0.400	0.150	0.234	0.367
Al2O3	12.093	17.950	14.927	9.825	16.817
Cr2O3	0	18.121	0	0.146	0
FeO	12.093	10.421	3.345	4.760	4.503
MnO	0	0	0	0	0
MgO	21.723	6.301	24.708	24.045	23.211
CaO	0	0.406	0	3.778	0
Na2O	0.539	0.674	0	0.809	0
K2O	6.384	5.782	9.035	5.300	9.757
Total	92.41	93.00	94.10	93.18	93.16
Si	5.898	5.083	5.918	6.306	5.577
AlIV	2.102	2.917	2.082	1.648	2.423
AlVI	0.020	0.344	0.399	0.000	0.445
Ti	0.000	0.046	0.016	0.025	0.040
Fe3	-	-	-	-	-
Fe2	1.507	1.344	0.395	0.567	0.545
Cr	0.000	2.208	0.000	0.016	0.000
Mn	0.000	0.000	0.000	0.000	0.000
Mg	4.826	1.449	5.199	5.104	5.011
Ca	0.000	0.067	0.000	0.576	0.000
Na	0.156	0.202	0.000	0.223	0.000
K	1.214	1.138	1.627	0.963	1.803

Microprobe analyses of brown (BRW), colourless (WHT) and green (GRN) phlogopite (n=50):

Sample	41	42	43	44	45
Analysis	57-8D	57-9D	454-5B	599-14F	646-3A
Location	PCR	PCR	L HZBG	L HZBG	L HZBG
Mineral	GRN	GRN	GRN	GRN	GRN
SiO2	40.000	38.1	34.900	38.500	39.800
TiO2	0	0	0.150	0	0
Al2O3	13.415	15.305	20.407	13.982	13.038
Cr2O3	0	0	0	0	0
FeO	5.275	5.017	15.567	11.064	10.935
MnO	0	0	0.387	0	0
MgO	24.371	23.542	13.761	20.226	21.221
CaO	2.099	0	0	0	0
Na2O	0.809	0.404	0	0.674	0.539
K2O	7.228	9.155	8.071	8.432	8.432
Total	93.20	91.52	93.24	92.88	93.97
Si	5.785	5.634	5.291	5.756	5.863
AlIV	2.215	2.366	2.709	2.244	2.137
AlVI	0.070	0.299	0.934	0.218	0.125
Ti	0.000	0.000	0.017	0.000	0.000
Fe3	-	-	-	-	-
Fe2	0.638	0.620	1.974	1.383	1.347
Cr	0.000	0.000	0.000	0.000	0.000
Mn	0.000	0.000	0.050	0.000	0.000
Mg	5.255	5.189	3.110	4.508	4.661
Ca	0.325	0.000	0.000	0.000	0.000
Na	0.227	0.116	0.000	0.195	0.154
K	1.334	1.727	1.561	1.608	1.585

Sample	46	47	48	49	49
Analysis	646-4A	646-5A	646-14C	646-15C	646-15C
Location	L HZBG	L HZBG	L HZBG	L HZBG	L HZBG
Mineral	GRN	GRN	GRN	GRN	GRN
SiO2	41.500	39.800	36.800	38.900	38.900
TiO2	0.217	0.217	4.671	0.484	0.484
Al2O3	13.227	12.849	12.849	12.471	12.471
Cr2O3	0	0	0	0	0
FeO	5.017	11.321	12.608	11.836	11.836
MnO	0	0	0	0	0
MgO	24.371	20.724	17.242	22.050	22.050
CaO	0.182	0	0	0	0
Na2O	0	0.539	0	0.539	0.539
K2O	8.794	8.312	8.914	7.348	7.348
Total	93.31	93.76	93.08	93.63	93.63
Si	5.965	5.883	5.573	5.761	5.761
AlIV	2.035	2.117	2.291	2.175	2.175
AlVI	0.204	0.120	0.000	0.000	0.000
Ti	0.023	0.024	0.532	0.054	0.054
Fe3	-	-	-	-	-
Fe2	0.603	1.399	1.597	1.466	1.466
Cr	0.000	0.000	0.000	0.000	0.000
Mn	0.000	0.000	0.000	0.000	0.000
Mg	5.223	4.567	3.892	4.868	4.868
Ca	0.028	0.000	0.000	0.000	0.000
Na	0.000	0.154	0.000	0.155	0.155
K	1.613	1.567	1.722	1.388	1.388

Sample	50	
Analysis	34/1	
Location	PCR	
Mineral	Cr-mica:	std
SiO2	49.7	1.2
TiO2	0.11	0.06
Al2O3	27	1.8
Cr2O3	6.28	0.3
FeO	0.69	0.3
MnO	0.01	0.007
MgO	3	1
CaO	1.61	0.4
Na2O	1.15	0.5
K2O	6.73	1.5
Total	95.85	
Si	8.56	
Al	1.82	
Al	*	
Ti	0.01	
Fe3	*	
Fe2	0.1	
Cr	0.28	
Mn	*	
Mg	0.77	
Ca	0.3	
Na	0.38	
K	1.48	

Microprobe analyses for serpentine (n=50):
s=standard deviation; ( )=number of analyses

	1		2		3		4		5		6	
	UD 5/A	s(4)	UD 5/C	s(6)	UD 5/D	s(2)	UD 1/4	s(5)	UD 34/4	s(4)	UD 5/C	s(10)
SiO2	43.43	0.49	41.18	2.01	43.43	1.21	42.66	0.54	44.77	2.70	43.02	3.05
TiO2	0	0	0.00	0.00	0	0	0	0	0	0	0	0
Al2O3	0	0	2.39	1.78	0	0	0.45	0.29	0.14	0.29	0.72	0.44
FeO	2.28	0.46	8.23	0.65	4.37	1.27	6.92	1.45	6.79	0.52	9.05	1.61
Cr2O3	0	0	0.80	0.68	0.00	0.00	0	0	0.13	0.15	0	0
MnO	0.03	0.06	0.00	0.00	0.06	0.08	0	0	0	0	0.11	0.04
MgO	38.51	0.25	32.47	1.39	36.73	1.06	34.86	1.66	33.79	2.32	31.13	1.23
CaO	0.03	0.07	0.56	1.05	0.08	0.12	0	0	0	0	0	0
Na2O	0.54	0.11	0.61	0.07	0.54	0.00	0.40	0.23	0.81	0	0.12	0.15
total	84.78	0.38	86.21	1.27	85.15	0.70	85.37	0.59	86.42		85.21	0.29
	7	8		9	10		11		12		13	14
	UD 45/C	UD 45/1	s(3)	UD 45/A	UD 45/3	s(3)	UD 1/1	s(3)	UD 1/2	s(5)	UD 1/3	UD 34/5
SiO2	44.93	44.39	0.76	44.93	46.00	0	43.93	0.25	42.07	0.46	42.57	44.50
TiO2	0	0	0	0	0	0	0	0	0	0	0	0
Al2O3	0	0.57	0.27	0.00	0.63	0.53	0	0	0.79	0.25	1.13	0
FeO	4.63	1.42	0.36	6.18	3.47	0.45	4.76	0.13	8.04	0.35	9.78	1.54
Cr2O3	0	0	0	0	0	0	0	0	0.15	0	0	0
MnO	0	0	0	0	0.04	0.09	0	0	0	0	0.13	0
MgO	34.49	37.97	0.23	33.83	35.21	0.12	37.20	0.35	34.22	0.45	32.67	39.14
CaO	0	0	0	0	0	0	0.04	0.06	0.02	0.05	0	0
Na2O	0.81	0	0	0.94	0	0	0.36	0.08	0.45	0.23	0	0.81
total	84.71	84.39	0.29	85.74	85.37	1.07	86.17	0.87	85.86	1.01	86.42	85.97

Microprobe analyses for chlorite (n=5):

Sample	1	2	3	4	5
Analysis	5/4-10E	45/4-6B	45/4-7B	34/7-1A	59/9-7C
Location	PCR	Lhzbg	Lhzbg	Lhzbg	Lhzbg
Mineral	Chl	Chl	Chl	Chl	Chl
SiO2	30.59	28.45	31.02	29.73	29.5
TiO2	0	0	0	0	0
Al2O3	16.25	20.60	18.52	14.74	17.8
Cr2O3	0	0	0	0	0
FeO	16.60	16.34	13.89	12.48	23.3
Fe2O3	0	0	0	0	0
MnO	0.15	0.52	0.39	0	0.5
MgO	21.72	19.40	22.71	26.36	18.7
CaO	0	0	0	0	0
Na2O	0.54	0	0	0.81	0
K2O	0	0.19	0.12	0	0.79
Total	85.85	85.50	86.65	84.12	90.59
Si	6.260	5.837	6.175	6.116	5.955
AlIV	1.740	2.163	1.825	1.884	2.045
Sum_T	8.000	8.000	8.000	8.000	8.000
AlVI	2.176	2.814	2.516	1.692	2.182
Ti	0.000	0.000	0.000	0.000	0.000
Fe3	0.000	0.000	0.000	0.000	0.000
Fe2	2.841	2.804	2.312	2.148	3.932
Cr	0.000	0.000	0.000	0.000	0.000
Mn	0.026	0.090	0.066	0.000	0.085
Mg	6.626	5.934	6.739	8.088	5.625
Ca	0.000	0.000	0.000	0.000	0.000
Na	0.214	0.000	0.000	0.323	0.000
K	0.000	0.050	0.030	0.000	0.203
Cations	19.883	19.692	19.663	20.251	20.027
O	36.000	36.000	36.000	36.000	36.000
Fe_FeMg	0.30	0.32	0.26	0.21	0.41
Mg_FeMg	0.70	0.68	0.74	0.79	0.59

Microprobe analyses for talc (n=8):

	1		2		3		4
	UD 5/1	s(2)	UD 1/4	s(2)	UD 1/3	s(3)	UD 34/8
SiO2	56.05	0	61.72	0.45	60.26	0.69	61.6
TiO2	0	0	0	0	0.22	0.06	0
Al2O3	2.83	0	0	0	0.38	0	0
Cr2O3	0.66	0.31	0	0	0.24	0.08	0
FeO	4.95	0.09	2.06	0	3.86	0.13	1.3
MnO	0	0	0	0	0	0	0
MgO	28.52	0.47	29.10	0.59	28.91	0.10	29.5
CaO	0	0	0	0	0	0	0
Na2O	0.27	0.38	0.61	0.10	0.63	0.08	0.8
[Total]	93.55	0.59	93.58	0.57	94.55	0.64	93.44
Si	8.31		8.76		8.60		8.75
Ti	0		0		0.02		0
Al	0.17		0		0.02		0
Cr	0.03		0		0.01		0
Fe	0.61		0.24		0.46		0.15
Mn	0		0		0		0
Mg	6.30		6.15		6.15		6.24
Ca	0		0		0		0
Na	0.08		0.17		0.17		0.22

Microprobe analyses of amphibole (n=59):

Sample	1_wht	2_wht	3_wht	4_wht	5_wht	6_wht	7_wht
Analysis	54_2a	54_3b	54_4b	54_6c	54_13f	45c_3b	451_18f
Location	PCR	PCR	PCR	PCR	PCR	PCR	PCR
Mineral	amp	amp	amp	amp	amp	amp	amp
SiO2	55.83665	57.33418	57.97598	54.33911	56.90631	29.95069	46.85144
TiO2	-	-	-	.333607	-	.150123	.200164
Al2O3	1.511571	-	-	2.645249	.377893	15.30466	12.28151
FeO	5.403242	6.175134	4.759999	3.216216	6.175134	14.28	4.502702
Cr2O3	.876934	.292311	.146156	1.02309	.584623	10.52321	.730778
MnO	-	.258245	.129123	-	.129123	.516491	-
MgO	20.23097	19.89931	21.06011	21.72342	20.06514	28.854	17.57773
CaO	12.7326	12.7326	13.57211	12.31284	12.7326	-	11.89309
Na2O	.943577	.539187	.539187	1.347968	.539187	.943577	2.830732
K2O	-	-	-	.108414	-	-	.302251
Total	97,40	97,42	98,26	97,14	97,39	100,53	97,17
TSi	7.830	8.071	8.049	7.591	7.980	3.751	6.664
TAl	0.170	0.000	0.000	0.400	0.023	2.257	1.336
TFe3	0.000	0.000	0.000	0.010	0.000	1.476	0.000
TTi	0.000	0.000	0.000	0.000	0.000	0.007	0.000
Sum_T	8.000	8.071	8.049	8.000	8.002	7.490	8.000
CAl	0.080	0.000	0.000	0.035	0.040	0.000	0.721
CCr	0.097	0.032	0.016	0.113	0.065	1.041	0.082
CFe3	0.000	0.000	0.000	0.111	0.002	0.020	0.081
CTi	0.000	0.000	0.000	0.035	0.000	0.008	0.021
CMg	4.230	4.176	4.359	4.524	4.194	3.932	3.727
CFe2	0.593	0.727	0.553	0.181	0.692	0.000	0.366
CMn	0.000	0.031	0.015	0.000	0.008	0.000	0.000
CCa	0.000	0.034	0.057	0.000	0.000	0.000	0.000
Sum_C	5.000	5.000	5.000	5.000	5.000	5.000	5.000
BMg	0.000	0.000	0.000	0.000	0.000	1.455	0.000
BFe2	0.040	0.000	0.000	0.073	0.031	0.000	0.088
BMn	0.000	0.000	0.000	0.000	0.008	0.055	0.000
BCa	1.913	1.887	1.961	1.843	1.913	0.000	1.812
BNa	0.046	0.113	0.039	0.084	0.049	0.106	0.100
Sum_B	2.000	2.000	2.000	2.000	2.000	1.616	2.000
ACa	0.000	0.000	0.000	0.000	0.000	0.000	0.000
ANa	0.210	0.034	0.106	0.281	0.098	0.123	0.681
AK	0.000	0.000	0.000	0.019	0.000	0.000	0.055
Sum_A	0.210	0.034	0.106	0.301	0.098	0.123	0.736
Sum_cat	15.210	15.105	15.155	15.301	15.100	14.229	15.736

Microprobe analyses of amphibole (n=59):

Sample	8_wht	9_wht	10_wht	11_wht	12_wht	13_wht	14_wht
Analysis	451_19f	452_4b	452_6c	453_3b	453_4b	347_5b	454_3a
Location	PCR	PCR	PCR	LHzbg	LHzbg	LHzbg	LHzbg
Mineral	amp	amp	amp	amp	amp	amp	amp
SiO2	54.98092	57.54811	52.62765	49.20471	50.70224	56.90631	59.04565
TiO2	.200164	-	-	.417008	.467049	-	-
Al2O3	4.534713	3.023142	8.502586	9.258372	8.124694	.377893	.755786
FeO	3.216216	2.315675	2.44324	6.046485	5.789188	3.344864	3.344864
Cr2O3	.438467	.584623	.584623	-	-	.146156	-
MnO	-	-	-	-	.129123	-	.129123
MgO	21.06011	21.39176	20.06514	19.236	18.24104	22.2209	21.22593
CaO	12.03301	12.7326	12.59268	11.19349	11.75317	14.13179	12.87252
Na2O	1.213171	.808781	1.752358	2.021952	2.291545	.808781	-
K2O	.096	-	.108414	.108414	.084	.132507	-
Total	97,79	98,54	98,74	97,46	97,58	98,22	97,45
TSi	7.591	7.879	7.235	6.873	7.162	7.893	8.152
TAl	0.409	0.121	0.765	1.127	0.838	0.062	0.000
TFe3	0.000	0.000	0.000	0.000	0.000	0.000	0.000
TTi	0.000	0.000	0.000	0.000	0.000	0.000	0.000
Sum_T	8.000	8.000	8.000	8.000	8.000	7.955	8.152
CAl	0.328	0.367	0.611	0.397	0.513	0.000	0.123
CCr	0.048	0.063	0.063	0.000	0.000	0.016	0.000
CFe3	0.123	0.000	0.000	0.349	0.091	0.000	0.000
CTi	0.021	0.000	0.000	0.044	0.050	0.000	0.000
CMg	4.335	4.366	4.112	4.006	3.841	4.595	4.369
CFe2	0.145	0.203	0.213	0.205	0.497	0.380	0.386
CMn	0.000	0.000	0.000	0.000	0.008	0.000	0.015
CCa	0.000	0.000	0.000	0.000	0.000	0.010	0.107
Sum_C	5.000	5.000	5.000	5.000	5.000	5.000	5.000
BMg	0.000	0.000	0.000	0.000	0.000	0.000	0.000
BFe2	0.103	0.062	0.068	0.153	0.096	0.008	0.000
BMn	0.000	0.000	0.000	0.000	0.008	0.000	0.000
BCa	1.780	1.868	1.855	1.675	1.779	1.992	1.797
BNa	0.117	0.070	0.077	0.172	0.118	0.000	0.000
Sum_B	2.000	2.000	2.000	2.000	2.000	2.000	1.797
ACa	0.000	0.000	0.000	0.000	0.000	0.099	0.000
ANa	0.208	0.144	0.390	0.376	0.510	0.218	0.000
AK	0.017	0.000	0.019	0.019	0.015	0.023	0.000
Sum_A	0.225	0.144	0.409	0.395	0.525	0.340	0.000
Sum_cat	15.225	15.144	15.409	15.395	15.525	15.295	14.949

Microprobe analyses of amphibole (n=59):

Sample	15_wht	16_wht	17_wht	18_wht	19_wht	20_wht	21_wht
Analysis	454_14d	45e_6c	45e_7c	646_1a	646_2a	647_12g	647_13g
Location	LHzbg	LHzbg	LHzbg	LHzbg	LHzbg	LHzbg	LHzbg
Mineral	amp	amp	amp	amp	amp	amp	amp
SiO2	57.33418	60.32925	59.90138	49.63258	53.91125	58.61778	58.83172
TiO2	.250205	-	-	.183484	.150123	-	-
Al2O3	1.889464	-	-	7.179962	3.778927	-	-
FeO	3.087568	3.344864	3.473513	6.303783	4.888648	1.801081	1.801081
Cr2O3	-	-	-	-	-	-	-
MnO	-	-	.387368	-	.129123	.258245	.258245
MgO	21.39176	21.55759	21.22593	19.73348	22.2209	23.87918	23.38169
CaO	12.59268	12.7326	12.87252	13.01244	12.87252	13.99187	13.71203
Na2O	.539187	-	-	1.347968	1.078374	-	-
K2O	-	-	-	.168645	-	-	-
Total	٩٧,٢٤	٩٨,١٤	٩٧,٧٠	٩٧,٤٧	٩٨,٩١	٩٣,٧٤	٩٧,٩٣
TSi	7.948	8.271	8.246	6.956	7.347	7.934	8.015
TAl	0.052	0.000	0.000	1.044	0.607	0.000	0.000
TFe3	0.000	0.000	0.000	0.000	0.046	0.063	0.000
TTi	0.000	0.000	0.000	0.000	0.000	0.000	0.000
Sum_T	8.000	8.271	8.246	8.000	8.000	7.997	8.015
CAl	0.256	0.000	0.000	0.141	0.000	0.000	0.000
CCr	0.000	0.000	0.000	0.000	0.000	0.000	0.000
CFe3	0.000	0.000	0.000	0.518	0.389	0.037	0.000
CTi	0.026	0.000	0.000	0.019	0.015	0.000	0.000
CMg	4.421	4.406	4.356	4.123	4.515	4.819	4.749
CFe2	0.297	0.384	0.400	0.199	0.073	0.104	0.205
CMn	0.000	0.000	0.045	0.000	0.007	0.027	0.030
CCa	0.000	0.211	0.199	0.000	0.000	0.014	0.016
Sum_C	5.000	5.000	5.000	5.000	5.000	5.000	5.000
BMg	0.000	0.000	0.000	0.000	0.000	0.000	0.000
BFe2	0.061	0.000	0.000	0.021	0.049	0.000	0.000
BMn	0.000	0.000	0.000	0.000	0.007	0.003	0.000
BCa	1.870	1.660	1.700	1.954	1.880	1.997	1.986
BNa	0.069	0.000	0.000	0.025	0.064	0.000	0.000
Sum_B	2.000	1.660	1.700	2.000	2.000	2.000	1.986
ACa	0.000	0.000	0.000	0.000	0.000	0.018	0.000
ANa	0.076	0.000	0.000	0.342	0.221	0.000	0.000
AK	0.000	0.000	0.000	0.030	0.000	0.000	0.000
Sum_A	0.076	0.000	0.000	0.372	0.221	0.018	0.000
Sum_cat	15.076	14.931	14.946	15.372	15.221	15.016	15.001

Microprobe analyses of amphibole (n=59):

Sample	22_wht	23_wht	24_wht	25_wht	26_wht	27_grn	28_grn
Analysis	18_17c	18_18c	18_19c	18_21e	18_23f	349_1a	45e_3a
Location	BGab	BGab	BGab	BGab	BGab	LHzbg	LHzbg
Mineral	amp	amp	amp	amp	amp	amp	amp
SiO2	54.98092	55.83665	55.40878	56.05058	55.40878	50.27438	44.28424
TiO2	-	-	-	-	-	.800656	3.836477
Al2O3	.377893	1.133678	1.133678	.755786	.755786	3.778927	10.95889
FeO	14.66594	11.32108	11.19243	11.19243	11.32108	13.25081	10.42054
Cr2O3	-	-	-	-	-	.292311	-
MnO	.258245	.387368	.258245	.258245	.258245	.11621	-
MgO	14.59283	16.91442	16.58276	16.91442	17.24607	14.92448	13.26621
CaO	12.45276	12.59268	12.59268	12.45276	12.31284	12.7326	11.05357
Na2O	.673984	.539187	.40439	.673984	.539187	1.078374	2.965529
K2O	-	-	-	-	-	.361381	1.011868
Total	97,96	98,77	97,46	98,36	97,65	98,00	97,75
TSi	7.989	7.900	7.931	7.972	7.890	7.346	6.558
TAl	0.014	0.100	0.069	0.028	0.101	0.650	1.442
TFe3	0.000	0.000	0.000	0.000	0.009	0.003	0.000
TTi	0.000	0.000	0.000	0.000	0.000	0.000	0.000
Sum_T	8.003	8.000	8.000	8.001	8.000	8.000	8.000
CAl	0.050	0.089	0.122	0.098	0.026	0.000	0.469
CCr	0.000	0.000	0.000	0.000	0.000	0.034	0.000
CFe3	0.000	0.055	0.010	0.011	0.128	0.078	0.000
CTi	0.000	0.000	0.000	0.000	0.000	0.088	0.427
CMg	3.161	3.568	3.539	3.586	3.661	3.251	2.929
CFe2	1.773	1.265	1.313	1.289	1.170	1.538	1.175
CMn	0.016	0.023	0.016	0.015	0.016	0.011	0.000
CCa	0.000	0.000	0.000	0.000	0.000	0.000	0.000
Sum_C	5.000	5.000	5.000	5.000	5.000	5.000	5.000
BMg	0.000	0.000	0.000	0.000	0.000	0.000	0.000
BFe2	0.009	0.019	0.016	0.031	0.041	0.000	0.115
BMn	0.016	0.023	0.016	0.016	0.016	0.003	0.000
BCa	1.939	1.909	1.931	1.898	1.878	1.993	1.754
BNa	0.036	0.049	0.037	0.055	0.065	0.004	0.131
Sum_B	2.000	2.000	2.000	2.000	2.000	2.000	2.000
ACa	0.000	0.000	0.000	0.000	0.000	0.000	0.000
ANa	0.154	0.099	0.075	0.131	0.084	0.302	0.721
AK	0.000	0.000	0.000	0.000	0.000	0.067	0.191
Sum_A	0.154	0.099	0.075	0.131	0.084	0.369	0.912
Sum_cat	15.157	15.099	15.075	15.131	15.084	15.369	15.912

Microprobe analyses of amphibole (n=59):

Sample	29_gm	30_gm	31_gm	32_gm	33_gm	34_gm	35_gm
Analysis	591_1a	591_4b	599_9d	599_10d	5912_1a	5912_2a	5912_5b
Location	LHzbg	LHzbg	LHzbg	LHzbg	LHzbg	LHzbg	LHzbg
Mineral	amp	amp	amp	amp	amp	amp	amp
SiO2	46.6375	50.27438	54.33911	53.91125	53.26944	52.84158	54.76698
TiO2	.48373	.767295	.250205	.183484	-	-	-
Al2O3	9.447318	5.857337	2.267356	2.267356	3.023142	3.212088	2.267356
FeO	10.93513	8.362161	12.60757	11.96432	13.63675	13.89405	9.905944
Cr2O3	-	-	.160771	.13154	-	.146156	-
MnO	-	.129123	.387368	.258245	.258245	.387368	.258245
MgO	16.41693	17.74355	16.41693	17.08024	15.42197	14.75866	18.07521
CaO	12.31284	13.43219	13.29227	13.43219	13.01244	13.29227	13.57211
Na2O	2.156749	1.347968	.673984	.539187	.673984	.943577	-
K2O	.240921	.180691	.120461	.108414	.156599	.204783	-
Total	98,61	98,60	100,58	100,CC	99,86	99,58	98,78
TSi	6.637	7.146	7.623	7.570	7.578	7.564	7.656
TAl	1.363	0.854	0.375	0.375	0.422	0.436	0.344
TFe3	0.000	0.000	0.002	0.055	0.000	0.000	0.000
TTi	0.000	0.000	0.000	0.000	0.000	0.000	0.000
Sum_T	8.000	8.000	8.000	8.000	8.000	8.000	8.000
CAl	0.221	0.127	0.000	0.000	0.084	0.106	0.029
CCr	0.000	0.000	0.018	0.015	0.000	0.017	0.000
CFe3	0.530	0.109	0.103	0.188	0.142	0.018	0.280
CTi	0.052	0.082	0.026	0.019	0.000	0.000	0.000
CMg	3.483	3.760	3.434	3.575	3.270	3.150	3.767
CFe2	0.714	0.885	1.374	1.162	1.480	1.645	0.879
CMn	0.000	0.016	0.045	0.031	0.023	0.047	0.031
CCa	0.000	0.021	0.000	0.010	0.000	0.018	0.015
Sum_C	5.000	5.000	5.000	5.000	5.000	5.000	5.000
BMg	0.000	0.000	0.000	0.000	0.000	0.000	0.000
BFe2	0.057	0.000	0.000	0.000	0.000	0.000	0.000
BMn	0.000	0.000	0.001	0.000	0.008	0.000	0.000
BCa	1.878	2.000	1.998	2.000	1.983	2.000	2.000
BNa	0.065	0.000	0.001	0.000	0.009	0.000	0.000
Sum_B	2.000	2.000	2.000	2.000	2.000	2.000	2.000
ACa	0.000	0.025	0.000	0.011	0.000	0.021	0.018
ANa	0.530	0.372	0.182	0.147	0.177	0.262	0.000
AK	0.044	0.033	0.022	0.019	0.028	0.037	0.000
Sum_A	0.574	0.429	0.204	0.177	0.205	0.320	0.018
Sum_cat	15.574	15.429	15.204	15.177	15.205	15.320	15.018

Microprobe analyses of amphibole (n=59):

Sample	36_grn	37_grn	38_grn	39_grn	40_grn	41_grn
Analysis	5912_6b	19_7c	19_8c	45g_1a	45g_2a	45g_3b
Location	LHzbg	BGab	BGab	BGab	BGab	BGab
Mineral	amp	amp	amp	amp	amp	amp
SiO2	55.40878	51.77191	51.13011	50.06044	49.63258	41.71704
TiO2	-	-	-	.767295	.867377	-
Al2O3	1.889464	2.645249	1.889464	4.723659	4.345767	10.2031
FeO	10.42054	21.74162	21.74162	16.08108	16.20973	26.63027
Cr2O3	-	-	-	-	-	-
MnO	.258245	.258245	.258245	.258245	-	.129123
MgO	17.57773	9.618002	9.949656	13.59786	13.59786	5.306484
CaO	13.85195	12.17292	12.17292	12.17292	12.17292	12.31284
Na2O	.539187	.943577	.673984	.943577	1.078374	1.078374
K2O	.096	.132507	-	.409566	.337289	1.084144
Total	100,33	99,27	97,66	98,93	98,52	98,71
TSi	7.744	7.697	7.687	7.249	7.255	6.446
TAl	0.256	0.303	0.313	0.751	0.733	1.554
TFe3	0.000	0.000	0.000	0.000	0.012	0.000
TTi	0.000	0.000	0.000	0.000	0.000	0.000
Sum_T	8.000	8.000	8.000	8.000	8.000	8.000
CAl	0.055	0.161	0.022	0.054	0.015	0.302
CCr	0.000	0.000	0.000	0.000	0.000	0.000
CFe3	0.040	0.005	0.137	0.308	0.270	0.674
CTi	0.000	0.000	0.000	0.084	0.095	0.000
CMg	3.662	2.132	2.230	2.935	2.963	1.222
CFe2	1.178	2.686	2.595	1.603	1.656	2.766
CMn	0.031	0.016	0.016	0.016	0.000	0.017
CCa	0.034	0.000	0.000	0.000	0.000	0.018
Sum_C	5.000	5.000	5.000	5.000	5.000	5.000
BMg	0.000	0.000	0.000	0.000	0.000	0.000
BFe2	0.000	0.012	0.002	0.036	0.044	0.000
BMn	0.000	0.016	0.016	0.016	0.000	0.000
BCa	2.000	1.939	1.961	1.889	1.907	2.000
BNa	0.000	0.033	0.021	0.060	0.050	0.000
Sum_B	2.000	2.000	2.000	2.000	2.000	2.000
ACa	0.040	0.000	0.000	0.000	0.000	0.021
ANa	0.146	0.239	0.176	0.205	0.256	0.323
AK	0.017	0.025	0.000	0.076	0.063	0.214
Sum_A	0.203	0.265	0.176	0.281	0.319	0.557
Sum_cat	15.203	15.265	15.176	15.281	15.319	15.557

Microprobe analyses of amphibole (n=59):

Sample	42_grn	43_grn	44_grn	45_lgrn	46_lgrn	47_lgrn	48_lgrn
Analysis	45g_4b	45g_5c	45g_12d	454_8c	454_13d	59I_6c	59I_7c
Location	BGab	BGab	BGab	LHzbg	LHzbg	LHzbg	LHzbg
Mineral	amp	amp	amp	amp	amp	amp	amp
SiO2	38.72197	48.99078	48.77684	47.06537	46.42358	55.62271	55.40878
TiO2	-	1.00082	1.167623	.667213	.750615	.200164	.266885
Al2O3	12.09257	5.101552	5.290498	10.39205	11.14784	2.07841	2.07841
FeO	28.3027	16.98162	16.98162	7.718918	7.847566	8.748107	8.619458
Cr2O3	-	-	-	.409236	-	.423851	.482314
MnO	-	.258245	.258245	-	.129123	.129123	-
MgO	3.48238	13.43204	13.43204	16.58276	16.08528	19.07018	19.236
CaO	12.03301	11.47333	11.75317	11.47333	11.47333	13.29227	13.57211
Na2O	1.347968	1.213171	1.213171	2.695935	2.830732	.539187	-
K2O	1.650308	.469796	.57821	.469796	.57821	-	-
Total	97,65	98,92	99,38	97,30	97,36	100,25	99,63
TSi	6.142	7.116	7.064	6.758	6.703	7.669	7.636
TAl	1.858	0.848	0.894	1.242	1.297	0.329	0.337
TFe3	0.000	0.037	0.042	0.000	0.000	0.002	0.027
TTi	0.000	0.000	0.000	0.000	0.000	0.000	0.000
Sum_T	8.000	8.000	8.000	8.000	8.000	8.000	8.000
CAl	0.401	0.025	0.008	0.515	0.598	0.008	0.000
CCr	0.000	0.000	0.000	0.046	0.000	0.046	0.052
CFe3	0.660	0.440	0.413	0.168	0.124	0.130	0.252
CTi	0.000	0.109	0.127	0.072	0.082	0.021	0.028
CMg	0.823	2.908	2.900	3.550	3.462	3.920	3.952
CFe2	3.095	1.501	1.535	0.649	0.726	0.868	0.714
CMn	0.000	0.016	0.016	0.000	0.008	0.008	0.000
CCa	0.021	0.000	0.000	0.000	0.000	0.000	0.002
Sum_C	5.000	5.000	5.000	5.000	5.000	5.000	5.000
BMg	0.000	0.000	0.000	0.000	0.000	0.000	0.000
BFe2	0.000	0.084	0.066	0.110	0.097	0.009	0.000
BMn	0.000	0.016	0.016	0.000	0.008	0.008	0.000
BCa	2.000	1.785	1.824	1.765	1.775	1.964	2.000
BNa	0.000	0.114	0.094	0.125	0.120	0.019	0.000
Sum_B	2.000	2.000	2.000	2.000	2.000	2.000	2.000
ACa	0.024	0.000	0.000	0.000	0.000	0.000	0.002
ANa	0.415	0.228	0.247	0.626	0.673	0.125	0.000
AK	0.334	0.087	0.107	0.086	0.107	0.000	0.000
Sum_A	0.773	0.315	0.354	0.712	0.779	0.125	0.002
Sum_cat	15.773	15.315	15.354	15.712	15.779	15.125	15.002

Microprobe analyses of amphibole (n=59):

Sample	49_lgm	50_lgm	51_lgm	52_type a	53_type a	54_type a
Analysis	59I_15e	646_12c	646_13c	55_4b	55_6b	55_11d
Location	LHzbg	LHzbg	LHzbg	PCR	PCR	PCR
Mineral	amp	amp	amp	amp	amp	amp
SiO2	54.76698	48.34898	50.06044	58.18992	58.18992	58.18992
TiO2	.51709	.183484	-	-	-	-
Al2O3	2.834196	8.880479	5.668391	-	-	-
FeO	6.947026	5.917837	11.19243	6.56108	6.175134	7.204323
Cr2O3	.672316	-	-	-	-	.146156
MnO	-	-	.258245	.180772	.206596	.129123
MgO	19.40183	19.56766	16.58276	34.8238	33.33135	34.65797
CaO	13.71203	13.43219	12.45276	.22387	.139919	.195886
Na2O	.673984	2.021952	.943577	-	.539187	.808781
K2O	.120461	.168645	.204783	-	-	-
Total	99,51	98,52	97,28	99,90	98,64	101,30
TSi	7.584	6.751	7.171	7.031	7.190	7.010
TAl	0.416	1.249	0.829	0.000	0.000	0.000
TFe3	0.000	0.000	0.000	0.545	0.447	0.585
TTi	0.000	0.000	0.000	0.000	0.000	0.000
Sum_T	8.000	8.000	8.000	7.576	7.637	7.595
CAl	0.047	0.212	0.128	0.000	0.000	0.000
CCr	0.074	0.000	0.000	0.000	0.000	0.014
CFe3	0.003	0.410	0.496	0.118	0.081	0.139
CTi	0.054	0.019	0.000	0.000	0.000	0.000
CMg	4.005	4.073	3.541	4.882	4.919	4.847
CFe2	0.802	0.281	0.819	0.000	0.000	0.000
CMn	0.000	0.000	0.016	0.000	0.000	0.000
CCa	0.016	0.004	0.000	0.000	0.000	0.000
Sum_C	5.000	5.000	5.000	5.000	5.000	5.000
BMg	0.000	0.000	0.000	1.390	1.221	1.377
BFe2	0.000	0.000	0.026	0.000	0.110	0.001
BMn	0.000	0.000	0.016	0.018	0.022	0.013
BCa	2.000	2.000	1.911	0.029	0.019	0.025
BNa	0.000	0.000	0.047	0.000	0.060	0.088
Sum_B	2.000	2.000	2.000	1.437	1.431	1.505
ACa	0.019	0.005	0.000	0.000	0.000	0.000
ANa	0.181	0.547	0.215	0.000	0.069	0.101
AK	0.021	0.030	0.037	0.000	0.000	0.000
Sum_A	0.221	0.583	0.252	0.000	0.069	0.101
Sum_cat	15.221	15.583	15.252	14.013	14.138	14.201

Microprobe analyses of amphibole (n=59):

Sample	55_type a	56_type b	57_amp2	58_amp2	59_amp2
Analysis	55_12d	55_2a	454_9c	454_10c	18_12b
Location	PCR	PCR	LHzbg	LHzbg	BGab
Mineral	amp	amp	amp	amp	amp
SiO2	56.26451	46.85144	56.05058	58.83172	55.83665
TiO2	-	-	.51709	.200164	-
Al2O3	1.511571	10.581	3.778927	1.511571	.944732
FeO	8.233512	5.274593	4.759999	2.701621	10.03459
Cr2O3	.146156	-	.204618	-	-
MnO	.258245	.129123	.129123	-	.258245
MgO	32.99969	19.73348	20.3968	21.72343	17.90938
CaO	.321813	11.89309	12.03301	13.15235	12.59268
Na2O	.40439	2.965529	1.482765	.539187	.808781
K2O	-	.228875	.228875	-	-
Total	100,2	97,72	99,76	98,39	98,16
TSi	6.871	6.581	7.690	8.038	7.894
TAl	0.217	1.419	0.310	0.000	0.106
TFe3	0.599	0.000	0.000	0.000	0.000
TTi	0.000	0.000	0.000	0.000	0.000
Sum_T	7.687	8.000	8.000	8.038	8.000
CAl	0.000	0.331	0.300	0.243	0.051
CCr	0.014	0.000	0.022	0.000	0.000
CFe3	0.242	0.368	0.038	0.000	0.042
CTi	0.000	0.000	0.053	0.021	0.000
CMg	4.744	4.132	4.172	4.425	3.775
CFe2	0.000	0.161	0.408	0.304	1.117
CMn	0.000	0.008	0.007	0.000	0.015
CCa	0.000	0.000	0.000	0.008	0.000
Sum_C	5.000	5.000	5.000	5.000	5.000
BMg	1.263	0.000	0.000	0.000	0.000
BFe2	0.000	0.091	0.101	0.005	0.028
BMn	0.027	0.008	0.008	0.000	0.016
BCa	0.042	1.790	1.769	1.917	1.907
BNa	0.045	0.112	0.123	0.078	0.049
Sum_B	1.377	2.000	2.000	2.000	2.000
ACa	0.000	0.000	0.000	0.000	0.000
ANa	0.051	0.696	0.271	0.065	0.172
AK	0.000	0.041	0.040	0.000	0.000
Sum_A	0.051	0.737	0.312	0.065	0.172
Sum_cat	14.115	15.737	15.312	15.103	15.172

Microprobe analyses of epidote-zoisite (n=12):

Sample	1	2	3	4	5	6
Analysis	45A-1A	454-1A	454-4B	455-6C	455-7C	591-12D
Location	M HZBG	L HZBG	L HZBG	L HZBG	L HZBG	L HZBG
Mineral	EPI	EPI	EPI	EPI	EPI	EPI
SiO2	38.294	39.792	40.433	39.578	40.433	39.364
TiO2	0	0	0	0	0	0
Al2O3	30.798	30.798	32.688	28.342	29.665	27.397
Fe2O3	0	0	0	0	0	0
FeO	2.830	4.117	3.216	6.947	5.532	6.690
MnO	0	0.129	0	0.516	0.516	0
MgO	0.663	0.166	0.332	0	0.663	0.829
CaO	25.745	23.506	23.366	23.087	22.527	24.626
Total	98.33	98.51	100.04	98.47	99.34	98.91
Si	2.934	3.019	3.004	3.032	3.048	3.015
AlIV	0.066	0.000	0.000	0.000	0.000	0.000
Sum_T	3.000	3.019	3.004	3.032	3.048	3.015
AlVI	2.713	2.752	2.860	2.557	2.634	2.471
Ti	0.000	0.000	0.000	0.000	0.000	0.000
Cr	-	-	-	-	-	-
Fe3	0.18	0.26	0.20	0.44	0.35	0.43
Fe2	0.000	0.000	0.000	0.000	0.000	0.000
Mn	0.000	0.008	0.000	0.033	0.033	0.000
Mg	0.076	0.019	0.037	0.000	0.075	0.095
Ca	2.113	1.911	1.860	1.895	1.819	2.021

Sample	7	8	9	10	11	12
Analysis	591-13E	5912-3A	5912-4A	5912-7B	5912-8B	5912-10C
Location	L HZBG	L HZBG	L HZBG	L HZBG	L HZBG	L HZBG
Mineral	EPI	EPI	EPI	EPI	EPI	EPI
SiO2	38.722	37.866	37.652	37.866	38.080	37.224
TiO2	0	0	0	0	0	0.400
Al2O3	26.075	23.429	22.674	21.729	22.484	22.674
Fe2O3	0	0	0	0	0	0
FeO	7.204	11.192	12.222	13.122	12.093	11.707
MnO	0	0.258	0.387	0	0	0
MgO	0.663	0	0	0	0	0.332
CaO	24.766	24.626	24.486	24.486	24.906	24.906
Total	97.43	97.37	97.42	97.20	97.56	97.24
Si	3.023	3.000	2.992	3.018	3.017	2.964
AlIV	0.000	0.000	0.008	0.000	0.000	0.036
Sum_T	3.023	3.000	3.000	3.018	3.017	3.000
AlVI	2.397	2.186	2.114	2.039	2.098	2.090
Ti	0.000	0.000	0.000	0.000	0.000	0.024
Cr	-	-	-	-	-	-
Fe3	0.47	0.74	0.81	0.87	0.80	0.78
Fe2	0.000	0.000	0.000	0.000	0.000	0.000
Mn	0.000	0.017	0.026	0.000	0.000	0.000
Mg	0.077	0.000	0.000	0.000	0.000	0.039
Ca	2.072	2.090	2.085	2.091	2.114	2.125

APPENDIX C

A mineral list compiled from the microscopic investigation on samples from the Uitkomst Complex

Mineral list:

Minerals:		Po	Pn	Vl	Mc	Cp	Py	Ml	Co	Cb	Ga	Sf	PGM	MtP	Mt	Ilm	Ox	Chr	Ol	Pl	Px	Bm	Gm	Cm	Am	Sp	Ta	Chl	Crb	Ep	Ss	Qtz
Section no:																																
UD 5/A	Mhzbg	*	*		*	*				*					*			*	*	*	*	*				*				*	*	
UD 5/B	Mhzbg	*	*		*	*				*					*			*	*		*	*				*	*	*				
UD 5/C	Mhzbg	*	*		*										*			*	*		*	*				*		*				
UD 5/D	Mhzbg	*	*		*	*				*					*			*			*	*				*						
UD 45/A	Mhzbg	*	*		*	*			?				?		*			*				*			*	*		*	*	*		
UD 5/1	PCR	*	*			*			*													*					*		*			
UD 5/3	PCR	*	*			*												*									*		*			
UD 5/4	PCR	*	*			*												*				*			*			*				
UD 5/5	PCR	*	*		*	*							?		*							*			*	*	*		*			
UD 5/6	PCR	*	*			*									*			*														
UD 5/7	PCR	*	*		*	*							*		*				*	*	*	*	*		*	*	*		*		*	
UD 1/1	PCR	*	*			*									*			*		*	*	*			*	*	*	*	*	*	*	
UD 1/2	PCR	*	*			*									*			*			*	*			*	*	*					
UD 1/3	PCR	*	*			*	*				?							*				*			*	*	*	*	*			
UD 1/4	PCR	*	*			*	*						?		*			*			*	*			*	*	*	*	*			
UD 45/B	PCR																	*									*					
UD 45/C	PCR	*	*	*		*												*				*			*	*	*	*	*	*		
UD 45/D	PCR	*	*	*		*			?						*				*		*				*	*		*	*			
UD 45/1	PCR	*	*	*		*									*			*	*		*	*			*	*	*	*	*			
UD 45/2	PCR	*	*	*		*			*						*			*		*		*			*	*	*	*				
UD 34/A	PCR	*				*	*	*			*							*				*			*	*	*		*			
UD 34/B	PCR	*	*	*		*																*			*	*	*	*	*			
UD 34/1	PCR						*											*						*	*	*		*				*
UD 34/3	PCR	*	*			*												*				*			*	*	*		*			
UD 34/4	PCR	*	*			*									*			*				*			*	*	*		*			
UD 34/5	PCR	*	*			*									*			*	*			*			*	*			*			
UD 34/6	PCR	*	*			*									*				*			*			*	*			*			

		Po	Pn	Vl	Mc	Cp	Py	Ml	Co	Cb	Ga	Sf	PGM	MtP	Mt	Ilm	Ox	Chr	Ol	Pl	Px	Bm	Gm	Cm	Am	Sp	Ta	Chl	Crb	Ep	Ss	Qtz
UD 5/8	Lhzbg	*	*		*	*									*				*	*	*	*	*			*	*			*			
UD 34/7	Lhzbg	*	*			*												*				*			*			*	*			
UD 34/8	Lhzbg	*				*	*	*										*				*			*		*	*				*
UD 34/9	Lhzbg	*	*			*								*		*				*	*	*	*			*	*	*	*				
UD 34/11	Lhzbg	*	*			*								*		*				*	*	*	*			*							
UD 45/3	Lhzbg	*	*	*		*			*				*		*			*				*	*			*	*		*	*			
UD 45/4	Lhzbg	*	*			*					?				*	*						*		*		*	*	*		*	*		
UD 45/E	Lhzbg	*	*			*							?		*	*	*					*	*			*		*	*	*			*
UD 45/F	Lhzbg	*	*			*									*		*	*			*	*	*			*			*			*	
UD 59/1	Lhzbg	*	*	*		*	*					*	?								*	*				*				*	*	*	
UD 59/2	Lhzbg																		*		*	*				*	*		*	*			
UD 59/4	Lhzbg	*	*			*	*						?		*	*	*	*			*	*	*			*	*					*	
UD 59/6	Lhzbg	*	*			*	*								*	*				*	*	*				*	*			*			
UD 59/9	Lhzbg	*	*			*	*								*		*	*		*	*	*	*			*	*	*		*		*	
UD 59/10	Lhzbg	*	*	*		*	*								*		*	*		*	*	*				*				*		*	
UD 59/12	Lhzbg					*	*										*	*			*					*					*	*	
UD 64/1	Lhzbg	*	*			*										*						*	*			*	*		*				
UD 64/2	Lhzbg	*	*			*										*					*					*				*	*		
UD 64/3	Lhzbg	*	*			*						*						*				*	*	*		*	*	*				*	
UD 64/4	Lhzbg	*	*			*										*					*	*	*	*		*	*	*		*		*	
UD 64/6	Lhzbg	*	*			*									*	*				*	*	*	*	*		*	*	*		*		*	
UD 64/7	Lhzbg	*	*			*									*	*	*				*	*	*			*	*		*	*		*	
UD 1/6	Bgab	*	*			*	*								*	*					*		*			*	*	*		*		*	
UD 1/8	Bgab	*	*			*					?				*		*				*	*	*			*	*	*	*	*			
UD 1/9	Bgab	*	*			*	*						?		*	*	*	*				*				*		*		*			
UD 45/G	Bgab	*	*			*	*								*		*	*			*	*	*			*						*	*
UD 45/H	Bgab					*	*										*	*								*						*	

(po=pyrrhotite, pn=pentlandite, vl=violarite, mc=mackinawite, cp=chalcopyrite, py=pyrite, ml=millerite, cob=cobaltite, cb=cubanite, ga=galena, sf=sphalerite, PGM=platinum group minerals, mtP=primary magnetite, mt=secondary magnetite, ilm=ilmenite, ox=Ti-oxides, chr=chromite, ol=olivine, pl=plagioclase, px=pyroxene, Bm=brown phlogopite, Gm=green phlogopite, Cm=Cr-rich mica, am=amphibole, sp=serpentine, ta=talc, chl=chlorite, crb=carbonate, ep=epidote-zoisite, ss=sericite/soussuriticite, qtz=quartz)

APPENDIX D

Data compiled on the grain size of disseminated and net-textured sulphide in boreholes UD 1, 2, 5, 13, 17, 21, 26, 28, 32, 34, 35, 36, 45, 56, 59, 64, 83, 89, 93.

Table 1: Quantitative data on flame and granular pentlandite:

Sample. no:	Lithology:	Total sulfide area (um^2)	Total sulfide area % (*1)	N (granular)	Granular Area (um^2)	%Granular pentlandite (*2)	N (flame)	Flame Area (um^2)	%Flame pentlandite (*2)
UD 5/C	Mhzbg	5295551	0.8335	11988	1324845	25.018	22	139.7	0.003
UD 45/A	Mhzbg	5874789	0.9247	4786	1223183	20.821	110	3090.7	0.053
UD 45/C	PCR	8521353	1.3412	7507	1007135	11.819	1764	44980.1	0.528
UD 45/1	PCR	8024516	1.263	3390	977105.5	12.177	509	6555.7	0.082
UD 45/3	Lhzbg	41952393	6.6032	4561	1921775	4.581	1875	70693.6	0.169
UD 45/F	Lhzbg	6987218	1.0998	145	33485.6	0.479	15	581.8	0.008
UD 45/G	Bgab	2026124	0.3189	339	14695.8	0.725	278	8180.4	0.404
				32716			**4573**		

*1= as % of sample surface
*2= as % of total sulphide

Table 2: Quantitative data on flame and granular pentlandite (with 4 pixels discarded):

Sample.no	Lithology	Total sulfide area (um^2)	Total sulfide area % (*1)	N (granular)	Granular Area (um^2)	%Granular pentlandite (*2)	N (flame)	Flame Area (um^2)	%Flame pentlandite (*2)
UD 5/C	Mhzbg	5295551	0.8335	7002	1316120	24.853	12	122.2	0.002
UD 45/A	Mhzbg	5874789	0.9247	3129	1220901	20.782	59	3019.3	0.051
UD 45/C	PCR	8521353	1.3412	4600	1002902	11.769	935	43843.3	0.515
UD 45/1	PCR	8024516	1.263	2456	975836.5	12.161	260	6172.7	0.077
UD 45/3	Lhzbg	41952393	6.6032	3053	1919726	4.576	1064	69645.7	0.166
UD 45/F	Lhzbg	6987218	1.0998	101	33433.3	0.478	11	576.3	0.008
UD 45/G	Bgab	2026124	0.3189	181	14452.8	0.713	168	8043	0.397
				20522			**2509**		

*1= as % of sample surface
*2= as % of total sulphide

Table 3:The difference (*) between Tables 1 and 2.

Sample no:	%Granular pentlandite (table1)	%Granular pentlandite (table 2)	*	%Flame pentlandite (table 1)	%Flame pentlandite (table 2)	*
UD 5/C	25.018	24.853	0.165	0.003	0.002	0.001
UD 45/A	20.821	20.782	0.039	0.053	0.051	0.001
UD 45/C	11.819	11.769	0.050	0.528	0.515	0.013
UD 45/1	12.177	12.161	0.016	0.082	0.077	0.005
UD 45/3	4.581	4.576	0.005	0.169	0.166	0.002
UD 45/F	0.479	0.478	0.001	0.008	0.008	0.000
UD 45/G	0.725	0.713	0.012	0.404	0.397	0.007

Sample no:	Lithology:	Frame no:	No of particles:	Volume % sulphide:	Area:	Min.pj:	Max.pj:	Mn.pj:	Sd.dv.pj:	Width:	Asp. rat.
UD 1:											
UD 1/1	PCR	1	74	4.33	237464.9	373.26	620.17	498.35	90.65	372.55	8.22
UD 1/2	PCR	8	282	4.11	58711.36	198.06	320.93	259.37	44.23	197.20	1.69
UD 1/3	PCR	9	124	4.10	133819.8	280.91	470.97	377.46	69.64	282.69	1.79
UD 1/4	PCR	2	135	3.16	94858.35	243.04	384.70	313.17	51.01	242.43	1.59
UD 1/7	Bgab	4	245	11.08	183485.6	306.34	516.36	413.32	78.00	310.25	1.66
UD 1/6	Bgab	3	249	16.18	264359.7	380.46	621.24	501.83	86.33	387.84	1.59
UD 1/8	Bgab	5	56	14.52	1053556	658.45	1100	886.94	150.38	708.21	1.70
UD 1/9	Bgab	6	297	32.40	439222.2	363.17	619.60	494.14	92.97	404.03	1.65
UD 2:											
UD2/1	PCR	11	43	0.65	59735.36	189.78	274.81	237.44	29.66	191.42	1.46
UD2/2	PCR	12	38	0.14	11510.79	85.65	142.99	113.96	23.68	88.10	1.61
UD2/3	PCR	1	523	18.30	141740.3	296.09	487.92	395.32	68.03	299.68	1.65
UD2/4	PCR	2	40	3.52	356287.5	379.32	680.11	532.02	107.06	383.01	1.74
UD2/5	PCR	17	86	3.81	179639	223.59	483.60	331.65	68.13	231.72	1.68
UD2/6	PCR	13	65	1.22	75765.25	204.78	360.31	281.02	55.59	209.64	1.70
UD2/7	PCR	3	23	10.16	1795163	902.34	1632.47	1307.4	256.14	955.49	1.73
UD2/8	PCR	4	118	6.78	233716.4	267.25	462.54	364.82	71.35	277.36	1.59
UD2/9	PCR	5	130	8.53	265989.7	281.25	548.66	420.33	95.23	295.08	1.76
UD2/10	PCR	6	202	8.61	172932.2	293.81	454.78	371.14	56.93	334.33	1.62
UD2/11	PCR	7	115	6.64	229713.8	362.46	677.55	527.62	112.35	371.24	1.80
UD2/12	PCR	14	49	10.24	848673.6	311.55	722.32	506.71	150.40	339.99	2.33
UD2/13	PCR	8	40	7.57	768531	456.49	746.08	614.68	98.25	459.81	1.65
UD2/14	PCR	15	251	15.87	256394.7	298.73	520.61	410.11	79.34	774.50	1.69
UD2/15	PCR	9	166	11.88	290421.3	465.87	571.17	460.61	77.49	357.07	1.73
UD2/16	PCR	49	49	4.42	365837.9	328.40	534.15	429.67	72.91	337.58	1.82
UD2/17	L Hzbg	10	61	7.78	518144	348.17	619.07	499.29	97.86	363.49	1.67

(min.pj.=minimum projection, max.pj.=maximum projection, mn.pj.=mean projection, all in micron
sd.dv.pj.=standard deviation projection, asp.rat.=aspect ratio, area=μm^2)

D

Sample no:	Lithology:	Frame no:	No of particles:	Volume % sulphide:	Area:	Min.pj:	Max.pj:	Mn.pj:	Sd.dv.pj:	Width:	Asp. rat.
UD 5:											
UD5/A	M Hzbg	5	61	1.9741	131462	290.754	513.84	400.68	79.024	295.74	1.76
UD5/B	M Hzbg	6	91	1.6872	74503.92	228.499	393.69	309.6	58.585	230.68	1.81
UD5/C	M Hzbg	7	119	1.4396	48722.78	167.894	287.72	229.28	44.444	167.46	1.76
UD5/D	M Hzbg	8	100	3.1275	126833.4	269.561	492.62	382.65	80.279	276.48	1.75
UD5/E	M Hzbg	9	39	0.90503	94060.29	224.502	406.68	311.11	71.598	220.2	1.73
UD5/1	PCR	1	48	2.3145	194953.9	243.03	389.57	318.69	50.596	259.28	1.41
UD5/3	PCR	12	37	6.6603	727634.4	372.882	820.36	643.63	159.49	414.06	1.76
UD5/4	PCR	10	63	3.8132	245443.1	337.472	571.65	459.03	84.998	308.38	1.67
UD5/5	PCR	2	173	8.8427	207668	317.722	559.25	441.62	84.993	327.14	1.66
UD5/6	PCR	11	197	5.9025	121340	214.865	352.03	285.34	49.537	288.81	1.71
UD5/7	PCR	3	97	4.6064	192912	331.538	535.1	436.85	70.37	334.58	1.62
UD5/8	L Hzbg	4	35	5.3287	618622.6	455.033	776.95	631.16	112.02	480.48	1.58
UD 13:											
13/17	M Hzbg	1	118	2.2916	78619.71	208.349	351.3	279.82	51.858	207.27	1.69
13/18	M Hzbg	2	53	1.984	151949.3	296.008	458.74	382.27	57.572	293.46	1.61
13/19	M Hzbg	3	76	3.0711	163906.3	318.818	502.71	412.26	69.497	325.46	1.53
UD 17:											
17/5	L Hzbg	5	148	14.253	390866.9	367.629	628.85	499.03	91.356	378.15	1.8
17/3	PCR	8	79	5.6766	291157.7	390.749	662.94	538.02	94.457	397.33	1.67
17/A	PCR	6	168	4.0684	98107	239.568	402.7	322.83	58.206	245.21	1.64
17/B	PCR	7	96	8.5008	359499.6	390.172	630.53	504.11	86.376	399.17	1.63

Sample no:	Lithology:	Frame no:	No of particles:	Volume % sulphide:	Area:	Min.pj:	Max.pj:	Mn.pj:	Sd.dv.pj:	Width:	Asp. rat.
UD 21:											
21/3	PCR	1	182	11.903	265638.5	377.222	614.7	498	83.451	383.89	1.69
21/4	PCR	2	158	6.4638	165987.2	263.849	514.82	393.23	90.926	265.72	1.87
21/2	PCR	3	54	4.632	348049.4	342.615	637.51	495.96	103.98	369.77	6.8
21/5	PCR	4	202	17.224	346248.1	393.491	654.68	528.11	152.26	403.39	1.66
21/7	PCR	5	20	0.40215	81044.9	206.78	393.91	298.56	69.405	210.7	1.8
21/A	PCR	6	74	2.4472	118449.5	257.387	442.75	347.09	67.323	263.45	1.64
21/B	PCR	7	155	3.0382	79386.27	221.111	369.44	320.38	53.746	218.77	1.74
21/C	PCR	8	45	2.8284	254794	275.059	456.42	375.57	59.928	280.94	1.72
21/E	PCR	9	27	1.9424	292181	358	565.33	469.15	71.024	358.83	1.85
21/1	PCR	10	31	3.4175	447617.4	437.532	756.05	621.89	112.07	487.85	1.77
21/D	PCR	11	65	3.7628	234813.2	310.023	487.31	400.76	62.185	323.55	1.56
UD 26:											
26/2	L Hzbg	1	182	6.6656	148692.5	315.671	518.84	422.06	71.143	322.65	1.63
26/5	L Hzbg	2	147	30.529	843628.8	499.164	832.41	673.18	116.58	530.48	1.6
26/7	L Hzbg	3	225	22.04	398129.4	485.574	1152	652.49	111.11	552.46	1.65
26/9	L Hzbg	4	272	5.619	83542.67	253.059	330.86	264.01	49.301	197.79	1.73
26/4	L Hzbg	5	48	21.674	507564.8	395.333	811.84	623.47	148.15	412.71	1.88
UD 28:											
28/3	L Hzbg	1	134	15.967	483757.8	317.366	513.55	416.04	69.542	332.12	1.77
28/6	L Hzbg	2	112	15.011	543931.5	418.739	733.98	586.22	109.32	441.31	1.65
28/4	L Hzbg	3	109	8.159	302976.7	332.079	561.59	432.77	82.303	337.47	1.73

Sample no:	Lithology:	Frame no:	No of particles:	Volume % sulphide:	Area:	Min.pj:	Max.pj:	Mn.pj:	Sd.dv.pj:	Width:	Asp. rat.
UD 32:											
32/A	PCR	4	59	2.03	139677.8	258.66	426.07	341.71	58.08	262.34	1.72
32/1	PCR	1	221	2.04	36573.68	149.96	265.58	207.44	43.36	147.65	1.74
32/2	LHzbg	5	25	0.25	40266.56	158.61	289.01	224.31	48.05	157.54	1.74
32/3	LHzbg	2	252	10.97	176745.3	379.14	493.51	399.99	67.39	311.79	1.61
32/6	LHzbg	6	15	0.58	155834.1	273.61	505.83	394.62	82.68	265.19	1.99
32/7	LHzbg	3	202	7.36	147646.2	230.94	402.86	317.36	64.85	236.31	1.66
UD 34:											
34/A	PCR	10	112	2.05	73801.92	206.58	335.34	269.36	47.72	207.12	1.64
34/B	PCR	11	47	5.62	481203.9	467.49	800.10	636.06	117.67	475.96	1.83
34/1	PCR	5	42	0.34	31502.09	135.01	189.73	164.50	20.23	142.53	1.36
34/3	PCR	1	63	1.16	74575.94	207.03	314.32	258.45	41.92	193.82	1.69
34/4	PCR	2	62	3.00	196464.3	285.44	510.65	386.95	78.65	290.30	1.69
34/5	PCR	6	213	6.62	125988.7	259.30	434.12	348.46	64.30	263.86	1.69
34/6	PCR	3	184	4.85	106899.4	239.05	368.51	304.05	46.67	241.23	1.57
34/7	LHzbg	7	136	3.45	102714.7	219.00	384.77	303.97	59.98	222.42	1.70
34/8	LHzbg	4	104	2.03	79180.68	217.92	342.68	281.20	44.01	220.02	1.52
34/9	LHzbg	8	82	5.89	291020.4	324.66	504.59	417.56	63.76	333.32	1.59
34/11	LHzbg	9	117	4.02	139174.8	282.02	500.35	394.71	78.91	284.10	1.72
UD 35:											
35/3	PCR	1	130	0.72	21655.74	125.31	185.14	157.72	23.40	118.46	1.59
35/4	PCR	2	94	7.77	335482.8	376.93	582.52	483.79	68.52	393.00	1.58
35/5	L Hzbg	3	117	4.85	166776.3	289.85	482.56	387.83	69.15	298.24	1.66
35/6	L Hzbg	4	56	2.27	164804.3	324.29	551.76	440.26	81.13	331.95	1.72
35/7	L Hzbg	5	89	5.34	243086.9	296.85	526.29	411.84	81.74	301.35	1.65
35/8	L Hzbg	6	104	3.93	152872.8	254.83	524.36	389.06	96.95	266.98	2.02
35/9	L Hzbg	7	210	8.23	152569.2	235.03	374.31	307.48	49.00	239.13	1.63

Sample no:	Lithology:	Frame no:	No of particles:	Volume % sulphide:	Area:	Min.pj:	Max.pj:	Mn.pj:	Sd.dv.pj:	Width:	Asp. rat.
UD 36:											
36/2	LHzbg	1	61	0.89	58967.18	187.48	307.91	250.45	44.92	193.05	1.60
36/3	LHzbg	2	38	0.83	88575.97	239.48	380.30	310.89	51.14	245.63	1.66
36/4	LHzbg	3	22	3.98	733599.3	626.98	942.66	793.61	111.07	648.05	1.70
UD 45:											
45/A	M Hzbg	12	79	1.48	76023.53	223.52	381.84	302.31	56.75	215.37	1.88
45/C	PCR	13	61	1.00	66087.01	200.09	320.43	260.87	46.12	191.75	1.75
45/D	PCR	14	61	3.20	212805.8	312.80	548.73	429.48	76.58	318.95	1.79
45/1	PCR	3	222	5.38	98243.29	238.74	382.91	311.96	52.40	240.57	1.63
45/2	PCR	4	99	2.20	89697.47	196.00	311.12	257.36	41.52	196.54	1.50
45/3	L Hzbg	5	104	8.36	326208.1	342.50	587.62	587.62	471.65	86.14	1.68
45/4	L Hzbg	6,18	41.5	8.92	806232.3	556.04	949.91	763.75	135.71	577.14	1.85
45/5	L Hzbg	2,7	92.5	24.09	1059727	561.76	1035.51	826.29	162.44	593.70	1.82
45/6	L Hzbg	1,8,9,10	268	16.18	510824.5	455.16	794.52	615.38	299.45	446.65	1.82
45/7	L Hzbg	11	245	11.42	189170.8	403.89	595.01	467.53	92.41	343.04	1.74
45/E	L Hzbg	15	51	6.26	498541.5	418.08	845.37	639.05	152.08	442.50	1.90
45/F	L Hzbg	19	40	0.72	72203.69	230.84	355.76	291.72	42.66	232.37	1.61
45/G	Gab	16	45	0.25	22060.10	122.20	185.31	154.93	23.98	124.28	1.52
45/H	Gab	17	16	0.15	37226.41	165.37	269.28	220.15	40.30	172.30	1.61
UD 56:											
56/1	L Hzbg	1	74	7.9945	199756.4	323.498	567.36	442.95	92.17	325.21	1.86
56/2	L Hzbg	2	71	3.1363	179119.1	305.394	478.38	392.96	59.679	302.87	1.65
56/3	L Hzbg	3	92	7.6263	336588.5	368.335	710.5	541.08	122.01	381.85	1.81
56/4	L Hzbg	4	630	8.3822	54458.38	176.731	307.55	241.34	47.244	176.6	1.72

Sample no:	Lithology:	Frame no:	No of particles:	Volume % sulphide:	Area:	Min.pj:	Max.pj:	Mn.pj:	Sd.dv.pj:	Width:	Asp. rat.
UD 59:											
59/1	L Hzbg	1	120	15.574	526959.8	285.079	489.4	388.71	75.448	297.36	1.58
59/2	L Hzbg	2	129	3.4831	109334.5	241.229	396.16	318.04	55.363	238.75	1.61
59/4	L Hzbg	3	116	8.5558	299282.1	276.609	452.12	369.79	63.4	285.87	1.61
59/6	L Hzbg	4	131	9.4536	293086.8	379.451	709.11	548.35	121.08	392.04	1.79
59/9	L Hzbg	5	106	12.227	468637	448.376	792.04	619.74	123.01	464.06	1.87
59/10	L Hzbg	6	71	7.5164	414755.3	370.406	655.25	523.29	98.777	389.4	1.75
UD 62:											
UD62/1	L Hzbg	1	281	8.48	122233.3	266.99	496.43	381.50	83.68	271.76	1.84
UD62/3	L Hzbg	2	165	4.90	117686.2	274.73	482.29	385.56	76.36	284.76	1.62
UD62/4	L Hzbg	3	368	5.17	56100.91	197.28	341.46	268.30	53.10	196.92	2.15
UD 64:											
64/1	L Hzbg	1	322	15.997	145947.8	212.528	352.57	283.55	51.827	215.14	1.63
64/3	L Hzbg	2	127	34.344	318781.4	408.201	699.69	559.93	101.38	428.57	1.79
64/4	L Hzbg	3	208	5.3668	104542.6	236.484	386.88	316.57	54.488	238.77	1.61
64/6	L Hzbg	4	274	18.648	201722.3	298.73	501.3	403.32	71.995	307.96	1.66
64/7	L Hzbg	5	75	11.007	235767	302.335	512.25	408.64	73.935	309.82	1.73

Sample no:	Lithology:	Frame no:	No of particles:	Volume % sulphide:	Area:	Min.pj:	Max.pj:	Mn.pj:	Sd.dv.pj:	Width:	Asp. rat.
UD 83:											
83/1	L Hzbg	1	501	29.611	240027.2	360.668	592.42	479.21	81.876	368.61	1.66
83/3	L Hzbg	2	52	11.932	711119.7	502.26	899.46	708.58	139.11	511.23	2.16
83/2	L Hzbg	3	63	6.3695	408084.8	443.894	767.29	608	112.87	460.73	1.67
UD 89:											
89/1	L Hzbg	1	172	5.8075	136875.5	290.324	500.48	399.67	74.902	297.44	1.74
89/2	L Hzbg	2	196	2.6361	53877.12	188.58	300.18	245.45	41.319	188.28	1.62
UD 93:											
93/1	L Hzbg	1	99	12.072	340160.8	316.228	623.55	482.23	110.37	329	1.88
93/2	L Hzbg	3	100	12.706	516252.4	527.032	860.69	700.65	116.58	550.59	1.65
93/3	L Hzbg	2,4	310	15.4925	224860.5	329.511	557.6	448.49	81.05	340.91	1.63

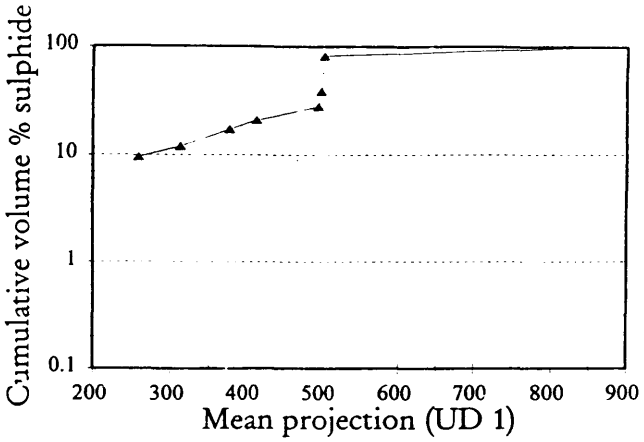

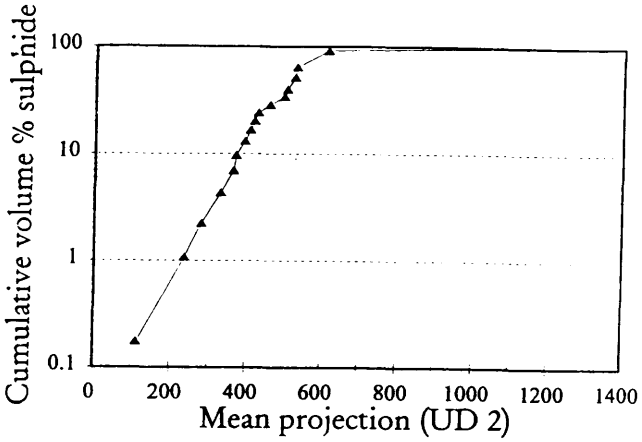

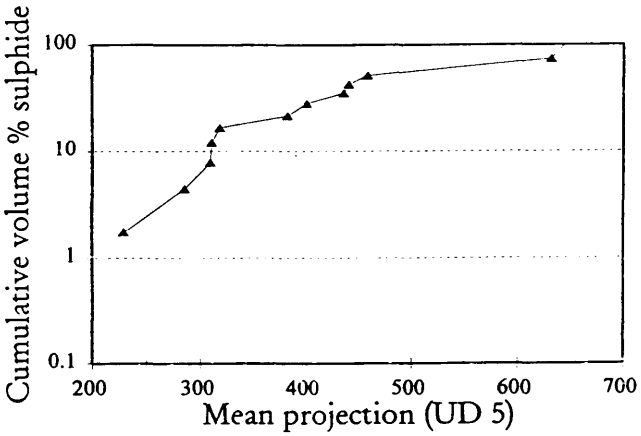

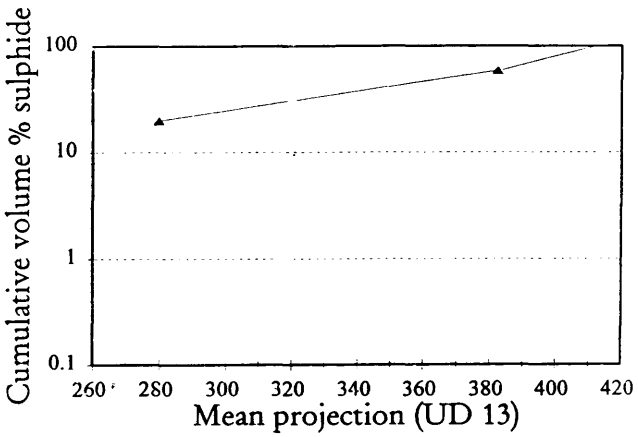

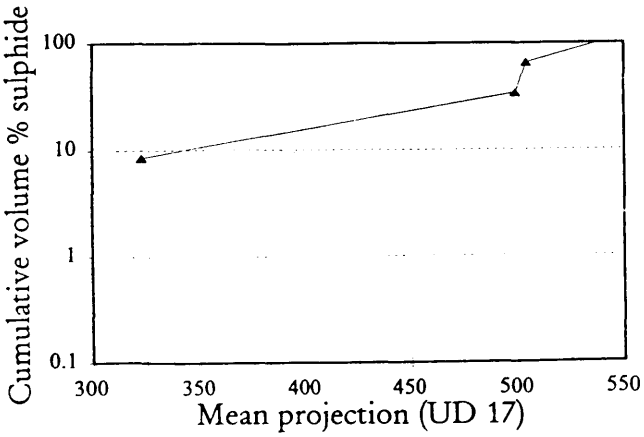

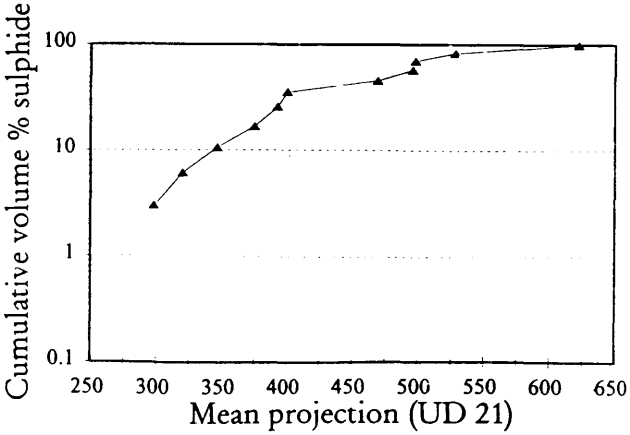

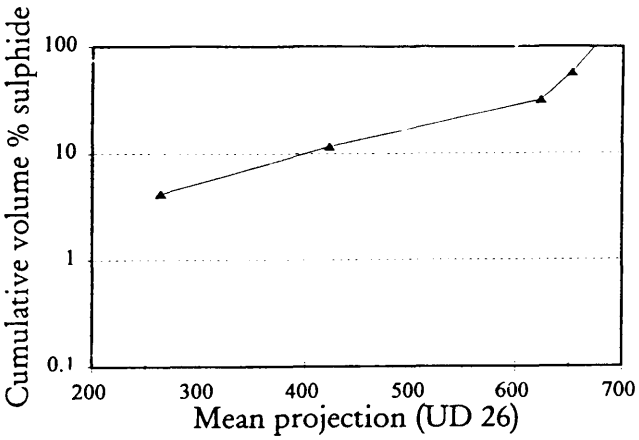

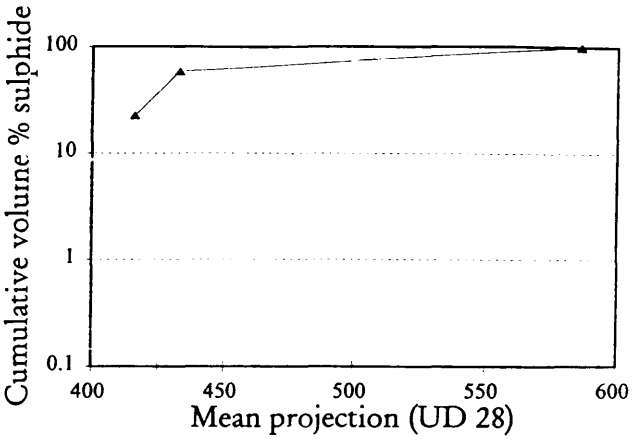

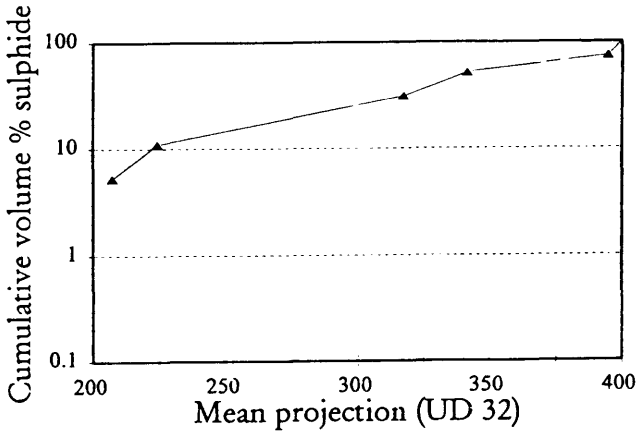

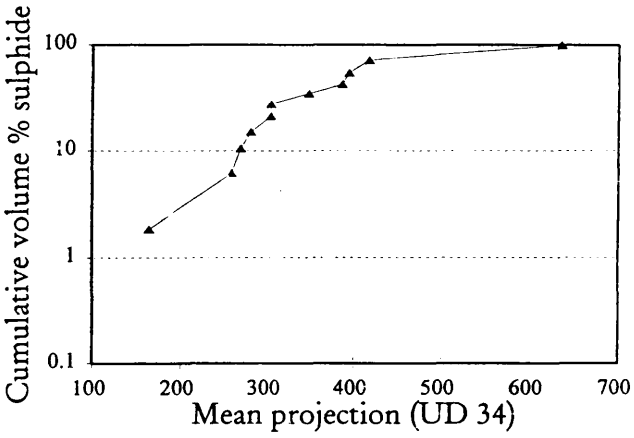

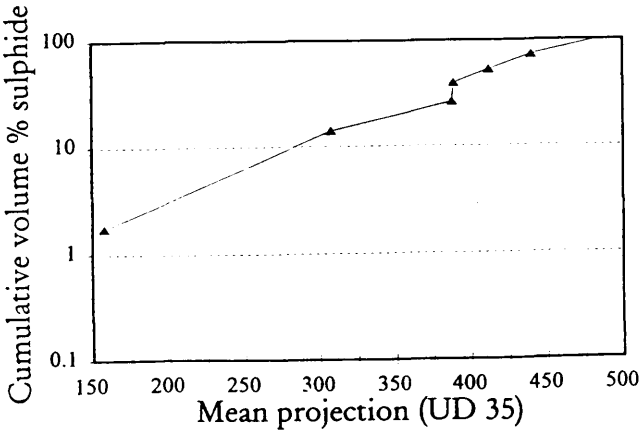

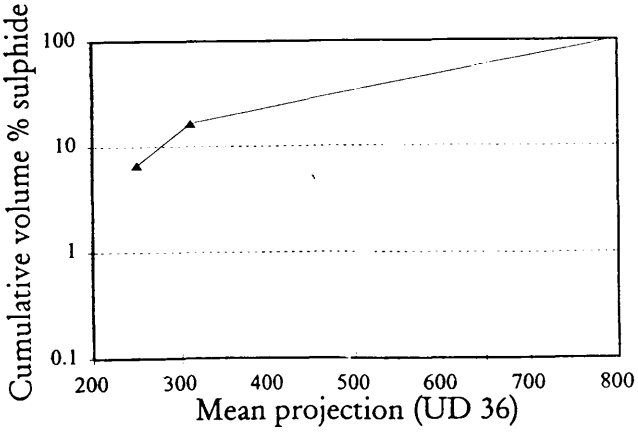

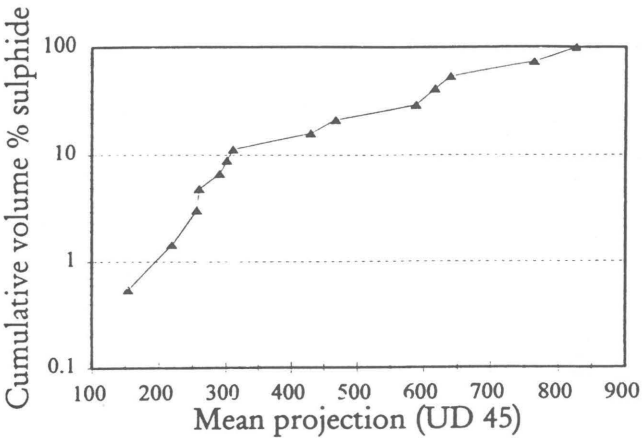

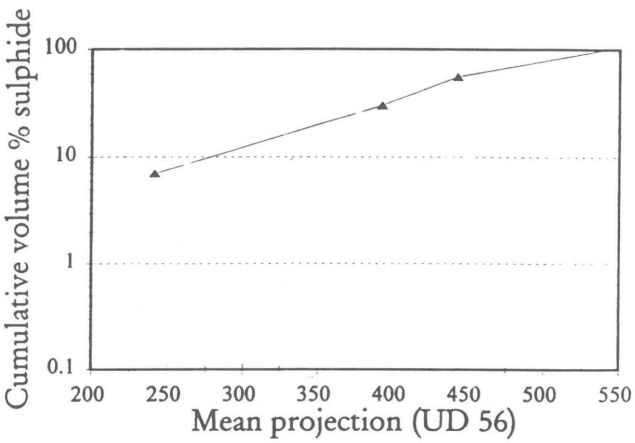

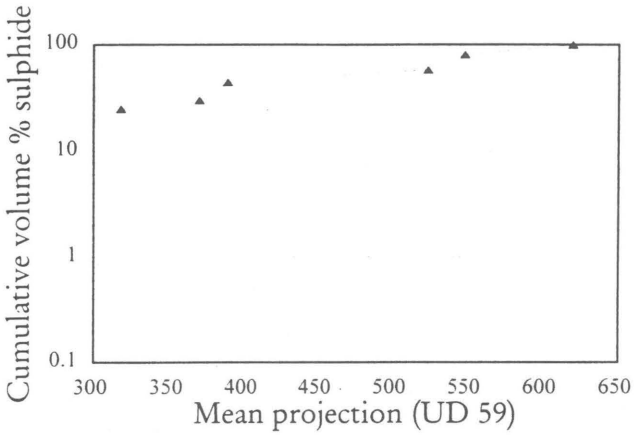

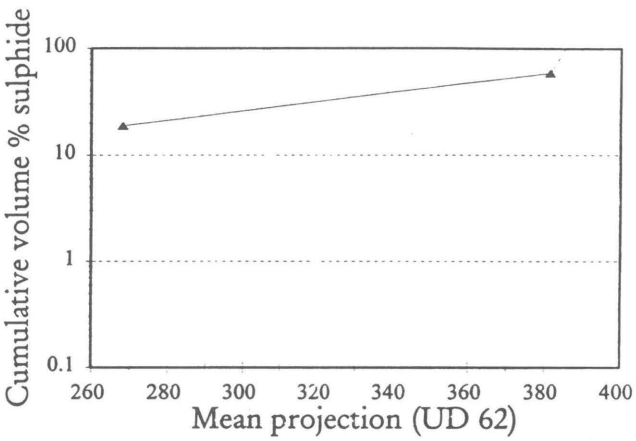

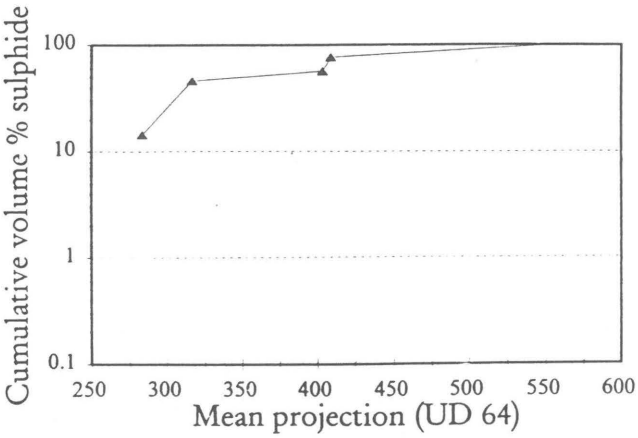

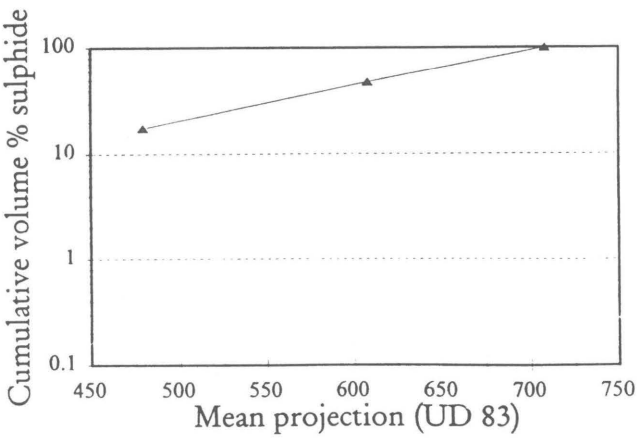

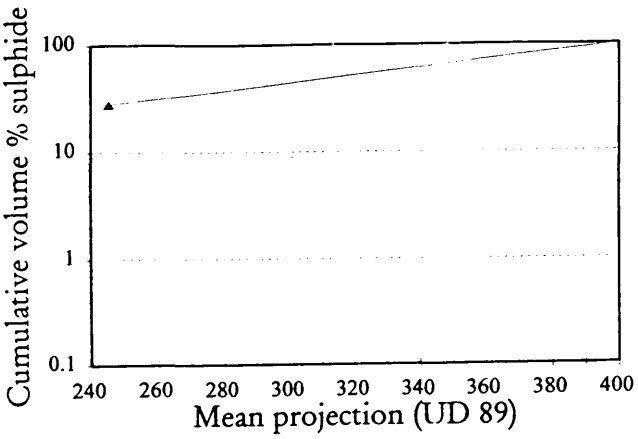

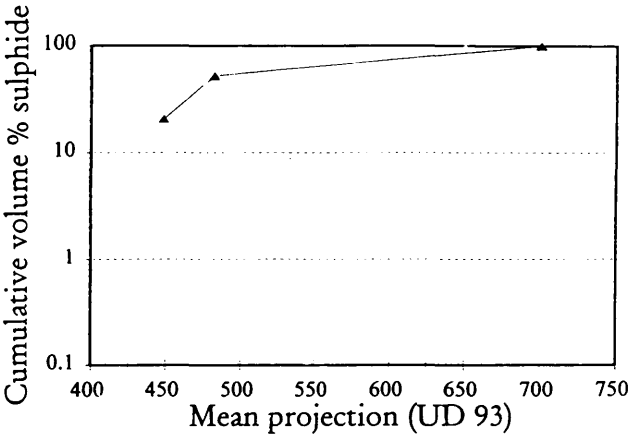

APPENDIX E

Assay values for boreholes UD 1, 5, 34, 45, 59, 64

Assay values for borehole UD 1:

Samp.no:	Depth:	Cu:	Ni:	Co:	S:	Pt:	Pd:
1005	175.03	0.15	0.40	0.02	1.04	0.17	0.4
1006	184.84	0.03	0.25	0.01	0.37	0.06	0.14
1001	197.05	0.02	0.25	0.01	0.31	0.05	0.13
1002	211.11	0.32	0.92	0.05	6.21	0.39	0.96
1003	216.41	0.55	0.81	0.04	6.21	0.84	2
1004	221.99	0.01	0.02	0.00	0.23	0	0

Samp.no:	Depth:	Cu/Ni:	Ni/S:	Pt/Pd:	Cu/Cu+Ni	Pt/Pt+Pd
1005	175.03	0.37	0.38	0.43	0.27	0.30
1006	184.84	0.13	0.68	0.43	0.12	0.3
1001	197.05	0.08	0.81	0.38	0.07	0.28
1002	211.11	0.35	0.15	0.41	0.26	0.29
1003	216.41	0.68	0.13	0.42	0.41	0.30
1004	221.99	0.65	0.09		0.39	

Assay values for borehole UD 5:

Samp.no:	Depth:	Cu:	Ni:	Co:	S:	Pt:	Pd:
1001	165.00	0.08	0.43	0.02	0.95	0.10	0.26
1002	174.92	0.03	0.28	0.01	0.33	0.05	0.14
1003	182.39	0.04	0.24	0.01	0.28	0.06	0.11
1004	194.80	0.03	0.12	0.01	0.23	0.05	0.09
1005	223.18	0.06	0.25	0.01	0.62	0.07	0.16
1006	230.76	0.10	0.33	0.02	1.46	0.20	0.50
1007	247.63	0.06	0.21	0.02	1.32	0.25	0.49
1008	257.63	0.10	0.31	0.02	2.04	0.26	0.55
1009	262.63	0.11	0.27	0.02	1.50	0.30	0.73
1010	267.63	0.14	0.48	0.03	3.41	0.20	0.54
1011	271.67	0.15	0.64	0.04	5.09	0.29	0.65

Samp.no:	Depth:	Cu/Ni:	Ni/S:	Pt/Pd:	Cu/Cu+Ni	Pt/Pt+Pd
1001	165.00	0.20	0.45	0.38	0.17	0.28
1002	174.92	0.11	0.83	0.36	0.10	0.26
1003	182.39	0.15	0.86	0.55	0.13	0.35
1004	194.80	0.30	0.50	0.56	0.23	0.36
1005	223.18	0.23	0.40	0.44	0.19	0.30
1006	230.76	0.29	0.23	0.40	0.22	0.29
1007	247.63	0.30	0.16	0.51	0.23	0.34
1008	257.63	0.32	0.15	0.47	0.24	0.32
1009	262.63	0.41	0.18	0.41	0.29	0.29
1010	267.63	0.30	0.14	0.37	0.23	0.27
1011	271.67	0.23	0.13	0.45	0.19	0.31

Assay values for borehole UD 34:

Samp.no:	Depth:	Cu:	Ni:	S:	Pt:	Pd:
1001	35.09	0.06	0.26	1.02	0.2	0.47
1002	43.84	0.08	0.32	1.2	0.2	0.44
1003	53.94	0.06	0.27	1.06	0.24	0.52
1004	62.160	0.07	0.29	1.33	0.29	0.54
1005	95.80	0.06	0.48	2.25	0.31	0.64
1006	104.46	0.10	0.35	1.67	0.26	0.60
1007	113.13	0.15	0.51	3.15	0.31	0.80
1008	122.17	0.22	0.67	4.82	0.34	0.81
1009	131.81	0.30	0.24	1.58	0.48	0.99

Samp.no:	Depth:	Cu/Ni:	Ni/S:	Pt/Pd:	Cu/Cu+Ni	Pt/Pt+Pd
1001	35.09	0.25	0.25	0.43	0.20	0.30
1002	43.84	0.25	0.26	0.45	0.20	0.31
1003	53.94	0.23	0.25	0.46	0.18	0.32
1004	62.160	0.23	0.22	0.54	0.19	0.35
1005	95.80	0.12	0.21	0.48	0.10	0.33
1006	104.46	0.28	0.21	0.43	0.22	0.30
1007	113.13	0.28	0.16	0.39	0.22	0.28
1008	122.17	0.33	0.14	0.42	0.25	0.30
1009	131.81	1.25	0.15	0.48	0.55	0.33

Assay values for UD 45:

Samp.no:	Depth:	Cu:	Ni:	Co:	S:	Pt:	Pd:
1001	28.70	0.04	0.17	0.02	0.61	0.16	0.32
1002	38.70	0.09	0.27	0.02	1.59	0.30	0.56
1003	48.49	0.08	0.24	0.02	1.09	0.34	0.66
1004	57.76	0.11	0.40	0.02	1.79	0.20	0.45
1005	63.38	0.19	0.73	0.04	5.07	0.24	0.58
1006	69.11	0.22	0.77	0.04	1.94	0.22	0.68
1007	85.32	0.33	0.82	0.04	5.70	0.43	1.10
1008	102.62	0.08	0.21	0.02	2.89	0.21	0.42
1009	109.75	0.09	0.04	0.01	0.38	0.10	0.19

Samp.no:	Depth:	Cu/Ni:	Ni/S:	Pt/Pd:	Cu/Cu+Ni	Pt/Pt+Pd
1001	28.70	0.22	0.27	0.50	0.18	0.33
1002	38.70	0.33	0.17	0.54	0.25	0.35
1003	48.49	0.35	0.22	0.52	0.26	0.34
1004	57.76	0.28	0.22	0.44	0.22	0.31
1005	63.38	0.25	0.14	0.41	0.20	0.29
1006	69.11	0.29	0.40	0.32	0.22	0.24
1007	85.32	0.40	0.14	0.39	0.29	0.28
1008	102.62	0.39	0.07	0.50	0.28	0.33
1009	109.75	2.20	0.11	0.53	0.69	0.34

Assay values for borehole UD 59:

Samp.no:	Depth:	Cu:	Ni:	Co:	S:	Pt:	Pd:
1001	16.58	0.15	0.41	0.02	2.18	0.31	0.82
1002	26.58	0.28	0.44	0.03	4.30	0.45	1.09
1003	36.58	0.21	0.24	0.02	2.61	0.23	0.42

Samp.no:	Depth:	Cu/Ni:	Ni/S:	Pt/Pd:	Cu/Cu+Ni	Pt/Pt+Pd
1001	16.58	0.37	0.19	0.38	0.27	0.27
1002	26.58	0.64	0.10	0.41	0.39	0.29
1003	36.58	0.87	0.09	0.55	0.47	0.35

Assay values for UD 64:

Samp.no:	Depth:	Cu:	Ni:	Co:	S:	Pt:	Pd:
1001	8.005	0.21	0.56	0.03	1.38	0.32	1.07
1002	12.44	0.34	1.27	0.05	5.59	0.35	1.08
1003	19.71	0.14	0.45	0.03	3.46	0.19	0.54
1004	30.02	0.09	0.09	0.01	0.84	0.10	0.23
1005	36.51	0.09	0.14	0.01	0.41	0.10	0.19

Samp.no:	Depth:	Cu/Ni:	Ni/S:	Pt/Pd:	Cu/Cu+Ni	Pt/Pt+Pd
1001	8.005	0.38	0.41	0.30	0.27	0.23
1002	12.44	0.27	0.23	0.32	0.21	0.24
1003	19.71	0.31	0.13	0.35	0.24	0.26
1004	30.02	0.98	0.11	0.43	0.49	0.30
1005	36.51	0.61	0.34	0.53	0.38	0.34